EVALUATION OF ASPHALT STRUCTURAL PERFORMANCE

by

S. C. Britton

D. Bynum, Jr.

W. B. Ledbetter

Research Report 127-4(F)

Research Study 2-8-69-127

Sponsored by

The Texas Highway Department
in cooperation with the
U. S. Department of Transportation
Federal Highway Administration

May 1971

TEXAS TRANSPORTATION INSTITUTE
Texas A&M University
College Station, Texas

PREFACE

This is the fourth and final report issued under Research Study 2-8-69-127, which is being conducted at the Texas Transportation Institute in the cooperative research program with the Texas Highway Department and the Federal Highway Administration. The first three reports are:

"Performance Requirements of High Quality Flexible Pavements," by Douglas Bynum, Jr., and R. N. Traxler, Research Report 127-1, Texas Transportation Institute, August 1969.

This report presents the results of an analytical determination of the performance requirements for 1) normal strain or stress at thermal equilibrium, 2) transient thermal stress, 3) shear stress, and 4) peel strength at the pavement-foundation interface, to maintain the structural integrity of a flexible pavement surface course.

"A Thermoviscoelastic Characterization of an Asphaltic Concrete," by Douglas Bynum, Jr., Research Report 127-2, Texas Transportation Institute, August 1970.

This report covers an experimental study to determine the mechanical behavior of two compacted asphaltic concrete mixtures under simple uniaxial tension and compression at several temperatures and several strain rates. One mixture was compacted at 300°F, and the other at 450°F; the results indicate the effects of asphalt embrittlement on uniaxial modulus and failure behavior.

"Loss of Durability in Bituminous Pavement Surfaces - Importance of Chemically Active Solar Radiation," by R. N. Traxler, F. H. Scrivner, and W. E. Kuykendall, Jr., Research Report 127-3, Texas Transportation Institute, April 1971.

This report gives the results of an investigation which involved the application of a new laboratory test for the hardening of asphalt cements by the action of chemically active short wave (solar) radiation and correlation of these test results with a Hardening Index obtained on 14 different asphalt cements after two years service in a pavement. The hardening action of solar radiation combined with air and heat was found to be accelerated significantly by the presence of small amounts (parts per million) of chemically active Vanadium in the asphalt cement.

The authors wish to acknowledge the guidance and assistance given by the advisory committee for this study. The members are as follows: (a) Texas Highway Department personnel - Mr. J. L. Brown, Study Contact Representative; Mr. Kenneth D. Hankins, Research Area Representative; and Mr. Weldon Chaffin, Materials and Test Division Representative; (b) Federal Highway Administration personnel - Mr. R. W. Barbour, Division Representative.

Special acknowledgement is made to Ralph N. Traxler, Research Chemist, who devoted many hours in providing the necessary guidance and advice on the asphalt and asphaltic concrete selection, characterization, and laboratory control.

Much of the experimental work, data reduction, and data presentation was done by graduate assistants. In particular, the authors wish to thank the following for their unstinting effort, willing cooperation, and extraordinary efforts in completing this phase of the study: Messrs. R. Agarwal, H. Ahmad, L. C. Askew, J. F. Evertson, P. R. Frye, D. R. Ray, and M. P. Sartori. Special thanks go to Mr. H. O. Fleisher who developed the extensive computer program used for data reduction and analysis in this study.

The advice and constructive criticism of other members of Texas Transportation Institute, and several other highway and aerospace engineers was also most helpful and very much appreciated.

TABLE OF CONTENTS

LIST OF TABLES

LIST OF FIGURES

Figure		Page

1.0 ABSTRACT

A method of fundamental evaluation of asphalt cement structural performance* was examined by measurement of the mechanical behavior (load response and failure) of candidate asphaltic concrete mixtures by application of direct uniaxial tension and compression, splitting tension, triaxial tension, and double lap shear test procedures. The mixtures were made by using two different representative asphalt cements (unmodified and modified by the addition of a synthetic elastomeric polymer). Test results were examined with respect to reliability of the test procedures and their capability of distinguishing among asphalt cements of significantly different composition and characteristics.

The results indicate that reliable test methods are available but require further development to make them suitable for practical application. The results also indicate that relative structural performance will vary with stress axiality and that adequate evaluation of asphalt cement structural performance requires more than uniaxial test methods. The viscoelastic (time dependent) nature of asphaltic concrete was confirmed and it was shown that addition of elastomeric polymers will significantly alter the structural performance of an asphalt cement.

*The term Structural Performance has been employed in this study to designate the behavioral characteristics of an asphalt cement which influence the ability of an asphaltic concrete to successfully withstand the repeated action of wheel loads or restrained volume changes brought about by changes in temperature.

2.0 SUMMARY

The research in this study was based on the premise that improvements in the prediction and control of a flexible pavement system can be achieved by suitable application of engineering design analysis techniques. In particular, this approach was considered to be a sub-system of the total system of design and analysis visualized in Study 1-8-69-123 (2). An important consideration in such an approach is that data characterizing the basic structural performance behavior of the asphaltic concrete are available and that this behavior will be greatly influenced by asphalt cement structural performance. Accordingly, constant strain rate tests to determine the mechanical behavior of representative asphaltic concrete samples were selected which represent the various conditions of stress axiality found in flexible pavement surface course. These tests were run on samples of asphaltic concrete mixtures made in the laboratory from two different representative asphalt cements (unmodified and modified by the addition of 3 percent of a synthetic elastomeric polymer). Other variables, such as the source and gradation of the aggregate were held constant in this study.

Based on the results of this study, the following conclusions were made:

1) The test modes examined in this study can be applied to obtain basic pavement design data, select asphalt cements, and for asphalt cement quality control.

2) These test methods give more reliable ultimate stress than ultimate strain data and more reliable secant modulus than tangent modulus values. Improved methods of measuring sample deformation are required.

3) Relative structural performance of asphaltic concrete cannot be judged solely on the basis of uniaxial tests; a combination of several test modes is required.

4) The simple power law dependence of modulus and failure data implies that the structural behavior of asphaltic concrete is linearly viscoelastic.

5) Certain elastomeric ploymers used as additives have a significant effect on asphalt cement structural performance.

6) Substitution of ground reclaimed rubber for up to 5 percent of the aggregate has little effect on the structural behavior of asphaltic concrete specimens examined in this study.

3.0 IMPLEMENTATION

Based on the results described in this report, the Texas Highway Department should apply the fundamental approach used herein to the acquisition of basic pavement design data and selection of asphalt cements. The final step, that of utilizing this approach to the control of asphalt quality, cannot be implemented without additional laboratory and field research.

4.0 INTRODUCTION

4.1 Objectives of the Study

The work presented in this report is part of a Texas Transportation Institute research study, sponsored by the Texas Highway Department and the Federal Highway Administration. The overall objectives of this research are to:

1. Determine the performance requirements of an asphaltic material needed to serve as a cohesive-adhesive waterproof binder for a first-class, long-life flexible pavement surface course.
2. Develop improved control tests for use in a specification for asphaltic materials that will meet the performance requirements in Objective 1.

4.2 Scope

The research reported herein is specifically part of Phase 3 of the 1969-70 work plan proposed to meet the program objectives. This part of the research comprised evaluation of the mechanical behavior (load response and failure) of candidate asphaltic concrete mixtures by application of available uniaxial tension, uniaxial compression, triaxial tension, and double lap shear procedures. The mixtures were prepared using two different representative asphalt cements (unmodified and modified by the addition of a synthetic elastomeric polymer) in order to determine how variations in the nature of the asphalt would influence basic mechanical behavior and thereby influence service performance. The results obtained were expected to indicate, in a fundamental way, how performance requirements of a bituminous pavement material might be determined, specified, and controlled.

5.0 APPROACH

5.1 Basic Philosophy

The approach followed in this part of the research program is based on the following premises:

1. Improvements in prediction and control of the performance of a flexible pavement system can be achieved by suitable application of rational engineering design analysis techniques. In the context of this report a rational design analysis is defined as one in which the mechanical state (stress, strain) of the pavement is determined as a function of coordinate position by application of the mathematical disciplines of the mechanics of continuous media. Performance is judged by comparison of the calculated mechanical state with stress and strain allowables; that is, by application of failure criteria.
2. Once pavement geometric design, failure modes, loading conditions, and environment are defined, rational engineering analysis can proceed if data are available which characterize the mechanical behavior of the materials making up the several parts of the pavement system. Such data are required for the asphaltic concrete, the base and sub-base courses, and the subgrade.
3. Mechanical behavior of asphaltic concrete depends on a number of factors. One of the most important is the nature of the asphalt cement employed. Accordingly, the usefulness of the asphalt cement can be evaluated most directly in the laboratory, in terms of pavement structural performance, by measurement of the mechanical behavior of samples representing the asphaltic concrete in a flexible pavement

4. Asphalt cement structural performance can be evaluated at any time during the life of a pavement. However, to separate asphalt cement structural performance from chemical performance, in this phase of this study, the effects of time and various environmental factors were not examined. Research Report 127-3 (90) treats the basic problem of asphalt cement chemical performance, with an emphasis on the effect of chemically active short wave solar radiation on asphalt hardening with age. Another aspect of chemical performance, not examined in this study, is the early failure of asphaltic concrete caused by the reaction of some mineral aggregates with asphalt cement.

Essentially, the approach followed in the present study represents the type of systems method suggested by Nair, Chang, Hudson, and McCullough (1). From another viewpoint this approach comprises a sub-system of the total system of design and analysis visualized in Study 1-8-69-123 (2). On the other hand the approach in this study is not that represented by the empirical sub-system suggested in Study 2-8-62-32 (6,7,8), primarily because in the empirical approach, material properties are inferred from pavement behavior, rather than from laboratory tests.

5.2 Background

As Nair, et al.,(1) suggest, the pavement sub-system is too complex to model simply in an engineering analysis. However, the field equations usually can be solved numerically, in a practical way, by one of the several computer oriented techniques which have become available in recent years. Even so, the material behavior must be idealized, if solutions are to be obtained in a reasonable time. Usually, an assumption of linear elastic or viscoelastic material behavior is made.

Early attempts to apply an elastic analysis to the rational design of flexible pavements are represented by the work of Burmister (3), Hank and

Scrivner (4), and Acum and Fox (5). More recent elastic analysis schemes are reported by Jeuffroy and Bacheley (9) and by Whiffin and Lister (10) who present a number of worked-out examples. Another approach is presented in a paper by Livneh and Shlarsky (11) who developed a method based on familiar techniques of soil mechanics which make use of an angle of internal friction (ϕ) and a cohesion constant (C) determined for the asphaltic concrete and other pavement layers from triaxial test data. Their method is based on one previously proposed by McLeod (13,14).

An important consideration is whether or not predictions based on rational engineering design analysis can be related to service performance. Skok and Finn (12) indicated that stresses and strains computed from three-layer elastic stress theory can be related to performance of a flexible pavement similar to that exhibited on test sections of the AASHO and WASHO road tests. Among the first to demonstrate the potential of the application of high-speed computers for solution of elastic field equations were Shiffman (31), Jones (15) and Peattie (16,17). Jones and Peattie also presented the results of their calculations in the form of design charts and curves. As a result of this analysis, Peattie (17) concluded that a critical factor in a flexible pavement structure was the horizontal tensile strain at the bottom of the bituminous layer. In another application of Peattie's results to design of flexible pavement, Dormon (18, 20) concluded that cracking may occur in the asphaltic concrete layer if the horizontal tensile stress or strain is excessive in cyclic loading (fatigue).

Behavior of real pavement materials (particularly the asphaltic concrete) is not elastic, but is also time dependent. The time dependence must be accounted for in a general rational analysis of a pavement structure because the time dependence may be particularly important when the load is applied over a significant time interval. Accordingly a number of solutions have been proposed based on a viscoelastic analysis. Such solutions involve handling the more complicated problems of computing the effect of moving loads and in deriving the time dependent behavior of the materials.

The problem of handling moving loads by superposition of stresses and deformations with respect to time is more complicated in a viscoelastic analysis. Methods for solving this problem are proposed by Pister and Westmann (19) and Perloff and Moavenzadeh (21). In general, viscoelastic solutions can be derived from elastic solutions by application of the correspondence principle (Alfrey (22), Lee (23), Blank (24). The correspondence principle states that if an elastic solution is known, a conversion to a viscoelastic solution is possible by application of Laplace or Fourier transforms to all time dependent functions. This is the point at which the constitutive equation (relating stress, strain, time, and temperature) for the material must be known. Application of the correspondence principle to solve structural analysis problems in layered pavement systems has been illustrated in papers by Ashton and Moavenzadeh (25), Huang (26), Ishihara and Kemura (27) and Barksdale and Leonards (28). These authors resorted to representing materials behavior by spring and dashpot models of varying complexity. Suitable constitutive equations also can be developed by curve fitting laboratory data on a given material by power law or modified power law models (a thorough discussion of such methods is given by Williams, Blatz, and Schapery (29). In the present study, this last approach has been followed to obtain the constitutive equations for asphaltic concrete, using the procedure proposed by Smith (29,30) for reduction of constant strain rate data.

Most of the techniques for structural analysis of highway pavements previously mentioned are limited to handling systems with only two or three layers. However, in recent years methods have been developed for analyzing systems comprising multiple layers, with different material behavior in each layer. The complications which arise in such multilayer solutions are resolved by application of high-speed digital computers. A choice among several numerical methods is possible; two have seen widespread application in flexible pavement structural analysis. One of these involves application of finite difference techniques for solving the differential equations for stresses, strains, and displacements. The other, called a finite element or a direct stiffness method, is based on energy theorems.

One of the finite-difference methods, which is well known, is the so-called "Chevron" program described by Michelow (33) and Dieckmann and Warren (34). Another, the "BISTRO" program, described in several publications by Peutz, Jones, and Van Klempen (35,36,37) has the advantage of being able to handle simultaneous input of two wheel loads and an assumption of either rough or smooth surfaces between layers.

Finite element techniques are represented by the programs developed by Duncan, Monismith and Wilson (38) and Westman (39). Quoting Duncan, "The finite element method of analysis provides an extremely powerful technique for solving problems involving the behavior of structures subjected to accelerations, loads, displacements, or changes in temperature. Problems involving the behavior of heterogeneous, anisotropic structures with complex boundary conditions may be handled." This powerful analytical tool has shown promise for application to solution of even the most difficult non-linear problems; Barksdale (61) used a finite element approach in problems involving the application of large numbers of wheel load repetions and viscoelastic creep loadings.

In summary, it appears that the state-of-the-art in rational engineering analysis of flexible pavement structures, as indicated in the foregoing review, is such that the approach selected for evaluating asphalt performance in this study is both useful and practical.

5.3 Rational Evaluation of Asphalt Structural Performance

Evaluation of asphalt cement structural performance is only a part, but an important part, of the whole system of design and analysis directed toward improvement in flexible pavement performance and performance prediction. The question is: how can a rational system design approach be implemented with respect to this segment? To help answer this question, Figure 5.1 is presented so that the relations among parts of the system might be visualized and thus illustrate the way the rational approach is applied to the study.

In this diagram, the output of the system shown is Pavement Performance Prediction and Assurance. Asphalt cement structural performance is one of the inputs which will influence this output. Other inputs, such as other raw material variables, asphalt hardening, preparation procedures, test procedures, pavement geometric design, loading and failure modes will also affect the output. However, if these are held constant, the mechanical behavior of the asphaltic concrete will depend only on asphalt structural performance. Of course, interaction among the system inputs may also be important. Probably, one of the most significant is the interaction among the raw material variables. For this reason, it is believed that asphalt cement structural performance is more definitively measured by testing representative asphaltic concrete mixtures than by simple laboratory tests on the asphalt cement alone.

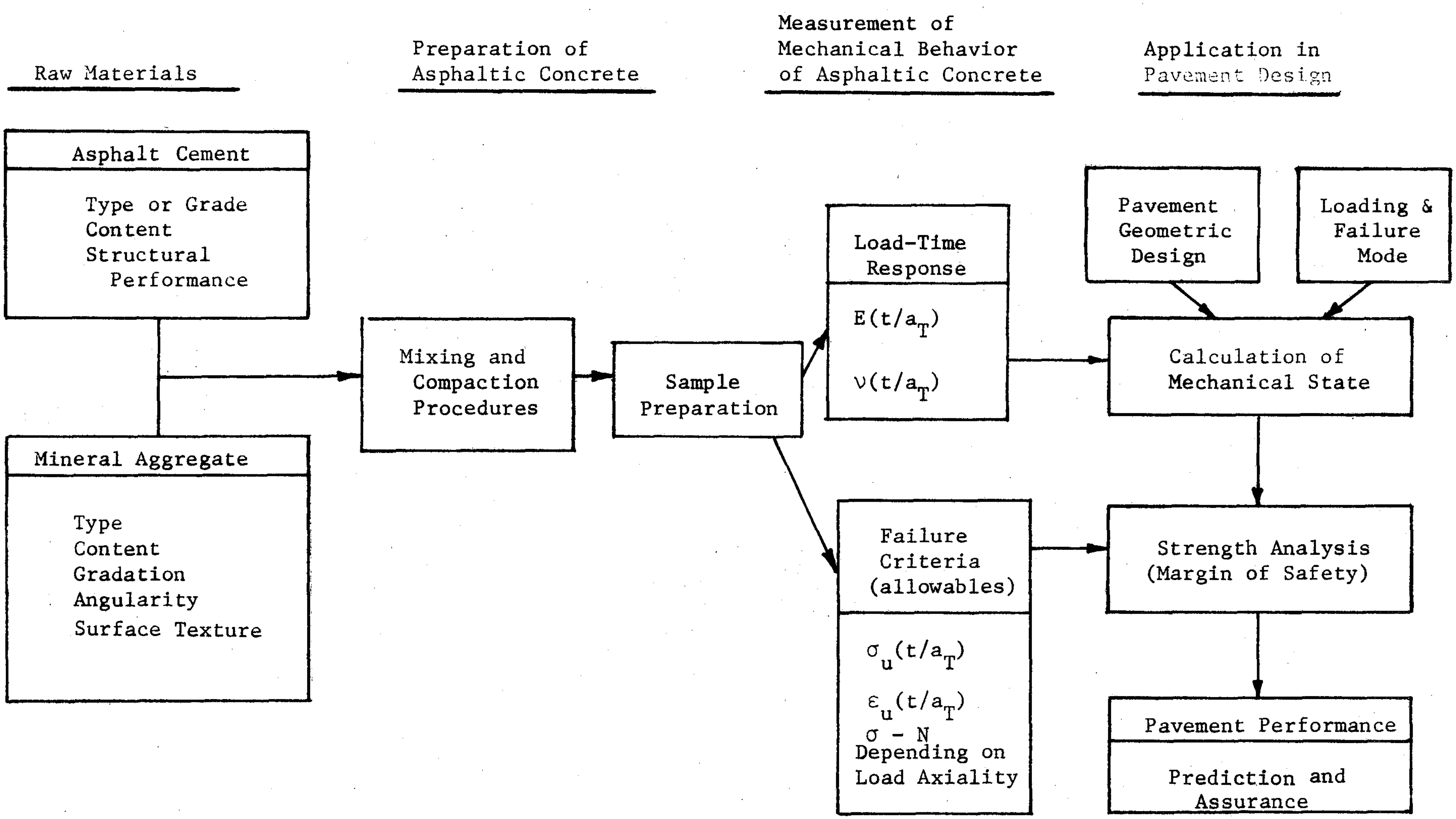

FIGURE 5.1 Input-Output Relations in a Rational Flexible Pavement Performance Prediction System

The approach to asphalt structural performance evaluation in this study may be summarized briefly as follows: laboratory measurement of mechanical behavior of representative samples of asphaltic concrete were used to make a rational assessment of the structural performance of an asphalt cement in terms of pavement performance. The samples and test procedures were selected accordingly, and results interpreted primarily to assess feasibility of these procedures and the sensitivity of test results to differences in asphalt structural performance.

5.4 Failure Mode Selection

The foregoing discussion points out that one of the essential elements in application of the proposed rational approach is a definition of approximate loading and failure modes. Considering only the structural performance factors, Research Report 127-1 (40) referred to the classification systems proposed by Hutchinson and Haas (42) and Hveem and Sherman (43) to describe the type of distress (i.e. failure mode) which will result in loss of pavement serviceability. Using such a classification, the asphalt structural performance evaluation in this study is based on the cracking mode as indicated in Table 5.1.

The reason for the emphasis on the cracking mode was indicated in Research Report 127-2 (41). That is, design by application of stability tests (as indicated by Hveem (44,45,46), U.S. Corps of Engineers (Marshall Test)(47,48), Nijboer (49), Smith (50), and Monismith (51) may alleviate rutting and shoving but tends to move the asphaltic concrete toward leaner mixtures. The lean mixtures, in turn, tend to be susceptible to cracking.

In addition, fatigue is an important mechanism for inducing cracking (and disintegration) but fatigue testing was not included in this particular phase of the research: it is a separate study in itself. However, some idea of

TABLE 5.1 Classification of Asphalt Pavement Load and Failure Modes*
As Used in This Study

Performance - Loss in Serviceability Resulting from (Failure Mode)	Major Influencing Loading Mode	Included in This Study?	Remarks
I Deformation			
A. Rutting	Traffic loads	no	Controlled by stability mix design.
B. Shear	Heavy traffic loads; deep seated foundation movement	no	
C. Waves	Traffic loads	no	
II Cracking			
A. Fatigue	Traffic loads	no**	No testing in phase being reported.
B. Longitudinal	Thermal loads; heavy traffic loads on cold pavement	yes	Significantly influenced by asphalt grade, type, and structural performance
C. Transverse	Thermal loads	yes	
D. Block	Thermal loads	yes	
III Disintegration			
A. Stripping	Moisture plus traffic	no	Significantly influenced by construction practices.
B. Ravelling	Traffic	no	
C. Pot holes	Traffic	no	

*After Hutchinson and Haas (42)

**Although included initially, fatigue has been dropped as a result of a change in the scope of the study.

relative fatigue performance might be gained from the ultimate stress and ultimate strain data obtained in this study, by application of methods like the one suggested by Heukelom and Klomp (52).

5.5 Program Variables and Constants

In general, determination of asphalt quality on the basis of measured mechanical behavior of representative asphaltic concrete samples implies that other variables in the system (indicated in Figure 5.1) are held constant. The variables receiving specific consideration in this study are as follows:

1. Mineral Aggregate; particle shape, surface texture, void ratio, particle size, particle gradation.
2. Asphalt; composition
3. Asphalt Content; percentage of asphalt (related to film thickness) and final void ratio.
4. Mixing Process; mixing apparatus, time, temperature and procedure. Critical considerations: uniformity of mix and completeness of coating of aggregate particles with asphalt.
5. Compacting Process; apparatus type, time, temperature, and procedure. Critical consideration: laboratory reproduction of asphalt concrete made in the field.
6. "Curing" Process; procedures affecting volatilization and oxidation of asphalt components during pavement construction.
7. Mechanical Behavior Test Variables; stress axiality, deformation of loading rate, temperature.

These are the principal variables influencing measurement of asphaltic concrete structural performance. Possible interactions among these variables also should be recognized. For example, the optimum asphalt content depends on service demands and mineral aggregate type and gradation, and asphalt composition.

In this phase of the study the mineral aggregate, asphalt content, mixing process, compacting process, and test temperature were held constant at selected values. In selecting the constant values for this study, consideration was given to experimental problems as well as the desire to make the material tested representative of asphalt concrete normally produced in highway pavement construction.

The variables in this program were: asphalt composition, stress axiality, and deformation rate. While the two asphalts selected for tests meets the same specification (AC-10) based on measurements commonly used for asphalt characterization, they varied materially with respect to their method of manufacture, and thus with respect to chemical composition. The effects of time (i.e. deformation rate) and temperature on asphalt structural performance are interrelated; their combined effects were already examined briefly in Research Report 127-2 (41). Accordingly, to save program time and expense, temperature was not included as a variable in this study.

5.6 Selection of Test Procedures

Selection of appropriate test methods and test conditions for measurement of the mechanical behavior of representative samples of asphaltic concrete was a decisive consideration to ensure successful implementation of the proposed approach to rational evaluation of asphalt structural performance. In making this selection, the most important factors to be considered were: 1) definition of loading and failure modes, 2) load axiality, 3) deformation (or loading) rate, and 4) specific details of the test specimen, apparatus and procedure. Definition of the loading and failure modes was discussed in section 5.4; the other factors are examined in the following discussion.

In general, the stress field in the pavement layer system under load will be multiaxial and the materials involved may be subjected to six stress components which can be resolved into three orthogonal principal stresses. Accordingly, material behavior (in this instance, the asphaltic concrete) can be examined in terms of response functionals in principal stress space. For example, Williams (53) and Blatz (54) show how material fracture behavior can be represented by a failure surface in principal stress (or strain) space. However, considering all strain histories and environmental variables involved, complete experimental definition of such functionals is indeed a formidable task. Fortunately, by limiting the conditions of load axiality to those corresponding to the major environmental, loading, and failure modes involved, the experimental problem can be reduced to one of manageable proportions. Specifically, Research Report 127-1 (40), indicated that for traffic loading and thermal loading inducing asphaltic pavement loading, measurement of material behavior in uniaxial tension and compression, shear, and triaxial (hydrostatic) tension would be necessary. Accordingly, for this phase of the study, the test specimens and method were selected to produce these four conditions of load axiality.

The spectrum of loading periods encountered in service can be summarized as follows (estimated from data given in references (40 and (55)).

Loading	Duration of Loading Period	Approx. Equivalent Strain Rate Range, Percent/min
Fast Traffic	0.05 sec	50 to 500
Braking/Accelerating Traffic	1 sec	5 to 50
Parked Vehicle	1 hr	1 to 5
Thermal (Cool-Down)	12 hr	.005 to .05 (temperature shift factor corrected rate)

The viscoelastic nature of asphaltic concrete requires characterization of behavior over a range of strain rates; the spectrum of rates indicated in this table suggests the range of rates over which the tests should be conducted. Actually, strain rates as low as 0.03 percent/min. and as high as 1000 percent/min. were employed in this study. Data were obtained using at least four strain rates for each kind of test so that the nature of the time dependency of the data could be inferred in some detail.

Since a major purpose of this part of the program was to assess the feasibility of applying tests giving basic mechanical behavior data reflecting asphalt characteristics, it was important that the time spent in developing test method be kept to a minimum. Thus the methods employed were selected from among those already existing for evaluation of composite viscoelastic materials, in particular, those previously developed for testing asphaltic concrete and those used for testing an analogous composite material, solid rocket propellant. In selecting and adapting such procedures for this study consideration was given to such factors as apparatus availability, potential of achieving acceptable test accuracy and precision, and practical application in the laboratory with respect to specimen size and quantity of material required, past experience with the procedures, and potential for field use of the procedure for quality control purposes.

6.0 EXPERIMENTAL

6.1 Materials

In selecting a mineral aggregate for making the asphaltic concrete specimens required for this study, the most important consideration was the necessity of minimizing factors which might introduce uncontrolled variation in the test results. Accordingly, a siliceous aggregate* was chosen for its low porosity, constant surface texture, controlled gradation and angularity, and continuing availability. Fractions were blended to produce a final gradation of near-optimum density as indicated by a straight-line plot on a Goode and Lufsey Chart (56) as shown in Figure 6.1. Other properties of the aggregate are shown in Table 6.1 and Figure 6.2. This aggregate was used in all experiments presented in this report. In one instance (in preparation of specimens for one series of hydrostatic tension tests), 5 percent devulcanized rubber+ was added to the siliceous aggregate before it was mixed with asphalt.

Four different asphalt cements which could be expected to vary significantly in their effect on pavement performance were selected from this study. Two of these were samples of commercial asphalts obtained from different producers. The remaining two samples were made by adding, to each of the above two commercial asphalts, 3 percent of an elastomeric polymer marketed as an asphalt additive. Characteristics of these samples are summarized in Table 6.2.

---

*Twenty-seven percent of the aggregate was local (Brazos County) pea gravel and 73 percent was from Brady, Texas.

+Particle size range: +4, 0 percent; -32, 45 percent.

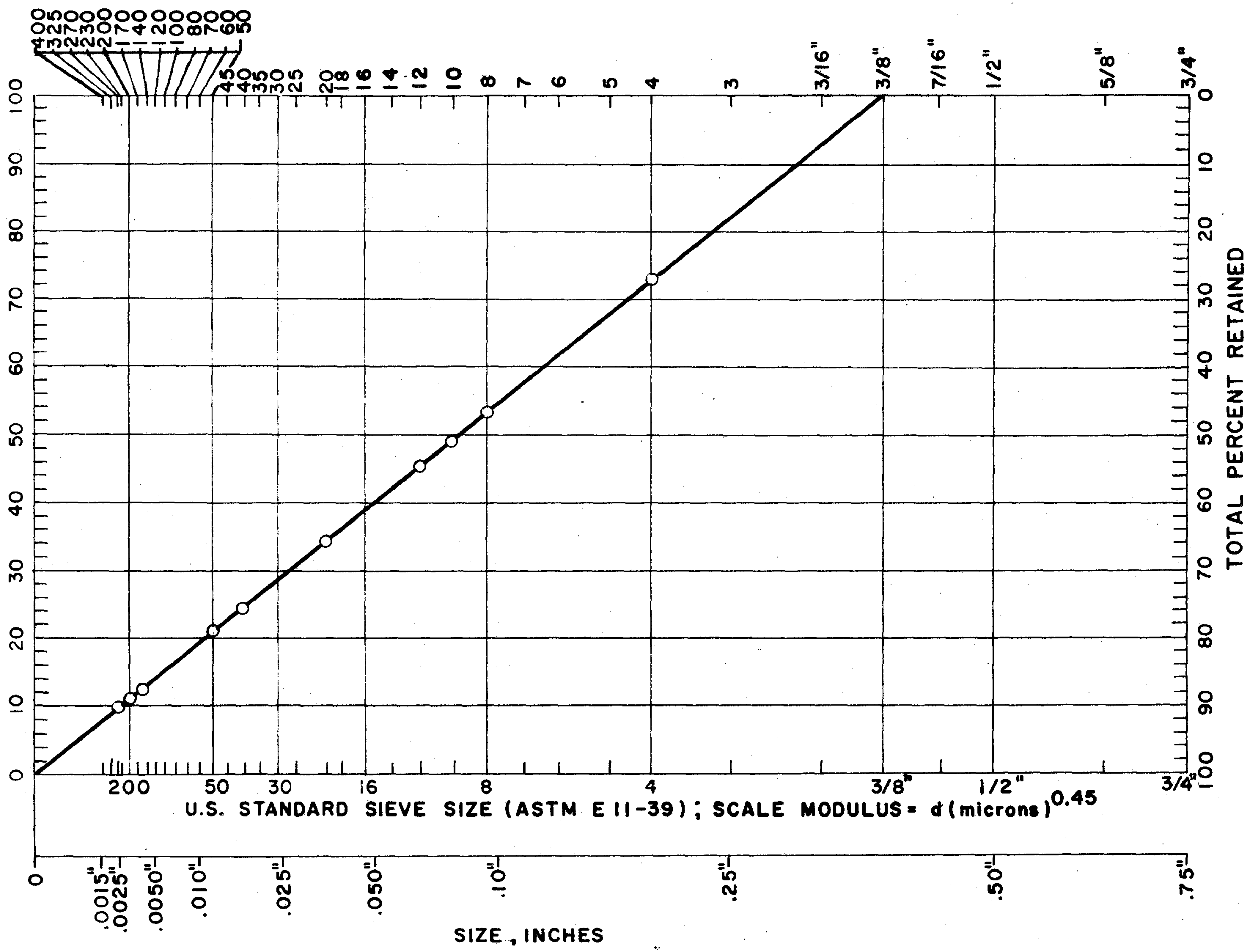

FIGURE 6.1 Gradation of Aggregate Used to Prepare Asphaltic Concrete Test Samples

TABLE 6.1 CHEMICAL AND PHYSICAL PROPERTIES OF BRADY, TEXAS, SILICEOUS AGGREGATE

1. Composition: Silica content $> 98^{o}$ percent

   Organic Impurities $<$ 0.1 percent

2. Specific Gravity: 2.66 (Determined)

3. Hardness: 13,850 psi, 3-point pressure loading (Manufacturers Data)

4. Angularity: 0.6 Krumbein roundness number, as indicated in chart (Manufacturers Data)

FIGURE 6.2 Krumbein Roundness Chart

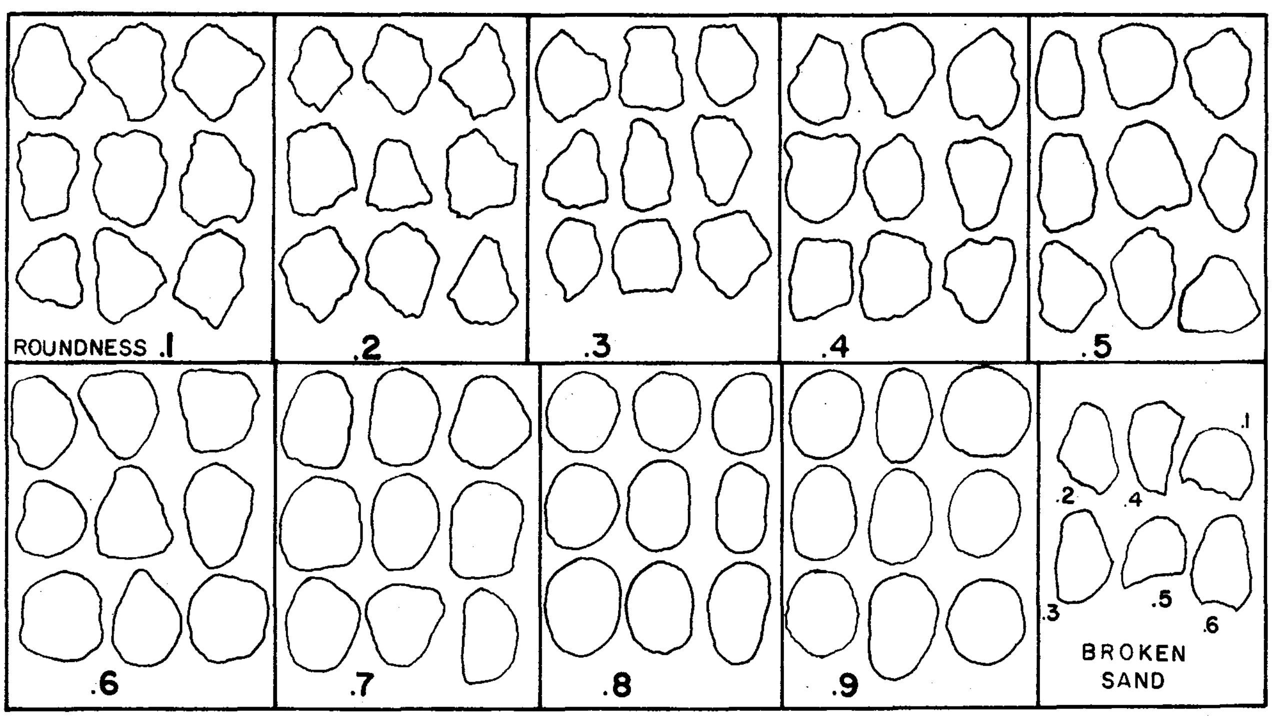

TABLE 6.2 CHARACTERISTICS OF ASPHALT AND ASPHALT-POLYMER BLENDS

Characteristic	Test Method	AC10; Producer Code 6	AC10; Producer Code 6, with 3% Polymer (d)	AC10; Producer Code 11	AC10; Producer Code 11, with 3% Polymer (d)
PENETRATION, 77F, 100g, 5 sec.	ASTM D5	85	75	95.5	70
VISCOSITY, 77F: megapoise	Proposed ASTM Sliding Plate	0.66	1.12	0.88	1.56
VISCOSITY, 140F: stokes	ASTM D2170	1294	3630	1542	6740
VISCOSITY, 275F: stokes	ASTM D2170	3.30	12.1	3.35	10.2
DUCTILITY, 39.2F, 5 cm/min: cm	ASTM D113	0.9	36(c)	8	150+
SOFTENING POINT: °F	ASTM D36	112	131	117	142
THIN FILM OXIDATION TEST	(a)				
Vis @ 77F after test: megapoise		2.80	3.24	2.06	5.30
Relative Hardening		4.2	2.9	2.3	3.4
THIN FILM U.V. RADIATION TEST	(b)				
Vis @ 77F after test: megapoise		80	41	16	22.5
Relative Hardening		121	36.5	18.5	14.5

Notes:

(a) 15 micron films of asphalt heated 2 hrs. at 225°F in air in a dark oven.

(b) 10 micron films of asphalt exposed, in air, for 18 hrs. at 95°F, to 1000 microwatts/cm^2 of 3600 Angstrom radiation.

The basic differences in the composition of the two commercial asphalt samples is indicated by the standard test values as well as the evident differences in their response in thin film oxidation and radiation tests. That significant modification of asphalt behavior can be expected from addition of elastomers is also well known. For example, Wood (57) reported that addition of 5 percent rubber to a particular asphalt increased the viscosity, improved aging resistance, and improved impact resistance by a factor of 45. Thompson (58) presented field data indicating decreased wheel tracking and pavement cracking, and increased stability with the use of rubber additives.

6.2 Test Procedures

The test procedures selected for experimental implementation of the previously discussed approach are illustrated concisely in Figure 6.3 which indicates the specimen geometries, loading modes, and strain rates applied to the asphalt concrete samples tested in this study. All test configurations were loaded on a model TT-D Instron Universal Tester. Two methods were followed for acquisition of uniaxial tensile data. Both have seen considerable application in testing asphalt concrete. Both were examined in an attempt to determine which one would be more suitable for routine evaluation of asphaltic concrete mechanical behavior. Also note that two versions of the triaxial tensile test method were applied. In one, representative asphaltic concrete samples were tested. The other version, called a "bead-test," was evaluated as a potential quality control method for asphalt cements. The test procedures are described and discussed in more detail in the following sections.

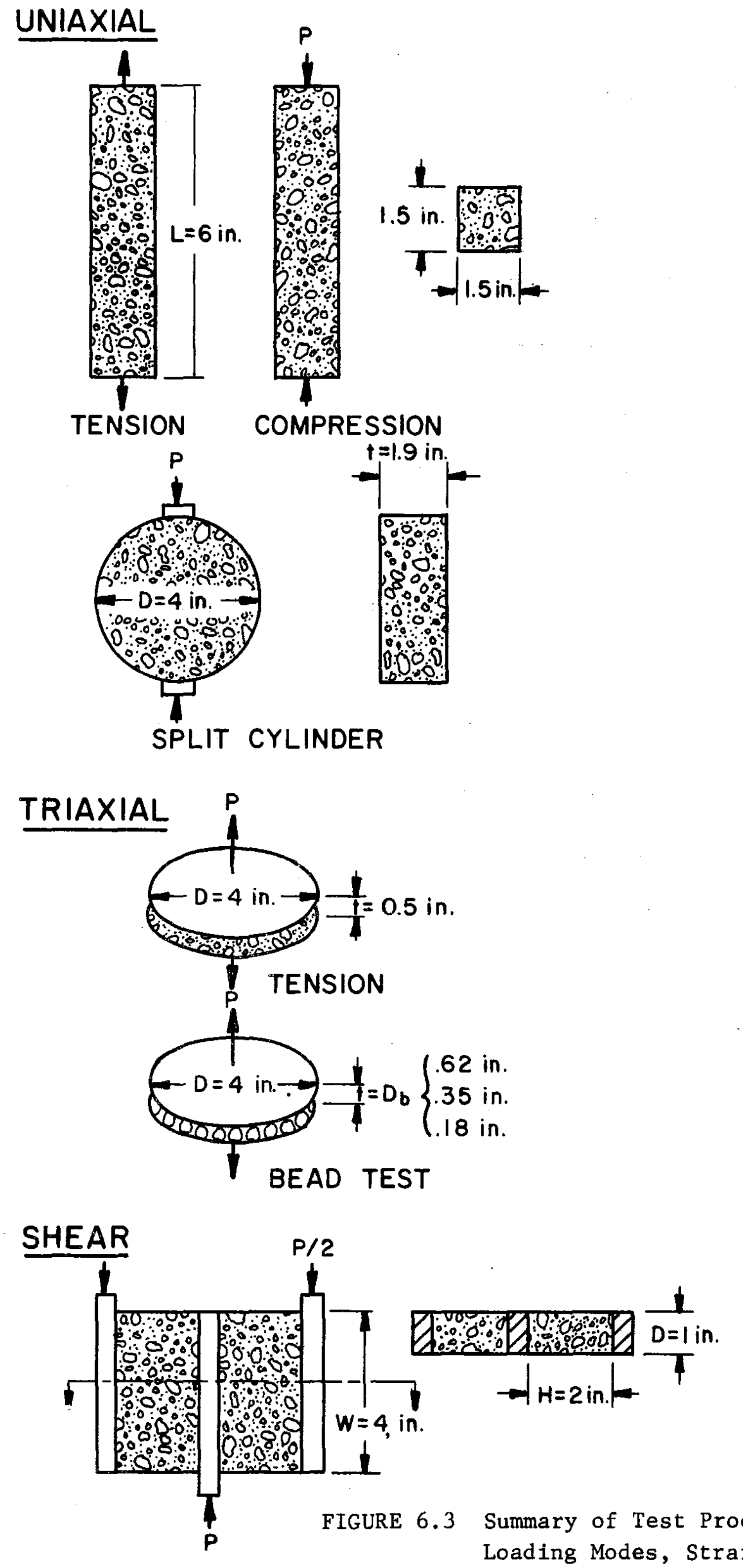

STRESS	STRAIN	NOMINAL STRAIN RATES, min^{-1}
P/A	ΔL/L	0.033 0.333 3.33 17. 34. 340.
$\frac{2P}{\pi tD}$	0.067 Δt	1.0 10. 100. 500. 1000.
$1.95 \cdot \frac{P}{A}$	$\frac{\Delta t}{t} \cdot 1.45$	.33 3.4 34. 340.
$\frac{P}{2HD}$	$\frac{\Delta W}{H}$	.1 1.0 10. 100.

FIGURE 6.3 Summary of Test Procedures: Specimen Configurations, Loading Modes, Strain Rates and Data Reduction

6.2.1 Shear

In pavement design, data on shear response and failure are often inferred from the results of triaxial compression tests on the layer materials. In particular, application of triaxial tests for evaluation of shear characteristics of asphalt concrete is illustrated in papers by Hargett (59), Goetz and Schaub (60), and Nair and Chang (1). However, for the approach followed in this report a more direct means of determining shear behavior is preferable. Pure shear tests, such as the one suggested for bituminous materials by Calderon (65), or a torsional shear test like the one described in Section 4.4.2 of the Solid Propellant Mechanical Behavior Manual (64) could be considered, but these tests pose theoretical and practical difficulties. Accordingly, for expeditious and efficient pursuit of the objectives of this study a simple and direct method was sought for determining asphaltic concrete behavior in shear. Thus, modification of a double-lap simple shear test described by Jones and Knauss (62), Kelley (63), and in Section 4.4.1 of the Solid Propellant Mechanical Behavior Manual (64) appeared to be the best approach.

In this test, two 1 in. x 2 in. x 4 in. blocks of asphaltic concrete were bonded to 1/2 in. x 1 in. x 6 in. aluminum bars to fabricate the test configuration illustrated in Figure 6.3. A completed test specimen is shown in Figure 6.4. Placement of the test specimen in the Instron machine is illustrated in Figure 6.5. The loading method and the data acquisition system is described in Section 6.2.6.

6.2.2 Uniaxial Tension and Compression

At least four different kinds of test methods have been applied for measurement of uniaxial tensile and compressive behavior of asphaltic concrete.

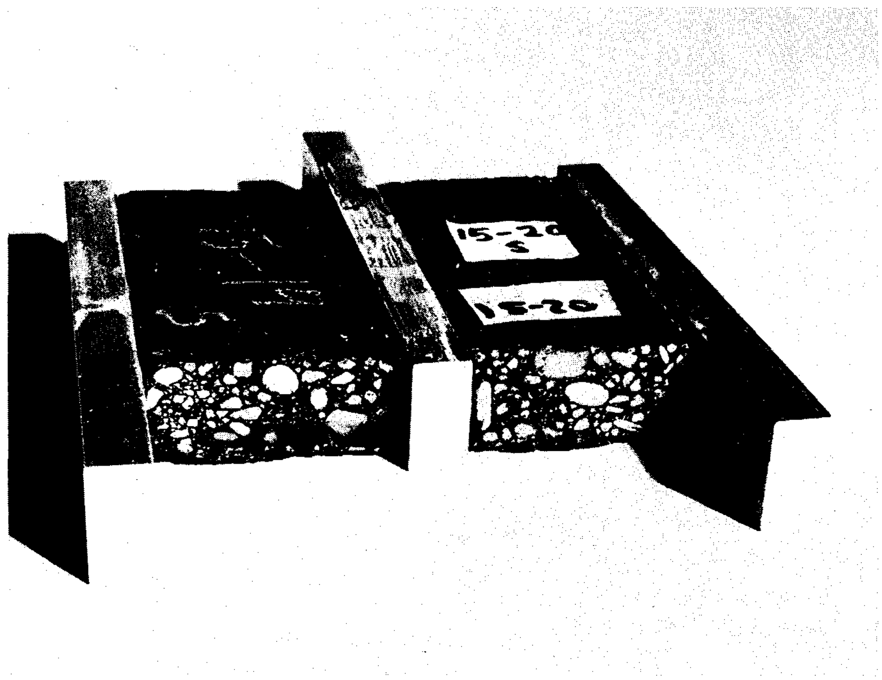

FIGURE 6.4 OBLIQUE VIEW OF DOUBLE LAP SHEAR CONFIGURATION

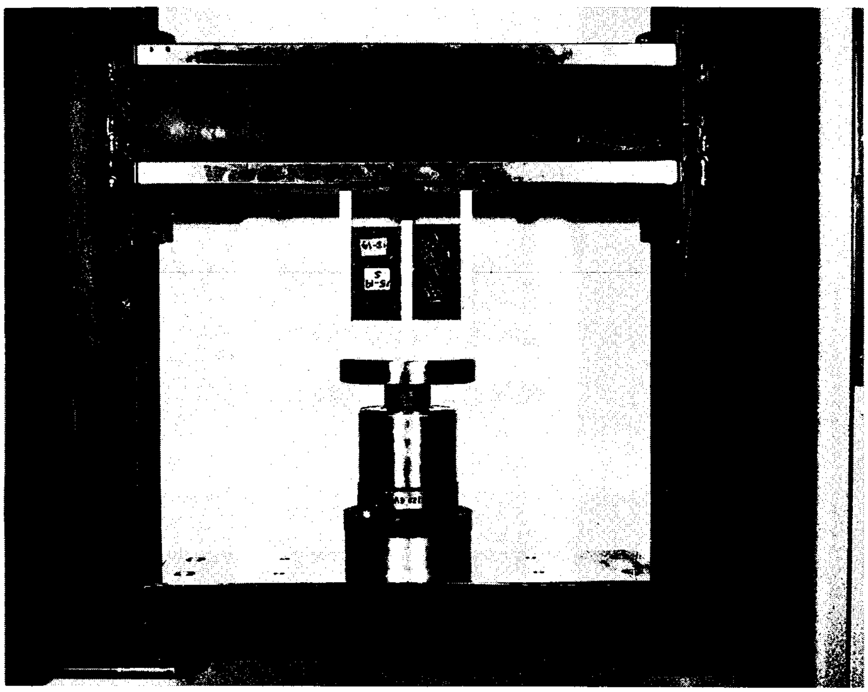

FIGURE 6.5 TEST SET-UP IN INSTRON

These are:

1) Tests requiring direct application of tensile or compressive loads.
2) Prism flexure tests.
3) Disk diametral compression tests (sometimes referred to as indirect tensile or splitting tensile tests).
4) Disk centrifugal tests.

Prism flexural tests include center loaded beam tests or cantilever beam tests (example: the Hveem Cohesiometer). Such tests give some indication of composite tensile and compressive characteristics, but as pointed out by Kennedy and Hudson (66), interpretation of results in terms of basic tensile or compressive behavior is uncertain at best. As a result, tests of this kind were not considered to be appropriate for this program. Disk centrifugal tests, such as the one mentioned by Calderon (67) have interesting possibilities, but have seen little application in testing bituminous materials. Accordingly, in this study, a direct uniaxial method and a splitting tensile method have been employed.

If loading misalignment is avoided (not difficult with the Instron Tester), and a reasonably uniform stress distribution across the specimen can be assumed, stress and strain state in a direct uniaxial test can be determined simply and reliably; this is an inherent advantage which usually encourages use of a direct test. Most of the uncertainty is related to the manner in which the load is applied to tensile specimens, and to stability problems with compression specimens. Such problems are reduced for a viscoelastic material by selecting an appropriate ratio of specimen length to cross-sectional area and by direct bonding of a tensile specimen to a rigid metal grip. This approach appears to have yielded satisfactory results in uniaxial tests of asphaltic concrete reported by Tons and Krokosky (69). They used a specimen 2 in. in diameter and 5 in. long cemented onto circular caps which were then attached to the grips of an Instron Tester. A similar test is represented by the uniaxial tensile test described in Section 4.3.2. of reference 64 and by Kelly (63) which employes a tab-end bonded specimen 2.8 in. long, 0.375 in. wide, and 0.5 in. thick, also loaded by an Instron Tester.

The direct uniaxial test applied in this study is essentially the same as the tests just discussed, the principal difference being the exact dimensions of the specimen. In the direct compression test used in this study, the 6 in. x 1.5 in. x 1.5 in. asphaltic concrete specimen sketched in Figure 6.3 is placed between platens fixed on the crosshead and on the compression bench of the Instron test machine. In the direct tension test, this specimen is bonded on each end to a 2 in. diameter, 2.5 in. long aluminum cylinder with epoxy cement (Shell Epon 828). Adhesive cure is accelerated by placing the capped specimen, mounted in a supporting fixture, in a 200°F oven for 30 minutes. Bending moments are minimized by connecting the metal caps to the test machine base and crosshead through unviersal joints. A completed tension test specimen is shown in Figure 6.6.

The splitting tensile test was developed in 1943 by Carneiro and Barcellos (70) and, independently by Akazawa (71), for measurement of portland cement concrete tensile strength. Even though a biaxial stress field exists it is now a commonly used standard method of test (72) for the uniaxial tensile behavior of this material. Application of this kind of test for determining asphaltic concrete tensile behavior is reported by Breen and Stephens (73)

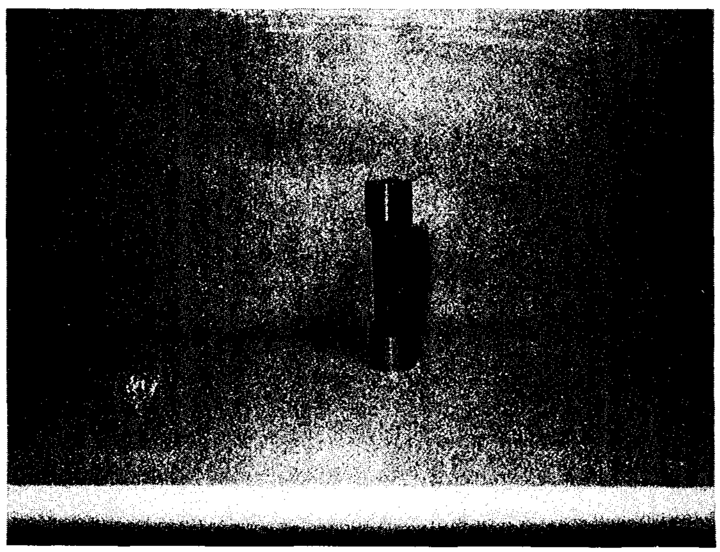

FIGURE 6.6 Direct Tension and Compression
Test Specimen

and Livneh and Shlarsky (74); although the latter appear to favor the use of specimens with a rectangular cross-section. Application of an indirect tensile test to cylindrical specimens of asphalt-treated pavement sub-base materials has been well developed by Kennedy and his co-workers (66,75,76,77,78). Particular care was taken in this work to apply the load uniformly by means of a curved loading strip; horizontal deformations were measured with a special cantilever arm strain gage.

A similar cylinder diametral compression test has been used successfully for examining the behavior of solid propellants, as described by Kelley (63) and in Section 4.5.1 of reference 64. In this procedure, deformations are followed by distortion of grid markings on the sample face as well as by gages and cross-head travel.

One of the major problems with indirect tests of this kind is that of determining the stress field imposed. If continuum elastic behavior and line loading is assumed, the stress field which is developed at the center of this test specimen is compression-tension. Taking the y axis to be the load application axis, the compressive stress, σ_y, is given by

$$\sigma_y = \frac{-2P_y}{\pi t} \left(\frac{2}{d-2y} + \frac{2}{d+2y} - \frac{1}{d} \right)$$

At the center, this reduces to

$$\sigma_{y0} = \frac{-6P_y}{\pi t d}$$

where d = specimen diameter, t = thickness, P_y = applied diametral force

The tensile stress normal to the axis of loading, σ_x is given by

$$\sigma_x = \frac{2P_y}{\pi t d}$$

The corresponding strains are:

$$\varepsilon_y = \frac{-2P_y}{\pi t E d} \left[\frac{(3 + \nu)d^2 + (1 + \nu)dy^2}{d^2 - 4y^2}\right]$$

at the center this becomes

$$\varepsilon_{y0} = \frac{-2P_y}{\pi t E d} (3 + \nu)$$

$$\varepsilon_x = \frac{2P_y (1 + 3\nu)}{\pi t E d}$$

where ν = Poissons Ratio; E = elastic modulus.

The total deformation u along the diameter in the x direction is given by

$$u = \frac{P_y}{\pi t E} [(1 - \nu)(2 - \pi) + 2 (1 + \nu)]$$

The curved loading strip used by Hadley and Kennedy (75) requires the use of somewhat more complicated relations (75,77) for calculating σ_x , σ_y, ε_x, ε_y, E, and ν.

In this program the load was applied diametrically to the specimen sketched in Figure 6.3 with a flat steel bar 0.5 in. wide, approximating line loading. The length of the bar was greater than the specimen thickness to minimize points of stress concentration. Because the experiments in this program were to be analyzed primarily to assess feasibility of the test methods selected and senstivity of test results to differences in asphalt performance, only the deformations in the y direction were determined (from measurement of crosshead motion).

Accordingly, Poisson's ratio was not found, but was assumed to be 0.4. The expression for vertical strain as a function of y was expanded in a Maclaurin series and integrated over the y axis to obtain:

$$E = \frac{5.22P_y}{tv}$$

where v = diametral deformation in the direction of P_y, the compressive load.

The tensile strain at the center becomes, for this specimen

$$\varepsilon_{x0} = \frac{0.35P_y}{tE}$$

or

$$\varepsilon_{x0} = 0.067v$$

6.2.3 Triaxial (Hydrostatic) Tension

Although, as indicated in Research Report 127-1 (40), behavior of asphaltic concrete in hydrostatic tension should be known for rational analysis of pavement performance, no reports of tests imposing this stress field on samples of bituminous paving materials could be found in the literature. However, mechanical behavior of materials in this stress field is also of importance in the structural design of solid propellant rocket motors. As a result, an appropriate experimental method has been proposed, given a thorough stress analysis, developed in the laboratory, and reduced to practice as a materials testing procedure for solid propellants.

Specifically, this is a test method where the material under test is bonded securely between two rigid circular platens which are then pulled apart, while measuring the load and deformation in the direction of the load. At a ratio of specimen diameter to thickness of 8 or more, it can be shown that a uniaxially applied tensile load results in a state of hydrostatic tension in most of the central plane of the disk of test material. A report by Lindsey, Schapery, Williams, and Zak (79) gives an analysis for stress and strain in this configuration (sometimes called a "poker-chip" test) and reports on some of the early experimental work done on elastomers. Further application of this method to the study of fracture initiation and propagation in solid propellants is presented by Lindsey (80). The method was further refined for general application to solid propellant testing by Harbert (81, 82), and is described by Kelley (63), and in Sections 4.5.5 and 4.7.3 of reference 64.

The hydrostatic tension method applied in this study is essentially the "poker-chip" test discussed above. The main variations from the method, as described by Harbert (81), is that a center load cell was not used nor was the axial extension determined from LVDT measurements in the tests in this study. The resulting simplification in this program was believed to be justified since these tests were exploratory in nature. A completed "poker chip" test specimen is shown in Figure 6.7.

In this procedure, the hydrostatic stress field imposed in the neighborhood of the center of the specimen cannot be calculated directly by dividing the load by the specimen cross-sectional area, as a result of end effects around the periphery of the specimen. Accordingly, corrections which depend on specimen geometry and material dilitational behavior must be made. Similar corrections are required in the calculation of strain and modulus.

Analysis (79, 83, 84) indicates that the axial stress occurring at the center of the specimen is the maximum and related to the P/A stress as shown

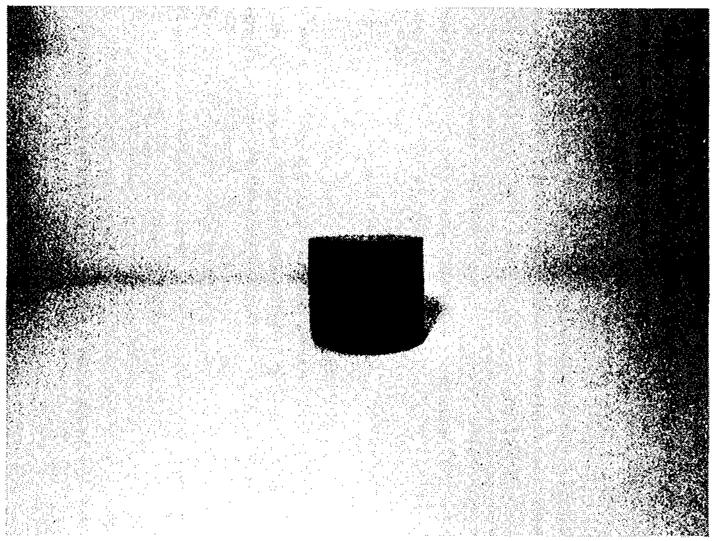

FIGURE 6.7 Hydrostatic Tension Test Specimen

in Figure 6.7. The axial stress, σ_{z0}, can be estimated from the P/A stress using this relationship. Also, for ratio of specimen diameter to thickness of 8 or over, the stress field is nearly hydrostatic, that is:

$$\sigma_{z0} \cong \sigma_{r0} \cong \sigma_{\theta 0}$$

The correlating parameters are specimen diameter-to-thickness ratio, and Poisson's ratio. Assuming a Poisson's ratio of 0.4, this figure indicates that for the specimen used in this study, the actual hydrostatic stress is about 1.16 times the P/A stress observed. However, the assumption of linear viscoelastic material behavior implies a Poisson's ratio closer to 0.5. Accordingly, the P/H values of ultimate stress reported in Appendix E-5 were multiplied by 1.95 to obtain the ultimate stress values used for curve plotting and data analysis.

A similar plot, Figure 6.9, for strain, shows that the apparent strain (Δ th/th) should be multiplied by a factor of 1.45 to get true strain at the center of the specimen. The resulting factor for converting apparent modulus to true modulus is 1.34.

6.2.4 Bead Test

This test is a modification of the hydrostatic tension test previously described, wherein glass beads were used to simulate the aggregate. In this way, aggregate variables including angularity, texture, and porosity were eliminated in this triaxial test for evaluating asphalt performance. A gradation of glass beads selected for optimum packing would produce an analog of the asphaltic concrete samples containing natural aggregate that were evaluated in this study. However, the bead test was examined with the idea that it might

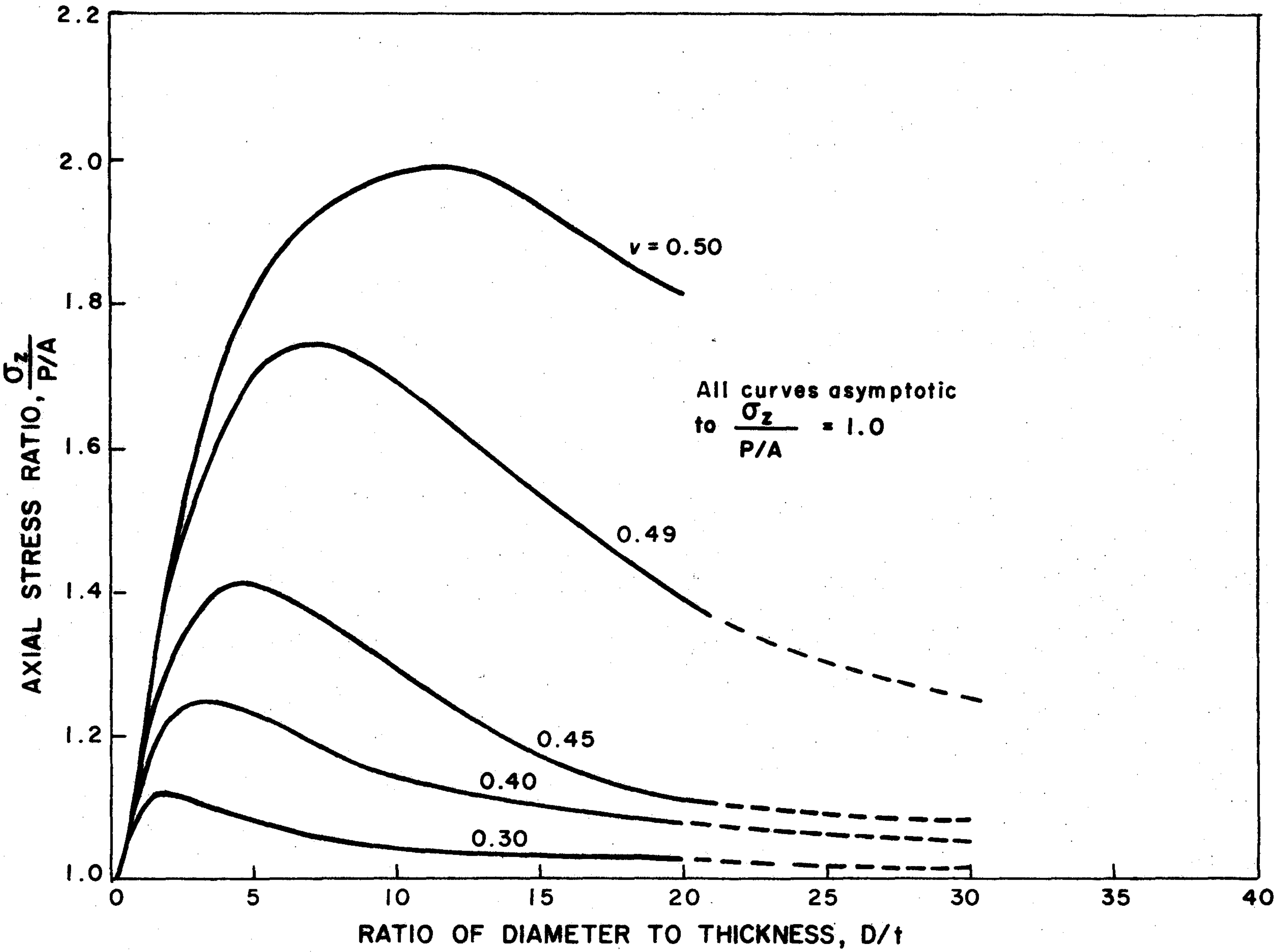

FIGURE 6.8 Axial Stress at Center of "Poker Chip" Specimen (Ref. 83)

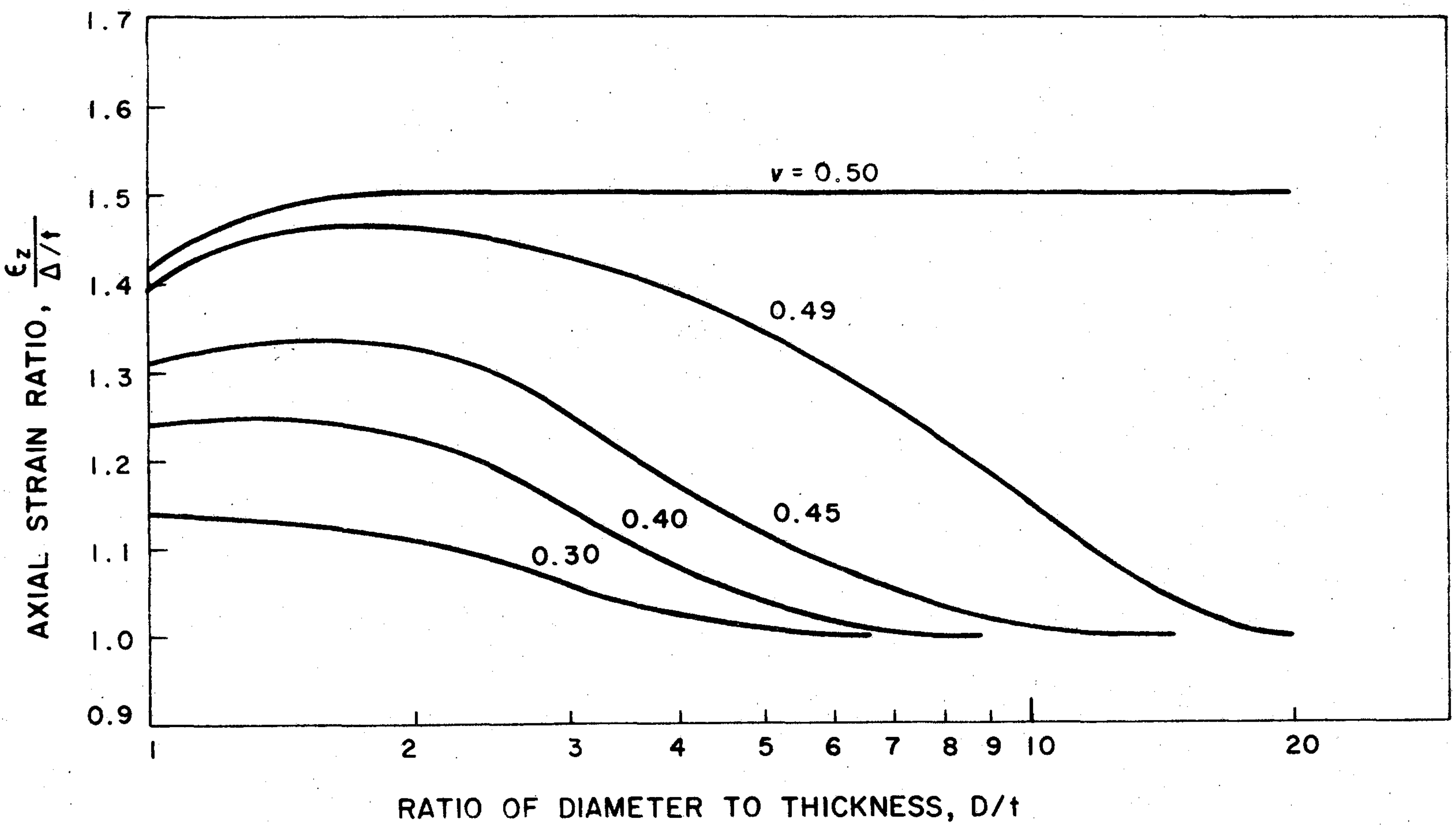

FIGURE 6.9 Axial Strain at Center of "Poker Chip" Specimen (Ref. 83)

ultimately be useful as a routine asphalt quality control test. Accordingly, single size glass beads were used for this program.

The beads were placed in a single layer, in a matrix of the asphalt being tested, between the platens of the "poker-chip" apparatus, as illustrated in Figure 6.10. Three different bead sizes were used: 0.620 in., 0.346 in., and 0.179 in. Theoretically, the total number of each of these sizes which can be packed between 4 in. platens is 38, 121, and 454 respectively. Actual packing was 32, 105, and 400 beads per platen as a result of the asphalt film thickness, imperfect packing at the platen outer boundary, and variation in true bead diameters.

In other respects, the test procedure was the same as in the hydrostatic tension test of asphaltic concrete. Data reduction was the same except that the area used in computing the P/A stress was taken as the net area of asphalt in the central plane of the test configuration. Theoretically, this net area is 9.40 percent of the platen area, and is independent of the bead diameter.

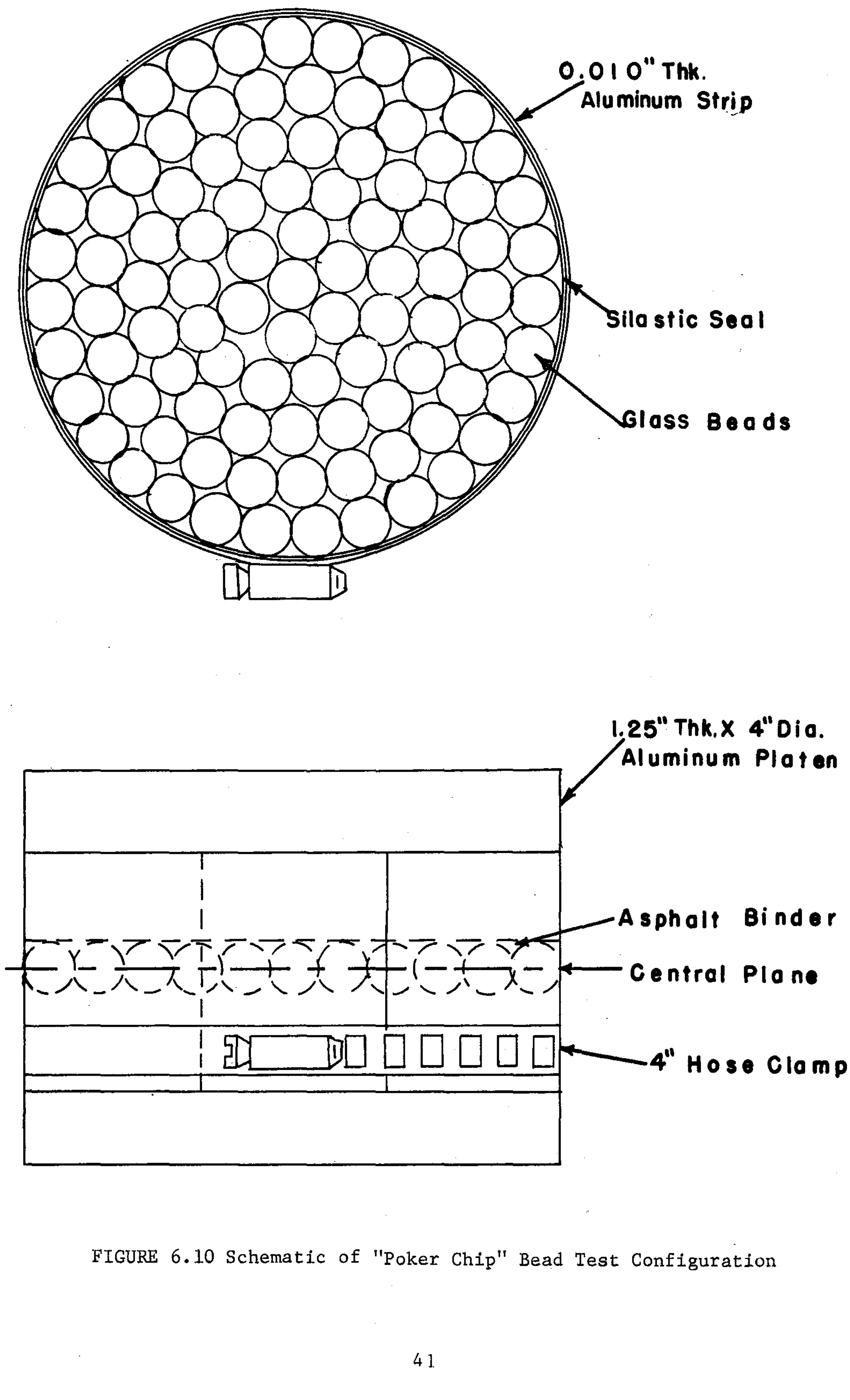

FIGURE 6.10 Schematic of "Poker Chip" Bead Test Configuration

6.2.5 Specimen Preparation

Mixing and compacting procedures followed in this study for preparation of test specimens were set up so as to 1) produce samples which could be repeated, i.e. so that successive samples reasonably could be expected to exhibit comparable behavior, 2) be practical with respect to forming the specimen configuration required for a particular test, and 3) produce an asphaltic concrete that would have a reasonable similarity to a field paving mixture. These procedures as well as other details of specimen preparation are presented in the following paragraphs.

The double lap shear test configuration required two prismatic specimens; these were most conveniently formed by cutting the specimens from a larger sheet of asphaltic concrete. To make this sheet, the binder and aggregate were heated separately (temperature shown in Table 6.3), and mixed in a Hobart model A-200 mixer. The mixture was placed immediately in a 17-1/2 in. diameter mold for compaction (Figure 6.11) using the machine developed and described by Jimenez (85,86) and by Layman (87). The mixture was compacted at a 5/16 in. tilt for 4 minutes and then leveled for 2 minutes.

The compacted sample was allowed to cool overnight before sawing the specimens (Figure 6.12) with a diamond bit blade to nominal dimensions of 1 in. x 2 in. x 4 in. The dimensions along the 12 edges of each specimen were measured and weight in air and water were determined. From these data specific gravities and void content were calculated on the basis of either specimen volume or water displacement. In this program the water displacement method was found to be the more repeatable of the two methods. Dimensional, specific gravity, and void content data on all double lap shear specimens are given in Appendix B1.

TABLE 6.3 ASPHALTIC CONCRETE MIXTURES

		Asphalt			Compaction			
					Temperature-°F			
Loading Mode	Mix No.	Source	Wt.* %	Additive	Pre-Heat	Com-paction	Com-pactor (d)	Voids %
Uniaxial Tension & Compression	9	11	5.5	0	250/325	325	J	2.6
	10	11	5.5	3% Polymer(a)			J	2.5
	11	6	5.5	0			J	2.0
	12	6	5.5	3% Polymer			J	2.2
	13	11	4.0	0			J	2.7
	14	11	5.5	0 (b)			J	1.5
Splitting Tension	39	6	5.5	0	250	250	TGC	0.7
	43	6	3.8	0	250	250	TGC	2.5
Hydrostatic (Triaxial) Tension	16	11	5.5	0	325	325	TGC	2.2
	17	6	5.5	0			TGC	2.8
	18	6	5.5	3% Polymer(a)			TGC	2.0
	19	6	5.5	5% Ground Rubber(c)			TGC	1.5
Shear	15	11	5.5	0	325	325	J	1.4
	20	6	5.5	0			J	1.4
	21	6	5.5	3% Polymer(a)			J	1.6

(a) Proportion of polymer in asphalt

(b) Specimens prepared from thin sheets to eliminate 2 saw cuts (also decreased void %)

(c) Proportion of ground rubber in aggregate

(d) J = Jimenez compactor
TGC = Texas Gyratory Compactor

*Based on dry weight of aggregate.

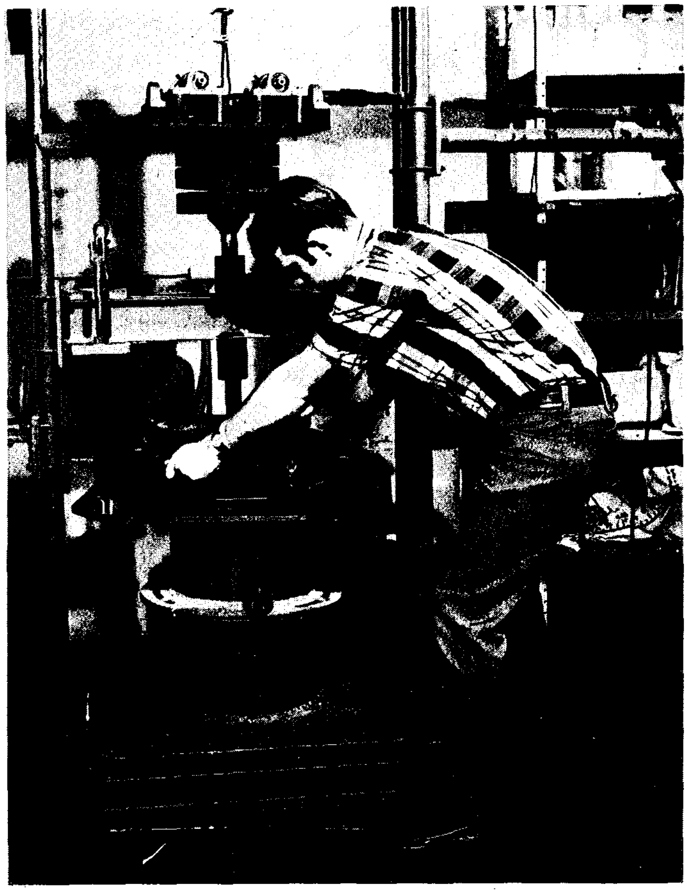

FIGURE 6.11 COMPACTION OF MIXTURE

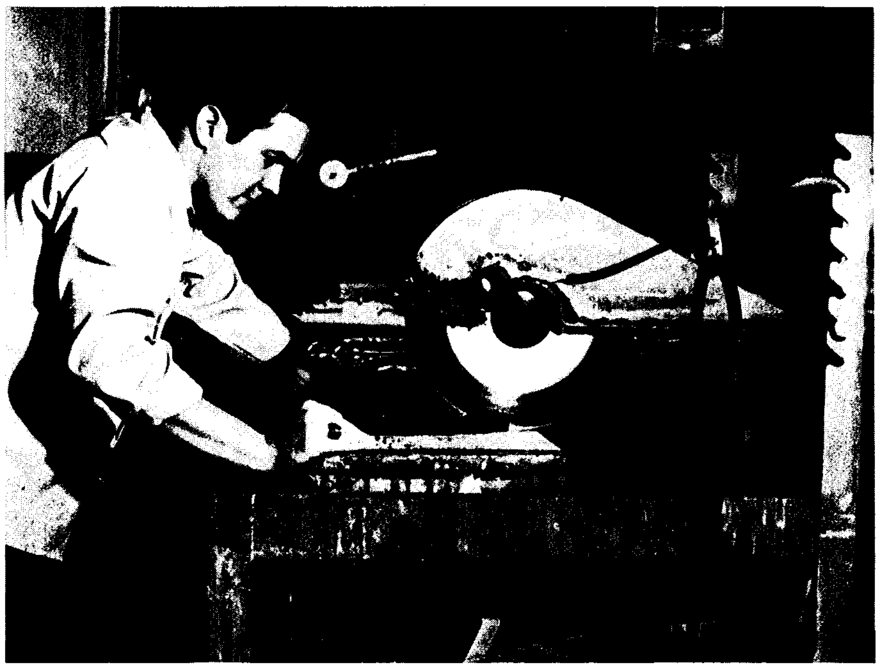

FIGURE 6.12 SAWING OPERATION TO CUT SAMPLE TO SPECIMEN CONFIGURATION

Resulting average void contents are summarized in Table 6.3, which also indicates asphalt source, mix design, and mix number. Mounting of the double lap shear specimens was described previously in this report.

Mixing, compacting, and sawing of the uniaxial specimens was essentially the same as for the double lap shear specimens. Normally, the sheet sample dimensions were such that all six faces were saw-cut to obtain the nominal specimen dimensions (1.5 in. x 1.5 in. x 6 in.). However, in molding the samples from Mix 14, the thickness was controlled at 1.5 in. so that these specimens have saw cuts only at the two ends and along two sides. Since, Mixes 9 and 14 were otherwise the same, possible stress-riser effects of the saw-cuts could be assessed by comparing uniaxial data from these two mixes.

Dimensional, specific gravity, and void content data for uniaxial tensile specimens are given in Appendix B2, and for uniaxial compression specimens in Appendix B3. These data are also summarized in Table 6.3. Specimen mounting has been described previously.

The disks for the splitting tensile test were made by forming the specimen directly from the mix to the nominal 4 in. diameter x 1.9 in. thick dimensions, in a Texas Gyratory Compactor. Prior to making the mix in a Hobart mixer, the asphalt was preheated for 30 minutes at 250°F, and the aggregate was preheated for two hours at 250°F. Dimensional, specific gravity, and void content data for these specimens are given in Appendix B4, and summarized in Table 6.3.

The disk-shaped specimens for the triaxial ("poker-chip") test were also formed directly from the mix in a Texas Gyratory Compactor. Nominal sample size was 4 in. diameter and 0.5 in. thick, giving an aspect ratio of 8. From the viewpoint of stress analysis, a thinner (i.e. larger aspect ratio) would be better, but then the thickness would approach the size of the largest aggregate particles, which is also undersirable. These specimens were attached to aluminum platens with epoxy cement. Dimensional, specific gravity, and void content data for these specimens are given in Appendix B5, and summarized in Table 6.3.

The bead test specimens (Figure 6.10) were prepared by forming a dam around the lower aluminum platen consisting of an aluminum strip and a hose clamp sealed with a narrow bead of silastic. The maximum number of the single size beads were then arranged on the top of the lower platen. The platens and beads were preheated for two hours at 325°F, and the asphalt was preheated for 30 minutes at 325°F. The asphalt was then poured on top of the beads to a level slightly higher than the bead diameter. A spatula was used to roll the beads to insure uniform coating of the bead surfaces. The upper platen was then set in place; the weight caused the asphalt to overflow until this platen contacted the top of the beads. This assembly was allowed to cool overnight at room temperature (76°F). Immediately before beginning a test, the aluminum strip and hose clamps were removed.

6.2.6. Loading Method and Data Acquisition

The tests in this program were conducted on the Instron machine at various constant crosshead extension rates selected so as to yield, as closely as possible, the nominal constant strain rates scheduled for each test mode, as indicated in Figure 6.3. All tests were conducted at the laboratory temperature (76°F±2°F).

The primary data shown on the chart produced by the Instron machine is a continuous record of load vs. time. From a knowledge of chart speed and cross-head rate, the Instron chart time axis can be converted to a total indicated deformation in the machine. This indicated deformation is the sum of the specimen extension and the machine deformation at the load shown on the chart. Accordingly, to obtain specimen extension, the machine deformation was subtracted from the indicated total deformation.

The machine deformation was determined from a calibration record obtained on the Instron machine for each kind of test set up. This calibration was made by loading only the machine and associated fixtures to a force greater than the load at failure for any of the specimens tested. The resulting calibration data for machine deformation, in each of the test modes, is recorded in Appendix D. Use of this calibration in data reduction is explained in the following section.

6.2.7 Data Reduction

The method of data reduction is illustrated by an example taken from one of the uniaxial tests (Sample 14 from Mix 10). The same general procedure was followed for the other tests, modified as required for the stress and strain analysis of a given configuration, as discussed previously and as outlined in Figure 6.3. Since a large amount of data had to be reduced in this study, actual data reduction was handled by computer. Details of the computer program are presented and discussed in Appendix A.

Considering the example from the uniaxial tension test, the following data are required in addition to the Instron chart for the test and the calibration data:

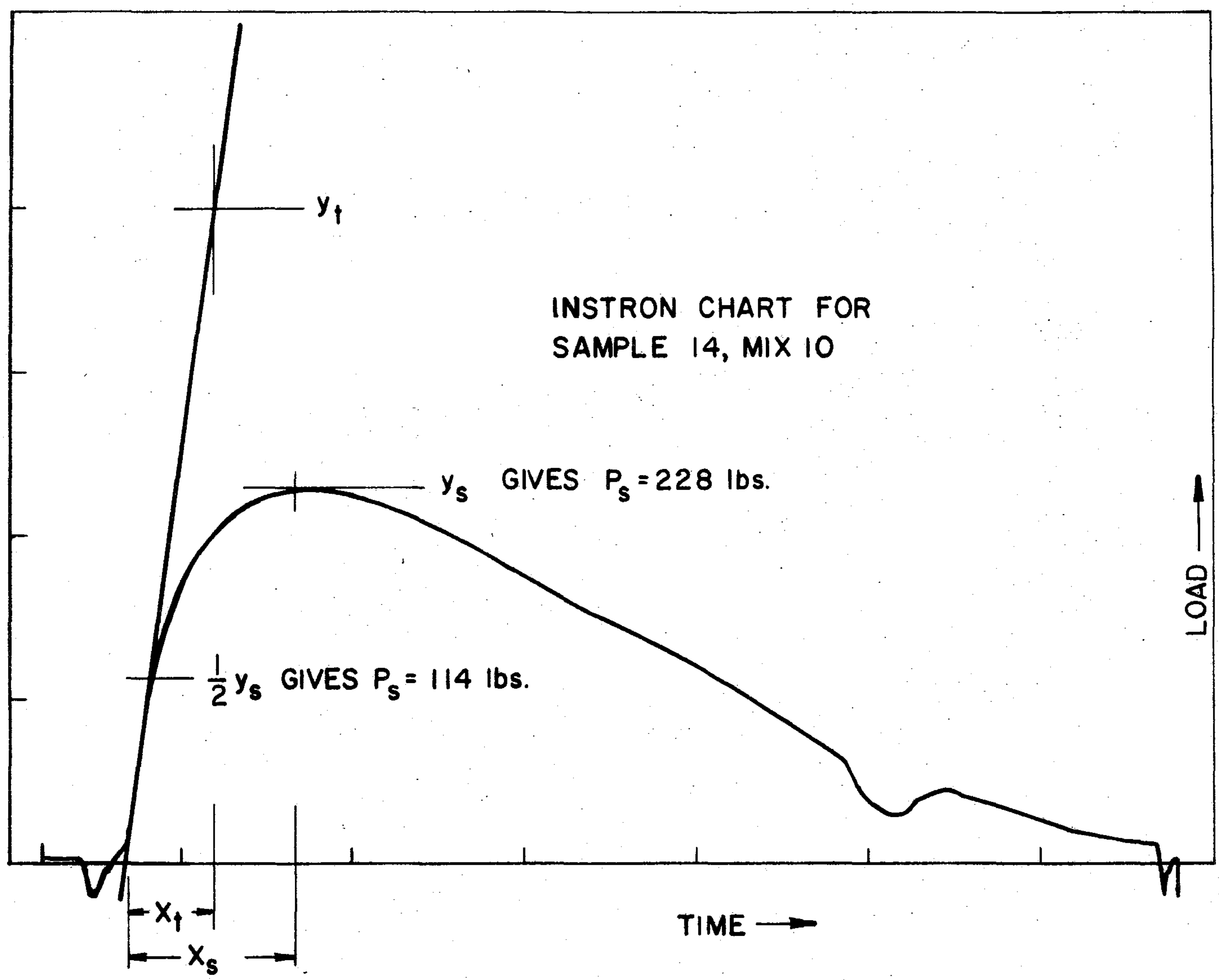

FIGURE 6.13 Typical Instron Chart Indicating Method of Data Reduction.

1. Load at Full Scale Chart Per Travel, P_{FS} 1000 lbs.

2. Cross-head Rate, R 2 in./min.

3. Chart Speed, S 50 in./min.

4. Dimensions (Appendix B2-B)

Average Height, $\overline{H}$	5.87 in.
Average Width, $\overline{W}$	1.52 in.
Average Depth, $\overline{D}$	1.4 in.

The strain rate is calculated as,

$$\dot{\varepsilon} = \frac{R}{\overline{H}} \times 100 = \frac{2}{5.87} \times 100 = 34.1 \text{ percent/min.}$$

The sample cross-sectional area is,

$$A = \overline{W} \times \overline{D} = 2.22 \text{ in.}^2$$

Refer now to the Instron chart for the test examples, Figure 6.13 . The maximum point on the curve is considered to indicate the force at ultimate stress. The y coordinate of this point is,

$$Y_s = 2.28$$

The force at ultimate stress is,

$$P_s = Y_s \frac{P_{FS}}{10} = 2.28 \frac{1000}{100} = 228 \text{ lbs.}$$

and ultimate stress is,

$$\sigma_u = P_s/A = \frac{228}{2.22} = 103 \text{ psi}$$

Many of the Instron charts showed erratic traces at the beginning of the curve. As a result, it was difficult to determine the starting point for computing axial deformation, and thus strain. Accordingly, it was necessary to establish a somewhat arbitrary method for consistent determination of the

$Y = 0.5\ Y_s$. This tangent line defines the tangent modulus which must go through the origin. Thus the intersection of the tangent line and the X-axis was considered to be the zero point of the test trace.

Using this zero point, the X coordinate corresponding to Y_s is,

$$X_s = 0.98$$

An arbitrary point Y_t is chosen on the tangent line, in this case;

$$Y_t = 4.0$$

$$X_t = 0.51$$

The corresponding force: $P_{t,d}$ is,

$$P_{t,d} = Y_t \times \frac{P_{FS}}{10} = 4 \times \frac{1000}{10} = 400 \text{ lbs.}$$

The actual force at the point of tangency is,

$$P_t = 0.5\ P_s = 114 \text{ lbs.}$$

A time fraction is now defined as

$$f_t = \frac{P_t}{P_{t,d}} = \frac{114}{400} = 0.285.$$

It is now possible to correct the total deformation for the machine deformation. A plot of the calibration data for the uniaxial configuration is given in Figure 6.14. This curve is approximated, for ease of machine calculation, by a series of straight lines tangent to the curve. The slopes and intercepts of these tangent lines to the calibration curves is given in Appendix D.

Figure 6.14 is entered at P_t. In the example, the slope of the curve is,

$$B = 0.448 \times 10^5$$

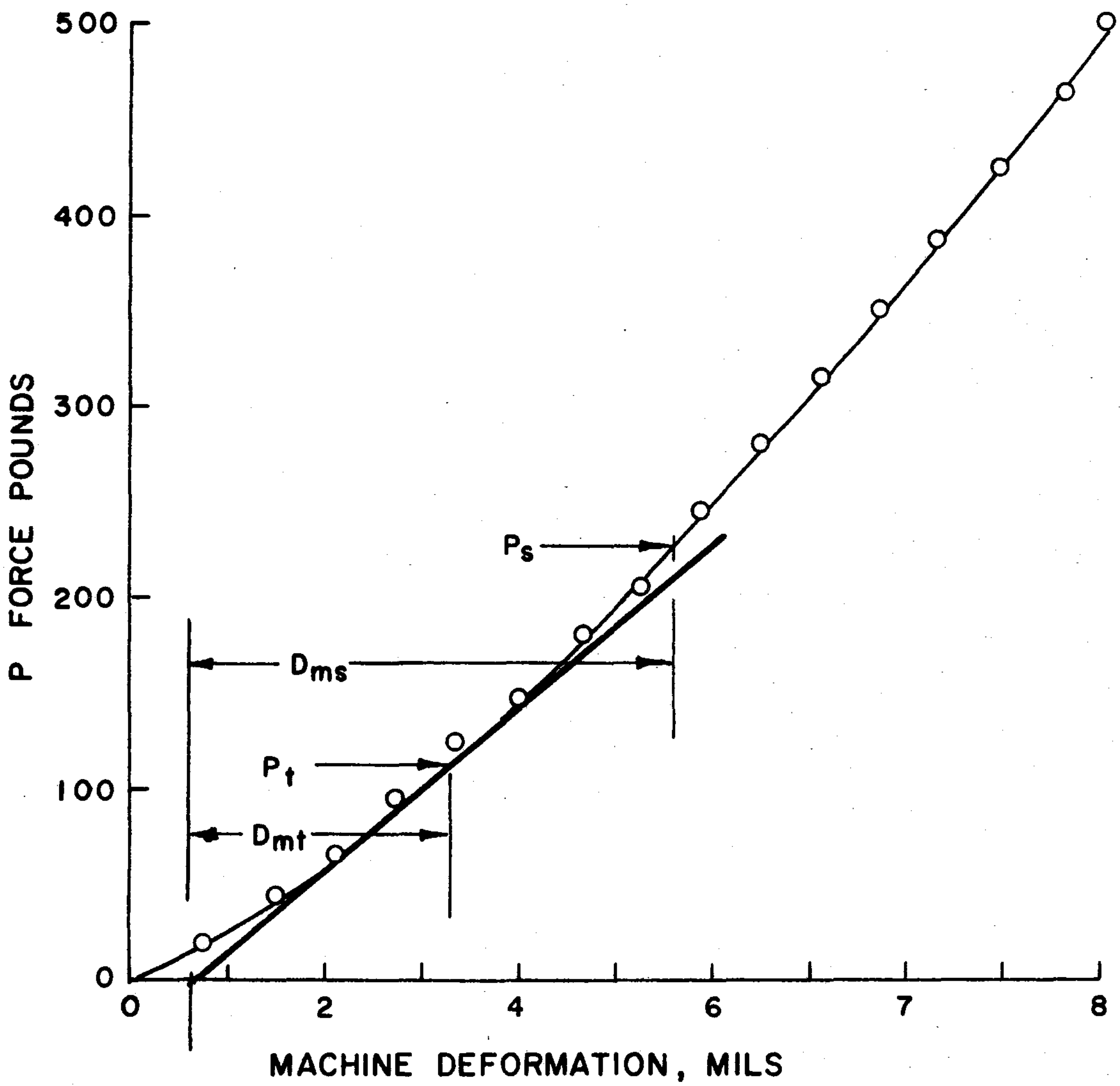

FIGURE 6.14 Force-Machine Deformation Calibration for Uniaxial Tension (NTS 7)

and the machine deformation is

$$D_{mt} = \frac{F_t}{B} = 0.00254 \text{ in.}$$

Total deformation at F_t is

$$D_t = X_t \frac{R}{S} \times F_t$$

$$= 0.51 \times \frac{2}{50} \times 0.285 = 0.581 \times 10^{-2} \text{ in.}$$

Thus, the specimen deformation is

$$D = D_t - D_{mt} = (0.581-0.254)\times 10^{-2}$$

$$= 0.327 \times 10^{-2} \text{ in.}$$

For the uniaxial case the strain is

$$\varepsilon_t = \frac{\Delta L}{L} = \frac{D}{H} = \frac{.327 \times 10^{-2}}{5.87} = 5.57 \times 10^{-4}$$

and the tangent modulus is:

$$E_t = \frac{\sigma_t}{\varepsilon_t} = \frac{51.4}{5.57} \times \frac{10^4}{10^3} = 92.4 \text{ kips/in.}^2$$

The machine deformation at the ultimate stress is D_{ms} as shown in Figure 6.14 . This figure is used to correct the total deformation in calculating ultimate strain and tangent modulus.

7.0 RESULTS AND DISCUSSION

Test results are presented in a manner to:

1) Produce a record of all basic and reduced test data obtained in this study.
2) Show how modulus and failure parameters varied with strain rate.
3) Indicate the degree of precision achieved with each test mode.
4) Demonstrate whether or not a given test mode can distinguish between asphalt concretes made with different asphalts.

The basic data taken from the Instron records are tabulated in Appendix C. Results of data reduction are summarized in Appendix E. These data, along with the calibration data presented in Appendix D, constitute the data record of the experimental work of this program, and are intended to be complete enough to permit detailed checking of the analyses and interpretations if desired. Specifically, the data are recorded in the appendices in accordance with the following schedule:

Test Mode	Data From Instron Records Are In Appendix	Reduced Data Are In Appendix
Double Lap Shear	C1-A through C1-C	E1-A through E1-C
Uniaxial Tension	C2-A through C2-F	E2-A through E2-F
Uniaxial Compression	C3-A through C3-F	E3-A through E3-F
Splitting Tension	C4-A through C4-B	E4-A through E4-B
Hydrostatic Tension	C5-A through C5-D	E5-A through E5-D
Bead Test	C6-A through C6-C	E6-A through E6-C

Various linear regression models were examined to determine the relation of ultimate strength, ultimate strain, secant modulus, and tangent modulus to strain rate. Considering all of the data and all test modes, a simple power law was found to give the best fit, i.e., the highest coefficient of correlation and highest student-t statistics. Accordingly, the modulus and strength parameters are presented in the form of plots of the log of the parameter vs log of strain rate. These plots also give the equation, coefficient of correlation, and student-t values found in the regression analyses.

7.1 Double Lap Shear Tests

The reduced data are plotted against strain rate in Figure 7.1. Average values of shear modulus and failure parameters at each strain rate are given in Table 7.1.

Replicate tests at a given strain rate were too few to estimate a meaningful standard deviation of the test data. However, an indication of the repeatability can be obtained by examining the relative scatter of the data points in Figure 7.1. Additionally, the coefficient of correlation and student-t values shown give an indication of test precision as well as evidence of the validity of the correlation equation chosen. The student-t statistic, as well as the coefficient of correlation, indicates how well the equations proposed (a power law in this case) fit the data. For example, for the number of samples tested, a student-t value of 3.2 indicates that the equation proposed fits the data with a probability of 99 percent, and a student-t value of 2.2 indicates that the probability of fit is 95 percent. For the number of samples tested, a student-t value of about 3 is required for a 99 percent confidence level. All shear test values shown give student-t values well above 3, except for the ultimate strain values obtained with Mix 21.

In general, it appears that the ultimate shear stress values are more reliable than ultimate shear strain data. In addition, these data indicate that the secant shear modulus values are more reliable than the tangent shear modulus.

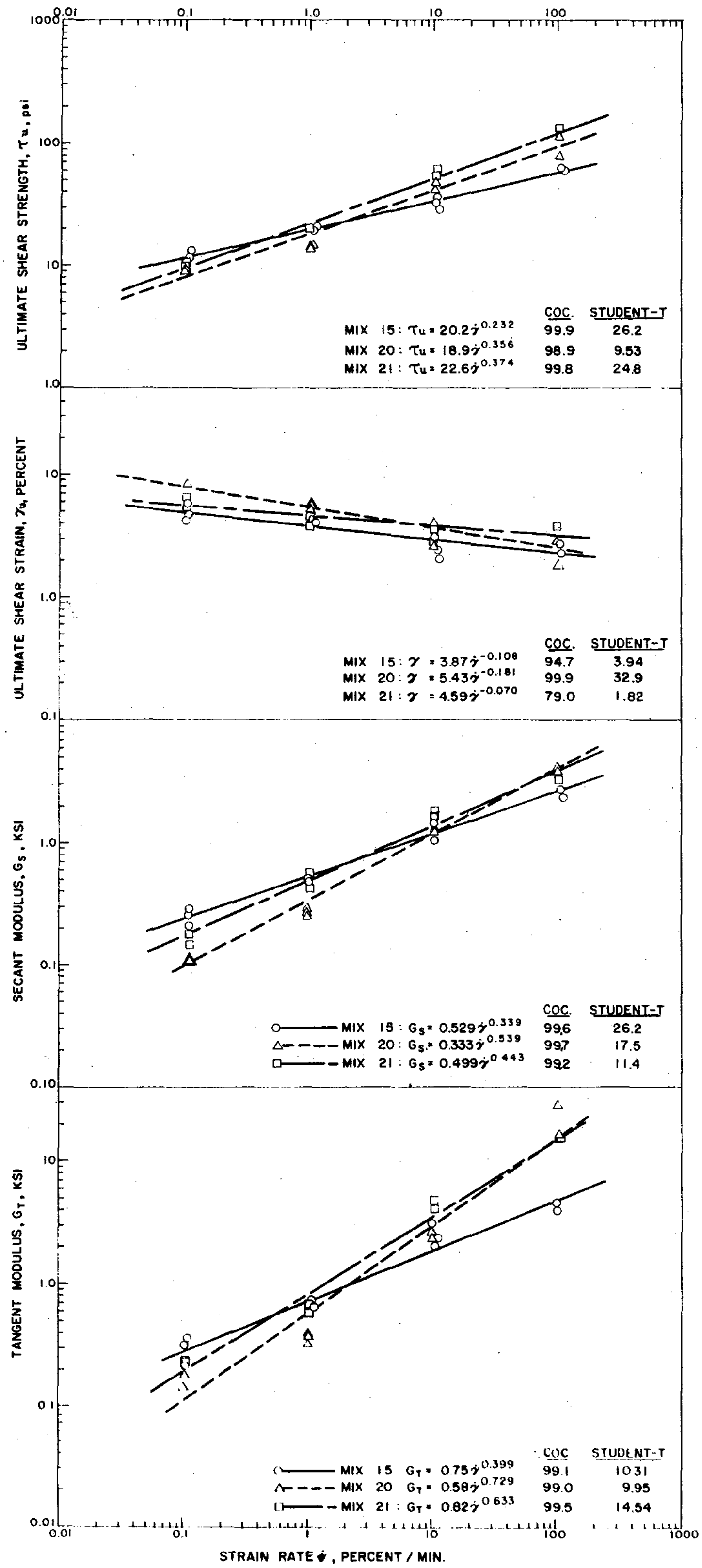

ULTIMATE SHEAR STRENGTH, τu, psi
COC. STUDENT-T
MIX 15: τu = 20.2γ̇^0.232 99.9 26.2
MIX 20: τu = 18.9γ̇^0.356 98.9 9.53
MIX 21: τu = 22.6γ̇^0.374 99.8 24.8
ULTIMATE SHEAR STRAIN, γu, PERCENT
COC. STUDENT-T
MIX 15: γ = 3.87γ̇^-0.108 94.7 3.94
MIX 20: γ = 5.43γ̇^-0.181 99.9 32.9
MIX 21: γ = 4.59γ̇^-0.070 79.0 1.82
SECANT MODULUS, Gs, KSI
COC. STUDENT-T
MIX 15: Gs = 0.529γ̇^0.339 99.6 26.2
MIX 20: Gs = 0.333γ̇^0.539 99.7 17.5
MIX 21: Gs = 0.499γ̇^0.443 99.2 11.4
TANGENT MODULUS, GT, KSI
COC STUDENT-T
MIX 15 GT = 0.75γ̇^0.399 99.1 10.31
MIX 20 GT = 0.58γ̇^0.729 99.0 9.95
MIX 21: GT = 0.82γ̇^0.633 99.5 14.54
STRAIN RATE γ̇, PERCENT / MIN.

TABLE 7.1

Double Lap Shear Modulus and Failure Data at Various Strain Rates

Mix No.	Number of Samples	Strain Rate %/min.	τ_u Ultimate Shear Stress (psi)	γ_u Ultimate Shear Strain (percent)	G_T Initial Tangent Modulus (ksi)	G_S Secant Modulus (ksi)
15	3	0.106	12.2	4.97	0.30	0.25
	2	1.11	20.8	4.14	0.70	0.50
	3	10.9	33.3	2.53	2.51	1.35
	2	110.0	62.3	2.54	4.29	2.46
20	2	0.101	9.1	8.30	0.16	0.11
	3	1.02	14.2	5.26	0.38	0.27
	2	10.2	45.4	3.66	2.53	1.24
	2	101.5	95.5	2.33	22.79	4.15
21	2	0.105	10.1	6.09	0.22	0.17
	2	1.03	20.9	4.16	0.62	0.51
	2	10.7	58.7	3.26	4.46	1.81
	1	106.2	127.6	3.86	15.05	3.30

All data taken at 76°F.

Most of the coefficients of correlation are greater than 99 percent, which strongly supports the use of the simple power law for strain rate dependence. This observation suggests that, in routine evaluation of asphalt concrete shear behavior, tests at just two different strain rates would be adequate.

Finally, considering the variation in slope and position of the data plots in Figure 7.1, in conjunction with the indicated reliability of the laws of each curve, it is evident that the double lap shear test will be sensitive to significant variations in asphalt performance. Further analysis and interpretation of the data obtained in this study with respect to asphalt structural performance is presented in Section 8 of this report.

7.2 Uniaxial Tension Tests

The data for uniaxial tension tests are plotted in Figures 7.2 and 7.3 and averages are given in Table 7.2

The precision of the uniaxial tension test indicated by the data presented in Figures 7.2 and 7.3 appears to be even better than that shown for the double lap shear test. The lowest student-t value found was 4.9 for the ultimate strain rate obtained with Mix 9. The ultimate tensile strength values appear to be most reliable. An example of the potential repeatability of this test mode is demonstrated by tensile strength values obtained for Mix 13 (Figure 7.3). Note that data from duplicate tests check so closely that it was difficult to separate them on the data plot. The high reliability of these data is further indicated by the student-t value of nearly 90 obtained for tensile strength tests in Mix 13.

As noted for the shear test, the ultimate tensile strain values are noticeably less reliable than tensile stress value. This difference is probably mostly the result of the relatively crude way that specimen extension was measured in this test, (i.e. estimation from crosshead separation corrected for

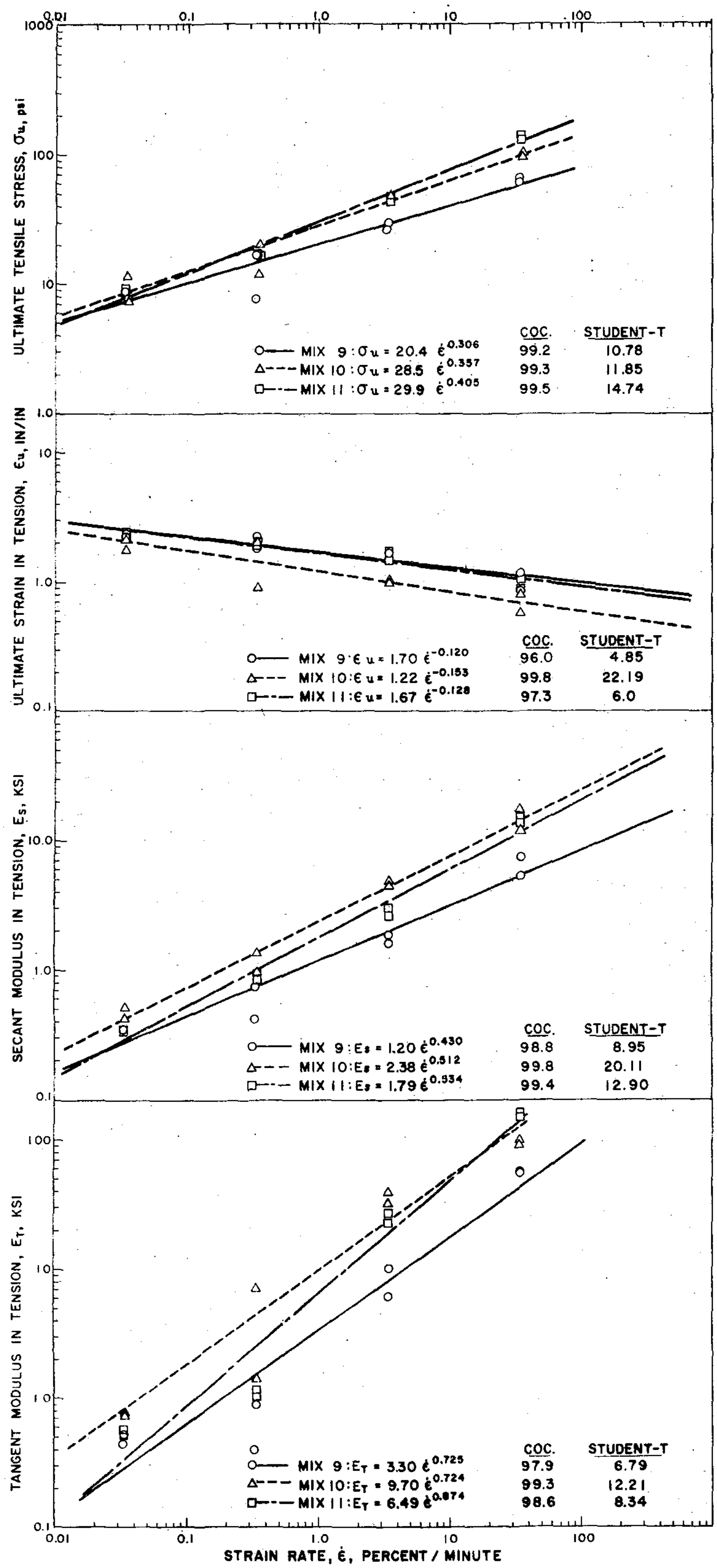

ULTIMATE TENSILE STRESS, σu, psi
COC. STUDENT-T
MIX 9 : σu = 20.4 ε̇^0.306 99.2 10.78
MIX 10 : σu = 28.5 ε̇^0.357 99.3 11.85
MIX 11 : σu = 29.9 ε̇^0.405 99.5 14.74
ULTIMATE STRAIN IN TENSION, εu, IN/IN
COC. STUDENT-T
MIX 9 : εu = 1.70 ε̇^-0.120 96.0 4.85
MIX 10 : εu = 1.22 ε̇^-0.153 99.8 22.19
MIX 11 : εu = 1.67 ε̇^-0.128 97.3 6.0
SECANT MODULUS IN TENSION, Es, KSI
COC. STUDENT-T
MIX 9 : Es = 1.20 ε̇^0.430 98.8 8.95
MIX 10 : Es = 2.38 ε̇^0.512 99.8 20.11
MIX 11 : Es = 1.79 ε̇^0.534 99.4 12.90
TANGENT MODULUS IN TENSION, ET, KSI
COC. STUDENT-T
MIX 9 : ET = 3.30 ε̇^0.725 97.9 6.79
MIX 10 : ET = 9.70 ε̇^0.724 99.3 12.21
MIX 11 : ET = 6.49 ε̇^0.874 98.6 8.34
STRAIN RATE, ε̇, PERCENT / MINUTE

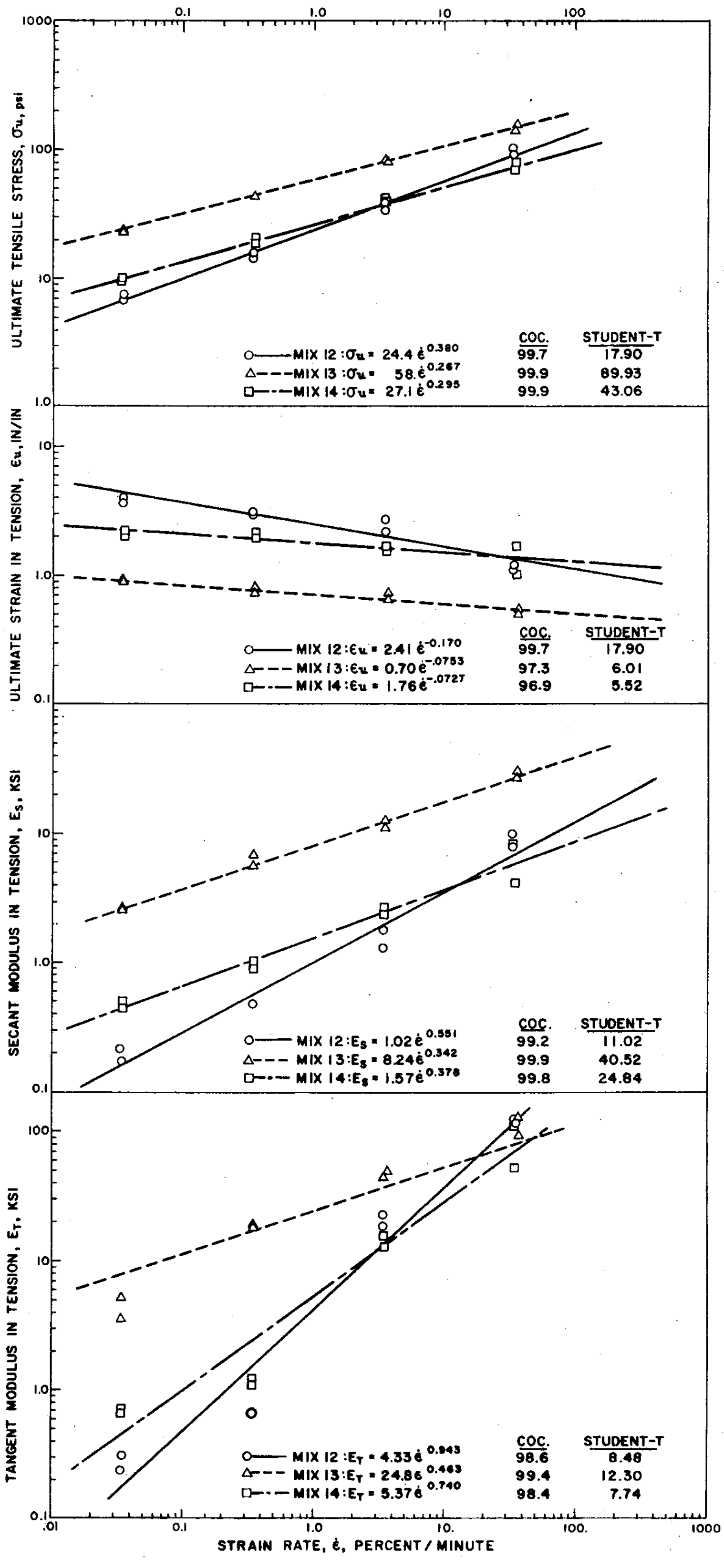

0.1
1.0
10
100
1000
ULTIMATE TENSILE STRESS, σu, psi
MIX 12 : σu = 24.4 ė^0.380
MIX 13 : σu = 58.ė^0.267
MIX 14 : σu = 27.1 ė^0.295
COC.
99.7
99.9
99.9
STUDENT-T
17.90
89.93
43.06
ULTIMATE STRAIN IN TENSION, εu, IN/IN
MIX 12 : εu = 2.41 ė^-0.170
MIX 13 : εu = 0.70 ė^-.0753
MIX 14 : εu = 1.76 ė^-.0727
COC.
99.7
97.3
96.9
STUDENT-T
17.90
6.01
5.52
SECANT MODULUS IN TENSION, Es, KSI
MIX 12 : Es = 1.02 ė^0.551
MIX 13 : Es = 8.24 ė^0.342
MIX 14 : Es = 1.57 ė^0.378
COC.
99.2
99.9
99.8
STUDENT-T
11.02
40.52
24.84
TANGENT MODULUS IN TENSION, ET, KSI
MIX 12 : ET = 4.33 ė^0.943
MIX 13 : ET = 24.86 ė^0.463
MIX 14 : ET = 5.37 ė^0.740
COC.
98.6
99.4
98.4
STUDENT-T
8.48
12.30
7.74
.01
0.1
1.0
10.
100.
1000
STRAIN RATE, ė, PERCENT / MINUTE

TABLE 7.2

Uniaxial Tensile Modulus and Failure Data

at Various Strain Rates

Mix No.	Number of Samples	$\dot{\varepsilon}$ Strain Rate %/min.	σ_u Ultimate Tensile Stress psi	ε_u Ultimate Tensile Strain %	E_T Initial Tangent Modulus ksi	E_S Secant Modulus ksi
9	2	0.033	8.1	2.36	0.48	0.34
	2	0.332	12.2	2.05	0.66	0.58
	2	3.34	28.9	1.66	8.12	1.75
	2	33.6	64.1	1.01	54.50	6.50
10	2	0.034	9.4	1.99	0.75	0.47
	2	0.339	15.9	1.49	4.22	1.14
	2	3.40	48.6	1.03	35.93	4.70
	2	34.1	100.5	0.70	95.59	14.87
11	2	0.034	8.5	2.46	0.53	0.35
	2	0.339	16.9	1.94	1.10	0.87
	2	3.41	44.7	1.62	25.26	2.78
	2	34.1	139.0	0.92	154.79	14.30
12	2	0.034	7.3	3.86	0.28	0.19
	2	0.338	14.6	3.04	0.65	0.48
	2	3.36	36.1	2.44	20.35	1.51
	2	33.4	100.4	1.13	121.26	8.94
13	2	0.034	23.3	0.89	4.37	2.62
	2	0.336	43.4	0.76	18.63	5.70
	2	3.46	82.3	0.69	47.36	11.93
	2	35.7	148.7	0.51	115.33	29.01
14	2	0.034	10.0	2.13	0.70	0.47
	2	0.342	19.4	2.05	1.16	0.95
	2	3.42	40.7	1.61	14.77	2.53
	2	34.0	74.8	1.32	87.28	6.13

machine deformation). Direct measurement of extension by suitable extensometers (by methods like those often used in uniaxial testing of solid propellants, as discussed by Kelley (63)), would probably produce a significant improvement of the precision of the ultimate tensile strain data obtained with asphaltic concrete specimens. Again, the secant modulus data appear to be more reliable than the tangent modulus data.

Coefficient of correlation numbers were 96 percent or above in all cases, and over 99 percent for many of the data. Thus the simple power law relation with strain rate is quite valid over the range of strain rates examined. The tension test appears to be quite sensitive to differences in asphalt performance.

It will be recalled that the only difference between Mix 9 and Mix 14 was in the specimen preparation: Mix 14 had fewer saw cuts and thus a lower probability of surface stress risers. A comparison of the data on these two mixes (in Figures 7.2 and 7.3) indicates that the difference in saw cut procedure resulted in a) somewhat higher ultimate tensile strength but no difference in strain rate sensitivity, and b) a marked improvement in test repeatability with fewer saw cuts. This later point is illustrated by the comparison of student-t values in the following:

	Student-t value for		
	Ultimate Stress σ_u	Ultimate Strain ε_u	Secant Modulus E_s
Mix 9, six saw cuts per specimen	11	4.9	9
Mix 14, four saw cuts per specimen	43	5.3	25

From these data it appears that further improvement in specimen preparation could result in increased test reliability.

7.3 Uniaxial Compression Tests

The data for uniaxial compression tests are plotted in Figures 7.4 and 7.5 and averages are given in Table 7.3.

In general, these data indicate 1) satisfactory test repeatability, 2) better reliability for ultimate stress values than for ultimate strain values, and, 3) better reliability for secant modulus values than for tangent modulus values.

The rather low student-t value obtained for ultimate strain on Mix 13 clearly is associated with the low coefficient of correlation (77 percent) rather than poor repeatability of test data at a given strain rate. The low coefficient of correlation means primarily that the simple power law for strain rate dependence does not fit this particular set of data very well. One of the problems with a prismatic specimen in compression is that of column stability. In some of these tests this could change the nature of the strain-rate sensitivity of the ultimate strain data. Otherwise, no test difficulty resulting from stability problems is evident from the data. In most cases the simple power law appears to correlate the data very well (correlation coefficients ranging from 96 to 100 percent). Also, significant differences in location and slope of the curves indicate that the uniaxial compression test is sensitive to differences in asphalt cement structural performance.

7.4 Splitting Tension Tests

Results from the splitting tensile tests are plotted in Figure 7.6. Data on Mix 39 in this figure can be compared with the results of the direct tensile

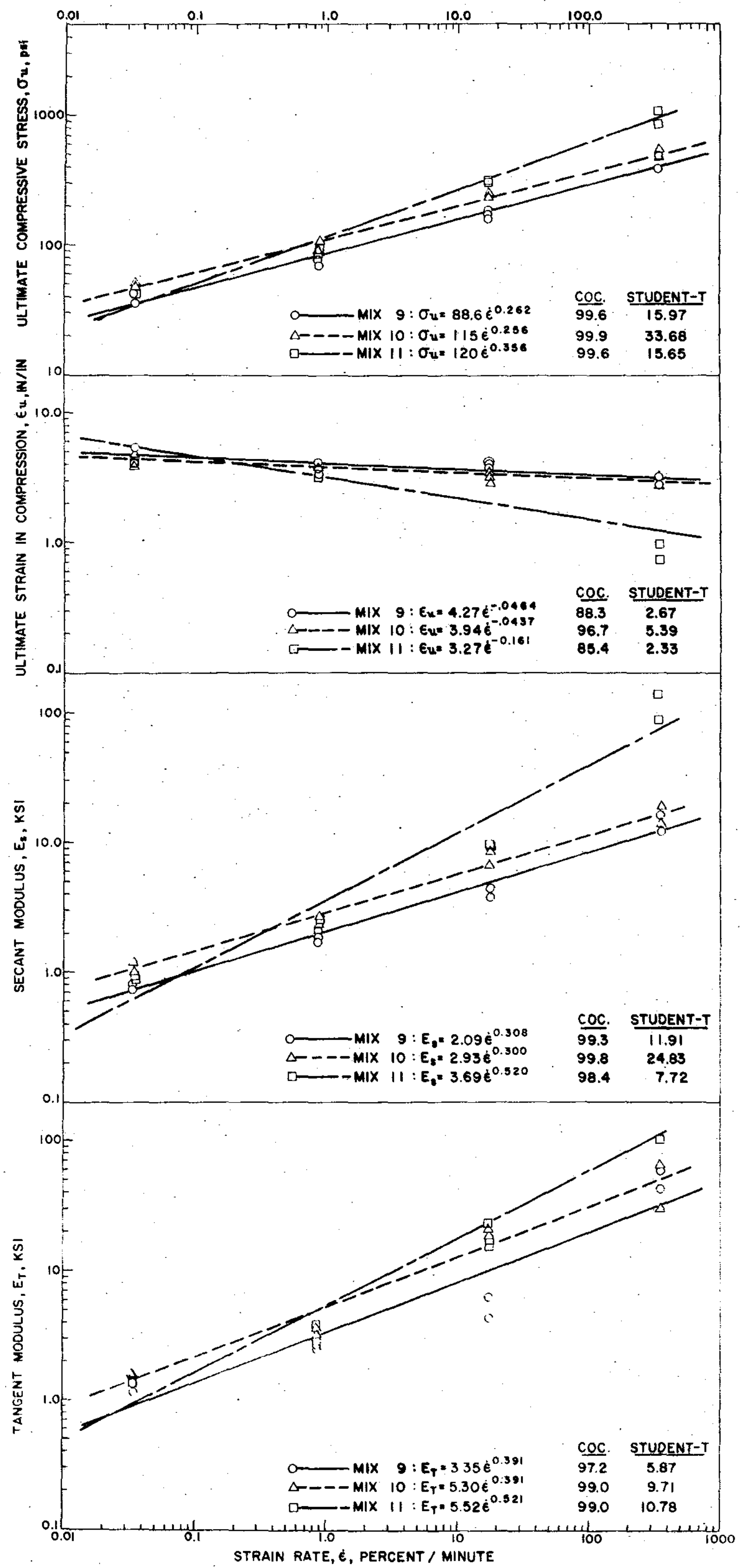

0.01
0.1
1.0
10.0
100.0
ULTIMATE COMPRESSIVE STRESS, σu, psi
1000
100
10
COC.
STUDENT-T
MIX 9 : σu= 88.6 έ^0.262
99.6
15.97
MIX 10 : σu= 115 έ^0.256
99.9
33.68
MIX 11 : σu= 120 έ^0.356
99.6
15.65
ULTIMATE STRAIN IN COMPRESSION, εu, IN/IN
10.0
1.0
0.1
COC.
STUDENT-T
MIX 9 : εu= 4.27έ^-.0464
88.3
2.67
MIX 10 : εu= 3.94έ^-.0437
96.7
5.39
MIX 11 : εu= 3.27έ^-0.161
85.4
2.33
SECANT MODULUS, Es, KSI
100
10.0
1.0
0.1
COC.
STUDENT-T
MIX 9 : Es= 2.09έ^0.308
99.3
11.91
MIX 10 : Es= 2.93έ^0.300
99.8
24.83
MIX 11 : Es= 3.69έ^0.520
98.4
7.72
TANGENT MODULUS, ET, KSI
100
10
1.0
0.1
COC.
STUDENT-T
MIX 9 : ET= 3.35έ^0.391
97.2
5.87
MIX 10 : ET= 5.30έ^0.391
99.0
9.71
MIX 11 : ET= 5.52έ^0.521
99.0
10.78
0.01
0.1
1.0
10
100
1000
STRAIN RATE, έ, PERCENT / MINUTE

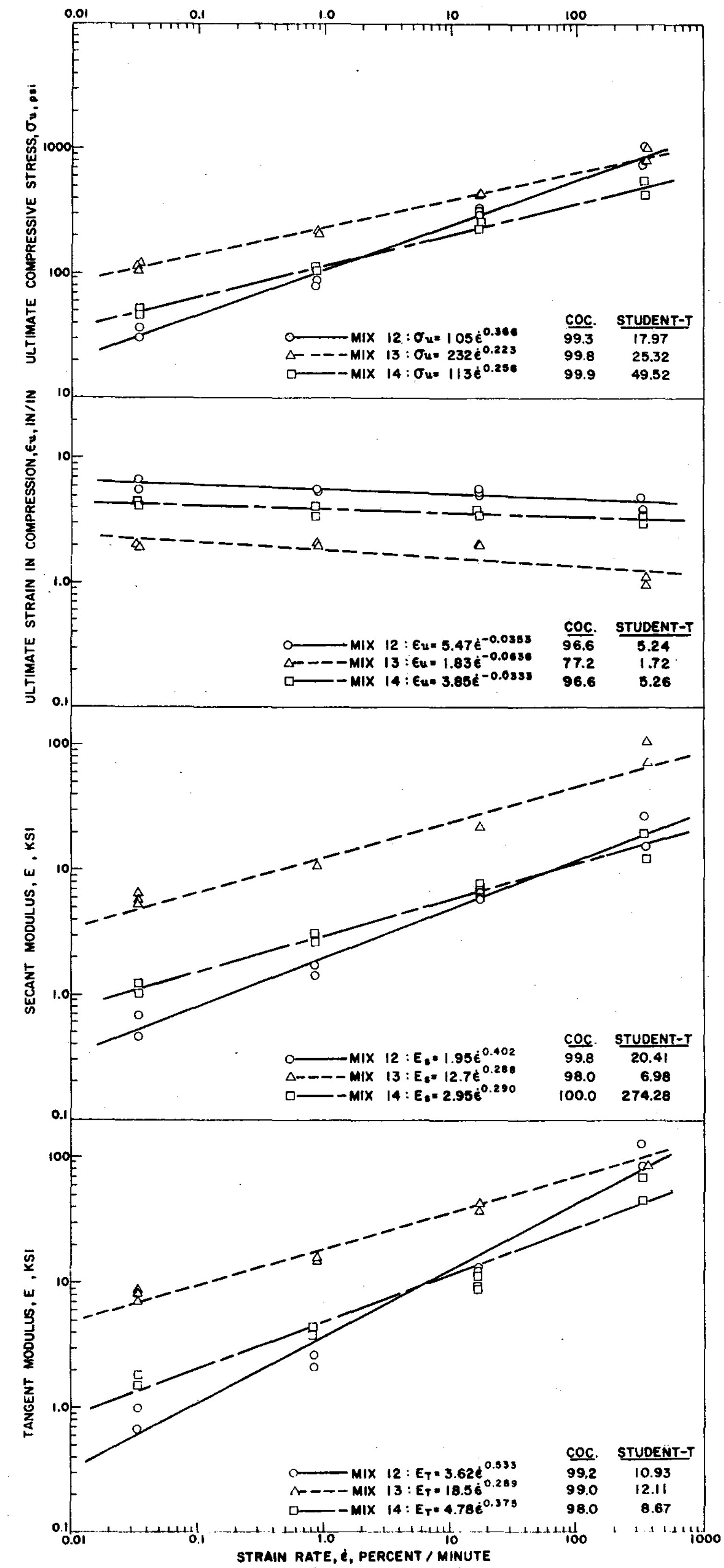

0.01
0.1
1.0
10
100
1000
ULTIMATE COMPRESSIVE STRESS, σu, psi
COC.
STUDENT-T
MIX 12 : σu = 105ε̇^0.366
99.3
17.97
MIX 13 : σu = 232ε̇^0.223
99.8
25.32
MIX 14 : σu = 113ε̇^0.256
99.9
49.52
ULTIMATE STRAIN IN COMPRESSION, εu, IN/IN
COC.
STUDENT-T
MIX 12 : εu = 5.47ε̇^-0.0353
96.6
5.24
MIX 13 : εu = 1.83ε̇^-0.0636
77.2
1.72
MIX 14 : εu = 3.85ε̇^-0.0333
96.6
5.26
SECANT MODULUS, E, KSI
COC.
STUDENT-T
MIX 12 : Es = 1.95ε̇^0.402
99.8
20.41
MIX 13 : Es = 12.7ε̇^0.288
98.0
6.98
MIX 14 : Es = 2.95ε̇^0.290
100.0
274.28
TANGENT MODULUS, E, KSI
COC.
STUDENT-T
MIX 12 : ET = 3.62ε̇^0.533
99.2
10.93
MIX 13 : ET = 18.5ε̇^0.289
99.0
12.11
MIX 14 : ET = 4.78ε̇^0.375
98.0
8.67
STRAIN RATE, ε̇, PERCENT / MINUTE

TABLE 7.3

Uniaxial Compressive Modulus and Failure Data

At Various Strain Rates

Mix No.	Number of Samples	ε Strain Rate %/min.	σ_u Ultimate Compressive Stress (psi)	ε_u Ultimate Compressive Strain (%)	E_T Tangent Modulus (ksi)	E_S Secant Modulus (ksi)
9	2	0.033	39.7	5.00	1.22	0.80
	3	0.835	76.5	4.02	2.53	1.91
	3	16.9	172.5	4.30	5.81	4.02
	2	336.0	441.3	3.04	50.96	14.62
10	2	0.034	50.2	4.60	1.60	1.10
	2	0.852	102.9	4.06	3.59	2.56
	3	17.1	239.6	3.26	21.11	7.62
	2	341.0	517.0	3.17	48.19	16.45
11	2	0.034	41.1	4.46	1.29	0.92
	2	0.853	92.7	3.69	3.51	2.51
	3	17.0	327.2	3.50	19.47	9.36
	2	341.0	1029.7	0.87	152.00	123.40
12	2	0.034	33.4	6.10	0.81	0.56
	2	0.841	82.2	5.45	2.31	1.51
	3	16.8	323.2	5.23	12.78	6.19
	2	335.0	884.8	4.31	107.14	21.15
13	3	0.034	113.8	1.97	7.95	5.79
	2	0.891	213.7	2.02	15.09	10.59
	2	17.5	423.6	1.96	38.99	21.60
	2	357.0	899.1	1.03	113.06	89.70
14	2	0.034	48.4	4.42	1.65	1.10
	2	0.852	103.8	3.68	3.94	2.84
	3	16.7	238.4	3.59	9.77	6.66
	2	340.0	498.4	3.17	56.01	15.95

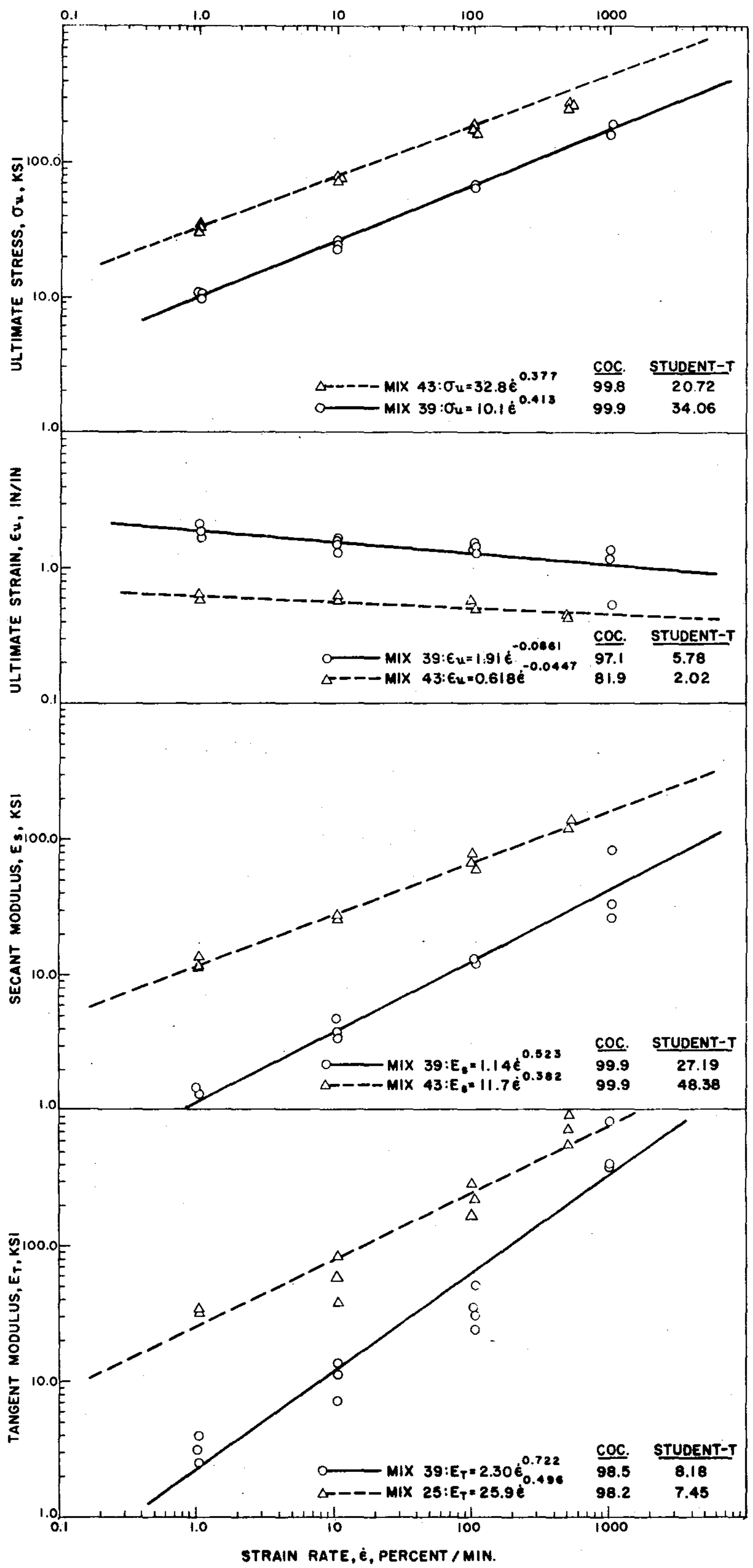

0.1
1.0
10
100
1000
ULTIMATE STRESS, σu, KSI
100.0
10.0
1.0
COC.
STUDENT-T
MIX 43: σu=32.8ė^0.377
99.8
20.72
MIX 39: σu=10.1ė^0.413
99.9
34.06
ULTIMATE STRAIN, εu, IN/IN
1.0
0.1
COC.
STUDENT-T
MIX 39: εu=1.91ė^-0.0861
97.1
5.78
MIX 43: εu=0.618ė^-0.0447
81.9
2.02
SECANT MODULUS, Es, KSI
100.0
10.0
1.0
COC.
STUDENT-T
MIX 39: Es=1.14ė^0.523
99.9
27.19
MIX 43: Es=11.7ė^0.382
99.9
48.38
TANGENT MODULUS, ET, KSI
100.0
10.0
1.0
COC.
STUDENT-T
MIX 39: ET=2.30ė^0.722
98.5
8.18
MIX 25: ET=25.9ė^0.496
98.2
7.45
0.1
1.0
10
100
1000
STRAIN RATE, ė, PERCENT / MIN.

test on Mix 9 plotted in Figure 7.2. Average values of modulus and failure parameters are summarized in Table 7.4.

Except for the tangent modulus data, the points for repeat tests shown on Figure 7.6 fall nearly on top of one another. This indicates the excellent repeatability possible with the splitting tension test on asphaltic concrete specimens. Comparing the data for Mix 9 and Mix 39, student-t values appear to be significantly higher for the splitting tension test mode. However, it is believed that this indicates a better fit to the power law model rather than inherently better test repeatability.

The two tension test modes also can be compared on the basis of relative strength and modulus values obtained. Since there is more uncertainty as to the actual stress and strain field at a given load in the splitting tension test than in a direct tension test, it was assumed that the latter values are correct. On this basis, at a strain rate of one percent per minute, it appears that the splitting tension test underestimates the ultimate stress by a factor of 2 and overestimates the ultimate strain by about 12 percent. The two tests also give somewhat different sensitivities to strain rate. Briefly, the splitting tension test is easier to conduct and appears to be capable of somewhat better precision than the direct tension test on asphaltic concrete. However, the accuracy of the splitting tension test results appears to be in doubt. Possibly the accuracy would have been improved in this study if the curved loading bar recommended by Kennedy (66,75) had been used.

The asphaltic concrete variable examined in the splitting tension tests in this study was asphalt content. A reduction of asphalt content from 5.5 percent to 3.8 percent increased ultimate stress by a factor of 3, decreased

TABLE 7.4

Splitting Tensile Modulus and Failure Data At Various Strain Rates

Mix No.	Number of Samples	ε Strain Rate %/min.	σ_u Ultimate Tensile Stress (psi)	ε_u Ultimate Tensile Strain (%)	E_T Initial Tangent Modulus (ksi)	E_S Initial Secant Modulus (ksi)
39	3	1.05	10.6	1.91	3.24	1.24
	4	10.4	24.7	1.48	10.7	3.71
	4	105	73.1	1.40	35.2	11.6
	3	1020	175	1.01	549	46.6
43	3	1.02	32.0	0.58	33.7	12.1
	3	10.4	73.6	0.59	58.4	27.3
	3	103	169	0.55	223	68.5
	3	509	250	0.43	718	128

ultimate strain 3-fold, and produced an order-of-magnitude increase in modulus. These differences indicate a useful sensitivity of this test to factors which may influence pavement structural performance.

7.5 Hydrostatic Tension Tests

Data for the hydrostatic tension tests are plotted in Figure 7.7 Average values of modulus and failure parameters are summarized in Table 7.5 In plotting the data in Figure 7.6, the values for ultimate stress listed in Appendix E5 were multiplied by 1.95, ultimate strain values were multiplied by 1.45, and modulus values were multiplied by 1.34, in accordance with the explanation given in Section 6.2.3. The same adjustments were made in calculating the data listed in Table 7.5

In this exploratory study of the application of a hydrostatic test configuration ("poker-chip" test) to asphaltic concrete specimens, the precision of the test results is evidently not as good as that observed in other test modes. In particular, the scatter of the ultimate strain data is clearly greater than any differences among the samples of asphaltic concrete mixes evaluated. It is believed that this is largely the result of the very small vertical specimen deformation at failure combined with the relative crudeness of the method of deformation measurement.

The ultimate stress data appears to be the most reliable and served to demonstrate the possibilities of this kind of test for determination of asphaltic concrete behavior in a hydrostatic stress field. Significant differences among the samples tested are indicated, although the sensitivity of this test to variations in asphalt characteristics is less than that observed in other test modes.

Ultimate strain appears to be little influenced by strain rate. Modulus and ultimate stress data show the expected simple power law dependence on strain rate.

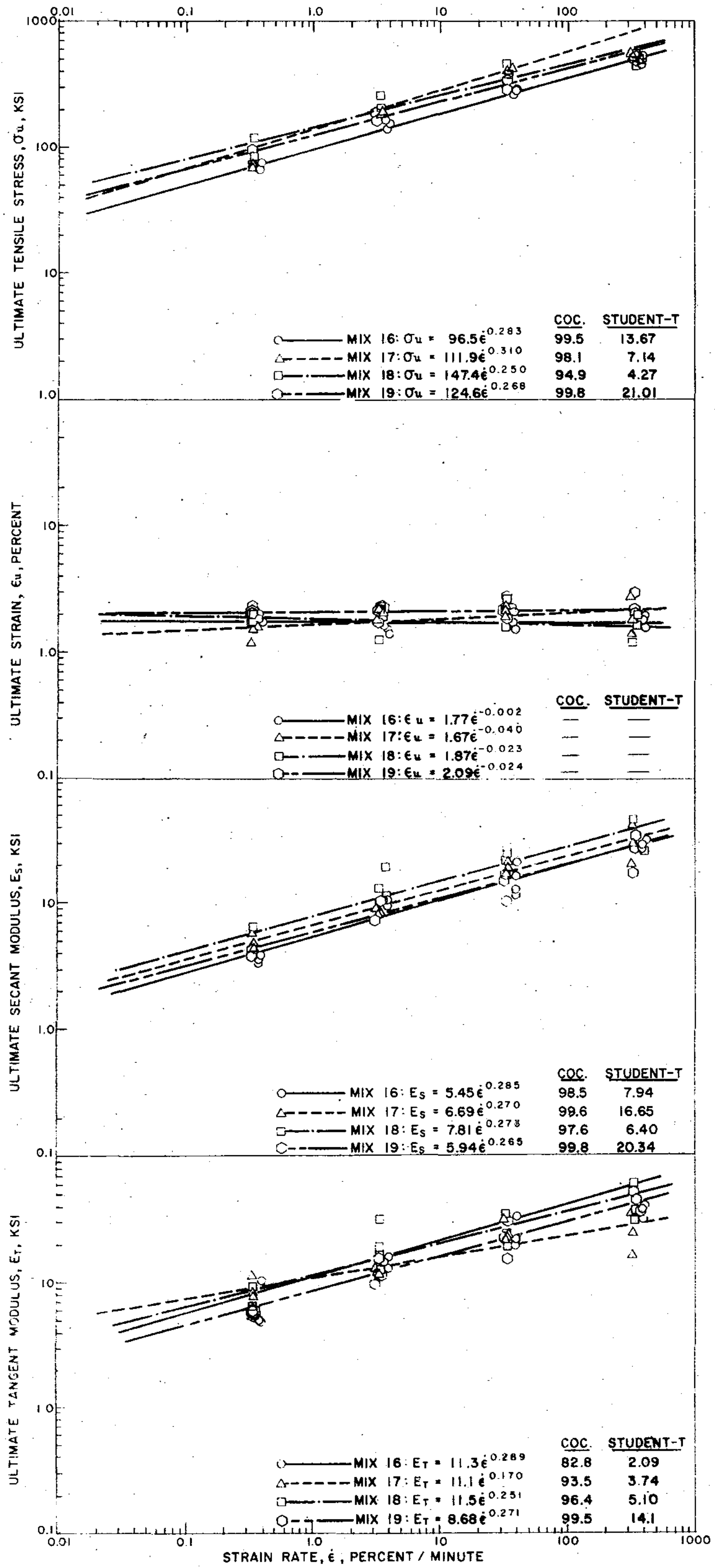

ULTIMATE TENSILE STRESS, σu, KSI
COC.
STUDENT-T
MIX 16: σu = 96.5ε̇^0.283 99.5 13.67
MIX 17: σu = 111.9ε̇^0.310 98.1 7.14
MIX 18: σu = 147.4ε̇^0.250 94.9 4.27
MIX 19: σu = 124.6ε̇^0.268 99.8 21.01
ULTIMATE STRAIN, εu, PERCENT
COC.
STUDENT-T
MIX 16: εu = 1.77ε̇^-0.002
MIX 17: εu = 1.67ε̇^-0.040
MIX 18: εu = 1.87ε̇^-0.023
MIX 19: εu = 2.09ε̇^-0.024
ULTIMATE SECANT MODULUS, Es, KSI
COC.
STUDENT-T
MIX 16: Es = 5.45ε̇^0.285 98.5 7.94
MIX 17: Es = 6.69ε̇^0.270 99.6 16.65
MIX 18: Es = 7.81ε̇^0.273 97.6 6.40
MIX 19: Es = 5.94ε̇^0.265 99.8 20.34
ULTIMATE TANGENT MODULUS, ET, KSI
COC.
STUDENT-T
MIX 16: ET = 11.3ε̇^0.269 82.8 2.09
MIX 17: ET = 11.1ε̇^0.170 93.5 3.74
MIX 18: ET = 11.5ε̇^0.251 96.4 5.10
MIX 19: ET = 8.68ε̇^0.271 99.5 14.1
STRAIN RATE, ε̇, PERCENT / MINUTE

TABLE 7.5

Hydrostatic Tensile Modulus and Failure Data at Various Strain Rates

Mix No.	Number of Samples	ε Strain Rate %/min.	σ_u Ultimate Tensile Stress (psi)	ε_u Ultimate Tensile Strain (%)	E_S Secant Modulus (ksi)	E_T Tangent Modulus (ksi)
16	3	0.39	68	1.88	3.59	6.71
	3	3.9	155	1.55	9.95	14.9
	4	39	291	1.92	15.7	.85
	4	397	488	1.77	27.6	35
17	3	0.34	70	1.43	4.98	8.88
	3	3.37	17.9	2.02	8.88	12.7
	3	33.5	415	2.18	19.0	27.4
	3	321	558	2.00	30.0	25.1
18	3	0.34	91	1.86	4.88	7.13
	4	3.4	246	1.93	13.4	20.3
	4	33.4	450	2.01	22.8	29.7
	3	341	506	1.58	33.3	43.1
19	4	0.35	89	2.10	4.23	6.0
	4	3.36	180	2.06	8.81	13.2
	4	34	338	2.26	15.3	23.7
	4	344	567	2.19	27.0	38.8

Further study and refinement of this test method is necessary before it will become a useful tool for evaluating the performance of asphaltic concrete. One obvious improvement would be the use of LVDT's for the measurement of vertical deflection of the specimen. Based on the experience with this test on solid propellants (81), additional care in preparation of the "poker-chip" specimens probably is necessary also. In particular, the two platens must be kept parallel, within very close tolerences, to produce a hydrostatic tension field within the specimen.

7.6 Bead Tests

Results obtained for this quality control version of the hydrostatic tension test are plotted in Figure 7.8. Average values of modulus and failure parameters are summarized in Table 7.6. In this test, the apparent stress and strain values were not multiplied by the factors used in hydrostatic tension tests of asphaltic concrete specimens because the more complicated stress analysis of the bead test configuration has not been accomplished. Nevertheless, examination of the apparent ultimate stress, ultimate strain, modulus data will serve to allow assessment of the bead test as a quality control procedure. In fact, relative values usually suffice in quality control applications and it may not be necessary to make such corrections at all.

In most instances values obtained in repeat tests in this series were in excellent agreement with one another. This observation is especially in evidence for the ulitmate strain data. The indicated potential of excellent repeatability of ultimate strain values is of particular interest because it was hoped that the bead test might be a logical improvement over the standard ductility test which essentially yields ultimate strain data.

Sensitivity to differences in asphalt characteristics was not determined in this study since bead diameter was the only test parameter varied in addition to strain rate. However, the test was quite sensitive to bead size (simulating aggregate size) and it is believed that the bead test will be comparable to the ductility test with respect to sensitivity to differences in asphalt structural performance.

In all but one instance the simple power law strain rate dependence served to correlate the data very well. Correlation coefficient of 93 to over 99

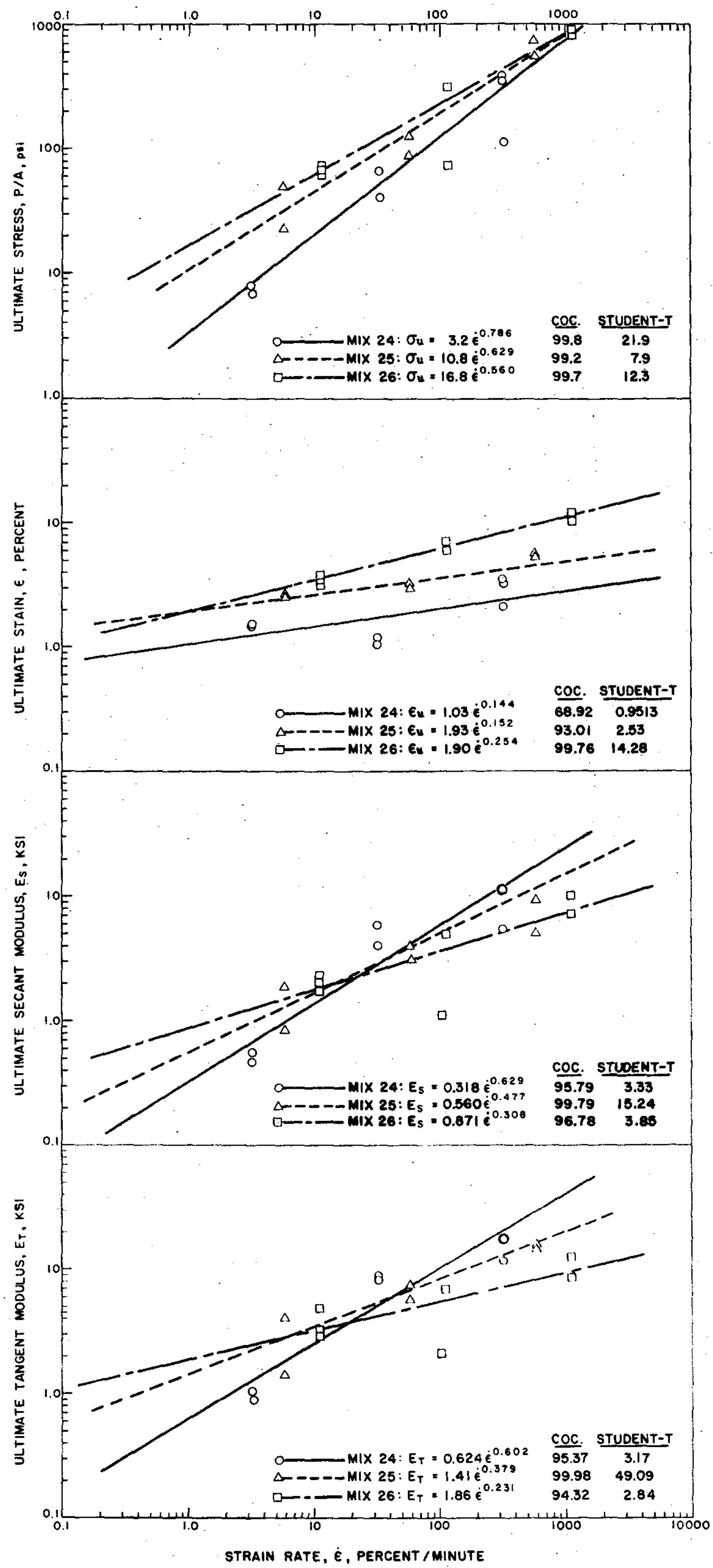

ULTIMATE STRESS, P/A, psi
MIX 24: $\sigma_u = 3.2\,\dot{\epsilon}^{0.786}$
MIX 25: $\sigma_u = 10.8\,\dot{\epsilon}^{0.629}$
MIX 26: $\sigma_u = 16.8\,\dot{\epsilon}^{0.560}$
COC. STUDENT-T
99.8 21.9
99.2 7.9
99.7 12.3
ULTIMATE STAIN, ϵ, PERCENT
MIX 24: $\epsilon_u = 1.03\,\dot{\epsilon}^{0.144}$
MIX 25: $\epsilon_u = 1.93\,\dot{\epsilon}^{0.152}$
MIX 26: $\epsilon_u = 1.90\,\dot{\epsilon}^{0.254}$
COC. STUDENT-T
68.92 0.9513
93.01 2.53
99.76 14.28
ULTIMATE SECANT MODULUS, E_S, KSI
MIX 24: $E_S = 0.318\,\dot{\epsilon}^{0.629}$
MIX 25: $E_S = 0.560\,\dot{\epsilon}^{0.477}$
MIX 26: $E_S = 0.871\,\dot{\epsilon}^{0.308}$
COC. STUDENT-T
95.79 3.33
99.79 15.24
96.78 3.85
ULTIMATE TANGENT MODULUS, E_T, KSI
MIX 24: $E_T = 0.624\,\dot{\epsilon}^{0.602}$
MIX 25: $E_T = 1.41\,\dot{\epsilon}^{0.379}$
MIX 26: $E_T = 1.86\,\dot{\epsilon}^{0.231}$
COC. STUDENT-T
95.37 3.17
99.98 49.09
94.32 2.84
STRAIN RATE, $\dot{\epsilon}$, PERCENT/MINUTE

TABLE 7.6

Bead Test Modulus and Failure Data at Various Strain Rates

Mix No.	Bead Size	Number of Samples	ε Strain Rate %/min.	σ_u Ultimate Tensile Stress (psi)	ε_u Ultimate Tensile Strain (%)	E_S Secant Modulus (ksi)
24		2	3.23	7.6	1.50	0.51
		2	32.3	55	1.11	4.92
		3	323	263	2.93	9.16
25		2	5.78	36.8	2.74	1.36
		2	57.8	109	3.05	3.54
		2	578	667	5.52	7.17
26		3	11.2	70	3.41	2.05
		2	112	206	6.58	2.98
		2	1120	918	11.0	8.5

percent were found except for the ultimate strain data from Mix 24. This suggests possible simplifications of this test mode. For constant strain rate tests, only two strain rates should be necessary. Another possibility is to load the bead test configuration at a constant stress. A creep test of this kind can be conducted with very simple apparatus.

8.0 ANALYSIS AND INTERPRETATION

The foregoing discussion considered the feasibility of the test methods selected for basic evaluation of asphalt cement structural performance, and the sensitivity of the test results to differences in asphalt composition. In this section, the experimental approach has been examined in greater depth. This section considers:

1) The effect of stress axiality on the behavior of the specimens tested.
2) Further examination of the effect of asphalt cement source and additives on the test results.
3) A viscoelastic interpretation of the data.
4) The application potential of the methods evaluated in this program.

8.1 Effect of Stress Axiality

The effect of stress axiality was examined to determine 1) the possibility of predicting combined stress behavior from uniaxial behavior, and 2) to what degree relative asphalt performance would vary with the stress field imposed.

Three theories of strength were selected for application to the data in this study from among those commonly used for correlation of combined stress behavior (such theories are discussed by Nadai (88) and Marin (89)). The theories selected were 1) maximum principal stress, 2) maximum principal strain, and 3) maximum strain energy. In this program only the data from the following asphalt concrete compositions were available to make this comparison:

1. 5.5 percent asphalt, source 11
2. 5.5 percent asphalt, source 6
3. 5.5 percent asphalt, source 11, with 3 percent polymer

Although the same three compositions were used for each test made, mix and specimen preparation procedures varied from mode to mode. Thus, a basic assumption had to be made: that the mix and specimen preparation variables have a minimal effect on asphaltic concrete behavior. Any conclusions reached were in the context of this assumption.

The application of the three failure theories selected can be tested by plotting, $\sigma_{u,m}/\sigma_{u,u}$ or $\varepsilon_{u,m}/\varepsilon_{u,u}$ against σ_2/σ_1, where:

$\sigma_{u,m}/\sigma_{u,u}$ = ratio of multiaxial to uniaxial ultimate stress

$\varepsilon_{u,m}/\varepsilon_{u,u}$ = ratio of multiaxial to uniaxial ultimate strain

σ_2/σ_1 = ratio of principal normal stresses

The data on asphaltic concrete specimens obtained in this study were plotted in this manner in Figures 8.1 and 8.2. For comparison, curves representing the three failure theories are also shown in these figures.

At low rates of strain, the maximum strain theory gives the best fit to the ultimate stress data. At high rates of strain, the failure stress points fall between the prediction of the maximum strain theory and the maximum stress theory. On the other hand, the data plotted in Figure 8.2 indicate that ultimate shear strain and ultimate strain in the hydrostatic tension test are significantly higher than either the maximum principal strain or maximum principal stress theories would predict. Accordingly, these data indicate that reliable prediction of asphaltic concrete mechanical behavior under combined stresses from uniaxial tests cannot be made by applying these theories.

The bead test data present another way in which the effect of load axiality on asphalt failure behavior can be examined. The ultimate strain values for

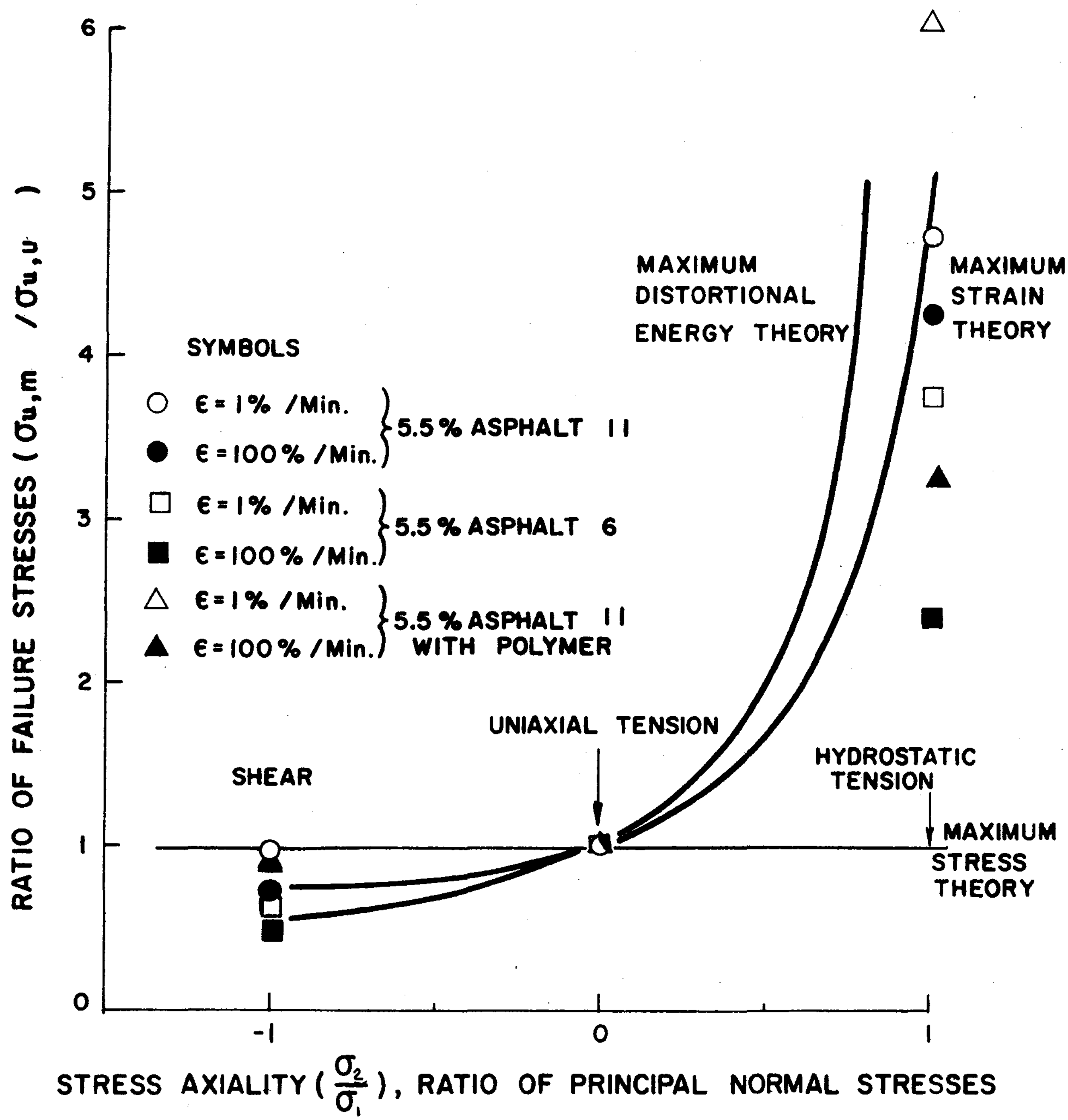

FIGURE 8.1 Effect of Stress Axiality on Ultimate Stress of Asphaltic Concrete

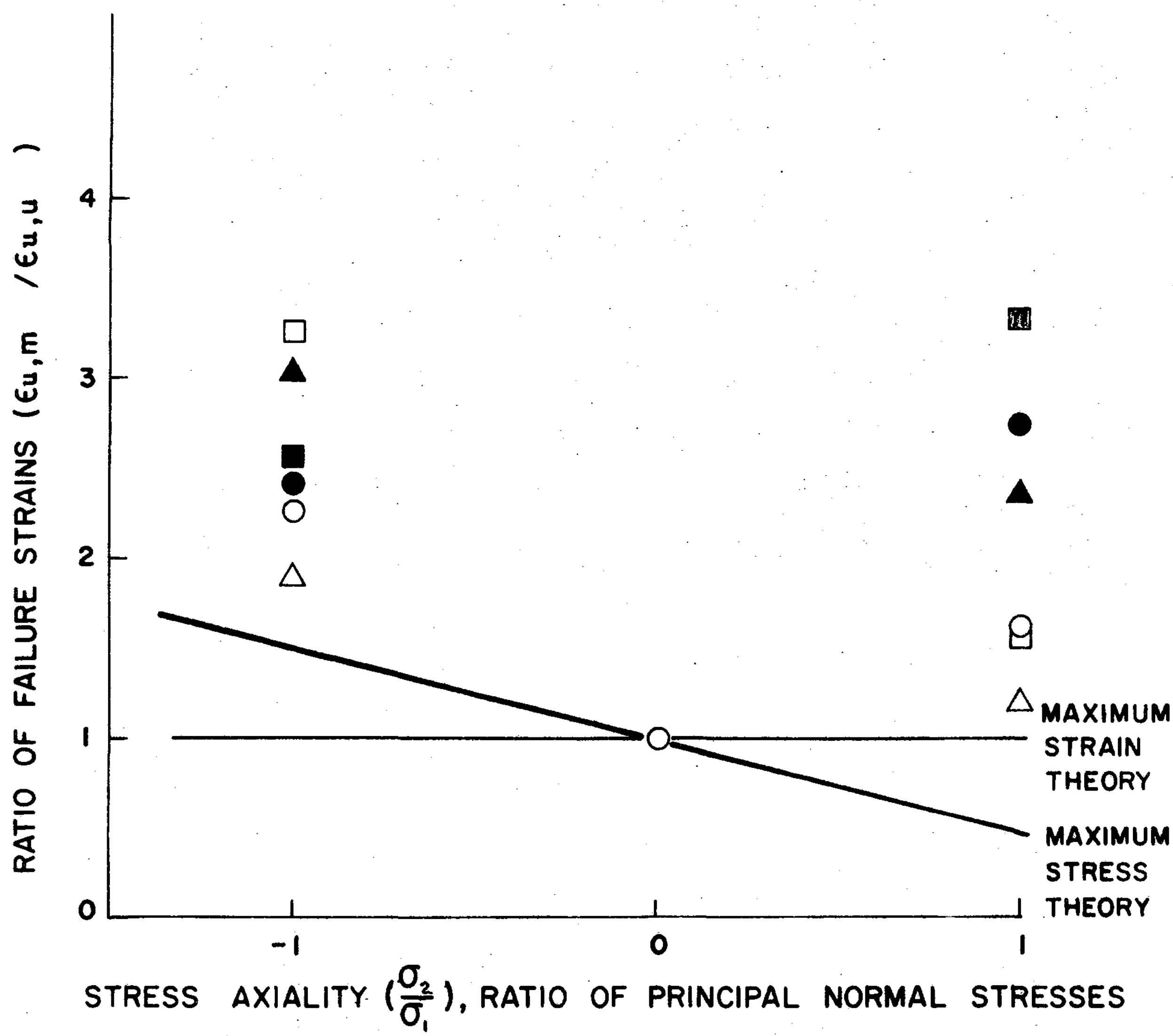

FIGURE 8. 2 Effect of Stress Axiality on Ultimate Strain of Asphaltic Concrete

asphalt 6 from the bead tests, at various strain rates, were divided by the corresponding ultimate strain obtained for asphalt concrete mixtures containing 5.5 percent asphalt 6 to determine an ultimate strain ratio. This ratio is plotted against strain rate for each of the test modes in Figure 8.3. Comparison of the curves demonstrates primarily that there is a marked difference in sensitivity of asphalt failure behavior to strain rate among the various test modes investigated in this program. Thus the need for determining asphalt behavior in multiaxial as well as uniaxial stress fields is indicated again. Additionally, these data suggest that the bead test should be run at more than one strain rate.

Effect of stress axiality on the relative ranking of the three asphaltic concrete compositions noted above was also investigated by:

1. Calculating, for each test mode, a relative value of modulus or failure parameter determined by dividing a given test value by the corresponding test value obtained from specimens of mixes of 5.5 percent asphalt 11. For example, at a strain rate of 1 percent/min the ultimate shear stress obtained from a mix of 5.5 percent asphalt 6 was 18.2 psi. The corresponding ultimate shear stress for mix 11 was 20.2 psi. The relative value of ultimate shear stress for specimens of 5.5 percent asphalt 6 was therefore 18.2/20.2 = 0.90.
2. Comparing the relative values of these performance parameters obtained in shear tests ($\sigma_2/\sigma_1 = -1$), uniaxial tensile tests ($\sigma_2/\sigma_1 = 0$), and hydrostatic tensile tests ($\sigma_2/\sigma_1 = 1$) for 1 percent/min and 100 percent/min strain rates.

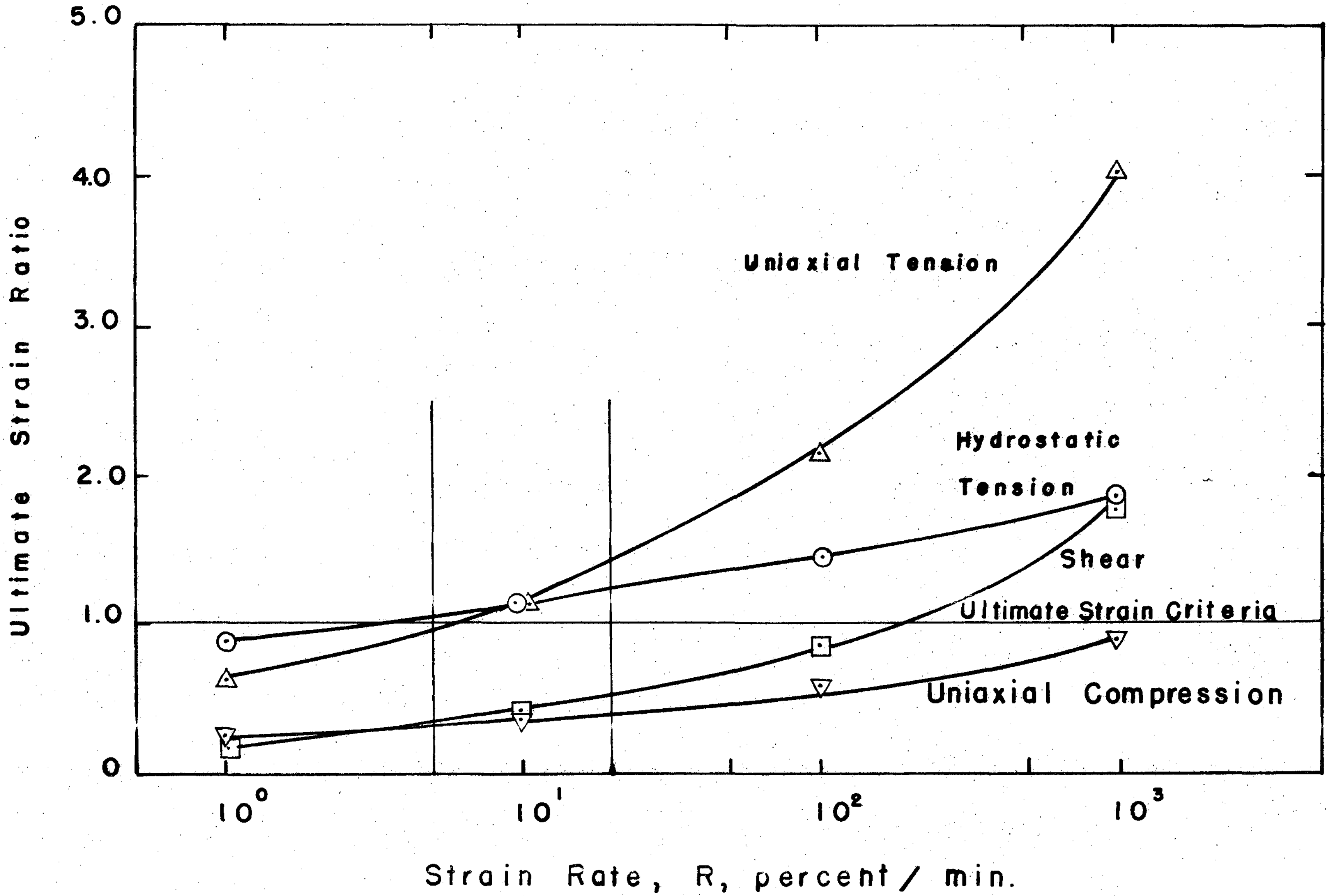

Ultimate Strain Ratio
5.0
4.0
3.0
2.0
1.0
0
Uniaxial Tension
Hydrostatic
Tension
Shear
Ultimate Strain Criteria
Uniaxial Compression
10^0
10^1
10^2
10^3
Strain Rate, R, percent / min.

3. Making a similar relative rating and comparison of the strain rate sensitivity of the modulus and failure data, as indicated by the slope of the log parameter - log strain rate plots (Figures 7.1 through 7.8).

Figure 8.4 shows the effect of load axiality on relative ratings calculated from data obtained at 1 percent/min. Figure 8.5 presents the same kind of comparison obtained from data obtained at 100 percent/min. Figure 8.6 compares the relative rate of change of modulus and failure criteria with strain rate under the three conditions of load axiality applied in these experiments.

These comparisons indicate that the relative ranking of different asphalts will depend, to some extent, on stress axiality. For example, asphalt 6 ranks lower in relative ultimate stress and modulus than asphalt 11 in the shear test mode, but ranks higher in uniaxial and triaxial tension tests. The effect of addition of 3 percent polymer to asphalt 11 appears to be more consistent. In all cases, addition of polymer appears to increase the relative ranking of the asphalt with respect to ultimate stress and ultimate strain. However, no very consistent trends were observed in the strain rate sensitivity data. In any event, it is evident that relative ranking on the basis of behavior in uniaxial tests alone would provide an incomplete evaluation of asphalt structural performance.

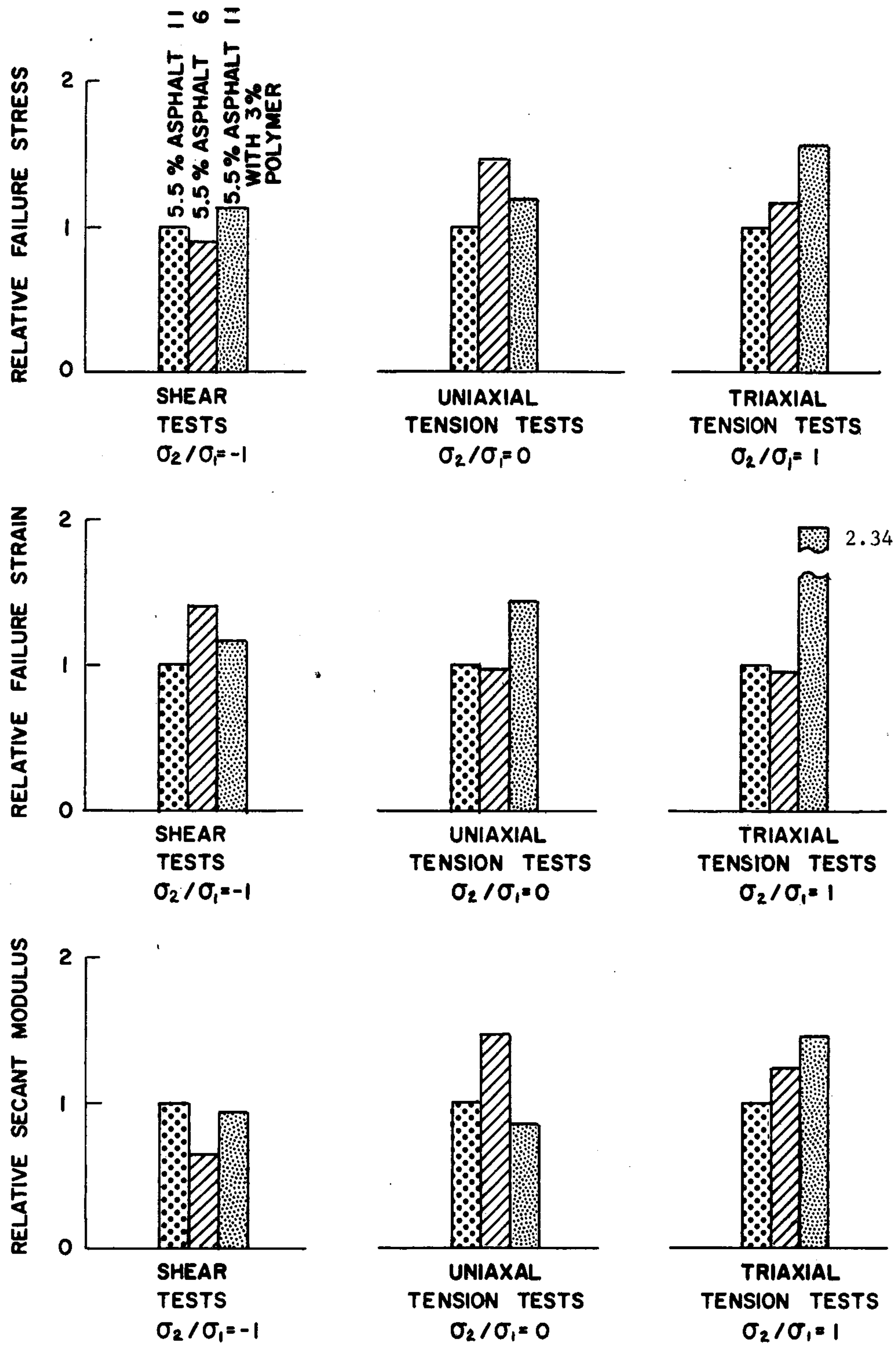

FIGURE 8.4 Effect of Load Axiality on Relative Asphalt Structural Performance: Modulus and Failure Data at 1 percent/min Strain Rate

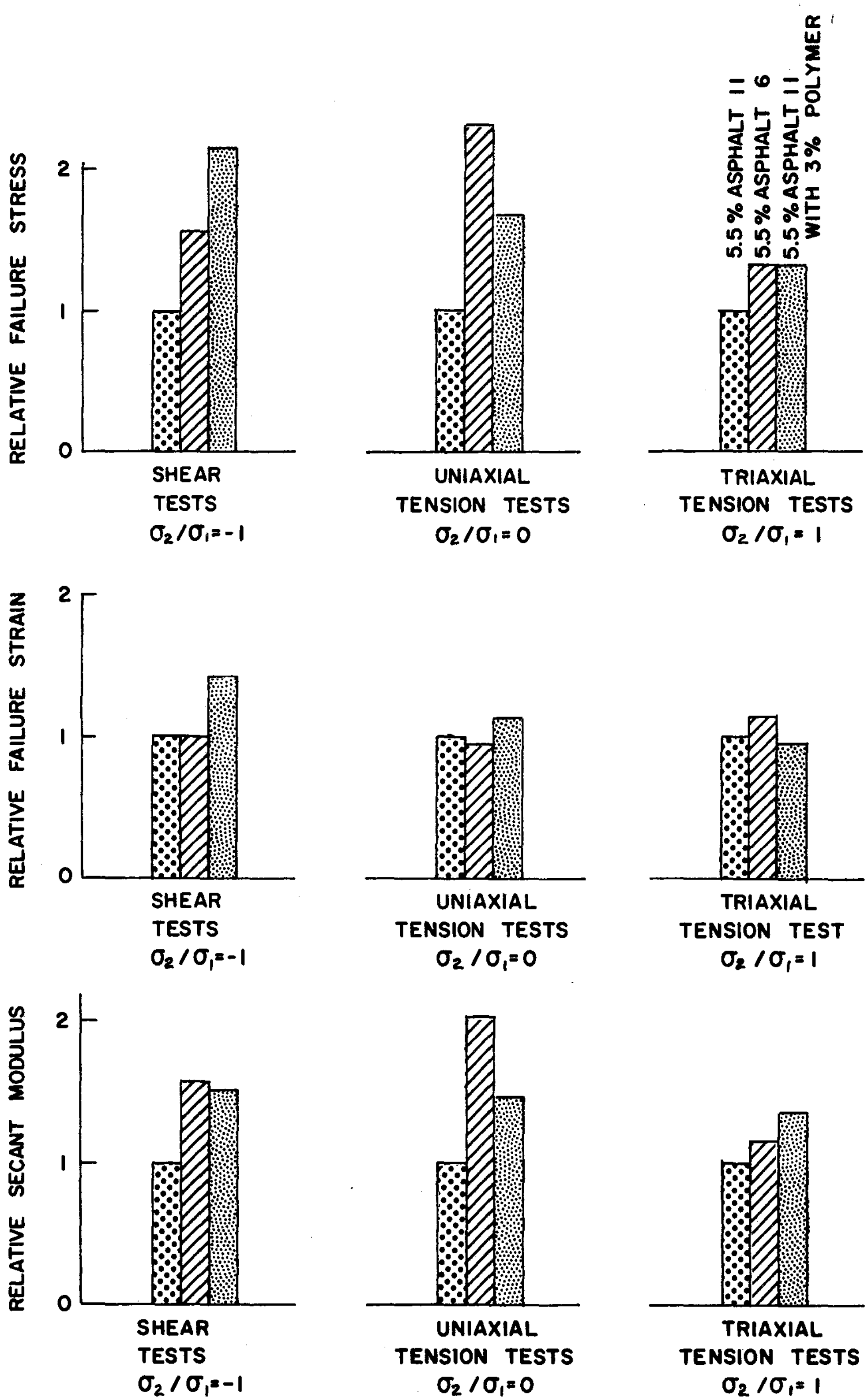

FIGURE 8.5 Effect of Load Axiality on Relative Asphalt Structural Performance: Modulus and Failure Data at 100 percent/min Strain Rate

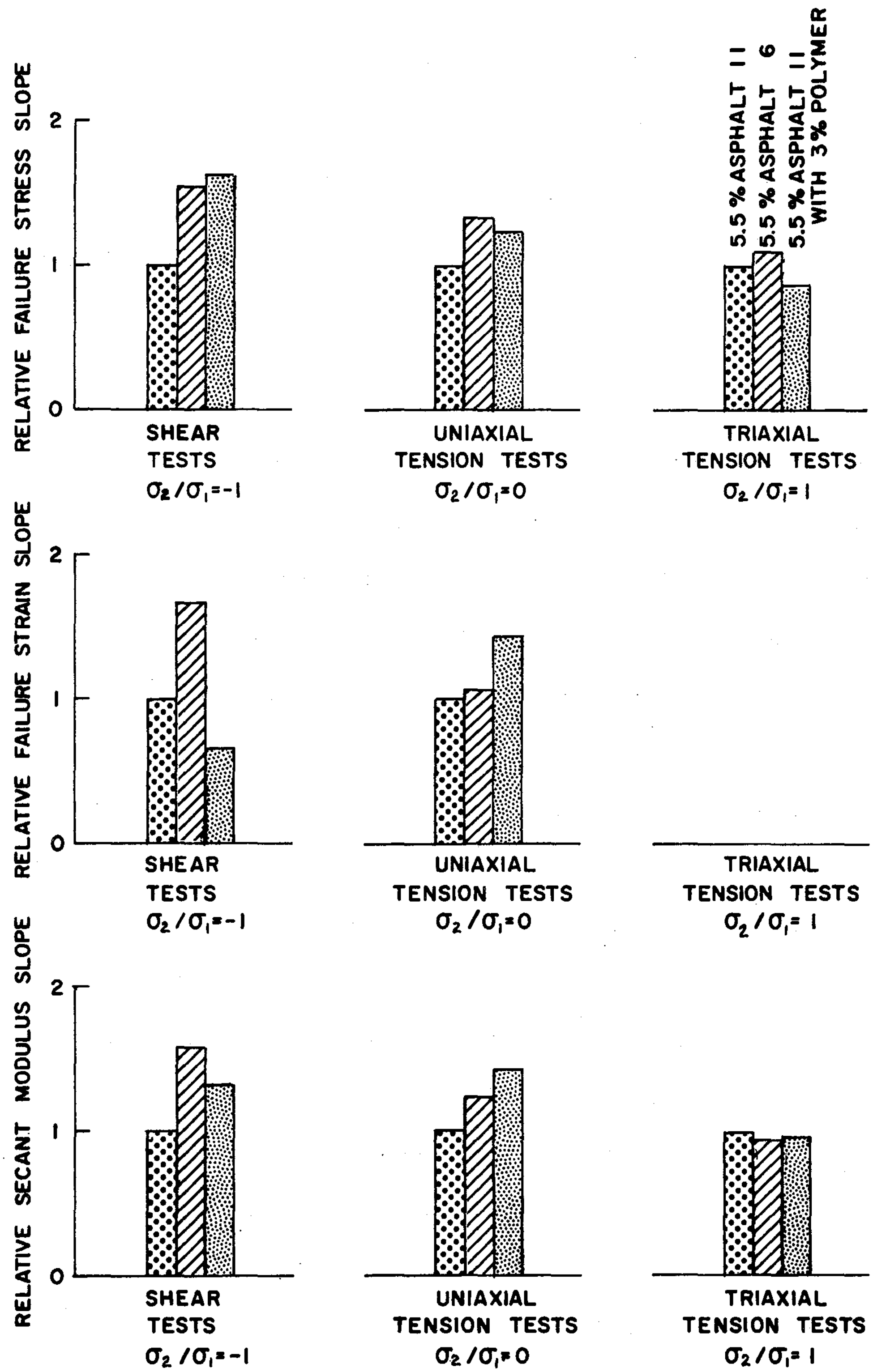

FIGURE 8.6 Effect of Load Axiality on Relative Asphalt Performance: Strain Rate Sensitivity

8.2 Effect of Asphalt Source, Additives and Content

The data presented in Figure 8.2, 8.5, and 8.6 and discussed in the preceding paragraphs indicated the effect of asphalt source and polymeric additives, as well as the effect of stress axiality, on asphalt structural performance. The evaluation can be extended further on the basis of additional data obtained in the direct uniaxial and hydrostatic tension tests.

Bar graph comparisons on the failure and modulus behavior of all of the asphaltic concrete mixes tested in direct uniaxial tention are given in Figure 8.7. In addition to the differences in uniaxial behavior of asphalt 11 and asphalt 6 previously noted, these comparisons clearly indicate that addition of 3 percent polymer to either asphalt significantly altered structural performance. However, where such addition increased ultimate stress and decreased ultimate strain with asphalt 11, it decreased ultimate stress and increased ultimate strain with asphalt 6. To resolve this apparent anomaly, an approximate strain energy density at failure was calculated for each test by multiplying ultimate stress by ultimate strain. The bar graph comparison of these data shows that addition of 3 percent polymer enhanced the structural performance of both asphalts in a uniaxial stress field. Note that this enhancement was more pronounced with asphalt 6 than with asphalt 11. However, the effect of polymer addition on modulus was not consistent; the polymer increases uniaxial tensile modulus of asphaltic concrete made with asphalt 11 and decreased the tensile modulus with asphalt 6.

As expected, a decrease of 1.5 percent in asphalt content resulted in a marked increase in ultimate strength, decrease in ultimate strain, and increase in tensile modulus.

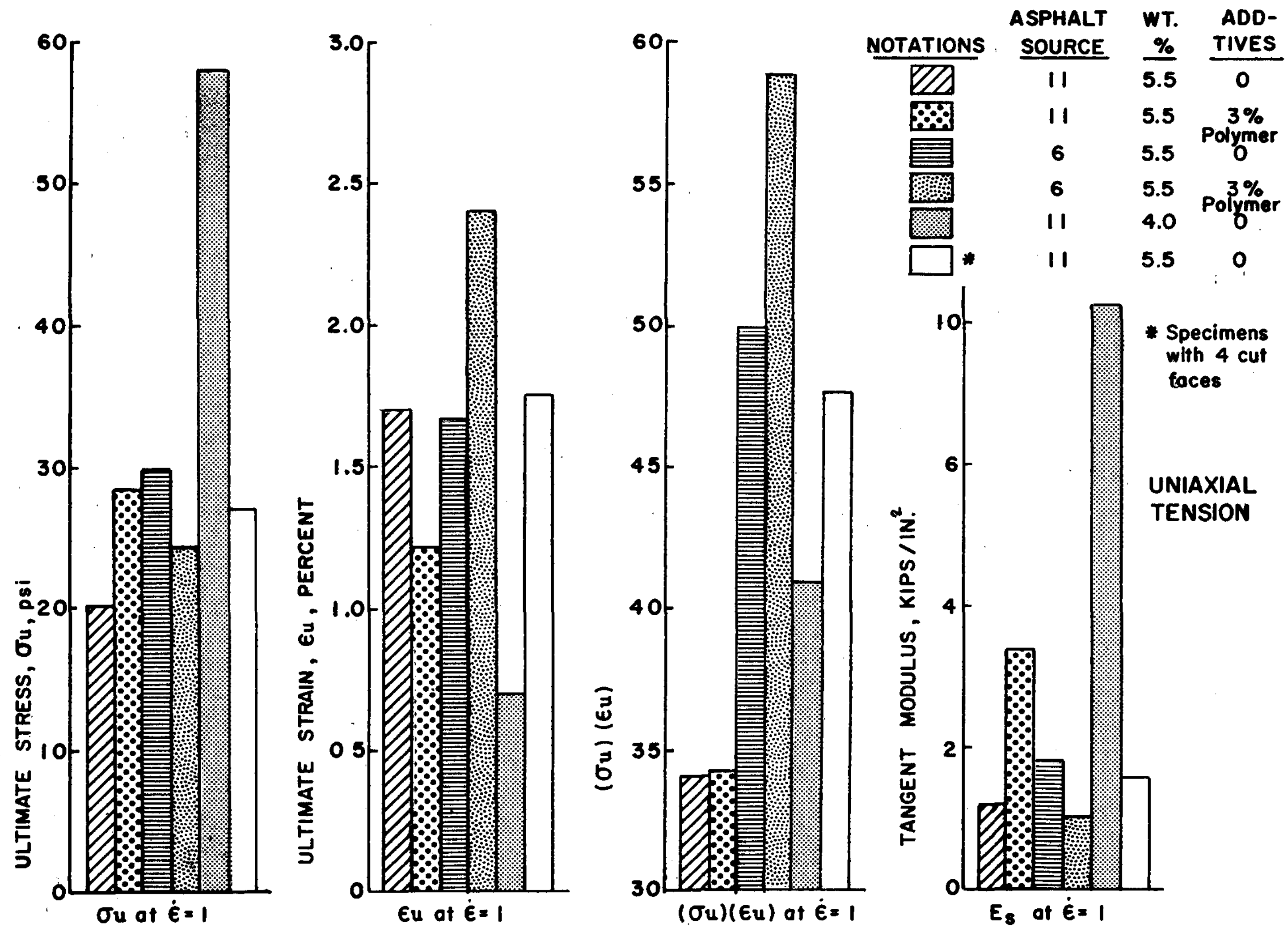

FIGURE 8.7 Effect of Asphalt Content, Source, and Additives on Uniaxial Tensile Structural Performance

The bar graphs in Figure 8.8 are presented to show a comparison of the effect of polymer addition to asphalt 6, with the effect of ground reclaimed rubber addition to the aggregate, on the modulus and failure behavior of asphaltic concrete in hydrostatic tension. All comparisons were made at a strain rate of one percent/min.

In this stress field, the addition of 3 percent polymer to asphalt 6 appeared to improve the performance. Note the marked increase in ultimate stress-ultimate strain product which occurred along with a rather small increase in modulus when the polymer addition was made.

Addition of reclaimed ground rubber to the aggregate decreases asphaltic concrete ultimate stress, increased ultimate strain, and decreased modulus. It appears that the overall effect of such additions on asphaltic concrete performance would be negligible. Accordingly, within the limits of this investigation application of reclaimed rubber in pavement construction would have to be justified on the basis of solid waste disposal rather than of enhancement of pavement structural performance.

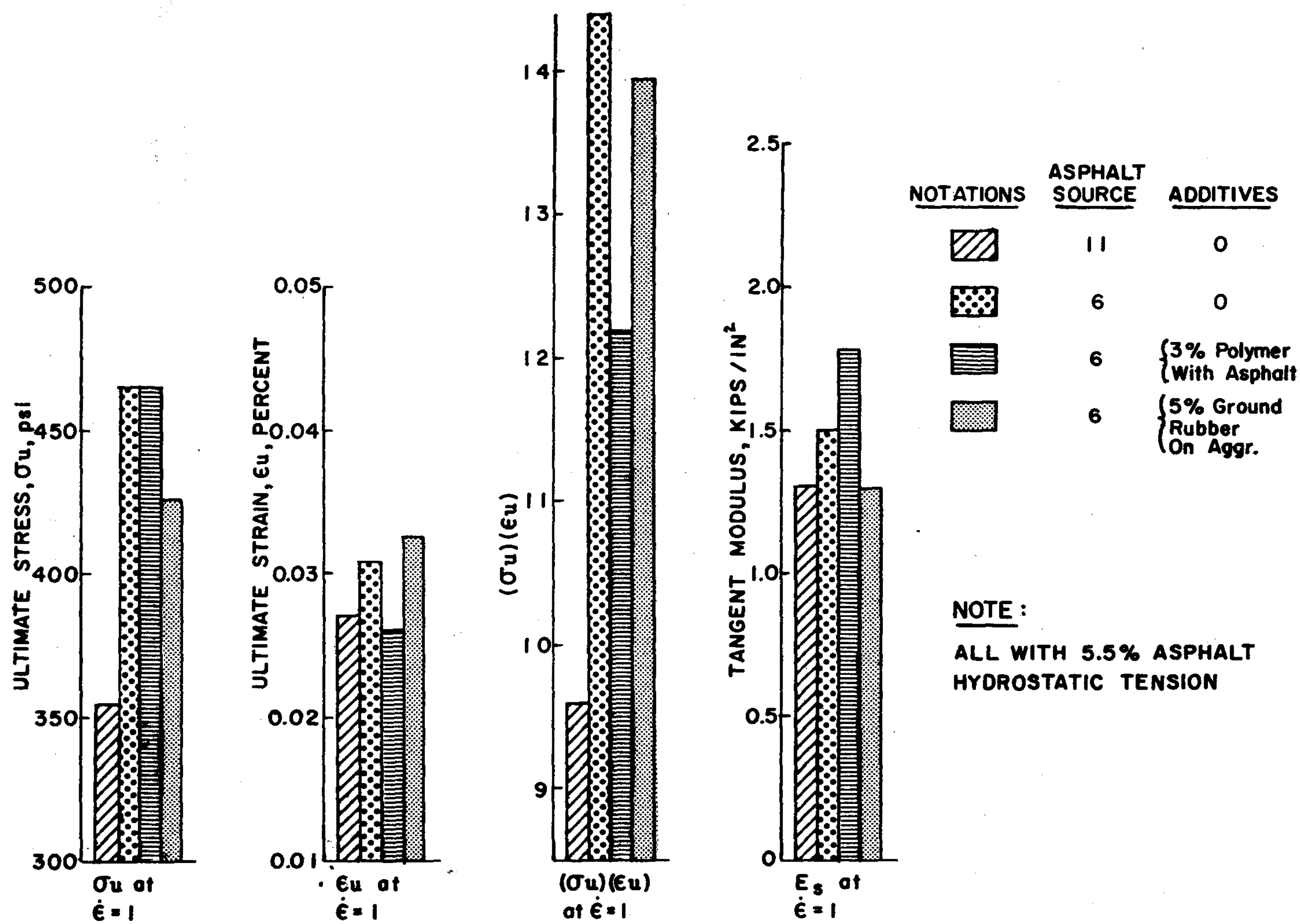

FIGURE 8.8 Effect of Asphalt Source and Additives and an Aggregate Additive on Hydrostatic Tensile Structural Performance

8.3 Viscoelastic Interpretation

In the discussion of the approach pursued in this study it was pointed out that behavior of real pavement materials was viscoelastic (i.e. time dependent) and that the time dependence must be accounted for in a rational analysis of pavement structural performance. Accordingly, viscoelastic interpretation of the modulus and failure data may be required as follows:

1) For estimation of the stress relaxation modulus (E(t)) needed for viscoelastic structural analysis.

2) To estimate a time to failure under constant stress or constant strain conditions.

3) To determine the effect of temperature variation on asphalt structural performance by application of time-temperature superposition.

If an asphaltic concrete material exhibits a simple power law dependence on strain rate and linear viscoelastic behavior, estimation of relaxation modulus and time to failure is straight forward, as shown by Smith (30,31). He begins by defining the relaxation modulus,

$$E\ (t) = \frac{\sigma(t,\varepsilon)}{\varepsilon_o}$$

and a constant strain rate modulus,

$$F\ (t) = \frac{\sigma(t,\varepsilon)}{\varepsilon}$$

where

$\sigma(t,\varepsilon)$ = stress level as a function of time and strain level

ε = strain level

ε_o = constant strain level in a stress relaxation experiment

He then assumes a simple power law relation for F(t),

$$F(t) = at^{-b}$$

where a, and b are experimentally determined constants and $t = \varepsilon/\dot{\varepsilon}$.

The two time dependent moduli are related by the equation

$$E(t) = F(t) \left[1 + \frac{d \ln F(t)}{d \ln t} \right]$$

In Figures 7.1 through 7.8, the strain rate dependence of secant modulus (E_s) was shown to follow the simple power law,

$$E_s = a_1 \dot{\varepsilon}^{b_1}$$

similarly,

$$\varepsilon = a_2 \dot{\varepsilon}^{b_2}$$

The constants a_1, a_2, b_1 and b_2 for each test are given in the referenced figures. Smith (30,31) then shows that the relaxation modulus can be represented by,

$$E(t) = a\,(1-b)t^{-b}$$

where

$$a = a_1 a_2^{\,b}$$

$$b = \frac{b_1}{1-b_2}$$

He then uses the following approach to relate time to failure in a constant stress (creep) test to constant strain rate data,

1) Call the ultimate stress (constant strain rate): σ_b, the corresponding ultimate strain: ε_b, and the time to failure: $t_{crb} = \varepsilon_b/\dot{\varepsilon}$.

2) In a constant stress (creep) test where $\sigma_0 = \sigma_b$, failure will occur when the strain has increased to ε_b. Call the time to reach this point t_{cb}.

3) Then,

$$\ln t_{cb} = \ln t_{crb} + \frac{1}{b} \ln \left[\frac{\pi b(1-b^2)}{\sin \pi b} \right].$$

As an example of the application of these relations, the time to failure--stress relations were estimated from the constant strain rate test data from double lap shear, direct tension, direct compression, and splitting tension tests run in this study. The resulting equations and stress-time to failure plots are presented in Figures 8.9 through 8.14. Actual creep tests were not conducted to verify these predictions. However, such verification would be worth-while because, if the prediction could be checked within engineering accuracy (say ± 10 percent), then asphaltic concrete behavior could be evaluated by means of constant load (creep) tests which require very simple apparatus.

The experiments in this study were conducted at constant temperature (76°F) but complete evaluation of asphalt structural performance will require knowledge of temperature effects. It has been demonstrated that the effects of temperature and time (e.g. strain rate) are interrelated in viscoelastic materials. Thus determination of the effect of temperature for asphaltic concrete can be simplified by application of time-temperature superposition. This principle has been outlined by Smith (94), Ferry (91), and Williams, Landel, and Ferry (92). Application of time-temperature superposition to correlation of the structural behavior of asphaltic concrete has been discussed by Haas (93,95), Schmidt (96), Marek (97), Majidzadeh (98) and Brodnyan (99). One of the most comprehensive

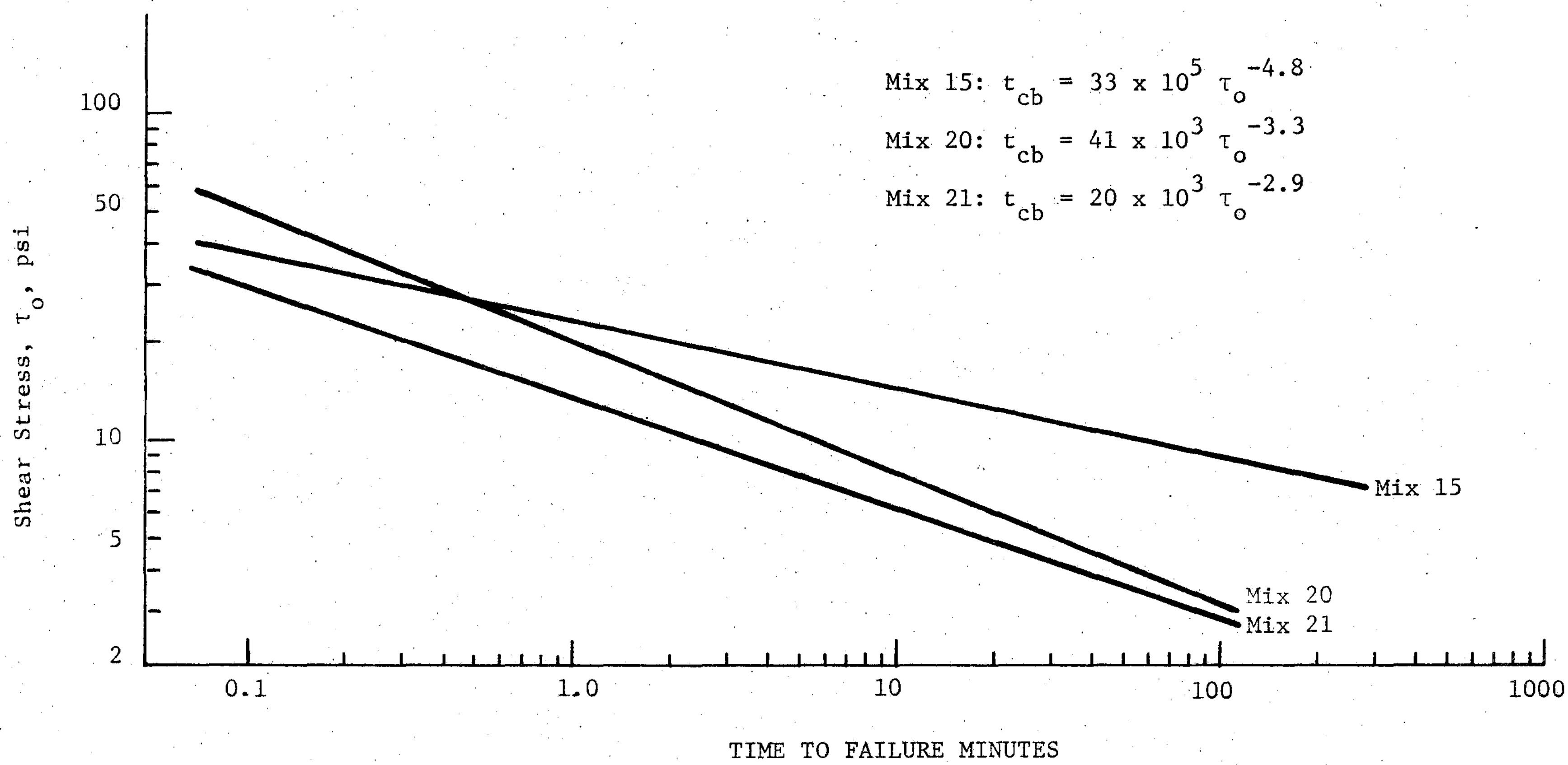

FIGURE 8.6 Estimated Time to Failure at Constant Shear Stress

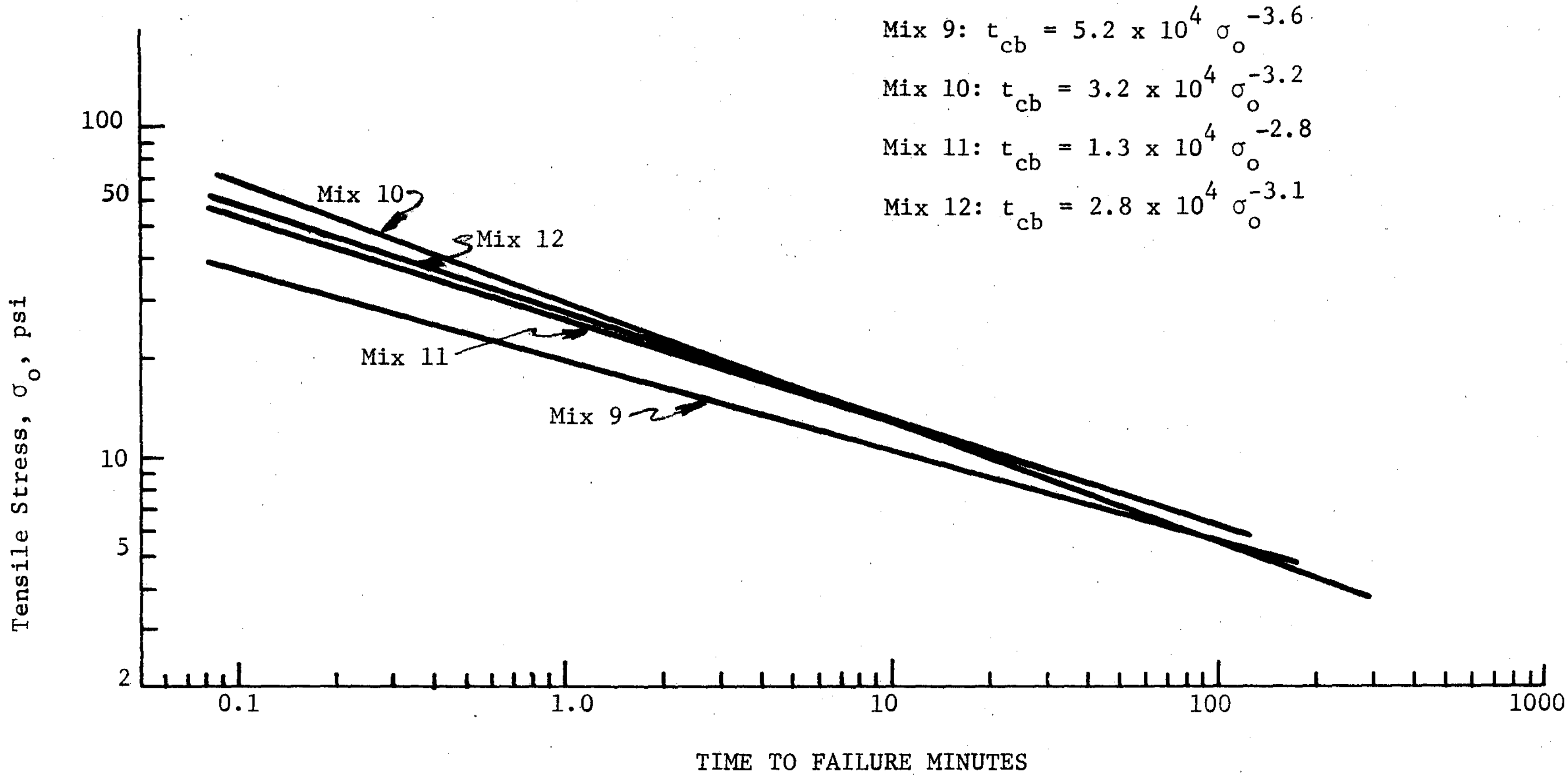

FIGURE 8.10 Estimated Time to Failure at Constant Uniaxial Tensile Stress

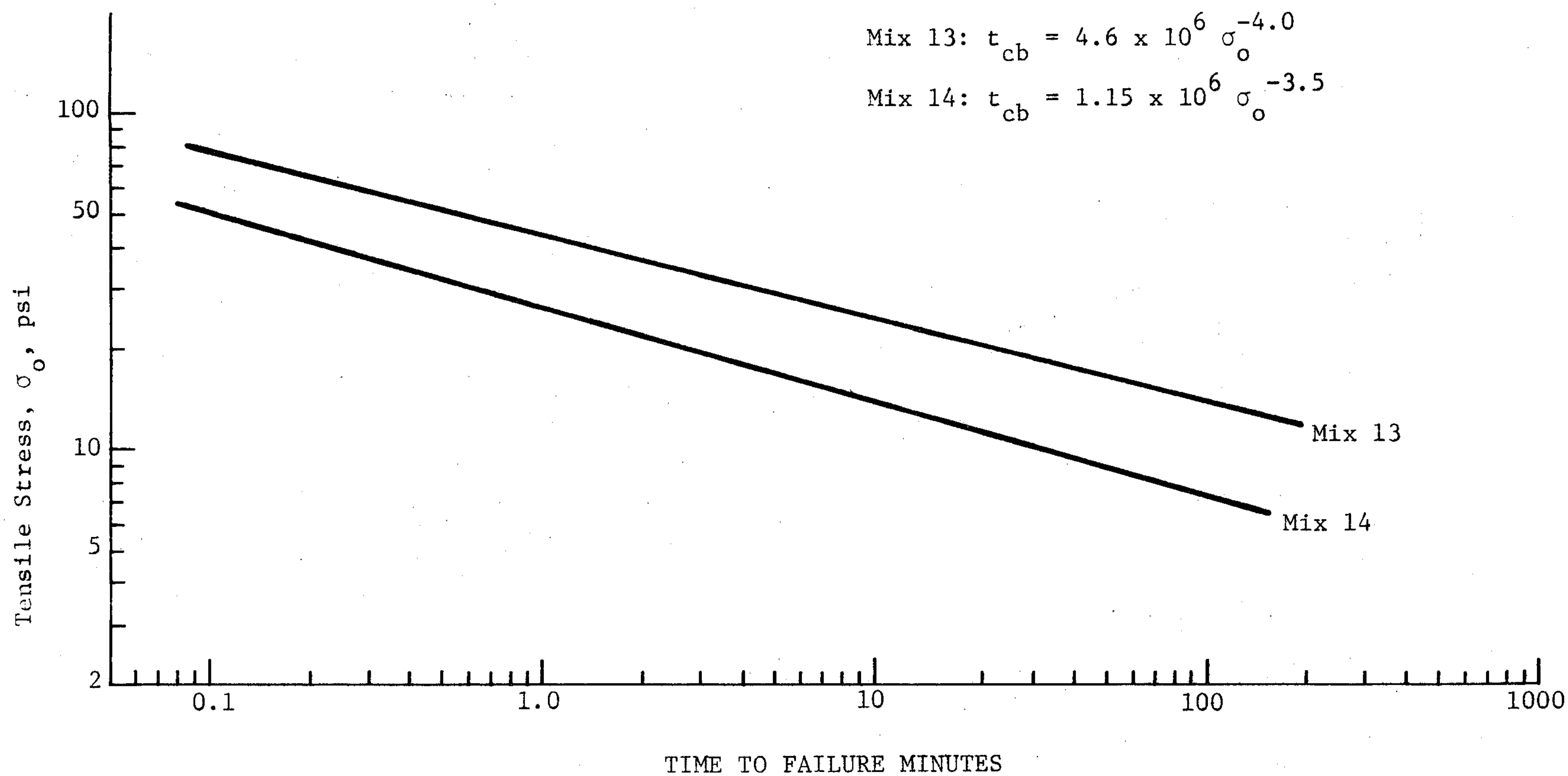

FIGURE 8.11 Estimated Time to Failure at Constant Uniaxial Tensile Stress

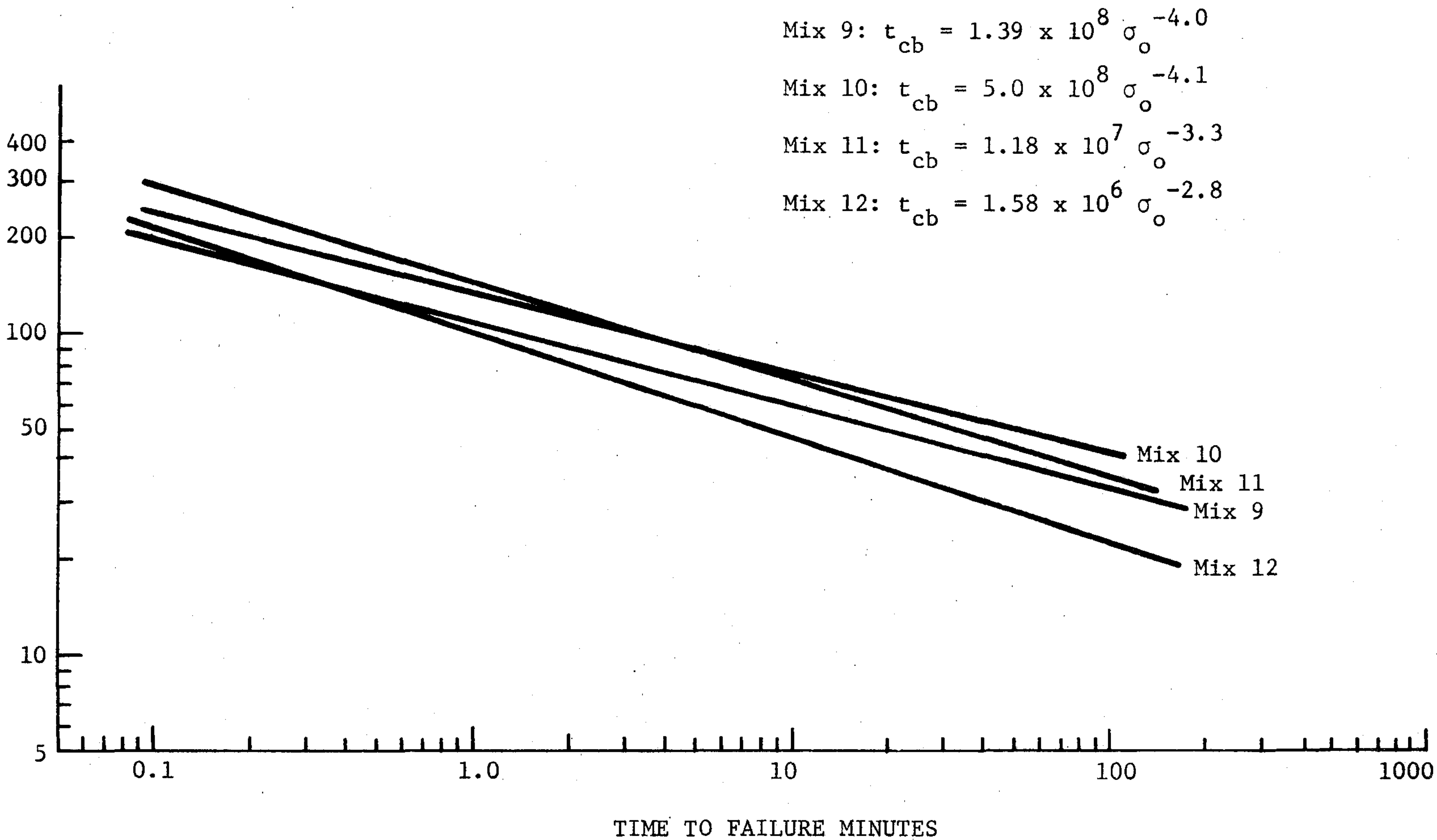

FIGURE 8.12 Estimated Time to Failure at Constant Uniaxial Compressive Stress

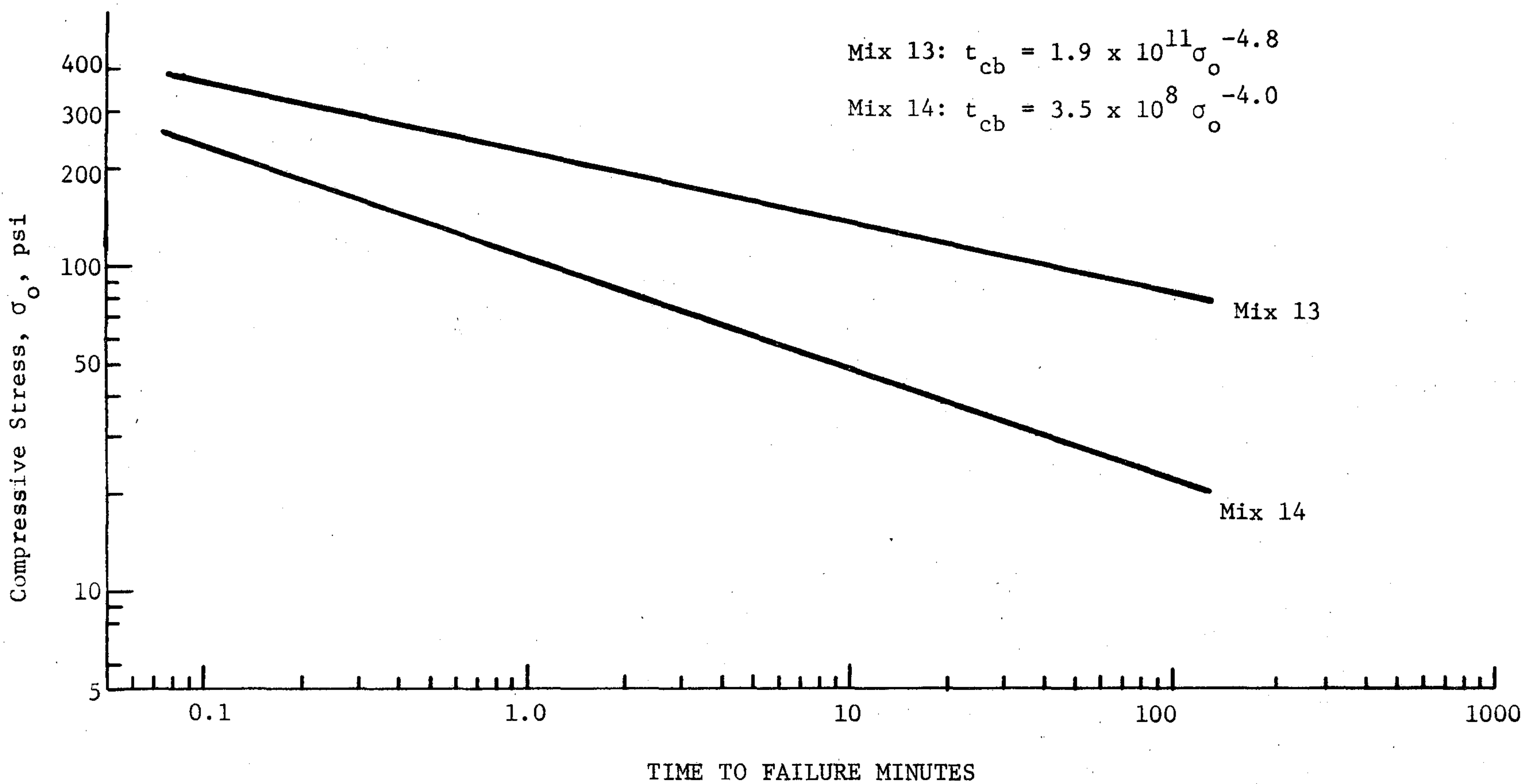

FIGURE 8.13 Estimated Time to Failure at Constant Uniaxial Compressive Stress

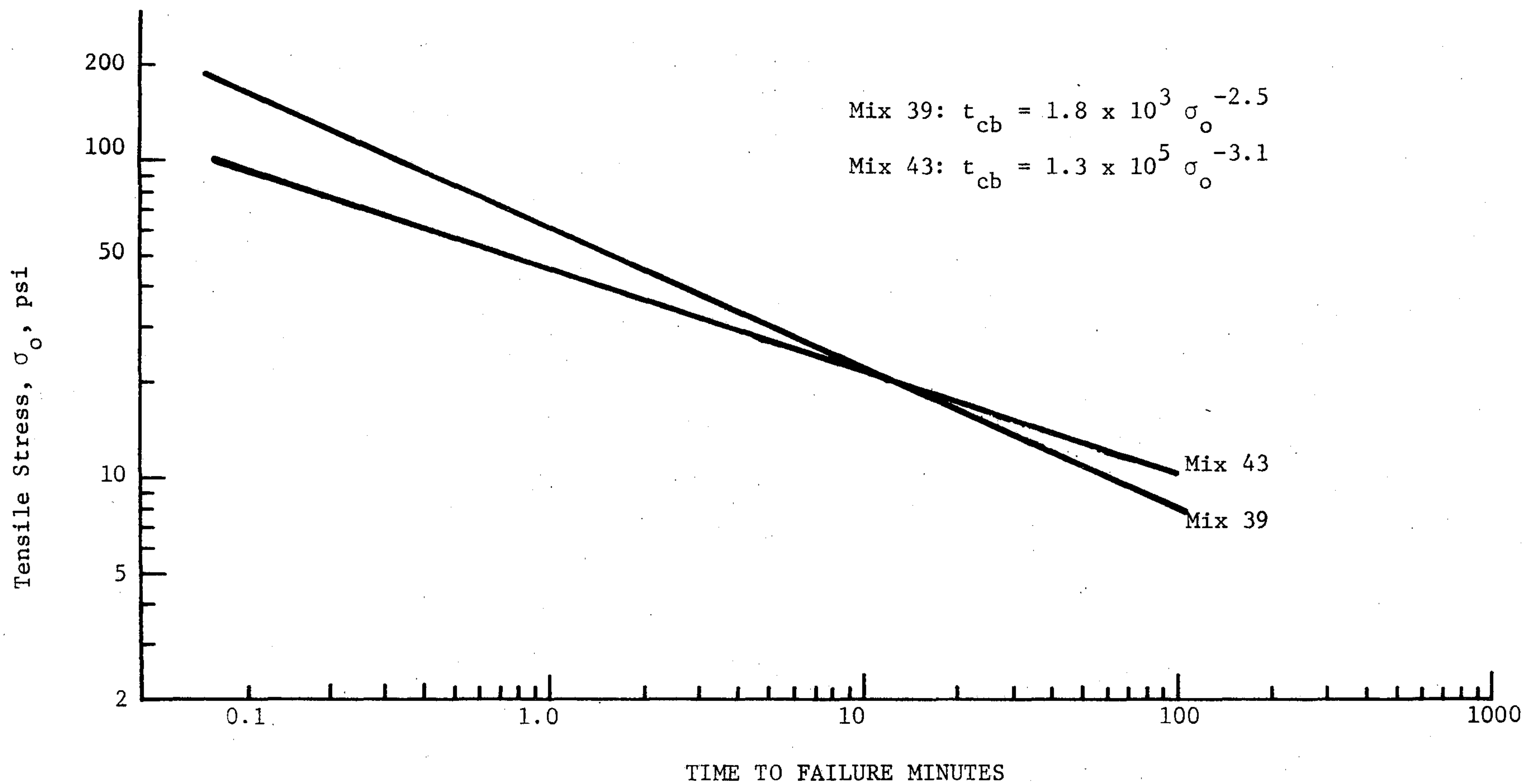

FIGURE 8.14 Estimated Time to Failure at Constant Uniaxial Tensile Stress (Splitting Tension Test)

studies was done by Alexander (100) who performed creep, relaxation, and constant strain rate tests on uniaxial tensile specimens of asphaltic concrete over a temperature range of 40°F to 110°F. He reported that all of his data could be superposed by using a shift factor which varied with temperature by a simple power law.

8.4 Application Potential

The determination of performance requirements of asphaltic material for a flexible pavement surface course was approached in this study be examining several tests for evaluation of the basic mechanical behavior of asphaltic concrete specimens. These tests were selected to reproduce the actual states of stress and strain in the pavement. In assessing the results of this study in terms of the ultimate usefulness of this approach, several questions were considered,

1) What kind of samples will truly represent the material in the pavement structure?
2) Are the test methods selected capable of giving accurate results with acceptable repeatability?
3) Are the results produced by those test methods sensitive to significant differences in asphalt structural performance?
4) How practical are the test methods for routine evaluation of asphalt structural performance?

Some of the answers to these questions have been considered in the foregoing discussion of test results and interpretation. They will be given a summary review in the following paragraphs.

All of the samples tested in this study were produced by laboratory mixing and compacting procedures which are supposed to reproduce asphaltic concrete made in the field. While these methods had been developed previously for this express purpose, no data were available to compare laboratory and field results, particularly with respect to the test methods used in this study. Obviously, this is one point which should be clarified before the approach proposed in this study could be considered to be ready for practical application.

Additionally, even when it is shown that laboratory preparation truly represents field produced asphaltic concrete, the data would be useful only in estimating the pavement performance immediately after construction. The chemical and physical changes that occur as time increases would be completely missing, and should be evaluated. One way to do this would be to compare test results on samples taken from a surface course after various time intervals with the results of similar samples subjected to an appropriate laboratory procedure simulating environmental conditions affecting the pavement.

A judgment and evaluation of the application potential of the proposed test methods was made on the basis of the practicality of the sample preparation procedures, the feasibility of the testing procedures, and the potential reliability and significance of the test results for evaluating asphalt cement structural performance. Such a summary and evaluation is presented in Table 8.1 . In general, it is believed that adequate uniaxial performance data can be obtained most practically by use of the splitting tension test. The double lap shear has the possibility of giving excellent data in a practical way. However, in this case, additional development relative to details of the test procedure appears to be necessary. The hydrostatic tension test clearly requires the most development effort before this procedure could be considered for practical application. In particular, attention should be given to sample preparation procedures and means of deformation measurement to make the "poker chip" test a reliable and practical method for measuring asphalt structural performance. In fact, it is believed that progress could be made most rapidly with the bead test version of this method.

TABLE 8.1 Summary Evaluation of Test Techniques

	REPEATABILITY		SENSITIVITY		PRACTICAL APPLICATION		
					EQUIPMENT		TEST
TEST	MODULUS	FAILURE	MODULUS	FAILURE	AS RUN(a)	MODIFIED(b)	TIME
Direct Uniaxial Tension/ Compression	Good	Good	Excellent	Good	Fair	Good	Good
Splitting Tension	Good	Good	Excellent	Good	Fair	Good	Excellent
Hydrostatic Tension	Fair	Poor-Fair	Poor	Fair	Fair	Fair	Good
Shear	Good	Good	Good	Fair	Fair	Good	Fair
Bead Test	Poor	Good	Not evaluated but correlation with other tests indicated		Fair	Good	Good

(a) Tests run with an Instron universal tester.

(b) Methods modified to obtain results from constant load (creep) test procedures.

9.0 CONCLUSIONS AND RECOMMENDATIONS

The experimental data and resulting analysis in this study indicate that:

1) Test methods are available which can be applied to reliably evaluate asphalt structural performance in a fundamental way. The test methods examined in this study are sensitive to significant differences in asphalt content and asphalt structural performance. Thus, these methods can be applied to obtain basic pavement design data, select asphaltic materials, and for asphalt quality control. However, additional research related to details of sample preparation, test procedure, and analysis of results should be completed before this approach can be put to practical use. Additionally, a cyclic loading (fatigue) method should be included in any complete asphalt structural performance evaluation scheme.

2) All of the test methods applied in this study give more reliable ultimate stress data than ultimate strain data, and more reliable secant modulus values than tangent modulus values. Improved methods of measuring sample deformation during test should improve the precision of the ultimate strain data.

3) Relative structural performance of asphaltic concrete will vary with stress axiality. Also, it appears that there is no consistent relation between uniaxial and multiaxial mechanical behavior. Accordingly, asphalt cement structural performance cannot be judged solely on the basis of uniaxial test results; a combination of several test modes is necessary for adequate performance evaluation.

4) Asphaltic concrete modulus and failure data demonstrate a simple power law dependence on strain rate. Such dependence implies that linear viscoelastic

behavior for this material is a reasonable engineering assumption. It also suggests that the test procedures might be simplified by substitution of a constant load (creep) schedule for the more commonly applied constant strain rate schedule.

5) Additions of elastomeric polymers (synthetic and natural rubber and the like) have a significant effect on asphalt cement structural performance. Failure behavior is improved but such additions may either increase or decrease the elastic modulus, depending on the base asphalt source.

6) Based on limited experiments performed in this study, substitution of ground reclaimed rubber for part of the aggregate has little effect on the mechanical behavior of asphaltic concrete. Thus such substitution should be justified primarily on the basis of being a possible method for solid waste disposal.

As a result of the findings of this study, the following recommendations are made:

1) Serious consideration should be given to application of the fundamental approach to asphalt structural performance, as proposed in this study, for acquisition of basic pavement design data, selection of asphalt cements, and for asphalt quality control. However, the required additional research to further develop and improve the test methods should be supported to completion so that this scheme can be applied in a practical way and with confidence.

2) Methods of sample preparation should be studied carefully, with respect to how well the samples represent asphaltic concrete produced in highway construction as well as to improvement of the accuracy and precision of the test methods themselves.

3) Further research on test methods to be used in the fundamental evalu-

and fatigue test methods.

4) The application of structural performance evaluation methods should be extended to include the study of the effects of asphalt aging on both field and laboratory samples.

10.0 REFERENCES

1. Nair, K., Chang, C-Y., Hudson, W. R., and McCullough, B. F., "Translating AASHO Road Test Findings - Basic Properties of Pavement Components," Final Report, NCHRP Projects 1-10 and 1-10/1, Materials Research and Development, Inc., August 1970.

2. Hudson, W. R., McCullough, B. F., Scrivner, F. H., and Brown, J. L., "A Systems Approach Applied to Pavement Design and Research," Research Report 123-1, Texas Highway Department, Center for Highway Research and Texas Transportation Institute, March 1970.

3. Burmister, D. H., "The Theory of Stress and Displacements in Layered Systems and Application to the Design of Airport Runways," Proceedings, Highway Research Board, Vol. 23, 1943, pp. 126-128.

4. Hank, R. J., and Scrivner, F. H., "Some Numerical Solutions of Stresses in Two and Three-Layered Systems," Proceedings, Highway Research Board, Vol. 28, 1948, pp. 457-468.

5. Acum, W. E. A., and Fox, L., "Computation of Load Stresses in a Three-Layered System," Geotechnique, Vol. 2, 1951, pp. 293-300.

6. Scrivner, F. H., Moore, W. M., McFarland, W. F., and Carey, G. P., "A Systems Approach to the Flexible Pavement Design Problem," Research Report 32-11, Texas Transportation Institute, February 1969.

7. Scrivner, F. H., and Moore, W. M., "An Empirical Equation for Predicting Pavement Deflections," Research Report 32-12, Texas Transportation Institute, February 1969.

8. Scrivner, F. H., and Michalak, C. H., "Flexible Pavement Performance Related to Deflections, Axle Applications and Foundation Movements," Research Report 32-13, February 1969.

9. Jeuffroy, G., and Bacheley, J., "Note on a Method of Analysis of Pavements," Proceedings, 1st Intl. Conf. on Structural Design of Asphalt Pavements, 1962, pp. 300-309.

10. Whiffin, A. C., and Lister, N. W., "The Application of Elastic Theory to Flexible Pavements," Proceedings, 1st Intl. Conf. on Structural Design of Asphalt Pavements, 1962, pp. 499-521.

11. Livneh, M., and Schlarsky, E., "The Bearing Capacity Asphaltic Concrete Carpets Surfacing," Proceedings, 1st Intl. Conf. on Structural Design of Asphalt Pavements, 1962, pp. 345-353.

12. Skok, E. L., and Finn, F. N., "Theoretical Concepts Applied to Asphalt Pavement Design," Proceedings, 1st Intl. Conf. on Structural Design of Asphalt Pavements, 1962, pp. 412-440.

13. McLeod, N. W., "Rational Design of Bituminous Paving Mixtures with Curved Mohr Envelopes," Proceedings, Association of Asphalt Paving Technologists, Vol. 21, 1952, pp. 349-437.

14. McLeod, N. W., "Some Basic Problems in Flexible Pavement Design," Proceedings, Highway Research Board, Vol. 32, 1953.

15. Jones, A., "Tables of Stresses in Three-Layer Elastic Systems," Bulletin 342, Highway Research Board, 1962, pp. 176-214.

16. Peattie, K. R., "Stress and Strain Factors for Three-Layer Elastic Systems," Bulletin 342, Highway Research Board, 1962, pp. 215-253.

17. Peattie, K. R., "A Fundamental Approach to the Design of Flexible Pavements," Proceedings, 1st Intl. Conf. on Structural Design of Asphalt Pavements, 1962, pp. 403-411.

18. Dormon, G. M., "The Extension to Practice of a Fundamental Procedure for the Design of Flexible Pavements," Proceedings, 1st Intl. Conf. on Structural Design of Asphalt Pavements, 1962, pp. 785-793.

19. Pister, K. S., and Westmann, W. A., "Analysis of Viscoelastic Pavements Subjected to Moving Loads," Proceedings, 1st Intl. Conf. on Structural Design of Asphalt Pavements, 1962, pp. 522-529.

20. Dormon,G. M., and Edwards, J. M., "Developments in the Application in Practice of a Fundamental Procedure for the Design of Flexible Pavements," Proceedings, 2nd Intl. Conf. on the Structural Design of Asphalt Pavements, 1967, pp. 99-107.

21. Perloff, W. H., and Moavenzadeh, F., "Deflection of Viscoelastic Medium Due to a Moving Load," Proceedings, 2nd Intl. Conf. on the Structural Design of Aspahlt Pavement, 1967, pp. 269-276.

22. Alfrey, T., and Doty, P., "The Methods for Specifying the Properties of Viscoelastic Materials," Journal of Applied Physics, Vol. 16, 1945, pp. 700-713.

23. Lee, E. H., "Stress Analysis in Viscoelastic Bodies," Quarterly of Applied Materials, Vol. 13, 1955.

24. Bland, D. R., The Theory of Linear Viscoelasticity, Pergamon Press, New York, 1960.

25. Ashton, J. E., and Moavenzadeh, F., "Analysis of Stresses and Displacements in a Three-Layered Viscoelastic System," Proceedings, 2nd Intl. Conf. on the Structural Design of Asphalt Pavements, 1967, pp. 209-219.

26. Huang, Y. H., "Stresses and Displacements in Viscoelastic Layered Systems Under Circular Loaded Areas," Proceedings, 2nd Intl. Conf. on the Structural Design of Asphalt Pavements, 1967, pp. 225-244.

27. Ishihara, K., and Kimura, T., "The Theory of Viscoelastic Two-Layer Systems and Conception of Its Application to the Pavement Design," Proceedings, 2nd Intl. Conf. on the Structural Design of Asphalt Pavements, 1967, pp. 245-254.

28. Barksdale, R. D., and Leonards, G. A., "Predicting Performance of Bituminous Surfaced Pavements," Proceedings, 2nd Intl. Conf. on the Structural Design of Asphalt Pavements, 1967, pp. 321-340.

29. Williams, M. L., Blatz, P. J., and Schapery, R. A., "Fundamental Studies Relating to Systems Analysis of Solid Propellants," Graduate Aeronautical Lab, California Institute of Technology, Report SM 61-5, February 1961.

30. Smith, T. L., "Nonlinear Viscoelastic Response of Amorphous Elastomers to Constant Strain Rates," Trans. of Soc. of Rheology, Vol. 6, 1962, pp. 61-80.

31. Smith, T. L., "Tensile Properties of Elastomers," Journal of Applied Science, Vol. A1, 1963, pp. 397-615.

32. Shiffman, R. L., "The Numerical Solution for Stresses and Displacements in a Three-Layer Soil System," Proceedings, 4th Intl. Conf. on Soil Mechanics and Foundation Engineering, 1957, pp. 169-173.

33. Michelow, J., "Analysis of Stresses and Displacements in an N-Layered Elastic System Under a Load Uniformally Distributed on a Circular Area," California Research Corporation, September 1963.

34. Dieckmann, W. L., and Warren, H., "Numerical Computation of Stresses and Strains in a Multiple-Layered Asphalt Pavement System," California Research Corporation, September 1963.

35. Peutz, M. G. F., and van Klempen, H. P. M., Prepared Discussion, Session II. Proceedings, 2nd Intl. Conf. on the Structural Design of Highway Pavements, 1967, pp. 202-204.

36. Peutz, M. G. F., and van Klempen, H. P. M., and Jones, A., "Layered Systems Under Normal Surface Loads," Highway Research Record No. 228, Highway Research Board, 1968, pp. 34-45.

37. Peutz, M. G. F., Jones, A., and van Klempen, H. P. M., "Computer Program: Layered Systems Under Normal Surface Loads - BISTRO," Koniklijke/ Shell-Laboratorium, Amsterdam, May 1968.

38. Duncan, J. M., Monismith, C. L., and Wilson, E. L., "Finite Element Analysis of Pavements," Highway Research Record No. 228, Highway Research Board, 1968, pp. 18-33.

39. Westmann, R. A., "Stress Analysis by Finite Elements," Highway Research Record No. 228, Highway Research Board, 1968, pp. 46-58.

40. Bynum, D., and Traxler, R. N., "Performance Requirements of High Quality Flexible Pavements," Research Report 127-1, Texas Transportation Institute, August 1969.

41. Bynum, D., "A Thermoviscoelastic Characterization of an Asphaltic Concrete," Research Report 127-2, Texas Transportation Institute, August 1970.

42. Hutchinson, B. G., and Haas, R. C. G., "A System Analysis of the Highway Design Process," Highway Research Record No. 239, Highway Research Board, 1968, pp. 1-24.

43. Hveem, F. N., and Sherman, G. B., "California Method for the Structural Design of Flexible Pavements," Proceedings, 1st Intl. Conf. on Structural Desing of Asphalt Pavements, 1962, p. 855.

44. Stanton, T. E., and Hveem, F. N., Proceedings, Highway Research Board, Vol. 14, 1934, part II.

45. State of California, Division of Highways, Test Method No. 304D, Materials Manual 1, 1963.

46. "Standard Method of Test for Resistance to Deformation and Cohesion of Bituminous Mixtures by Means of the Hveem Apparatus," ASTM D1560-65, 1965.

47. U. S. Corps of Engineers, "Flexible Airfield Pavements," EM 1110-45-302, Pt. 12, Ch. 2, 1958.

48. "Standard Method of Test for Resistance to Plastic Flow of Bituminous Mixtures Using Marshall Apparatus," ASTM D1559-56, 1965.

49. Nijboer, L. W., "Plasticity as a Factor in the Design of Dense Bituminous Road Carpets," Elseiver Publishing Co., Amsterdam, 1948.

50. Smith, V. R., "Triaxial Stability Method for Flexible Pavement Design," Proceedings, Asphalt Paving Technologists, Vol. 18, 1949, pp. 63-94.

51. Monismith, C. L., "Some Applications of Theory in the Design of Asphalt Pavements," 5th Annual Nevada Streets and Highways Conf., University of Nevada, 1970.

52. Heukelom, W., and Klomp, A. J. G., "Road Design and Dynamic Loading," Proceedings, Association of Asphalt Paving Technologists, Vol. 33, 1965, pp. 92-123.

53. Williams, M. L., "Structural Analysis of Viscoelastic Materials," Journal of American Institute of Aeronautics and Astronautics, Vol. 2, 1964, p. 785.

54. Blatz, P. J., "The Yield Surface in Normal Stress and Normal Strain Space," Bulletin of 19th Meeting, JANAF Panel on Physical Properties of Solid Propellants, SPIA Pub. No. PP13, 1960, p. 165.

55. "The Testing of Bituminous Materials," Report of the Koniklijke/Shell Laboratorium, Amsterdam, December 1966, p. 1.

56. Goode, J. F., and Lufsey, L. A., "A New Graphical Chart for Evaluating Aggregate Gradations," Association of Asphalt Paving Technologists, Vol. 31, 1962, pp. 172-207.

57. Wood, P. R., "Rheology of Asphalts and Its Relation to Behavior of Paving Mixtures," Highway Research Record No. 192, 1967, pp. 20-25.

58. Thompson, P. D., "Merits of Adding Natural Rubber to Bituminous Road Surfacing Materials," Highway Research Record No. 273, 1969, pp. 87-98.

59. Hargett, E. R., "Basic Material Properties for the Design of Bituminous Concrete Surfaces," Proceedings, 1st Int'l Conf. Structural Design of Asphaltic Pavements, 1962, pp. 606-610.

60. Goetz, W. H., and Schaub, J. H., "Triaxial Testing of Bituminous Mixtures," ASTM Special Technical Publication NO. 252, 1959, pp. 51-69.

61. Barksdale, R. D., "A Nonlinear Theory for Predicting the Performance of Flexible Highway Pavements," Highway Research Record No. 337, 1970, pp. 22-39.

62. Jones, J. W., and Knauss, W. G., American Institute of Aeronautics and Astronautics, 6th Solid Propellant Rocket Conference, Paper 65-157, 1965.

63. Kelley, F. N., "Solid Propellant Mechanical Properties Testing, Failure Criteria, and Ageing," Advances in Chemistry Series No. 88, American Chemical Society, 1969, pp. 188-243.

64. "ICRPG Solid Propellant Mechanical Behavior Manual," CPIA, Johns Hopkins Applied Physics Laboratory, Silver Springs, Maryland, 1963.

65. Calderon, H. M., "A Possible New Approach to Develop a Mohr Diagram," Proceedings, Association of Asphalt Paving Technologists, Vol. 22, 1953, pp. 302-314.

66. Kennedy, T. W., and Hudson, W. R., "Application of the Indirect Tensile Test to Stabilized Materials," Highway Research Record No. 235, 1968, pp. 36-48.

67. Livneh, M., and Shlarsky, E., "The Splitting Test for Determination of Bituminous Concrete Strength," Proceedings, Association of Asphalt Paving Technologists, Vol. 31, 1962, pp. 457-474.

68. Calderon, H. M., "Discussion of Livneh and Schlarsky Paper (68), Proceedings, Association of Asphalt Paving Technologists, Vol. 31, 1962, pp. 474-475.

69. Tons, E., and Krokosky, E., "Tensile Properties of Dense Graded Bituminous Concrete," Proceedings, Association of Asphalt Paving Technologists, Vol. 32, 1963, pp. 497-529.

70. Carneiro, F. L. B., and Barcellos, A., "Tensile Strength of Concretes," RILEM (International Association of Testing and Research Laboratories Materials and Structures, Paris), Bulletin No. 13, March 1953, pp. 99-125.

71. Azazawa, T., "Tension Test Method for Concretes," RILEM (International Association of Testing and Research Laboratories Materials and Structures, Paris), Bulletin No. 16, November 1953, pp. 13-23.

72. "Splitting Tensile Strength of Molded Concrete Cylinders," ASTM C496-66, American Society for Testing and Materials, 1966.

73. Breen, J. J., and Stephens, "Split Cylinder Test Applied to Bituminous Mixtures at Low Temperatures," Journal of Materials, Vol. 1, 1966, pp. 66-76.

74. Livneh, M., and Schlarsky, E., "The Splitting Test for Determination of Bituminous Concrete Strength," Proceedings, Association of Asphalt Paving Technologists,Vol. 31, 1962, pp. 457-474.

75. Hadley, W. O., Hudson, W. R., and Kennedy, T. W., "An Evaluation of Factors Affecting the Tensile Properties of Asphalt-Treated Materials," Research Report 98-2, Center for Highway Research, The University of Texas, Austin, March 1969.

76. Hadley, W. O., Hudson, W. R., and Kennedy, T. W., "Correlation of Tensile Properties with Stability and Cohesiometer Values for Asphalt-Treated Materials," Research Report 98-6, Center for Highway Research, The University of Texas, Austin, June 1970.

77. Hadley, W. O., and Hudson, W. R., and Kennedy, T. W., "A Method of Estimating Tensile Properties of Materials Treated in Indirect Tension," Research Report 98-7, Center for Highway Research, The University of Texas, Austin, July 1970.

78. Hadley, W. O., Hudson, W. R., and Kennedy, T. W., "A Statistical Experiment to Evaluate Tensile Properties of Asphalt-Treated Materials," Proceedings, Association of Asphalt Paving Technologists, Vol. 38, 1969, pp.

79. Lindsey, G. H., Schapery, R. A., and Williams, M. L., and Zak, A. R., "The Triaxial Tension Failure of Viscoelastic Materials," Report ARL 63-152, Aerospace Research Laboratories, U. S. Air Force, September 1963.

80. Lindsey, G. H., "Triaxial Fracture Studies," Journal Applied Physics, Vol. 38, 1967, pp. 4843-4852.

81. Harbert, B. C., "Triaxial Testing of Solid Propellants," Bulletin, 4th Meeting ICRPG Working Group on Mechanical Behavior, Vol. 1, CPIA Publication No. 94u, 1965, pp. 217-234.

82. Harbert, B. C., and Britton, S. C., "Influence of Solids Particle Size on Propellant Mechanical Behavior in A Triaxial Stress Field," Bulletin, 5th Meeting ICRPG Working Group on Mechanical Behavior, Vol. 1, CPIA Publication No. 119, 1966, pp. 157-168.

83. Brisbane, J. J., "Stress Distributions in 'Poker-Chip' Tensile Specimens," Bulletin, 3rd Meeting, ICRPG Working Group on Mechanical Behavior, CPIA Publication No. 27, 1963, p. 337.

84. Messner, A. M., "Stress Distributions in Poker-Chip Tensile Specimens," Bulletin, 3rd Meeting ICRPG Working Group on Mechanical Behavior, CPIA Publication No. 27, 1963, pp. 109-129.

85. Jimenez, R. A., "An Apparatus for Laboratory Investigations of Asphaltic Concrete Under Repeated Flexural Deformations," Ph.D. Dissertation, January 1962, Texas A&M University.

86. Jimenez, R. A., "Aspects on the Binding Strength of Asphaltic Concrete," AAPT, Vol. 36, 1967, pp. 703-730.

87. Layman, A. H., "A Study of the Flexural Properties of a Black Base," Ph.D. Dissertation, January 1968, Texas A&M University.

88. Nadai, A., "Theory of Flow and Fracture of Solids," Vol. I, 2nd Ed., McGraw-Hill Book Co., 1950, pp. 208-228.

89. Marin, J.,"Mechanical Behavior of Engineering Materials," Chapter III, Prentice-Hall, Inc., 1962, pp. 104-169.

90. Traxler, R. N., Scrivner, F. H., and Kuykendall, W. E., "Loss of Durability in Bituminous Pavement Surfaces--Importance of Chemically Active Solar Radiation," Research Report 127-3, Texas Transportation Institute, April 1971.

91. Ferry, J. D., "Mechanical Properties of Substances of High Molecular Weight. VI. Dispersion in Concentrated Polymer Solutions and Its Dependence on Temperature and Concentration," Journal of American Chemical Society, Vol. 72, 1950, p.3746.

92. Williams, M. L., Landel, R. F., and Ferry, J. D., "The Temperature Dependence of Relaxation Mechanisms in Amorphous Polymers and Other Glass-Forming Liquids," Journal of American Chemical Society, Vol. 77, 1955, p. 3701.

93. Haas, R. C. G., "The Low-Temperature Behavior of Flexible Pavement Surfaces," presented to Canadian Technical Asphalt Association, Ottawa, November 1968.

94. Smith, Thor L., "Measurement and Analysis of Small Deformation and Ultimate Tensile Properties of Amorphous Elastomers," Instron Application Series, PC-5, 1960.

95. Haas, R. C. G., and Phang, W. A., "Case Studies of Pavement Shrinkage Cracking as Feedback for a Design Subsystem," HRB presentation (to be published), January 1970.

96. Schmidt, R. J., "The Relationship of the Low-Temperature Properties of Asphalt to the Cracking of Pavements," Proceedings of the Association of Asphalt Paving Technologists, Vol. 35, 1966.

97. Markek, C. R., "Estimation of the Tensile Strength of Asphalt Cements in Thin Films," Journal of Materials, Vol. 5, No. 1, March 1970, pp. 3-17.

98. Majidzadeh, Kamran, "Rheological Aspects of Aging," Highway Research Record No. 231, Highway Research Board, 1968, pp. 68-81.

99. Brodnyan, John C., "Use of Rheological and Other Data in Asphalt Engineering Problems, Highway Research Bulletin 192, Highway Research Board, 1967, pp. 1-19.

100. Alexander, R. L., "Limits of Linear Viscoelastic Behavior of an Asphalt Concrete in Tension and Compression," Ph.D. Dissertation, University of California, Berkeley, California, June 1964.

APPENDIX A

Computer Data Reduction Program:

Methodology, User's Guide, Program Listing

APPENDIX A

Table of Contents

METHODOLOGY

Machine Deformation

All materials testing was performed with an Instron Universal Testing Machine Model No. TTD. The indicated deformation obtained from the Instron pen trace includes both the actual specimen deformation and the machine deformation. A method of accurately correcting for the machine deformation was incorporated in the computer routine (Figure 2).

For each mode of testing, a different test set-up was required. A calibration trace for each test set up was obtained by loading only the machine and associated fixtures to a force greater than any failure load of the materials to be tested.

Dimensions and Data

The pertinent dimensions of each specimen were recorded accurately to the nearest one-hundredth of an inch. In the case of the uniaxial and double-lap shear specimens, four lengths, widths, and weights were recorded and averaged to obtain the final dimensions used for calculations. The hydrostatic and split-cylinder specimens were of a poker chip configuration with a constant diameter of four inches making it necessary to record only three heights or thicknesses for each specimen. The single size aggregate hydrostatic specimens had a constant thickness equal to the glass bead diameter used in the specimens. The orientation of these dimensions varied with the specimen configuration.

The weight in air and the weight in water of each specimen were recorded accurately to the nearest tenth of a gram. The theoretical specific gravity calculations were based upon the mix design and were read into the routine. Using the theoretical specific gravity, the weights in air and water, and the specimen dimensions according to the two methods described by Rice provided the specific gravity and void content per specimen. One method used the theoretical specific gravity, the weight in air, and the average dimensions whereas the other method used the weight in air and the weight in water. Both methods were employed as it was not known initially which one would give the better results. The latter method proved to be the most reliable.

Test Results and Data Reduction

Four values taken directly from the Instron trace of each specimen tested were required. These values represented the x and y coordinates of the point on the trace at which the first maximum load occurred and the point at which a load equal to one-half of the maximum load occurred before failure.

Because of the slow material response at the lower strain rates, many of the traces were erratic at the beginning of the curve. This caused difficulty in determining the exact starting point for computing the strain. To provide consistency in the location of this starting point, a line was drawn tangent to the curve at the point equal to half of the ultimate load. This tangent line was then extrapolated to the zero force level. The point of intersection was then referenced as the initial point of zero strain thus eliminating the erratic section of the trace. The slope of this tangent line was labeled the initial tangent modulus (Figure 3).

Because the computer routine was developed specifically for reducing Instron test data, the raw test values could be entered directly into the data deck. Along with these values the crosshead rate, chart speed, full scale setting, and test set-up number must be entered for each specimen tested. The conversion of the raw test data from chart units to stress and strain was written into the routine. The routine in its present form is therefore useful only for Instron test data.

Analysis

The calculated values of ultimate stress, ultimate strain, tangent modulus, and secant modulus for the specimens in each mix were grouped according to strain rate and were averaged. A simple deviation from these averages for each strain rate group was calculated. By averaging the deviations of each strain rate group for each mix, a single value indicating the spread of the data for the calculated quantities in each mix was obtained.

Simple deviations were used because the small number of points in each average eliminated the use of standard deviations. Finally the four average deviations in each mix were averaged to obtain a single value termed the field average deviation. This term was used only as a crude measure of the data scatter for each mix as a means of quick comparison.

Constitutive Relations and Statistical Evaluation

The constitutive relations for the characterization were determined by applying geometric laws and power laws to the average values calculated for stress, strain, secant modulus, and tangent modulus. The relations were calculated using two sets of units for the fundamental properties to provide for quick application of the relations without converting units.

For each constitutive relation , a coefficient of correlation and a Student t value was calculated. The coefficient of correlation indicated the extent of dependency of the dependent variable upon the independent variable for each relation. Application of the Student t test indicated how well these relations represented the data. By finding the working probability in a Student t table corresponding to the degrees of freedom and the Student t value for a given relation, the probability of that relation being valid was established.

USER'S GUIDE

The purpose of this guide is to provide a brief explanation of the formats required for keypunching the data cards and to show the proper order of the cards in the data deck. Enough explanation will be given to allow a person reasonably familiar with computer programming to code and punch the test data without understanding the logic of the routine.

Program Language

The program is written in Fortran IV for use with a Watfor compiler. The program in its present form is designed for use in the IBM 360-65 central processing unit available at the Data Processing Center of Texas A&M University. The program can be readily adapted for use with another compiler or installation. The operating procedures of the facilities available to the user should be checked before implementing the program.

Data Formats

Calibration Data:

The data immediately following the data entry card is the calibration data. The first card for each set of calibration data is called the calibration title card. The test set-up number, full scale setting, crosshead rate, and chart speed are entered on this card. The latter three values pertain to the Instron settings at which the calibration trace was run for that particular test set-up. The remaining cards contain the x and y coordinates of a series of points taken from the calibration trace. Each card contains a single set of coordinates. A maximum of twenty points can be stored for each test set-up including the zero point. The zero point is written into the program thus eliminating the need to enter this point with a data card. Examples 1 and 2 illustrate the read formats for the calibration title and data cards.

Example 1 -- <u>Calibration Title Card</u>

READ (5,105) NTSC, FSC, CHC, CSC

```
Col.
No.    1 2 3 4 5 6 7 8 9 10 11 12 13 14 15 16 17 18 19 20 21 22 23 24 25 26
       0 0 0 0 2 b 1 0 0  0  0  b  0  0  .  0  0  2  b  0  0  .  5  b  b  b
Field     I5    1x   F5.0       1x       F6.3         1x    F4.1
```

Example 2 -- <u>Calibration Data Card</u>

READ (5,107) XC(NTSC,I), YC(NTSC,I), LCIS, LS

```
Col.
No.    1 2 3 4 5 6 7 8 9 10 11 12 13 14 15 16 17 18 19 20
       0 2 . 0 0 b 0 2 .  0  0  b  0  0  b  b  b
Field    F5.2   1x   F5.2       1x  2I1
```

<u>Specimen Data</u>:

<u>Mix Title Card</u> - The first card in each set of specimen data cards is called the mix title card. This card contains the mix number, the code number for the mode of testing, the theoretical specific gravity, and if applicable the bead diameter. Example 3 illustrates the read format for this card.

Example 3 -- <u>Mix Title Card</u>

READ (5,109) MIX, G, MODE, FRAC, SGT, BD

```
Col.
No.    1 2 3 4 5 6 7 8 9 10 11 12 13 14 15 16 17 18 19 20 21 22 23 24 25 26
       0 2 1 B 0 2 b 0 .  5  0  0  b  2  .  1  3  9  b  0  .  5  0  0
Field   I3  1A1 I2 1x  F5.3         1x    F5.3          1x    F5.3
```

The term mix denotes all the specimens which came from the same mixture of binder and aggregate. Each mix has a particular percentage of binder or other additives and is unique in its composition. For ease of identification, each mix is assigned a number termed the mix number. Therefore, the variable 'MIX' in the read statement represents the mix number.

The variable 'G' represents a field allocation for a single literal character which can be included in the mix number to denote a subdivision within the mix. For example, a group of specimens from a mix numbered 15 which are to be tested differently or treated differently from the remaining specimens in the mix could be labeled 15B. This allows ready identification of the specimen composition yet indicates that a different test procedure was used. If a letter is to be part of the mix number, it should be entered in the field designated for the 'G' variable. If no letter is desired, the field should be left blank.

The variable 'MODE' represents a code number for the stress state and stress sign imposed upon the specimens in the mix during testing. For the purposes of this computer program, a change of stress state and/or a change of stress sign are considered different modes of loading. Table 1 lists the modes and corresponding code numbers.

The variable 'FRAC' represents a fractional value dependent upon the mode of loading. This value indicates the fractional part of the ultimate load at which the initial tangent was drawn to the Instron trace of each specimen tested in a particular mix. Table 1 also lists the 'FRAC' values corresponding to the modes of loading.

The variable 'SGT' represents the theoretical specific gravity of the mix material. This value varies with each mix design.

The variable 'BD' represents the average glass bead diameter. This variable is used only for Mode 6. For all other modes the field should be left blank.

Dimension Card

The cards which follow the Mix Title Card are termed the Dimension Cards. Upon these cards are entered the dimensions pertinent to the specimen configuration along with the weight in air and the weight in water. One card for each specimen in the mix is punched.

xample 4 — Dimension Cards for Uniaxial and Shear Specimen Configurations

READ(5,142) NS(I),W1,W2,W3,W4,D1,D2,D3,D4,H1,H2,H3,H4,WA(I),WW(I),LCIS,LS

```
ol. No. 1 2 3 4 5 6 7 8 9 10 11 12 13 14 15 16 17 18 19 20 21 22 23 24 25 26 27 28 29
        0 0 1|1 . 6 0 1 .  6  4  1  .  6  6  1  .  6  2  1  .  5  6  1  .  6  4  1  .
ield     I3                         12 F5.2

ol. No. 30 31 32 33 34 35 36 37 38 39 40 41 42 43 44 45 46 47 48 49 50 51 52
         6  0  6  .  0  4  6  .  0  6  6  .  0  6  6  .  0  6| 0  5  9  3  .
ield                                                            F6.1

ol. No.  53 54 55 56 57 58 59 60 61 62 63
          2| 0  3  2  7  .  5| 0  0|  b  b
ield              F6.1         2I1
```

xample 5 — Dimension Cards for Poker Chip and Split Cylinder Specimen Configurations

READ(5,150) NS(I),H1,H2,H3,WA(I),WW(I),LCIS,LS

```
ol. No. 1 2 3 4 5 6 7 8 9 10 11 12 13 14 15 16 17 18 19 20 21 22 23 24 25 26 27 28 29 30
        0 0 1|0 . 5 2 2|0  .  5  2  7| 0  .  5  2  1| 0  2  4  3  .  2| 0  1  4  0  .  8|
ield     I3    F5.3       F5.3          F5.3             F6.1              F6.1

ol. No. 31 32 33
         0  0| b
ield
```

Test Result Card

The test result cards are placed directly after the dimension cards. A single card is punched for each specimen. Each card contains the specimen number, test set-up number, full-scale setting, crosshead rate, chart speed, X and Y values for the secant modulus, and the X and Y values for the initial tangent modulus. Examples 6 and 7 show the formats for these cards.

Example 6 — Test Result Card for Uniaxial, Poker Chip, Shear, and Split Cylinder

```
READ(5,111) NS(I),NTS(I),FS(I),CH(I),CS(I),YS(I), XS(I),YT(I),XT(I), LCIS

Col. No. 1 2 3 4 5 6 7 8 9 10 11 12 13 14 15 16 17 18 19 20 21 22 23 24 25 26 27 28 29
         0 1 0 6 6 1 0 0 0 0  6  0  0  .  0  2  0  6  2  .  0  0  6  0  8  .  6  0  6
Field     I2  I2 1x   F5.0    1x         F6.3       1x     F4.1   1x      F5.2      1x

Col. No. 30 31 32 33 34 35 36 37 38 39 40 41 42 43 44 45 46 47 48 49 50 51
          0  9  .  5  0  6  0  4  .  3  0  0  6  0  3  .  6  0  6  0
Field          F5.2      1x       F6.3       1x      F5.2      1x I1
```

Example 7 — Test Result Card for Binder Hydrostatic (Single Size Aggregate)

```
READ(5,176) NS(I),NTS(I),NB(I),FS(I),CH(I),CS(I),YS(I),XS(I),YT(I),XT(I),LCIS,LS

Col. No. 1 2 3 4 5 6 7 8 9 10 11 12 13 14 15 16 17 18 19 20 21 22 23 24 25 26 27
         0 1 0 6 6 1 3 8 6  1  0  0  0  0  6  0  0  .  2  0  0  6  1  0  .  0  6
Field     I2  I2 1x I3  1x      F5.0       1x        F6.3        1x     F4.1    1x

Col. No. 28 29 30 31 32 33 34 35 36 37 38 39 40 41 42 43 44 45 46 47 48 49 50 51 52
          0  9  .  6  0  6  1  0  .  5  0  6  0  4  .  3  0  0  6  0  6  .  2  5  6
Field          F5.2      1x     F5.2      1x       F6.3        1x      F5.2

Col. No. 53 54 55 56 57
          0  0  6  6  6
Field      2I1
```

The terms 'LCIS' and 'LS' which appear at the end of each read statement except those for the title cards are the execution terminators of the computer program. The term 'LCIS' is an abbreviation for 'last card in set', and 'LS' is 'last set'. A set is defined as the group of calibration data cards for a test set-up or the group of dimension cards for a mix or the group of test result cards for a mix.

If the card is the last one in the set, the integer '1' should be punched in the field allocated to 'LCIS'. If the card is the last card of the last set in the data deck, the integer '1' should also be punched in the field allocated to 'LS'. The fields for 'LCIS' and 'LS' should be left blank for all cards except those to which the above conditions apply.

The proper sequence of the cards in the data deck is extremely important for correct execution of the program logic. Fig. 1 illustrates the correct sequence of the data cards.

Table 1 - Modes of Testing

Stress State and Sign	MODE	FRAC
Uniaxial Tension	1	0.50
Uniaxial Compression	2	0.50
Hydrostatic Tension	3	0.50
Hydrostatic Compression	4	0.05
Biaxial Shear	5	0.50
Hydrostatic Tension (Single Size Aggregate)	6	0.50
Split Cylinder	7	0.50

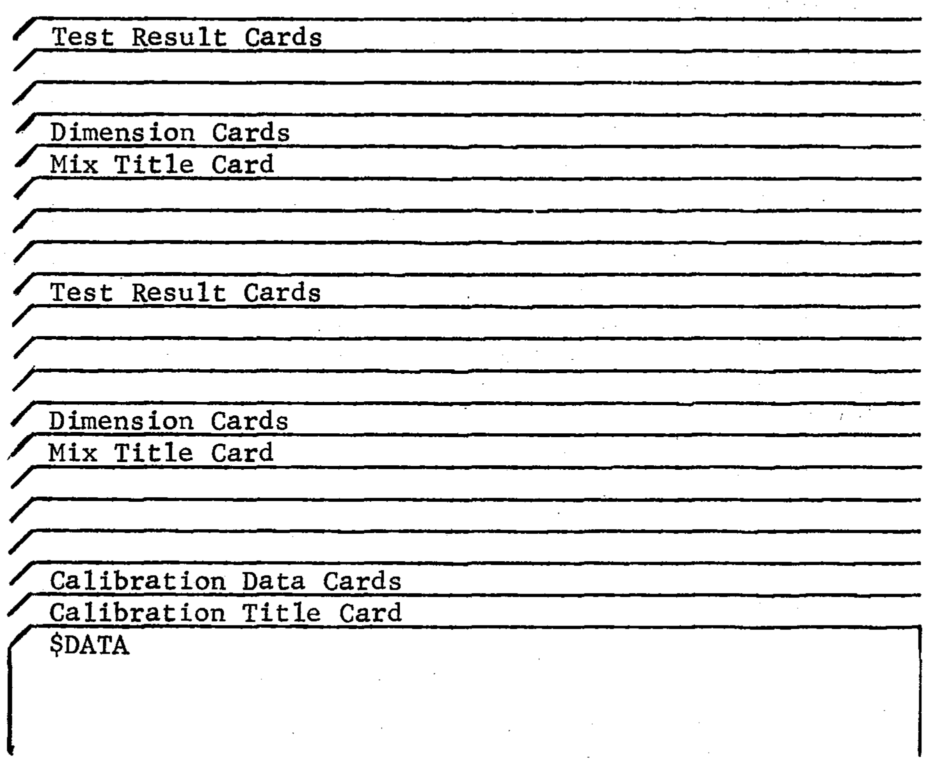

Fig. 1 - Sequence of Data Cards

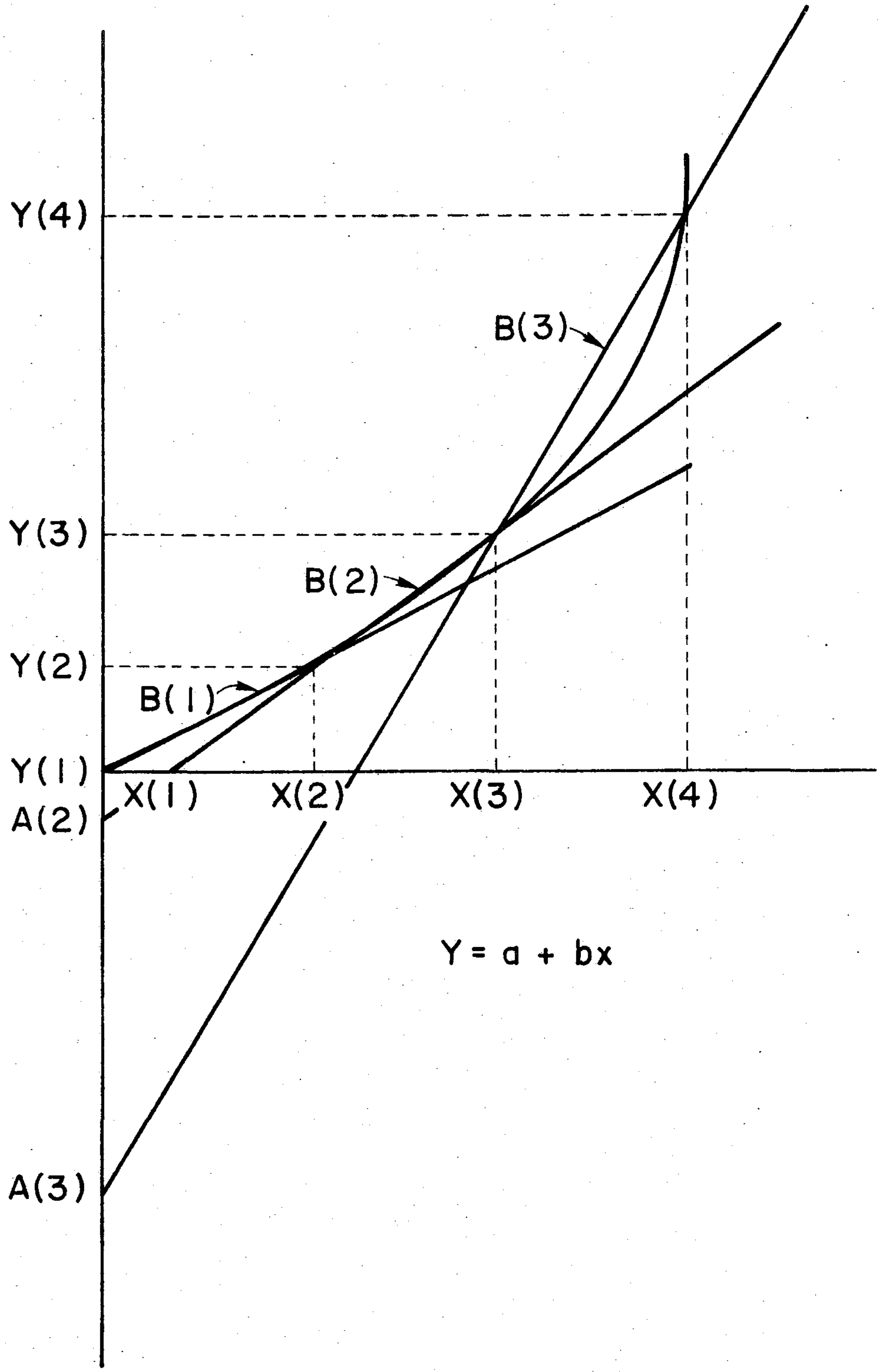

TANGENTIAL APPROXIMATION OF CALIBRATION CURVES

FIG. 2

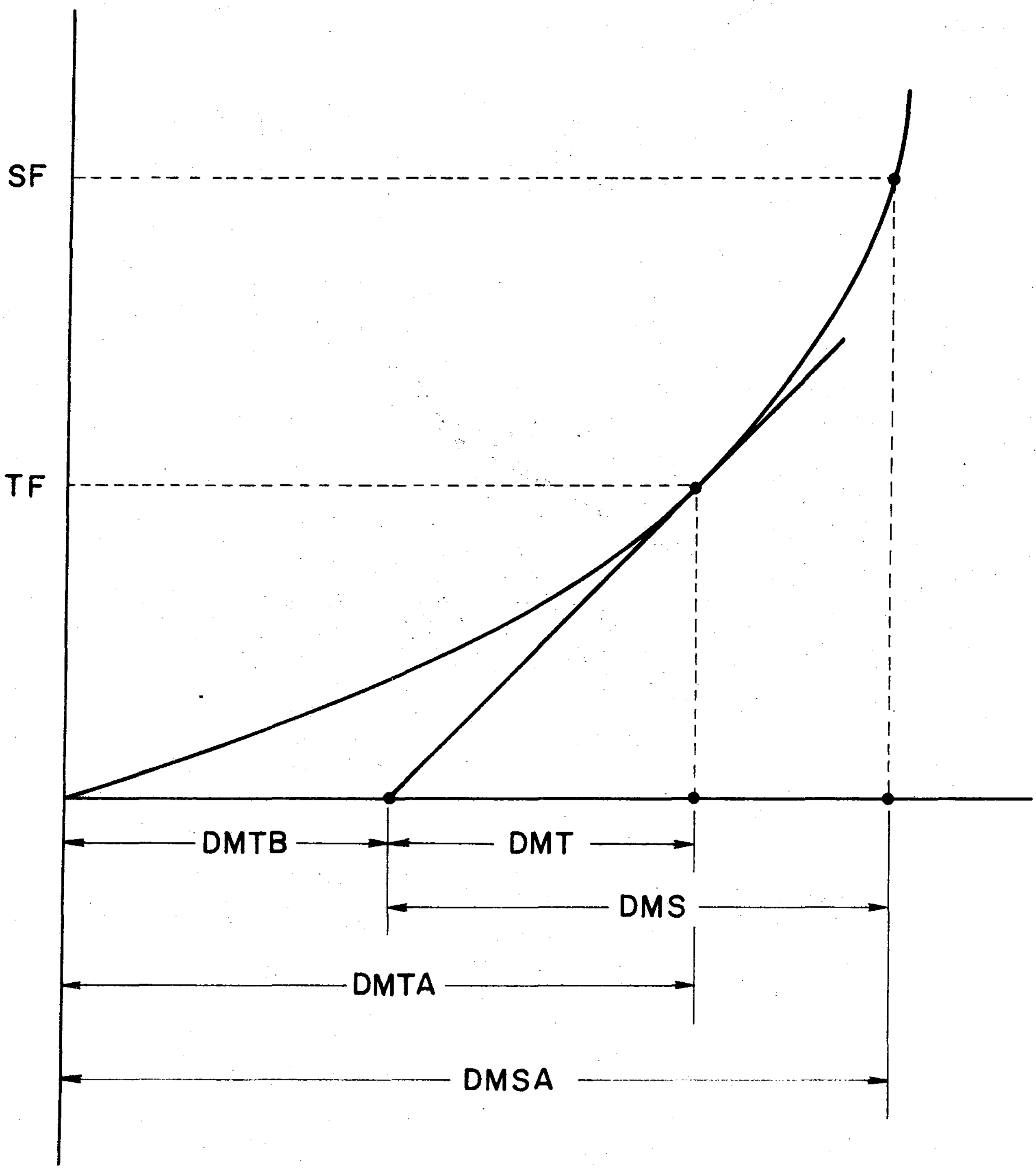

CORRECTION FOR MACHINE DEFORMATION
FIG. 3

PROGRAM LISTING

```
C
C
C********A COMPREHENSIVE ANALYSIS OF ASPHALTIC CONCRETE TEST DATA*******
C
C
      INTEGER OPT,DEGF
      DIMENSION XC(20,20),YC(20,20),DC(20,20),FC(20,20),AC(20,20),BC(20,
     *20),NS(30),AW(30),AD(30),AH(30),WA(30),WW(30),AREA(30),AHD(30),TFD
     *(30),NTS(30),FS(30),CH(30),CS(30),YS(30),XS(30),YT(30),XT(30),SF(3
     *0),TF(30),S(30),E(30),SEC(30),TAN(30),ET(30),DMT(30),DIT(30),DMS(3
     *0),DIS(30),AR(15),AS(15),AE(15),ASEC(15),ATAN(15),AFIT(10),BFIT(10
     *),R(30),DS(15),DE(15),DSEC(15),DTAN(15),NB(30)
C
C******************MACHINE DEFORMATION*********************************
C
  404 WRITE(6,101)
      READ(5,105) NTSC,FSC,CHC,CSC
      WRITE(6,106) NTSC,FSC,CHC,CSC
      I=1
  400 I=I+1
      READ(5,107) XC(NTSC,I),YC(NTSC,I),LCIS,LS
      IF(LCIS) 999,400,401
  401 NCP=I
      XC(NTSC,1)=0.0
      YC(NTSC,1)=0.0
      FC(NTSC,1)=0.0
      DC(NTSC,1)=0.0
      DO 402 I=2,NCP
      FC(NTSC,I)=(YC(NTSC,I))*FSC/10.0
      DC(NTSC,I)=(XC(NTSC,I))*CHC/CSC
      BC(NTSC,I-1)=(FC(NTSC,I)-FC(NTSC,I-1))/(DC(NTSC,I)-DC(NTSC,I-1))
  402 AC(NTSC,I-1)=FC(NTSC,I-1)-BC(NTSC,I-1)*DC(NTSC,I-1)
      BC(NTSC,NCP)=BC(NTSC,NCP-1)
      AC(NTSC,NCP)=AC(NTSC,NCP-1)
      NROW=0
      DO 403 I=1,NCP
      NROW=NROW+1
      WRITE(6,108) XC(NTSC,I),YC(NTSC,I),DC(NTSC,I),FC(NTSC,I),AC(NTSC,I
     *),BC(NTSC,I)
      IF(NROW-5) 403,750,403
  750 WRITE(6,178)
      NROW=0
  403 CONTINUE
      IF(LS) 999,404,406
C
C******************INITIAL INPUT***************************************
C
  406 READ(5,109) MIX,G,MODE,FRAC,SGT,BD
      JILT=1
      GO TO (411,411,412,412,411,443,412),MODE
  411 WRITE(6,140)
      GO TO 407
  412 WRITE(6,148)
  407 GO TO (431,432,433,434,435,436,437),MODE
  431 WRITE(6,110) MIX,G
      GO TO (420,421,999,423,424,425,426,427,590),JILT
  432 WRITE(6,125) MIX,G
      GO TO (420,421,999,423,424,425,426,427,590),JILT
  433 WRITE(6,126) MIX,G
```

```
      GO TO (444,999,999,423,424,425,426,427,590),JILT
  434 WRITE(6,127) MIX,G
      GO TO (444,999,999,423,424,425,426,427,590),JILT
  435 WRITE(6,128) MIX,G
      GO TO (420,421,999,423,424,425,426,427,590),JILT
  436 WRITE(6,153) MIX,G
      GO TO (999,999,999,423,424,425,426,427,590),JILT
  437. WRITE(6,181) MIX,G
      GO TO (444,999,999,423,424,425,426,427,590),JILT
C
C*****************DIMENSIONS FOR UNIAXIAL OR SHEAR********************
C
  420 WRITE(6,141)
      NROW=0
      I=0
  440 I=I+1
      READ(5,142) NS(I),W1,W2,W3,W4,D1,D2,D3,D4,H1,H2,H3,H4,WA(I),WW(I),
     *LCIS,LS
      ND=NS(I)
      AW(ND)=(W1+W2+W3+W4)/4.0
      AD(ND)=(D1+D2+D3+D4)/4.0
      AH(ND)=(H1+H2+H3+H4)/4.0
      WA(ND)=WA(I)
      WW(ND)=WW(I)
      NROW=NROW+1
      WRITE(6,143) NS(I),W1,W2,W3,W4,D1,D2,D3,D4,H1,H2,H3,H4
      IF(NROW-5) 600,610,600
  610 WRITE(6,178)
      NROW=0
  600 NSAMP=I
      IF(LCIS) 999,440,441
C
C*****************DATA FOR UNIAXIAL OR SHEAR***************************
C
  441 WRITE(6,144)
      JILT=2
      GO TO 407
  421 WRITE(6,145)
      SSGW=0.0
      SSGM=0.0
      SVSGW=0.0
      SVSGM=0.0
      NROW=0
      DO 442 I=1,NSAMP
      ND=NS(I)
      VOL=AW(ND)*AD(ND)*AH(ND)
      SGM=WA(ND)/(16.42*VOL)
      SGW=WA(ND)/(WA(ND)-WW(ND))
      VSGM=100.0*(1.0-SGM/SGT)
      VSGW=100.0*(1.0-SGW/SGT)
      SSGM=SSGM+SGM
      SSGW=SSGW+SGW
      SVSGM=SVSGM+VSGM
      SVSGW=SVSGW+VSGW
      NROW=NROW+1
      WRITE(6,146) NS(I),AW(ND),AD(ND),AH(ND),VOL,WA(ND),WW(ND),SGM,SGW,
     *VSGM,VSGW
      IF(NROW-5) 442,620,442
  620 WRITE(6,178)
      NROW=0
```

```
  442 CONTINUE
      ASGM=SSGM/NSAMP
      ASGW=SSGW/NSAMP
      AVSGM=SVSGM/NSAMP
      AVSGW=SVSGW/NSAMP
      IF(NSAMP .EQ. 10 .OR. NSAMP .EQ. 15 .OR. NSAMP .EQ. 20) GO TO 630
      WRITE(6,147) ASGM,ASGW,AVSGM,AVSGW,SGT
      GO TO 443
  630 WRITE(6,179) ASGM,ASGW,AVSGM,AVSGW,SGT
      GO TO 443
C
C******************DIMENSIONS AND DATA FOR HYDROSTATIC MODES(3,4)*******
C
  444 WRITE(6,149)
      I=0
      SSGM=0.0
      SSGW=0.0
      SVSGM=0.0
      SVSGW=C.0
      NROW=0
  445 I=I+1
      READ(5,150) NS(I),H1,H2,H3,WA(I),WW(I),LCIS,LS
      ND=NS(I)
      AH(ND)=(H1+H2+H3)/3.0
      VOL=12.56*AH(ND)
      WA(ND)=WA(I)
      WW(ND)=WW(I)
      SGM=WA(ND)/(16.42*VOL)
      SGW=WA(ND)/(WA(ND)-WW(ND))
      VSGM=1C0.0*(1.0-SGM/SGT)
      VSGW=100.0*(1.0-SGW/SGT)
      SSGM=SSGM+SGM
      SSGW=SSGW+SGW
      SVSGM=SVSGM+VSGM
      SVSGW=SVSGW+VSGW
      NROW=NROW+1
      NSAMP=I
      WRITE(6,151) NS(I),H1,H2,H3,AH(ND),VOL,WA(ND),WW(ND),SGM,SGW,VSGM,
     *VSGW
      IF(NROW-5) 650,660,650
  660 WRITE(6,178)
      NROW=0
  650 IF(LCIS) 999,445,490
  490 ASGM=SSGM/NSAMP
      ASGW=SSGW/NSAMP
      AVSGM=SVSGM/NSAMP
      AVSGW=SVSGW/NSAMP
      IF(NSAMP .EQ. 10 .OR. NSAMP .EQ. 15 .OR. NSAMP .EQ. 20) GO TO 640
      WRITE(6,152) ASGM,ASGW,AVSGM,AVSGW,SGT
      GO TO 443
  640 WRITE(6,180) ASGM,ASGW,AVSGM,AVSGW,SGT
      GO TO 443
C
C******************TEST RESULTS*******************************************
C
  443 JILT=4
      WRITE(6,102)
      GO TO 407
  423 WRITE(6,112)
      I=0
```

```
  452 I=I+1
      GO TO (493,493,491,491,493,494,491),MODE
  493 READ(5,111) NS(I),NTS(I),FS(I),CH(I),CS(I),YS(I),XS(I),YT(I),XT(I)
     *,LCIS
      GO TO 492
  491 READ(5,172) NS(I),NTS(I),FS(I),CH(I),CS(I),YS(I),XS(I),YT(I),XT(I)
     *,LCIS
      GO TO 492
  494 READ(5,176) NS(I),NTS(I),NB(I),FS(I),CH(I),CS(I),YS(I),XS(I),YT(I)
     *,XT(I),LCIS,LS
  492 ND=NS(I)
      GO TO (446,446,447,447,448,449,447),MODE
  446 AREA(I)=AW(ND)*AD(ND)
      AHD(I)=AH(ND)
      GO TO 450
  447 AREA(I)=12.56
      AHD(I)=AH(ND)
      GO TO 450
  448 NDP=NS(I+1)
      AREA(I)=AD(ND)*AW(ND)+AD(NDP)*AW(NDP)
      AHD(I)=(AH(ND)+AH(NDP))/2.0
      GO TO 450
  449 AHD(I)=BD
      AREA(I)=12.56-0.785*NB(I)*BD**2.0
  450 NT=I
      IF(I .EQ. 1) GO TO 680
      IF(CH(I)-CH(I-1)) 670,680,670
  670 WRITE(6,178)
  680 WRITE(6,113) NS(I),NTS(I),FS(I),CH(I),CS(I),YS(I),XS(I),YT(I),XT(I
     *),AHD(I),AREA(I)
      IF(LCIS) 999,452,451
C
C*****************DATA REDUCTION****************************************
C
  451 WRITE(6,103)
      JILT=5
      GO TO 407
  424 WRITE(6,114)
      KT=0
      KS=0
      DO 453 I=1,NT
      R(I)=100.0*CH(I)/AHD(I)
      NTSD=NTS(I)
      SF(I)=YS(I)*FS(I)/10.0
      IF(MODE .NE. 7) GO TO 800
      D=4.0
      S(I)=(2.0*SF(I))/(3.14*AHD(I)*D)
      GO TO 801
  800 S(I)=SF(I)/AREA(I)
  801 TFD(I)=YT(I)*FS(I)/10.0
      TF(I)=FRAC*SF(I)
      FRACT=TF(I)/TFD(I)
  454 KT=KT+1
      M=TF(I)-FC(NTSD,KT)
      IF(M) 455,455,454
  455 DMT(I)=TF(I)/BC(NTSD,KT-1)
      DIT(I)=XT(I)*FRACT*CH(I)/CS(I)
      DMTA=(TF(I)-AC(NTSD,KT-1))/BC(NTSD,KT-1)
  456 KS=KS+1
      M=SF(I)-FC(NTSD,KS)
```

```
      IF(M) 457,457,456
  457 DMSA=(SF(I)-AC(NTSD,KS-1))/BC(NTSD,KS-1)
      DMTB=DMTA-DMT(I)
      DMS(I)=DMSA-DMTB
      DIS(I)=XS(I)*CH(I)/CS(I)
      IF(MODE .NE. 7) GO TO 803
      C=(5.22*FS(I))/(10.0*AHD(I))
      TAN(I)=(C*YT(I))/((DIT(I)-DMT(I))*1000.0)
      SEC(I)=(C*YS(I))/((DIS(I)-DMS(I))*1000.0)
      E(I)=(0.350*YS(I)*FS(I))/(100.0*AHD(I)*SEC(I))
      GO TO 804
  803 E(I)=(DIS(I)-DMS(I))*100.0/AHD(I)
      ET(I)=(DIT(I)-DMT(I))*100.0/AHD(I)
      SEC(I)=S(I)/(E(I)*10.0)
      TAN(I)=TF(I)/(AREA(I)*ET(I)*10.0)
  804 KT=0
      KS=0
      WRITE(6,115) NS(I),R(I),SF(I),TF(I),DMS(I),DIS(I),DMT(I),DIT(I),S(
     *I),E(I),SEC(I),TAN(I)
      IF(I .EQ. NT) GO TO 453
      IF(CH(I)-CH(I+1)) 690,453,690
  690 WRITE(6,178)
  453 CONTINUE
C
C*****************ANALYSIS********************************************
C
      WRITE(6,104)
      JILT=6
      GO TO 407
  425 WRITE(6,116)
      IF(MODE-4) 459,458,459
  458 J=0
      DO 460 I=1,NT
      IF(E(I) .LT. 0.0 .OR. TAN(I) .LT. 0.0) GO TO 460
      J=J+1
      NS(J)=NS(I)
      R(J)=R(I)
      S(J)=S(I)
      E(J)=E(I)
      SEC(J)=SEC(I)
      TAN(J)=TAN(I)
      CH(J)=CH(I)
  460 CONTINUE
      NT=J
  459 AR(1)=0.0
      AS(1)=0.0
      AE(1)=0.0
      ASEC(1)=0.0
      ATAN(1)=0.0
      NIA=0
      NAD=0
      KR=1
      CH(NT+1)=0.0
      DO 461 I=1,NT
      AR(KR)=AR(KR)+R(I)
      AS(KR)=AS(KR)+S(I)
      AE(KR)=AE(KR)+E(I)
      ASEC(KR)=ASEC(KR)+SEC(I)
      ATAN(KR)=ATAN(KR)+TAN(I)
      NIA=NIA+1
```

```
      IF(CH(I)-CH(I+1)) 463,461,463
  462 GO TO 461
  463 DNIA=NIA
      AR(KR)=AR(KR)/DNIA
      AS(KR)=AS(KR)/DNIA
      AE(KR)=AE(KR)/DNIA
      ASEC(KR)=ASEC(KR)/DNIA
      ATAN(KR)=ATAN(KR)/DNIA
      DS(KR)=0.0
      DE(KR)=0.0
      DSEC(KR)=0.0
      DTAN(KR)=0.0
      IF(NIA-1) 999,465,466
  466 IP=I+1
      DO 464 J=1,NIA
      DS(KR)=DS(KR)+ABS(AS(KR)-S(IP-J))
      DE(KR)=DE(KR)+ABS(AE(KR)-E(IP-J))
      DSEC(KR)=DSEC(KR)+ABS(ASEC(KR)-SEC(IP-J))
  464 DTAN(KR)=DTAN(KR)+ABS(ATAN(KR)-TAN(IP-J))
      DS(KR)=100.0*DS(KR)/(DNIA*AS(KR))
      DE(KR)=100.0*DE(KR)/(DNIA*AE(KR))
      DSEC(KR)=100.0*DSEC(KR)/(DNIA*ASEC(KR))
      DTAN(KR)=100.0*DTAN(KR)/(DNIA*ATAN(KR))
      NAD=NAD+1
  465 WRITE(6,117) AR(KR),AS(KR),AE(KR),ASEC(KR),ATAN(KR),DS(KR),DE(KR),
     *DSEC(KR),DTAN(KR),NIA,NS(I)
      IF(NIA-1) 999,467,468
  468 NIAM=NIA-1
      DO 469 J=1,NIAM
  469 WRITE(6,118) NS(I-J)
  467 KR=KR+1
      NIA=0
      AR(KR)=0.0
      AS(KR)=0.0
      AE(KR)=0.0
      ASEC(KR)=0.0
      ATAN(KR)=0.0
  461 CONTINUE
      NAR=KR-1
      DNAD=NAD
      ADS=0.0
      ADE=0.0
      ADSEC=0.0
      ADTAN=0.0
      DO 470 J=1,NAR
      ADS = ADS + DS(J)
      ADE = ADE + DE(J)
      ADSEC = ADSEC + DSEC(J)
  470 ADTAN=ADTAN+DTAN(J)
      ADS = ADS / DNAD
      ADE=ADE/DNAD
      ADSEC = ADSEC / DNAD
      ADTAN = ADTAN / DNAD
      FAD = (ADS +ADE +ADSEC +ADTAN)/4.0
      WRITE(6,119) ADS,ADE,ADSEC,ADTAN,FAD
C
C*****************EQUATIONS FOR RESULTS BY LEAST SQUARES FIT***********
C
      IF(NAR-1) 999,472,481
  481 NRUN=1
```

```
471 WRITE(6,121)
    JILT=7
    GO TO 407
426 WRITE(6,154)
    NE=1
    OPT=2
    CALL FIT(NAR,OPT,AS,AR,A,B,RES,NE,MODE,COC,DEGF,STUDT)
    IF(OPT .EQ. 0) GO TO 503
    AFIT(NE)=A
    BFIT(NF)=B
    WRITE(6,161) BFIT(NE),NE,AFIT(NE),RES,COC,DEGF,STUDT
503 NE=NE+1
    OPT=2
    CALL FIT(NAR,OPT,AE,AR,A,B,RES,NE,MODE,COC,DEGF,STUDT)
    AFIT(NE)=A
    BFIT(NE)=B
    WRITE(6,162) BFIT(NE),NE,AFIT(NE),RES,COC,DEGF,STUDT
    NE=NE+1
    OPT=3
    CALL FIT(NAR,OPT,AR,AE,A,B,RES,NE,MODE,COC,DEGF,STUDT)
    AFIT(NF)=A
    BFIT(NE)=B
    WRITE(6,163) NE,AFIT(NE),BFIT(NE),RES,COC,DEGF,STUDT
    NE=NE+1
    OPT=2
    CALL FIT(NAR,OPT,ASEC,AR,A,B,RES,NF,MODE,COC,DEGF,STUDT)
    AFIT(NE)=A
    BFIT(NE)=B
    WRITE(6,164) BFIT(NE),NE,AFIT(NE),RES,COC,DEGF,STUDT
    NE=NE+1
    OPT=2
    CALL FIT(NAR,OPT,ATAN,AR,A,B,RES,NE,MODE,COC,DEGF,STUDT)
    AFIT(NF)=A
    BFIT(NE)=B
    WRITE(6,165) BFIT(NE),NE,AFIT(NE),RES,COC,DEGF,STUDT
    NE=NE+1
    WRITE(6,155)
    OPT=2
    CALL FIT(NAR,OPT,AS,AE,A,B,RES,NE,MODE,COC,DEGF,STUDT)
    IF(OPT .EQ. 0) GO TO 507
    AFIT(NE)=A
    BFIT(NE)=B
    WRITE(6,166) BFIT(NE),NE,AFIT(NE),RES,COC,DEGF,STUDT
507 NE=NE+1
    OPT=2
    CALL FIT(NAR,OPT,AE,AS,A,B,RES,NF,MODE,COC,DEGF,STUDT)
    AFIT(NE)=A
    IF(OPT .EQ. 0) GO TO 500
    BFIT(NE)=B
    WRITE(6,167) BFIT(NE),NE,AFIT(NE),RES,COC,DEGF,STUDT
500 NE=NE+1
    OPT=3
    CALL FIT(NAR,OPT,AE,AS,A,B,RES,NE,MODE,COC,DEGF,STUDT)
    IF(OPT .EQ. 0) GO TO 501
    AFIT(NE)=A
    BFIT(NE)=B
    WRITE(6,173) NE,AFIT(NE),BFIT(NE),RES,COC,DEGF,STUDT
501 NE=NE+1
    OPT=3
    CALL FIT(NAR,OPT,AS,AE,A,B,RES,NE,MODE,COC,DEGF,STUDT)
```

```
      IF(OPT .EQ. 0) GO TO 502
      AFIT(NF)=A
      BFIT(NE)=B
      WRITE(6,168) NE,AFIT(NE),BFIT(NE),RES,COC,DEGF,STUDT
  502 IF(NRUN-1) 999,475,476
  475 WRITE(6,169)
      DO 480 I=1,NAR
      AR(I)=AR(I)/100.0
      AS(I)=AS(I)
      AE(I)=AE(I)/100.0
      ASEC(I)=ASEC(I)*1000.0
  480 ATAN(I)=ATAN(I)*1000.0
      NRUN=NRUN+1
      GO TO 471
  476 WRITE(6,170)
C
C******************CONVERSIONS AND TIME TO FAILURE**********************
C
      WRITE(6,130)
      JILT=8
      GO TO 407
  427 BS=BFIT(4)/(1.0-BFIT(2))
      IF(AFIT(7) .EQ. 0.0) GO TO 505
      BR=1.0/BS
      BSN=-BS
      BRN=-BR
      ASM=AFIT(4)*AFIT(2)**BS
      H=3.14*BS*(1.0-BS*BS)/SIN(3.14*BS)
      ACSR=SIN(3.14*BS)/(3.14*ASM*BS*(1.0-BS*BS))
      ACE=ASM*(1.0-BS)
      ACS=SIN(3.14*BS)/(3.14*ASM*BS*(1.0-BS))
      AFCER=AFIT(2)
      BFCER=BFIT(2)-1.0
      BFCSR=(BFIT(2)-1.0)/(BFIT(4)+1.0)
      AFCSR=AFIT(2)*H**BR*(H**BR/AFIT(4))**BFCSR
      AFCE=(ASM*(1.0-BS)/AFIT(7))**BR
      BFCE=(1.0-BFIT(7))*BR
      AFCS=(AFIT(7)/ACS)**BR
      BFCS=(BFIT(7)-1.0)*BR
      AQ=AFIT(4)*H**BRN
      BQ=BFIT(4)+1.0
      WRITE(6,131) BSN,BFCER,ASM,AFCER,BS,BFCSR,ACSR,AFCSR,BQ,AQ,BSN,BFC
     *E,ACE,AFCE,BSN,ACE,BS,BFCS,ACS,AFCS,BS,ACS
      WRITE(6,171)
C
C**************SAMPLE CALCULATIONS OF TIME TO FAILURE*****************
C
      WRITE(6,177)
      JILT=9
      GO TO 407
  590 CALL TIME(NAR,AR,AE,AFCER,BFCER)
      GO TO 472
  505 WRITE(6,175)
  472 IF(LS) 999,406,999
  999 CONTINUE
      WRITE(6,136)
      STOP
C
C******************FORMAT STATEMENTS*************************************
C
```

```
101 FORMAT('1'///' ',56X'MACHINE DEFORMATION')
102 FORMAT('1'///' ',60X'TEST RESULTS')
103 FORMAT('1'///' ',59X'DATA REDUCTION')
104 FORMAT('1'///' ',62X'ANALYSIS')
105 FORMAT(I5,1X,F5.0,1X,F6.3,1X,F4.1)                                    11480
106 FORMAT('0',39X,'NTS = ',I2,5X,'FS = ',F6.0,5X,'CH = ',F6.3,5X,'CS
   *= ',F4.1// ' ',28X,'X',14X,'Y',13X,'D',14X,'F',14X,'A',14X,'B'/)     115
107 FORMAT(2(F5.2,1X),2I1)
108 FORMAT(' ',25X,F6.3,9X,F6.3,7X,4(E10.3,5X))
109 FORMAT(I3,1A1,I2,3(1X,F5.3))
110 FORMAT('0'45X'MIX = 'I3,1A1,9X'MODE = UNIAXIAL TENSION')
111 FORMAT(2I2,1X,F5.0,1X,F6.3,1X,F4.1,1X,2(F5.2,1X),F6.3,1X,F5.2,1X,1
   *I1)
112 FORMAT('0',21X,'NS'3X'NTS'4X'FS'7X'CH'6X'CS'5X'YS'6X'XS'6X'YT'6X'X
   *T'6X'AH'5X'AREA'/)
113 FORMAT(' ',21X,2(I2,3X),F6.0,3X,F6.3,3X,F4.1,6(2X,F6.3))
114 FORMAT('0'17X'NS'6X'R'5X'SF'5X'TF'6X'DMS'6X'DIS'6X'DMT'6X'DIT'7X'S
   *'8X'E'7X'SEC'6X'TAN'/)
115 FORMAT(' '17X,I2,1X,F8.3,2(1X,F6.1),1X,F8.5,3(1X,F8.5),1X,F7.1,3F9
   *.2)
116 FORMAT('0',34X'AR'4X'AS'6X'AE'7X'ASEC'6X'ATAN'4X'DS'5X'DE'4X'DSEC'
   *3X'DTAN'3X'N'2X'NS'/)
117 FORMAT(' ',30X,F8.3,F6.1,F7.2,2(1X,F9.2),4F7.2,2(2X,I2))
118 FORMAT(' ',105X,I2)
119 FORMAT(' ',74X,'ADS'4X'ADE'3X'ADSEC'2X'ADTAN'4X'FAD'/' ',71X,4F7.2
   *,1X,F7.2)
121 FORMAT('1'///' '35X'EQUATIONS OF CONSTANT STRAIN RATE RESULTS BY L
   *EAST SQUARES FIT')
125 FORMAT('0',43X,'MIX = 'I3,1A1,9X,'MODE = UNIAXIAL COMPRESSION')
126 FORMAT('0',43X'MIX = 'I3,1A1,9X'MODE = HYDROSTATIC TENSION')
127 FORMAT('0',42X'MIX = 'I3,1A1,9X'MODE = HYDROSTATIC COMPRESSION')
128 FORMAT('0',45X'MIX = 'I3,1A1,9X'MODE = DOUBLE LAP SHEAR')
130 FORMAT('1'///' '50X'CONVERSIONS AND TIME TO FAILURE')
131 FORMAT('-'34X'CONSTANT STRAIN RATE MODULUS'//' '53X,E10.3,25X,E1o.
   *3/' '34X'CERM = 'E10.3' T'17X'TTF = 'E10.3' R'///' '34X'CONSTANT S
   *TRESS RATE COMPLIANCE'//' '53X,E10.3,25X,E10.3/' '34X'CSRC = 'E10.
   *3' T'17X'TTF = 'E10.3' Q'/' '53X,E10.3/' '34X'Q    = 'E10.3' R'///
   *' '34X'CONSTANT STRAIN MODULUS'//' '53X,E10.3,25X,E10.3/' '34X'CEM
   *  = 'E10.3' T'17X'TTF = 'E10.3' E'/' '53X,E10.3,25X,'0'/' '34X'S(T
   *) = 'E10.3' T'11X'F'/' '65X'0'///' '34X'CONSTANT STRESS COMPLIANCE
   *'//' '53X,E10.3,25X,E10.3/' '34X'CSC  = 'E10.3' T'17X'TTF = 'E10.3
   *' S'/' '53X,E10.3,25X'0'/' '34x'E(T) = 'E10.3' T'11X'S'/' '65X'0')
136 FORMAT('1'59X'AD HADES TECUM')
140 FORMAT('1'///' '61X'DIMENSIONS')
141 FORMAT('0',23X'NS'4X'W1'5X'W2'5X'W3'5X'W4'5X'D1'5X'D2'5X'D3'5X'D4'
   *5X'H1'5X'H2'5X'H3'5X'H4'/)
142 FORMAT(I3,12F5.2,2F6.1,2I1)
143 FORMAT(' ',23X,I2,12(2X,F5.2))
144 FORMAT('1'///' '64X'DATA')
145 FORMAT('0',20X'NS'5X'AW'7X'AD'7X'AH'7X'VOL'6X'WA'7X'WW'7X'SGM'6X'S
   *GW'5X'VSGM'5X'VSGW'/)
146 FORMAT(' ',19X,I3,4(3X,F6.3),2(3X,F6.1),4(3X,F6.3))
147 FORMAT('0',70X'AVERAGE'2X,F6.3,3(3X,F6.3)//' '73X'SGT = 'F6.3)
148 FORMAT('1'///' '56X'DIMENSIONS AND DATA')
149 FORMAT('0',22X'NS'3X'H1'5X'H2'5X'H3'5X'AH'6X'VOL'5X'WA'6X'WW'6X'SG
   *M'5X'SGW'4X'VSGM'4X'VSGW'/)
150 FORMAT(I3,3F5.3,2F6.1,2I1)
151 FORMAT(' ',22X,I2,4(2X,F5.3),1X,F7.3,2(2X,F6.1),4(2X,F6.3))
152 FORMAT('0',69X,'AVERAGE'2X,F6.3,3(2X,F6.3)//' '72X'SGT = 'F6.3)
153 FORMAT('0',32X'MIX = 'I3,1A1,9X'MODE = HYDROSTATIC TENSION (SINGLE
```

```
     * SIZE AGGREGATE)')
 154 FORMAT('-',21X'EQUATION'17X'FUNCTION'21X'RESIDUAL'6X'COC'5X'DEGF'5
     *X'STUDT')
 155 FORMAT('-',58X'FAILURE ENVELOPE')
 161 FORMAT('0',53X,E10.3/' '24X,I1,10X'S    = 'E10.3' R'20X,E10.3,5X,F6
     *.4,5X,I1,4X,F8.4)
 162 FORMAT('0',53X,E10.3/' '24X,I1,10X'E    = 'E10.3' R'20X,E10.3,5X,F6
     *.4,5X,I1,4X,F8.4)
 163 FORMAT('0',24X,I1,10X'E    = 'E10.3' +('E10.3')LOG R'3X,E10.3,5X,F6
     *.4,5X,I1,4X,F8.4)
 164 FORMAT('0',53X,E10.3/' '24X,I1,10X'SEC = 'E10.3' R'20X,E10.3,5X,F6
     *.4,5X,I1,4X,F8.4)
 165 FORMAT('0',53X,E10.3/' '24X,I1,10X'TAN = 'E10.3' R'20X,E10.3,5X,F6
     *.4,5X,I1,4X,F8.4)
 166 FORMAT('0',53X,E10.3/' '24X,I1,10X'S    = 'E10.3' E'20X,E10.3,5X,F6
     *.4,5X,I1,4X,F8.4)
 167 FORMAT('0',53X,E10.3/' '24X,I1,10X'E    = 'E10.3' S'20X,E10.3,5X,F6
     *.4,5X,I1,4X,F8.4)
 168 FORMAT('0',24X,I1,10X'E    = 'E10.3' +('E10.3')LOG S'3X,E10.3,5X,F6
     *.4,5X,I1,4X,F8.4)
 169 FORMAT('-',35X'WHERE MOD IN KSI, S IN PSI, E IN PERCENT, T IN MIN,
     * R IN PERCENT/MIN')
 170 FORMAT('-',35X'WHERE MOD IN PSI, S IN PSI, E IN IN/IN, T IN MIN, R
     * IN IN/(IN-MIN)')
 171 FORMAT('-',43X'WHERE MOD IN PSI, S IN PSI, E IN IN/IN, T IN MIN,'/
     *' '38X'R IN IN/(IN-MIN), Q IN PSI/MIN')
 172 FORMAT(2I2,1X,F5.0,1X,F6.3,1X,F4.1,1X,2(F5.2,1X),F6.3,1X,F5.2,2X,1
     *I1)
 173 FORMAT('0',24X,I1,10X'S    = 'E10.3' +('E10.3')LOG E'3X,E10.3,5X,F6
     *.4,5X,I1,4X,F8.4)
 175 FORMAT('-',24X'CONSTITUITIVE RELATIONS NOT APPLICABLE BECAUSE ''E'
     *' CANNOT BE DEFINED IN TERMS OF ''S''')
 176 FORMAT(2I2,1X,I3,1X,F5.0,1X,F6.3,1X,F4.1,1X,2(F5.2,1X),F6.3,1X,F5.
     *2,1X,2I1)
 177 FORMAT('1'///' ',41X'COMPARISON OF SAMPLE TIME TO FAILURE COMPUTAT
     *IONS')
 178 FORMAT(' ')
 179 FORMAT(' ',70X'AVERAGE'2X,F6.3,3(3X,F6.3)//' '70X'SGT = 'F6.3)
 180 FORMAT(' ',69X,'AVERAGE'2X,F6.3,3(2X,F6.3)//' '72X'SGT = 'F6.3)
 181 FORMAT('0',46X'MIX = 'I3,1A1,9X'MODE = SPLIT CYLINDER')
     END
C
C*****************SUBROUTINE FIT FOR LEAST SQUARES CALCULATIONS********
C

      SUBROUTINE FIT(N,OPT,Y,X,A,B,RES,NE,MODE,COC,DEGF,STUDT)
      INTEGER OPT,DEGF
      REAL X(15),Y(15),DX(15),DY(15)
C     OPT=1  Y=A+BX
C     OPT=2  Y=AX**B, LOGY=LOGA + BLOGX
C     OPT=3  Y=AB**X, LOGY=LOGA + X LOGB, X=A + B LOGY
      IF(MODE-4) 617,616,617
 616 GO TO (609,617,617,617,617,609,609,609,609),NE
 617 DN=N
     SUMX=0.0
     SUMY=0.0
     SUMXX=0.0
     SUMXY=0.0
     YA=0.0
     DO 600 I=1,N
```

```
      DX(I)=X(I)
      DY(I)=Y(I)
      YA=YA+Y(I)
      GO TO (601,602,603),OPT
  602 DX(I)=ALOG10(X(I))
  620 DY(I)=ALOG10(Y(I))
      GO TO 601
  603 DY(I)=ALOG10(Y(I))
  601 SUMX=SUMX+DX(I)
      SUMY=SUMY+DY(I)
      SUMXX=SUMXX+DX(I)*DX(I)
  600 SUMXY=SUMXY+DX(I)*DY(I)
      YA=YA/DN
      DYA=ALOG10(YA)
      DEN= DN*SUMXX - SUMX*SUMX
      A=(SUMXX*SUMY-SUMX*SUMXY)/DEN
      B=(DN*SUMXY-SUMX*SUMY)/DEN
      RES=0.0
      SEV=0.0
      STV=0.0
      GO TO (611,607,611),OPT
  607 A=10.0**A
  611 DO 615 I=1,N
      GO TO (612,613,614),OPT
  612 YE=A+B*X(I)
      RES=RES+(ABS(Y(I)-YE))**2.0
      SEV=SEV+(ABS(YE-YA))**2.0
      STV=STV+(ABS(Y(I)-YA))**2.0
      GO TO 615
  613 YE=A*X(I)**B
      DYE=ALOG10(YE)
      RES=RES+(ABS(DY(I)-DYE))**2.0
      SEV=SEV+(ABS(DYE-DYA))**2.0
      STV=STV+(ABS(DY(I)-DYA))**2.0
      GO TO 615
  614 YE=A+B*X(I)
      RES=RES+(ABS(DY(I)-YE))**2.0
      SEV=SEV+(ABS(YE-DYA))**2.0
      STV=STV+(ABS(DY(I)-DYA))**2.0
  615 CONTINUE
      GO TO (850,850,608),OPT
  608 A=-A/B
      B=1.0/B
  850 DEGF=N-2
      COC=SQRT(SEV/STV)
      COCD=1.0-COC*COC
      IF(COCD .LE. 0.0) GO TO 618
      STUDT=(COC*SQRT(DN-2.0))/SQRT(COCD)
      GO TO 606
  618 STUDT=0.0
      GO TO 606
  609 WRITE(6,174) NE
      OPT=0
      A=0.0
  606 RETURN
  174 FORMAT('0',24X,I1,10X'EQUATION IS NOT APPLICABLE')
      END
C
C********SUBROUTINE TIME FOR SAMPLE CALCULATIONS OF TIME TO FAILURE*****
C
```

```
      SUBROUTINE TIME(N,AR,AE,A,B)
      REAL AR(15),AE(15)
      WRITE(6,200)
      SRAT=0.0
      DN=N
      DO 700 I=1,N
      TTFT=AE(I)/AR(I)
      TTFE=A*AR(I)**B
      RATIO=TTFT/TTFE
      SRAT=SRAT+RATIO
  700 WRITE(6,201) AR(I),TTFT,TTFE,RATIO
      AVRAT=SRAT/DN
      WRITE(6,202) AVRAT
      RETURN
  200 FORMAT('0',39X'AR'12X'TTFT'14X'TTFE'13X'RATIO'/' ',35X'(IN/IN-MIN)
     *'3X'(AE/AR,MIN)'3X'(FROM EQUATION,MIN)'3X'(TTFT/TTFE)'/)
  201 FORMAT(' ',35X,F10.6,5X,F8.4,10X,F8.4,7X,F11.4)
  202 FORMAT(' ',69X,'AVERAGE TTFT/TTFE'F8.4)
      END
C
C************************NOMENCLATURE**********************************
C
C     A,B              INTERCEPT AND SLOPE IN Y= A + BX
C     AREA             CROSS SECTIONAL AREA OF SPECIMEN, SQUARE INCHES
C     BD               AVERAGE BEAD DIAMETER
C     CH               CROSSHEAD SPEED, IN/MIN
C     COC              COEFFICIENT OF CORRELATION
C     CS               CHART SPEED, IN/MIN
C     DEGF             DEGREES OF FREEDOM
C     D,F              DEFORMATION AND FORCE IN CALIBRATION, IN., LB.
C     DIS,DMS          DEFORMATION INDICATED AND MACHINE FOR SECANT, IN.
C     DIT,DMT          DEFORMATION INDICATED AND MACHINE FOR TANGENT, IN.
C     E                ULTIMATE STRAIN, PERCENT
C     ET               INITIAL TANGENT STRAIN, PERCENT
C     FAD              FIELD AVERAGE DEVIATION
C     FRAC             FRACTION OF ULTIMATE LOAD FOR DETERMINING TANGENT
C     FS               FULL SCALE
C     H, W, D          SPECIMEN HEIGHT, WIDTH, DEPTH
C     JILT             CONTROL TO PRINT HEADINGS
C                           1   DIMENSIONS
C                           2   DATA
C                           3   DIMENSIONS AND DATA
C                           4   TEST RESULTS
C                           5   DATA REDUCTION
C                           6   ANALYSIS
C                           7   CONSTITUITIVE RELATIONS
C                           8   CONVERSIONS
C     KR               COUNTER OF AVERAGE RATES
C     KS               COUNTER ON SECANT FORCE INCREMENT FROM CALIBRATION
C     KT               COUNTER ON TANGENT FORCE INCREMENT FROM CALIBRATION
C     LCIS             LAST CARD IN SET
C     LS               LAST SET
C     MODE OF LOADING
C               1      UNIAXIAL TENSION
C               2      UNIAXIAL COMPRESSION
C               3      HYDROSTATIC TENSION
C               4      HYDROSTATIC COMPRESSION
C               5      DOUBLE LAP SHEAR
C               6      HYDROSTATIC TENSION(SINGLE SIZE AGGREGRATE)
C               7      SPLIT CYLINDER
```

```
C      NAD             NUMBER OF AVERAGE DEVIATIONS
C      NAR             NUMBER OF AVERAGE STRAIN RATES
C      NB              NUMBER OF BEADS PER SPECIMEN
C      NCP             NUMBER OF CALIBRATION POINTS
C      NE              NUMBER OF EQUATIONS
C      NIA             NUMBER IN AVERAGE
C      NS              SPECIMEN NUMBER
C      NSAMP           NUMBER OF SAMPLES
C      NT              NUMBER OF TESTS IN MIX
C      PREFIX A        AVERAGE
C      PREFIX D        DEVIATION
C      PREFIX S        SUM
C      Q               STRESS RATE, PSI/MINUTE
C      R               STRAIN RATE, PERCENT/MIN
C
C      RES             RESIDUAL
C      S               ULTIMATE STRESS,PSI
C      SEC             ULTIMATE SECANT MODULUS, KSI
C      SEV             SUM OF EXPLAINED VARIANCE
C      SF,TF           SECANT AND TANGENT FORCE, LBS.
C      SGM             SPECIFIC GRAVITY MEASURED, NUMERIC
C      SGT             SPECIFIC GRAVITY THEORETICAL, NUMERIC
C      SGW             SPECIFIC GRAVITY WEIGHED IN WATER, NUMERIC
C      STUDT           VALUE OF 'T' FOR OBTAINING THE LEVEL OF SIGNIFICANCE
C                           OF THE COEFFICIENT OF CORRELATION FROM A STUDENT
C                           'T' DISTRIBUTION TABLE
C      STV             SUM OF TOTAL VARIANCE
C      SUFFIX C        CALIBRATION
C      SUFFIX D        DUMMY
C      T               TIME, MINUTES
C      TAN             INITIAL TANGENT MODULUS, KSI
C      TTF             TIME TO FAILURE, MINUTES
C      TTFE            TIME TO FAILURE BASED UPON EQUATIONS
C      TTFT            TIME TO FAILURE BASED UPON TEST RESULTS
C      VOL             VOLUME OF SPECIMEN, CUBIC INCHES
C      VSGM, VSGW      AIR VOID, PERCENT
C      WA              WEIGHT IN AIR, GRAMS
C      WW              WEIGHT IN WATER, GRAMS
C      XA,YA           AVERAGE X OR Y DATA
C      XC,YC           GRAPH DIVISIONS IN CALIBRATION
C      XE,YE           ESTIMATE OF X OR Y FROM EQUATION
C      XS,YS           GRAPH DIVISIONS TO ULTIMATE SECANT
C      XT,YT           GRAPH DIVISIONS TO INITIAL TANGENT
C      FOR SHEAR SPECIMEN DIMENSIONS, AH IS DISTANCE BETWEEN PLATES, AW
C           IS MEASURED ALONG THE PLATES, AND AD IS THE THICKNESS

$DATA
```

APPENDIX B1

Double Lap Shear Specimen Dimensions, Specific Gravity and Void Content

APPENDIX B1-A; Mix 15

NS Spec. No.	AW Avg. Width $\overline{W}$ (in.)	AD Avg. Depth $\overline{D}$ (in.)	AH Avg. Height $\overline{H}$ (in.)	VOL Volume V (cu. in.)	WA Wt. in Air (gms)	WW Wt. in Water (gms)	SGM Sp.Gr. from Dimen.	SGW Sp.Gr. from Water Displ.	VSGM Void Volume from SGM (percent)	VSGW Void Volume from SGW (percent)
1	3.917	0.917	1.890	6.793	269.3	157.2	2.414	2.402	1.014	1.504
2	3.920	0.872	1.820	6.225	257.1	150.2	2.515	2.405		1.392
3	3.877	0.910	1.807	6.378	255.8	149.8	2.443	2.413	-0.148	1.058
4	3.927	0.902	1.790	6.345	252.7	147.8	2.426	2.409	0.550	1.232
5	3.930	0.905	1.775	6.313	270.7	158.0	2.611	2.402		1.519
6	3.930	0.902	1.897	6.730	268.6	156.9	2.431	2.405	0.345	1.408
7	3.827	0.937	1.905	6.836	268.6	156.9	2.393	2.405	1.884	1.408
8	3.832	0.925	1.795	6.363	253.5	147.8	2.426	2.398	0.527	1.669
9	3.835	0.932	1.805	6.455	250.1	145.9	2.360	2.400	3.253	1.591
10	3.837	0.915	1.795	6.303	251.9	147.2	2.434	2.406	0.205	1.356
11	3.842	0.930	1.813	6.477	254.3	148.4	2.391	2.401	1.964	1.545
12	3.832	0.910	1.837	6.408	256.3	149.7	2.436	2.404	0.135	1.422
13	4.037	0.942	1.785	6.793	267.4	156.1	2.397	2.403	1.702	1.496
14	4.032	0.920	1.767	6.557	260.2	151.8	2.417	2.400	0.917	1.584
15	4.030	0.927	1.780	6.653	264.1	154.2	2.417	2.403	0.884	1.472
16	4.025	0.935	1.773	6.671	262.5	153.2	2.397	2.402	1.739	1.532
17	4.040	0.937	1.825	6.912	272.9	159.3	2.404	2.402	1.417	1.505
18	4.020	0.925	1.885	7.009	278.9	163.0	2.423	2.406	0.646	1.337
19	4.015	0.912	2.135	7.822	309.2	180.8	2.407	2.408	1.295	1.267
20	4.072	0.927	2.033	7.677	309.9	181.2	2.458	2.408		1.274
21	4.002	0.907	1.987	7.219	283.9	166.6	2.395	2.420	1.804	0.767
22	3.965	0.927	1.865	6.859	275.8	161.3	2.449	2.409		1.241
						AVERAGE	2.429	2.405		1.390

Theoretical Specific Gravity 2.439

APPENDIX B1-B; Mix 20

NS	AW	AD	AH	VOL	WA	WW	SGM	SGW	VSGM	VSGW
Spec. No.	Avg. Width W (in.)	Avg. Depth D (in.)	Avg. Height H (in)	Volume V (cu. in.)	Wt. in Air (gms)	Wt. in Water (gms)	Sp.Gr. from Dimen.	Sp.Gr. from Water Displ.	Void Volume from SGM (percent)	Void Volume from SGW (percent)
1	3.962	0.960	2.002	7.618	298.4	174.6	2.386	2.410	2.186	1.175
2	3.962	0.980	1.967	7.640	297.6	174.6	2.372	2.420	2.739	0.799
3	3.975	0.982	2.015	7.869	304.1	177.9	2.353	2.410	3.509	1.203
4	4.005	0.970	1.985	7.711	297.1	173.1	2.346	2.396	3.798	1.764
5	3.870	0.982	1.982	7.538	296.5	173.8	2.395	2.416	1.784	0.924
6	3.890	0.970	1.942	7.330	285.9	167.1	2.376	2.407	2.603	1.330
7	3.875	0.930	1.955	7.045	285.2	166.5	2.465	2.403	-1.080	1.489
8	3.870	0.947	1.907	6.994	273.5	159.2	2.381	2.393	2.362	1.893
9	3.892	0.942	1.925	7.062	280.1	163.7	2.415	2.406	0.965	1.338
10	3.890	0.947	1.972	7.270	284.1	166.0	2.380	2.406	2.424	1.370
11	3.922	0.980	2.025	7.784	307.7	180.2	2.407	2.413	1.297	1.052
12	3.915	0.962	1.915	7.216	287.2	168.1	2.424	2.411	0.620	1.131
13	3.912	0.950	1.940	7.211	285.0	166.1	2.407	2.397	1.308	1.723
14	3.915	0.955	1.955	7.309	285.2	166.4	2.376	2.401	2.572	1.571
15	3.927	0.945	1.910	7.089	279.0	162.5	2.397	2.395	1.726	1.810
16	3.940	0.962	1.927	7.310	286.9	167.3	2.390	2.399	1.994	1.647
17	3.797	0.957	2.010	7.309	284.2	166.1	2.368	2.406	2.903	1.335
18	3.785	0.935	1.937	6.857	272.0	159.2	2.416	2.411	0.948	1.134
19	3.785	0.952	1.927	6.949	270.5	157.9	2.371	2.402	2.802	1.504
20	3.773	0.942	1.930	6.862	273.3	159.2	2.425	2.395	0.554	1.793
21	3.783	0.952	1.975	7.116	282.0	164.6	2.414	2.402	1.041	1.515
22	3.780	0.957	1.902	6.886	274.8	160.7	2.430	2.408	0.350	1.254
						AVERAGE	2.395	2.405	1.791	1.398

Theoretical Specific Gravity 2.439

APPENDIX B1-C; Mix 21

NS	AW	AD	AH	VOL	WA	WW	SGM	SGW	VSGM	VSGW
Spec. No.	Avg. Width $\overline{W}$ (in.)	Avg. Depth $\overline{D}$ (in.)	Avg. Height $\overline{H}$ (in.)	Volume V (cu. in.)	Wt. in Air (gms)	Wt. in Water (gms)	Sp.Gr. from Dimen.	Sp.Gr. from Water Displ.	Void Volume from SGM (percent)	Void Volume from SGW (percent)
1	3.910	0.997	1.890	7.371	288.5	167.8	2.384	2.390	2.274	2.000
2	3.907	0.997	1.895	7.386	286.0	165.3	2.358	2.370	3.315	2.849
3	3.910	0.990	1.932	7.481	290.0	168.2	2.361	2.381	3.199	2.380
4	3.925	0.985	1.962	7.587	294.2	172.0	2.361	2.408	3.178	1.290
5	3.937	0.975	1.902	7.304	286.9	168.4	2.392	2.421	1.917	0.734
6	3.835	0.975	1.917	7.170	282.0	164.9	2.395	2.408	1.789	1.263
7	3.827	0.967	1.845	6.832	273.9	160.4	2.442	2.413	-0.103	1.057
8	3.817	0.965	1.877	6.916	277.8	162.8	2.446	2.416	-0.291	0.957
9	3.822	0.967	1.892	6.999	276.1	161.3	2.402	2.405	1.497	1.392
10	3.827	0.970	1.875	6.961	274.8	160.2	2.404	2.398	1.430	1.685
11	3.855	1.000	2.010	7.749	302.9	175.2	2.381	2.372	2.390	2.748
12	3.850	0.985	1.842	6.987	275.6	160.1	2.402	2.386	1.510	2.167
13	3.865	0.985	1.895	7.214	279.3	162.7	2.358	2.395	3.330	1.789
14	3.845	0.975	1.840	6.898	271.2	158.3	2.394	2.402	1.828	1.512
15	3.835	0.972	1.882	7.021	277.9	162.5	2.411	2.408	1.164	1.265
16	3.852	0.965	2.073	7.705	302.5	177.0	2.391	2.410	1.966	1.174
						AVERAGE	2.393	2.399	1.900	1.641

Theoretical Specific Gravity 2.439

APPENDIX B2

Uniaxial Tension Specimen Dimensions, Specific Gravity and Void Content

APPENDIX B2-A; Mix 9

NS Spec. No.	AW Avg. Width $\overline{W}$ (in.)	AD Avg. Depth $\overline{D}$ (in.)	AH Avg. Height $\overline{H}$ (in.)	VOL Volume V (cu.in.)	WA Wt. in Air (gms)	WW Wt. in Water (gms)	SGM Sp.Gr. from Dimen.	SGW Sp.Gr. from Water Displ.	VSGM Void Volume from SGM (percent)	VSGW Void Volume from SGW (percent)
13	1.450	1.575	5.957	13.605	516.3	298.2	2.311	2.367	5.244	2.941
14	1.587	1.385	5.962	13.110	501.2	288.8	2.328	2.360	4.537	3.251
15	1.582	1.345	5.932	12.627	483.2	278.8	2.331	2.364	4.448	3.075
16	1.310	1.505	6.025	11.879	461.9	267.3	2.368	2.374	2.905	2.682
17	1.375	1.525	6.030	12.644	491.0	284.2	2.365	2.374	3.037	2.654
18	1.597	1.367	6.015	13.140	506.8	293.4	2.349	2.375	3.695	2.629
19	1.427	1.587	6.025	13.654	523.0	302.8	2.333	2.375	4.353	2.619
20	1.412	1.537	6.042	13.123	514.8	297.8	2.389	2.372	2.043	2.733
						AVERAGE	2.347	2.370	3.783	2.823

Theoretical Specific Gravity 2.439

APPENDIX B2-B; Mix 10

NS Spec. No.	AW Avg. Width $\overline{W}$ (in.)	AD Avg. Depth $\overline{D}$ (in.)	AH Avg. Height $\overline{H}$ (in.)	VOL Volume V (cu.in.)	WA Wt. in Air (gms)	WW Wt. in Water (gms)	SGM Sp.Gr. from Dimen.	SGW Sp.Gr. from Water Displ.	VSGM Void Volume from SGM (percent)	VSGW Void Volume from SGW (percent)
13	1.550	1.367	5.862	12.426	482.6	280.8	2.365	2.391	3.025	1.949
14	1.517	1.460	5.870	13.005	509.6	296.4	2.386	2.390	2.158	1.999
15	1.537	1.270	5.852	11.428	453.0	263.7	2.414	2.393	1.019	1.885
16	1.450	1.422	5.915	12.200	470.1	272.1	2.347	2.374	3.788	2.655
17	1.528	1.370	5.905	12.357	485.5	280.9	2.393	2.373	1.897	2.709
18	1.477	1.390	5.892	12.102	466.2	268.9	2.346	2.363	3.806	3.120
19	1.530	1.417	5.910	12.817	498.7	288.0	2.370	2.367	2.848	2.957
20	1.450	1.392	5.907	11.928	473.5	273.2	2.418	2.364	0.878	3.077
						AVERAGE	2.380	2.377	2.427	2.544
						Theoretical Specific Gravity	2.439			

APPENDIX B2-C; Mix 11

NS Spec. No.	AW Avg. Width $\overline{W}$ (in.)	AD Avg. Depth $\overline{D}$ (in.)	AH Avg. Height $\overline{H}$ (in.)	VOL Volume V (cu.in.)	WA Wt. in Air (gms)	WW Wt. in Water (gms)	SGM Sp.Gr. from Dimen.	SGW Sp.Gr. from Water Displ.	VSGM Void Volume from SGM (percent)	VSGW Void Volume from SGW (percent)
13	1.535	1.445	5.870	13.020	508.1	296.0	2.377	2.396	2.557	1.781
14	1.502	1.397	5.857	12.299	477.1	277.2	2.362	2.387	3.139	2.145
15	1.542	1.470	5.852	13.270	512.4	297.8	2.352	2.388	3.586	2.103
16	1.528	1.430	5.882	12.849	512.4	298.2	2.429	2.392	0.426	1.921
17	1.507	1.362	5.902	12.124	472.0	274.8	2.371	2.394	2.786	1.865
18	1.457	1.460	5.905	12.566	492.3	286.5	2.386	2.392	2.172	1.922
19	1.545	1.412	5.892	12.859	510.9	297.0	2.420	2.388	0.795	2.071
20	1.480	1.427	5.915	12.497	488.2	284.1	2.379	2.392	2.451	1.928
						AVERAGE	2.384	2.391	2.239	1.967

Theoretical Specific Gravity 2.439

APPENDIX B2-D; Mix 12

NS Spec. No.	AW Avg. Width $\overline{W}$ (in.)	AD Avg. Depth $\overline{D}$ (in.)	AH Avg. Height $\overline{H}$ (in.)	VOL Volume V (cu.in.)	WA Wt. in Air (gms)	WW Wt. in Water (gms)	SGM Sp.Gr. from Dimen.	SGW Sp.Gr. from Water Displ.	VSGM Void Volume from SGM (percent)	VSGW Void Volume from SGW (percent)
13	1.580	1.470	5.992	13.918	527.8	305.5	2.309	2.374	5.310	2.654
14	1.552	1.367	5.990	12.717	487.0	282.5	2.332	2.381	4.378	2.361
15	1.590	1.477	5.975	14.037	539.8	313.0	2.342	2.380	3.975	2.416
16	1.542	1.430	5.917	13.053	507.4	294.4	2.367	2.382	2.934	2.331
17	1.523	1.495	5.927	13.492	518.0	300.5	2.338	2.382	4.132	2.353
18	1.552	1.292	5.917	11.874	457.9	266.1	2.349	2.387	3.709	2.116
19	1.542	1.357	5.922	12.401	475.9	275.2	2.337	2.371	4.179	2.780
20	1.437	1.405	5.945	12.007	460.8	267.7	2.337	2.386	4.172	2.160
						AVERAGE	2.339	2.381	4.099	2.396

Theoretical Specific Gravity 2.439

APPENDIX B2-E; Mix 13

NS	AW	AD	AH	VOL	WA	WW	SGM	SGW	VSGM	VSGW
Spec. No.	Avg. Width $\overline{W}$ (in.)	Avg. Depth $\overline{D}$ (in.)	Avg. Height $\overline{H}$ (in.)	Volume V (cu.in.)	Wt. in Air (gms)	Wt. in Water (gms)	Sp.Gr. from Dimen.	Sp.Gr. from Water Displ.	Void Volume from SGM (percent)	Void Volume from SGW (percent)
13	1.547	1.425	5.597	12.344	497.7	291.5	2.456	2.414	1.619	3.298
14	1.547	1.430	5.607	12.409	476.6	278.8	2.339	2.410	6.287	3.465
15	1.467	1.450	5.600	11.916	481.8	281.9	2.462	2.410	1.346	3.437
16	1.395	1.402	5.967	11.675	476.2	280.0	2.484	2.427	0.482	2.760
17	1.502	1.430	5.957	12.800	523.9	305.9	2.493	2.403	0.134	3.718
18	1.410	1.490	5.952	12.506	508.0	299.4	2.474	2.435	0.884	2.433
19	1.512	1.410	5.952	12.694	514.8	303.9	2.470	2.441	1.052	2.205
20	1.472	1.323	5.942	11.572	475.3	280.6	2.501	2.441	-0.214	2.196
						AVERAGE	2.460	2.423	1.449	2.939

Theoretical Specific Gravity 2.496

APPENDIX B2-F; Mix 14

NS Spec. No.	AW Avg. Width $\overline{W}$ (in.)	AD Avg. Depth $\overline{D}$ (in.)	AH Avg. Height $\overline{H}$ (in.)	VOL Volume V (cu.in.)	WA Wt. in Air (gms)	WW Wt. in Water (gms)	SGM Sp.Gr. from Dimen.	SGW Sp.Gr. from Water Displ.	VSGM Void Volume from SGM (percent)	VSGW Void Volume from SGW (percent)
13	1.412	1.452	5.870	12.043	471.8	275.6	2.386	2.405	2.179	1.407
14	1.323	1.440	5.902	11.241	437.2	255.6	2.369	2.407	2.882	1.292
15	1.377	1.440	5.882	11.669	459.1	268.1	2.396	2.404	1.756	1.449
16	1.392	1.430	5.830	11.609	461.3	269.0	2.420	2.399	0.780	1.646
17	1.385	1.457	5.857	11.824	458.3	267.5	2.361	2.402	3.218	1.517
18	1.422	1.465	5.852	12.196	480.8	280.8	2.401	2.404	1.565	1.435
19	1.347	1.427	5.857	11.267	444.8	259.2	2.404	2.397	1.426	1.740
20	1.420	1.432	5.840	11.879	467.5	272.9	2.397	2.402	1.734	1.502
						AVERAGE	2.392	2.402	1.942	1.499

Theoretical Specific Gravity 2.439

APPENDIX B3

Uniaxial Compression Specimen Dimensions, Specific Gravity and Void Content

APPENDIX B3-A; Mix 9

NS Spec. No.	AW Avg. Width $\overline{W}$ (in.)	AD Avg. Depth $\overline{D}$ (in.)	AH Avg. Height $\overline{H}$ (in.)	VOL Volume V (cu.in.)	WA Wt. in Air (gms)	WW Wt. in Water (gms)	SGM Sp.Gr. from Dimen.	SGW Sp.Gr. from Water Displ.	VSGM Void Volume from SGM (percent)	VSGW Void Volume from SGW (percent)
1	1.542	1.483	5.985	13.686	540.7	313.2	2.406	2.377	1.352	2.554
2	1.652	1.645	5.957	16.195	737.7	370.7	2.774	2.010	******	
3	1.512	1.648	5.887	14.671	587.4	340.6	2.438	2.380	0.024	2.416
4	1.542	1.650	5.875	14.953	527.2	305.8	2.147	2.381	11.961	2.369
5	1.477	1.515	5.985	13.397	513.0	297.2	2.332	2.377	4.384	2.534
6	1.400	1.527	5.947	12.719	482.5	278.9	2.310	2.370	5.274	2.836
7	1.492	1.507	5.970	13.432	521.8	302.5	2.366	2.379	2.999	2.444
8	1.532	1.432	6.047	13.276	488.9	283.7	2.243	2.383	8.047	2.314
9	1.407	1.552	6.020	13.155	513.2	296.8	2.376	2.372	2.585	2.766
10	1.510	1.570	6.002	14.230	560.7	325.3	2.400	2.382	1.613	2.341
11	1.395	1.565	5.945	12.979	494.0	285.8	2.318	2.373	4.961	2.718
12	1.340	1.597	5.945	12.726	496.5	287.1	2.376	2.371	2.582	2.786
						AVERAGE	2.374	2.346	2.670	2.465

Theoretical Specific Gravity 2.439

APPENDIX B3-B; Mix 10

NS	AW	AD	AH	VOL	WA	WW	SGM	SGW	VSGM	VSGW
Spec. No.	Avg. Width $\overline{W}$ (in.)	Avg. Depth $\overline{D}$ (in.)	Avg. Height $\overline{H}$ (in.)	Volume V (cu.in.)	Wt. in Air (gms)	Wt. in Water (gms)	Sp.Gr. from Dimen.	Sp.Gr. from Water Displ.	Void Volume from SGM (percent)	Void Volume from SGW (percent)
1	1.487	1.492	5.815	12.910	504.9	292.8	2.382	2.380	2.344	2.399
2	1.552	1.497	5.865	13.635	534.9	309.0	2.389	2.368	2.046	2.917
3	1.500	1.462	5.905	12.954	524.0	300.4	2.463	2.343	-1.004	3.917
4	1.547	1.477	5.882	13.450	519.8	301.2	2.354	2.378	3.499	2.507
5	1.572	1.552	5.770	14.086	553.7	323.0	2.394	2.400	1.850	1.595
6	1.542	1.502	5.902	13.680	524.3	302.9	2.334	2.368	4.298	2.907
7	1.537	1.435	5.897	13.012	508.1	294.2	2.378	2.375	2.494	2.607
8	1.580	1.482	5.845	13.691	531.3	308.5	2.363	2.385	3.101	2.228
9	1.523	1.505	5.850	13.404	527.0	305.5	2.394	2.379	1.831	2.451
10	1.492	1.372	5.872	12.030	469.8	272.4	2.378	2.380	2.483	2.422
11	1.575	1.500	5.857	13.838	546.4	317.4	2.405	2.386	1.408	2.172
12	1.530	1.387	5.867	12.456	480.8	279.1	2.351	2.384	3.617	2.266
						AVERAGE	2.382	2.377	2.331	2.532

Theoretical Specific Gravity 2.439

APPENDIX B3-C; Mix 11

NS	AW	AD	AH	VOL	WA	WW	SGM	SGW	VSGM	VSGW
Spec. No.	Avg. Width $\overline{W}$ (in.)	Avg. Depth $\overline{D}$ (in.)	Avg. Height $\overline{H}$ (in.)	Volume V (cu.in.)	Wt. in Air (gms)	Wt. in Water (gms)	Sp.Gr. from Dimen.	Sp.Gr. from Water Displ.	Void Volume from SGM (percent)	Void Volume from SGW (percent)
1	1.592	1.560	5.822	14.465	571.5	333.4	2.406	2.400	1.345	1.589
2	1.592	1.537	5.807	14.219	565.2	330.8	2.421	2.411	0.749	1.137
3	1.613	1.438	5.782	13.404	529.9	310.3	2.408	2.413	1.284	1.065
4	1.528	1.537	5.870	13.786	539.0	314.3	2.381	2.399	2.373	1.650
5	1.455	1.472	5.880	12.598	496.1	288.0	2.398	2.384	1.669	2.257
6	1.537	1.510	5.902	13.703	539.8	314.5	2.399	2.396	1.640	1.766
7	1.485	1.400	5.900	12.266	482.2	280.4	2.394	2.389	1.840	2.030
8	1.557	1.467	5.820	13.302	525.0	307.0	2.404	2.408	1.452	1.261
9	1.507	1.477	5.900	13.141	514.2	300.3	2.383	2.404	2.296	1.438
10	1.470	1.542	5.915	13.412	529.5	308.7	2.404	2.398	1.421	1.677
11	1.435	1.407	5.842	11.800	466.0	271.1	2.405	2.391	1.394	1.969
12	1.500	1.407	5.875	12.404	471.5	273.2	2.315	2.378	5.082	2.513
						AVERAGE	2.393	2.398	1.879	1.696

Theoretical Specific Gravity 2.439

APPENDIX B3-D; Mix 12

NS Spec. No.	AW Avg. Width $\overline{W}$ (in.)	AD Avg. Depth $\overline{D}$ (in.)	AH Avg. Height $\overline{H}$ (in.)	VOL Volume V (cu.in.)	WA Wt. in Air (gms)	WW Wt. in Water (gms)	SGM Sp.Gr. from Dimen.	SGW Sp.Gr. from Water Displ.	VSGM Void Volume from SGM (percent)	VSGW Void Volume from SGW (percent)
1	1.557	1.457	5.860	13.303	525.2	307.3	2.404	2.410	1.416	1.178
2	1.495	1.465	5.840	12.791	494.6	284.5	2.355	2.354	3.444	3.480
3	1.382	1.515	5.912	12.384	482.4	279.6	2.372	2.379	2.731	2.472
4	1.452	1.492	5.937	12.872	495.4	287.2	2.344	2.379	3.897	2.442
5	1.532	1.512	5.965	13.826	550.0	319.6	2.423	2.387	0.672	2.126
6	1.462	1.457	5.992	12.774	496.7	290.0	2.368	2.403	2.905	1.476
7	1.460	1.432	5.992	12.533	491.5	285.5	2.388	2.386	2.077	2.176
8	1.572	1.445	5.905	13.418	520.7	302.7	2.363	2.389	3.100	2.069
9	1.500	1.555	5.905	13.773	537.2	313.3	2.375	2.399	2.611	1.628
10	1.545	1.502	5.922	13.748	518.2	302.0	2.295	2.397	5.884	1.728
11	1.577	1.395	5.967	13.132	508.0	295.1	2.356	2.386	3.408	2.169
12	1.517	1.315	5.972	11.918	459.1	265.9	2.346	2.376	3.814	2.571
						AVERAGE	2.366	2.387	2.997	2.126
						Theoretical Specific Gravity	2.439			

APPENDIX B3-E; Mix 13

NS	AW	AD	AH	VOL	WA	WW	SGM	SGW	VSGM	VSGW
Spec. No.	Avg. Width $\overline{W}$ (in.)	Avg. Depth $\overline{D}$ (in.)	Avg. Height $\overline{H}$ (in.)	Volume V (cu.in.)	Wt. in Air (gms)	Wt. in Water (gms)	Sp.Gr. from Dimen.	Sp.Gr. from Water Displ.	Void Volume from SGM (percent)	Void Volume from SGW (percent)
1.	1.470	1.475	5.925	12.847	517.0	304.8	2.451	2.436	1.808	2.389
2	1.547	1.447	5.835	13.070	524.8	308.9	2.445	2.431	2.031	2.614
3	1.495	1.517	5.775	13.102	521.8	308.4	2.426	2.445	2.823	2.036
4	1.482	1.452	5.685	12.242	490.0	289.4	2.438	2.443	2.335	2.137
5	1.547	1.547	5.587	13.381	541.0	318.0	2.462	2.426	1.349	2.804
6	1.480	1.497	5.612	12.439	501.2	295.0	2.454	2.431	1.687	2.618
7	1.492	1.395	5.610	11.680	472.7	277.9	2.465	2.427	1.255	2.781
8	1.575	1.460	5.942	13.665	566.2	344.0	2.523	2.548	-1.100	-2.090
9	1.533	1.560	5.982	14.302	560.8	330.0	2.388	2.430	4.328	2.652
10	1.550	1.555	5.980	14.413	568.5	333.9	2.402	2.423	3.761	2.914
11	1.470	1.432	5.592	11.777	484.8	285.0	2.507	2.426	-0.445	2.787
12	1.477	1.462	5.607	12.117	496.5	291.5	2.495	2.422	0.021	2.967
						AVERAGE	2.455	2.441	1.655	2.217

Theoretical Specific Gravity 2.496

APPENDIX B3-F; Mix 14

NS	AW	AD	AH	VOL	WA	WW	SGM	SGW	VSGM	VSGW
Spec. No.	Avg. Width $\overline{W}$ (in.)	Avg. Depth $\overline{D}$ (in.)	Avg. Height $\overline{H}$ (in.)	Volume V (cu.in.)	Wt. in Air (gms)	Wt. in Water (gms)	Sp.Gr. from Dimen.	Sp.Gr. from Water Displ.	Void Volume from SGM (percent)	Void Volume from SGW (percent)
1	1.467	1.470	5.962	12.862	496.7	289.9	2.352	2.402	3.576	1.524
2	1.712	1.475	5.985	15.118	592.0	345.9	2.385	2.406	2.220	1.372
3	1.622	1.450	6.030	14.186	552.4	322.3	2.371	2.401	2.770	1.570
4	1.667	1.482	6.045	14.944	575.3	336.6	2.345	2.410	3.871	1.183
5	1.380	1.440	5.900	11.724	459.7	267.9	2.388	2.397	2.097	1.732
6	1.475	1.450	5.900	12.619	522.6	304.9	2.522	2.401	-3.413	1.577
7	1.457	1.447	5.875	12.395	487.2	284.7	2.394	2.406	1.850	1.356
8	1.382	1.457	5.837	11.763	466.9	272.9	2.417	2.407	0.885	1.324
9	1.385	1.440	5.832	11.632	460.6	268.7	2.411	2.400	1.128	1.591
10	1.492	1.460	5.852	12.753	499.4	291.4	2.385	2.401	2.219	1.560
11	1.337	1.438	5.882	11.310	438.9	256.2	2.363	2.402	3.101	1.505
12	1.392	1.452	5.875	11.883	461.8	269.4	2.367	2.400	2.960	1.591
						AVERAGE	2.392	2.403	1.939	1.490

Theoretical Specific Gravity 2.439

APPENDIX B4

Splitting Tension Specimen Dimensions,

Specific Gravity and Void Content

APPENDIX B4-A; Mix 39

NS Spec. No.	H_1 Height Measurement (in.)	H_2 (in.)	H_3 (in.)	AH Avg. Height $\bar{H}$ (in.)	VOL Volume V (cu.in.)	WA Wt. in Air (gms)	WW Wt. in Water (gms)	SGM Sp.Gr. from Dimen.	SGW Sp.Gr. from Water Displ.	VSGM Void Volume from SGM (percent)	VSGW Void Volume from SGW (percent)
1	1.862	1.863	1.868	1.864	23.416	945.0	555.1	2.458	2.424	-0.771	0.627
2	1.951	1.946	1.956	1.951	24.505	974.3	571.5	2.421	2.419	0.720	0.827
3	1.908	1.906	1.899	1.904	23.918	949.0	557.4	2.416	2.423	0.928	0.640
4	1.922	1.929	1.919	1.923	24.157	968.8	568.7	2.442	2.421	-0.139	0.722
5	1.916	1.910	1.900	1.909	23.973	961.8	564.8	2.443	2.423	-0.180	0.670
6	1.893	1.895	1.892	1.893	23.780	945.0	555.5	2.420	2.426	0.773	0.525
7	1.906	1.918	1.916	1.913	24.031	965.0	568.1	2.446	2.431	-0.268	0.314
8	1.971	1.982	1.968	1.974	24.789	998.7	586.5	2.454	2.423	-0.597	0.662
9	1.942	1.953	1.940	1.945	24.429	980.1	575.3	2.443	2.421	-0.179	0.730
10	1.874	1.885	1.901	1.887	23.697	955.7	562.8	2.456	2.432	-0.705	0.270
11	1.828	1.824	1.831	1.828	22.955	924.2	544.1	2.452	2.431	-0.530	0.309
12	1.800	1.789	1.811	1.800	22.608	913.9	539.2	2.462	2.439	-0.937	-0.001
13	1.887	1.899	1.916	1.901	23.872	959.2	562.0	2.447	2.415	-0.329	0.988
14	1.999	2.002	1.995	1.999	25.103	1016.0	595.4	2.465	2.416	-1.060	0.960
15	1.887	1.896	1.894	1.892	23.768	980.0	573.4	2.511	2.410	-2.957	1.180
16	1.985	1.992	1.966	1.981	24.881	1013.2	592.9	2.480	2.411	-1.680	1.162
17	1.893	1.873	1.910	1.892	23.764	976.2	571.9	2.502	2.415	-2.575	1.003
18	1.948	1.939	1.939	1.942	24.392	979.0	573.2	2.444	2.413	-0.221	1.086
19	1.801	1.798	1.786	1.795	22.545	914.8	534.9	2.471	2.408	-1.318	1.271
20	1.929	1.919	1.932	1.927	24.199	984.2	579.0	2.477	2.429	-1.555	0.413
21	1.946	1.939	1.934	1.940	24.362	975.8	572.5	2.439	2.420	-0.014	0.798
22	1.966	1.940	1.949	1.952	24.513	995.1	584.3	2.472	2.422	-1.365	0.683
23	2.013	2.002	1.996	2.004	25.166	1013.2	594.1	2.452	2.418	-0.530	0.879
24	1.957	1.964	1.961	1.961	24.626	995.0	582.5	2.461	2.412	-0.889	1.102
							AVERAGE	2.456	2.421	-0.682	0.742
							Theoretical Specific Gravity	2.439			

APPENDIX B4-B; Mix 43

NS	H_1	H_2	H_3	AH	VOL	WA	WW	SGM	SGW	VSGM	VSGW
Spec. No.	Height Measurement (in.)	(in.)	(in.)	Avg. Height $\bar{H}$ (in.)	Volume V (cu.in.)	Wt. in Air (gms)	Wt. in Water (gms)	Sp.Gr. from Dimen.	Sp.Gr. from Water Displ.	Void Volume from SGM (percent)	Void Volume from SGW (percent)
1	1.940	1.942	1.939	1.940	24.371	967.1	570.3	2.417	2.437	3.523	2.705
2	1.932	1.933	1.939	1.935	24.299	962.9	569.0	2.413	2.445	3.660	2.414
3	1.972	1.974	1.973	1.973	24.781	967.0	566.0	2.376	2.411	5.130	3.734
4	1.910	1.911	1.914	1.912	24.011	956.1	565.3	2.425	2.447	3.190	2.335
5	1.914	1.912	1.915	1.914	24.036	958.0	566.3	2.427	2.446	3.099	2.365
6	1.919	1.914	1.917	1.917	24.073	958.8	566.8	2.426	2.446	3.170	2.359
7	1.993	1.994	1.996	1.994	25.049	992.3	585.9	2.413	2.442	3.689	2.528
8	1.969	1.968	1.971	1.969	24.735	981.3	578.6	2.416	2.437	3.548	2.722
9	1.907	1.913	1.919	1.913	24.027	948.8	559.6	2.405	2.438	3.996	2.682
10	1.980	1.984	1.986	1.983	24.911	981.9	579.5	2.401	2.440	4.170	2.590
11	1.976	1.985	1.955	1.972	24.768	969.8	572.0	2.385	2.438	4.807	2.678
12	1.984	1.984	1.985	1.984	24.923	990.8	586.6	2.421	2.451	3.350	2.145
13	2.016	2.024	2.028	2.023	25.405	1006.3	595.5	2.412	2.450	3.699	2.211
14	1.901	1.899	1.897	1.899	23.851	946.0	557.7	2.415	2.436	3.574	2.744
15	1.945	1.945	1.949	1.946	24.446	970.0	572.5	2.417	2.440	3.532	2.585
16	1.925	1.925	1.926	1.925	24.182	956.8	564.5	2.410	2.439	3.807	2.637
17	1.882	1.880	1.879	1.880	23.617	937.0	553.5	2.416	2.443	3.543	2.464
18	1.931	1.933	1.933	1.932	24.270	964.0	569.0	2.419	2.441	3.434	2.575
19	1.931	1.925	1.926	1.927	24.207	962.0	569.0	2.420	2.448	3.384	2.282
20	1.949	1.952	1.952	1.951	24.505	973.0	575.0	2.418	2.445	3.465	2.406
21	1.993	1.993	1.992	1.993	25.028	984.0	581.0	2.394	2.442	4.415	2.527
22	1.994	1.996	1.993	1.994	25.049	994.7	587.2	2.418	2.441	3.456	2.556
23	1.903	1.903	1.906	1.904	23.914	946.1	559.5	2.409	2.447	3.817	2.306
24	1.982	1.973	1.971	1.975	24.810	982.0	580.0	2.411	2.443	3.772	2.484
25	1.973	1.970	1.973	1.972	24.768	983.8	581.9	2.419	2.448	3.433	2.281
26	1.883	1.885	1.890	1.886	23.688	938.3	553.1	2.412	2.436	3.699	2.759

APPENDIX B5

Hydrostatic Tension Specimen Dimensions,

Specific Gravity and Void Content

APPENDIX B5-A; Mix 16

NS	H_1	H_2	H_3	AH	VOL	WA	WW	SGM	SGW	VSGM	VSGW
Spec. No.	Height Measurement (in.)	(in.)	(in.)	Avg. Height $\bar{H}$ (in.)	Volume V (cu.in.)	Wt. in Air (gms)	Wt. in Water (gms)	Sp.Gr. from Dimen.	Sp.Gr. from Water Displ.	Void Volume from SGM (percent)	Void Volume from SGW (percent)
1	0.522	0.527	0.521	0.523	6.573	243.2	140.8	2.253	2.375	7.613	2.624
2	0.512	0.512	0.514	0.513	6.439	239.2	138.4	2.262	2.373	7.242	2.705
3	0.518	0.495	0.507	0.507	6.364	238.9	139.5	2.286	2.403	6.261	1.459
4	0.549	0.543	0.548	0.547	6.866	258.3	150.0	2.291	2.385	6.065	2.212
5	0.510	0.519	0.510	0.513	6.443	239.0	138.7	2.259	2.383	7.380	2.302
6	0.494	0.498	0.502	0.498	6.255	238.2	138.8	2.319	2.396	4.909	1.748
7	0.525	0.512	0.510	0.516	6.477	240.5	140.0	2.261	2.393	7.280	1.885
8	0.515	0.508	0.523	0.515	6.473	240.2	139.2	2.260	2.378	7.336	2.492
9	0.509	0.508	0.512	0.510	6.401	240.9	140.2	2.292	2.392	6.033	1.917
10	0.514	0.505	0.491	0.503	6.322	236.8	138.0	2.281	2.397	6.470	1.732
11	0.503	0.495	0.522	0.507	6.364	241.3	140.3	2.309	2.389	5.320	2.046
12	0.513	0.502	0.505	0.507	6.364	239.2	139.0	2.289	2.387	6.143	2.123
13	0.502	0.513	0.501	0.505	6.347	237.0	137.3	2.274	2.377	6.761	2.537
14	0.496	0.495	0.486	0.492	6.184	235.8	137.1	2.322	2.389	4.784	2.048
28	0.469	0.504	0.503	0.492	6.180	232.0	134.3	2.286	2.375	6.255	2.640
							AVERAGE	2.283	2.386	6.390	2.165

Theoretical Specific Gravity 2.439

APPENDIX B5-B; Mix 17

NS	H_1	H_2	H_3	AH	VOL	WA	WW	SGM	SGW	VSGM	VSGW
Spec. No.	Height Measurement (in.)	(in.)	(in.)	Avg. Height $\bar{H}$ (in.)	Volume V (cu.in.)	Wt. in Air (gms)	Wt. in Water (gms)	Sp.Gr. from Dimen.	Sp.Gr. from Water Displ.	Void Volume from SGM (percent)	Void Volume from SGW (percent)
1	0.589	0.592	0.600	0.594	7.456	276.9	160.9	2.262	2.387	7.273	2.129
2	0.575	0.579	0.584	0.579	7.276	274.5	160.2	2.297	2.402	5.802	1.534
3	0.603	0.598	0.596	0.599	7.523	283.0	164.8	2.291	2.394	6.074	1.835
4	0.594	0.588	0.582	0.588	7.385	272.0	152.9	2.243	2.284	8.036	6.363
5	0.570	0.571	0.564	0.568	7.138	267.1	155.7	2.279	2.398	6.568	1.695
6	0.634	0.622	0.623	0.626	7.867	289.5	168.0	2.241	2.383	8.110	2.308
7	0.598	0.597	0.590	0.595	7.473	275.8	160.2	2.248	2.386	7.848	2.181
8	0.616	0.601	0.609	0.609	7.653	280.7	162.8	2.234	2.381	8.417	2.385
9	0.577	0.594	0.584	0.585	7.348	266.1	154.3	2.206	2.380	9.570	2.413
10	0.629	0.626	0.618	0.624	7.842	287.3	165.6	2.231	2.361	8.516	3.209
11	0.620	0.634	0.615	0.623	7.825	282.3	163.0	2.197	2.366	9.916	2.981
12	0.620	0.598	0.632	0.617	7.745	275.8	158.6	2.169	2.353	11.086	3.516
							AVERAGE	2.241	2.373	8.101	2.712
							Theoretical Specific Gravity	2.439			

APPENDIX B5-C; Mix 18

NS	H_1	H_2	H_3	AH	VOL	WA	WW	SGM	SGW	VSGM	VSGW
Spec. No.	Height Measurement (in.)	(in.)	(in.)	Avg. Height $\bar{H}$ (in.)	Volume V (cu.in.)	Wt. in Air (gms)	Wt. in Water (gms)	Sp.Gr. from Dimen.	Sp.Gr. from Water Displ.	Void Volume from SGM (percent)	Void Volume from SGW (percent)
1	0.589	0.600	0.595	0.595	7.469	275.3	159.0	2.245	2.367	7.964	2.946
2	0.576	0.581	0.588	0.582	7.306	266.4	154.9	2.221	2.389	8.949	2.040
3	0.589	0.605	0.575	0.590	7.406	275.2	161.1	2.263	2.412	7.217	1.110
4	0.590	0.580	0.580	0.583	7.327	270.7	158.3	2.250	2.408	7.743	1.256
5	0.560	0.588	0.583	0.584	7.331	269.8	157.0	2.241	2.392	8.103	1.933
6	0.590	0.593	0.595	0.593	7.444	266.8	155.5	2.183	2.397	10.505	1.717
7	0.611	0.606	0.627	0.615	7.720	279.0	162.3	2.201	2.391	9.762	1.978
8	0.593	0.592	0.589	0.591	7.427	269.8	156.3	2.212	2.377	9.294	2.538
9	0.595	0.591	0.601	0.596	7.482	269.1	156.7	2.191	2.394	10.188	1.840
10	0.599	0.597	0.612	0.603	7.569	272.2	158.1	2.190	2.386	10.208	2.188
14	0.584	0.589	0.590	0.588	7.381	271.5	157.3	2.240	2.377	8.153	2.525
15	0.595	0.593	0.593	0.594	7.456	274.0	159.9	2.238	2.401	8.244	1.542
16	0.586	0.581	0.589	0.585	7.352	272.7	158.9	2.259	2.396	7.379	1.750
17	0.590	0.589	0.592	0.590	7.415	270.8	157.8	2.224	2.396	8.804	1.744
18	0.577	0.582	0.595	0.585	7.343	273.2	158.8	2.266	2.388	7.104	2.086
19	0.573	0.578	0.568	0.573	7.197	271.1	157.1	2.294	2.378	5.941	2.498
							AVERAGE	2.232	2.391	8.472	1.981

Theoretical Specific Gravity 2.439

APPENDIX B5-D; Mix 19

NS	H_1	H_2	H_3	AH	VOL	WA	WW	SGM	SGW	VSGM	VSGW
Spec. No.	Height Measurement (in.)	(in.)	(in.)	Avg. Height H (in.)	Volume V (cu.in.)	Wt. in Air (gms)	Wt. in Water (gms)	Sp.Gr. from Dimen.	Sp.Gr. from Water Displ.	Void Volume from SGM (percent)	Void Volume from SGW (percent)
1	0.577	0.575	0.590	0.581	7.293	265.1	149.2	2.214	2.287	4.869	1.705
2	0.595	0.583	0.571	0.583	7.322	264.4	149.3	2.199	2.297	5.500	1.283
3	0.580	0.582	0.580	0.581	7.293	266.3	150.2	2.224	2.294	4.438	1.431
4	0.578	0.585	0.568	0.577	7.247	260.9	146.7	2.192	2.285	5.781	1.823
5	0.627	0.617	0.619	0.621	7.800	284.8	160.7	2.224	2.295	4.437	1.378
6	0.575	0.582	0.587	0.581	7.302	265.0	149.4	2.210	2.292	5.014	1.487
7	0.585	0.570	0.586	0.580	7.289	264.8	150.1	2.212	2.309	4.922	0.789
8	0.601	0.585	0.611	0.599	7.523	267.2	149.9	2.163	2.278	7.050	2.109
9	0.587	0.587	0.584	0.586	7.360	266.1	149.6	2.202	2.284	5.379	1.843
10	0.590	0.590	0.590	0.590	7.410	266.4	150.0	2.189	2.289	5.914	1.648
11	0.572	0.594	0.586	0.584	7.335	263.7	149.1	2.189	2.301	5.911	1.115
12	0.585	0.593	0.573	0.584	7.331	266.1	150.0	2.211	2.292	5.001	1.505
13	0.582	0.568	0.585	0.578	7.264	258.2	145.0	2.165	2.281	6.971	1.980
14	0.585	0.582	0.579	0.582	7.310	265.4	150.3	2.211	2.306	4.979	0.910
15	0.572	0.582	0.588	0.581	7.293	266.3	150.3	2.224	2.296	4.438	1.346
16	0.587	0.584	0.572	0.581	7.297	268.4	151.7	2.240	2.300	3.740	1.164
							AVERAGE	2.204	2.293	5.271	1.470

Theoretical Specific Gravity 2.327

APPENDIX C1

Double Lap Shear Results Taken From Instron Chart and Records

Interpretation of Tabular Column Headings

NS . . . . . Specimen Number

NTS. . . . . Test Set Up Number

FS . . . . . Instron Full Scale Load Setting - Pounds

CH . . . . . Instron Cross Head Separation Rate - in./min.

CS . . . . . Instron Chart Speed - in./min.

YS . . . . . Y-Coordinate of Ultimate Load from Instron Chart - chart divisions

XS . . . . . X-Coordinate of Ultimate Load from Instron Chart - chart divisions

YT . . . . . Y-Coordinate of Initial Tangent from Instron Chart (selected on tangent line) - chart divisions

XT . . . . . X-Coordinate of Initial Tangent

AH . . . . . Average Specimen Height

AREA . . . . Specimen Area in Shear

APPENDIX C1-A; Mix 15

NS	NTS	FS	CH	CS	YS	XS	YT	XT	AH	AREA
17	6	500.	0.002	0.2	1.990	8.840	2.000	6.950	1.822	7.208
19	6	500.	0.002	0.2	1.590	8.620	2.000	8.590	1.971	7.192
21	6	500.	0.002	0.2	1.690	11.240	1.000	6.370	1.889	7.177
13	6	500.	0.020	2.0	3.110	7.540	5.000	9.680	1.780	7.362
15	6	500.	0.020	2.0	2.990	8.000	5.000	9.110	1.839	7.285
7	6	500.	0.200	10.0	4.750	3.180	5.000	1.830	1.905	7.177
9	6	500.	0.200	10.0	4.160	1.990	5.000	1.540	1.800	7.121
11	6	1000.	0.200	2.0	2.690	0.480	5.000	0.490	1.809	7.150
1	6	2000.	2.000	50.0	2.260	1.380	5.000	1.720	1.842	7.106
5	6	1000.	2.000	50.0	4.350	1.190	5.000	0.960	1.794	7.130

APPENDIX C1-B; Mix 20

NS	NTS	FS	CH	CS	YS	XS	YT	XT	AH	AREA
19	6	500.	0.002	0.2	1.380	16.770	1.000	7.440	1.947	7.488
21	6	500.	0.002	0.2	1.360	16.230	1.000	9.540	1.995	7.508
13	6	500.	0.020	2.0	2.180	11.370	2.000	7.930	1.962	7.602
15	6	500.	0.020	2.0	2.150	10.490	2.000	7.030	1.946	7.514
17	6	500.	0.020	2.0	2.060	9.720	2.000	6.630	1.976	7.409
9	6	500.	0.200	10.0	7.040	4.120	5.000	1.620	1.940	7.272
11	6	500.	0.200	10.0	6.360	3.470	5.000	1.370	1.966	7.511
1	6	2000.	2.000	50.0	4.120	1.570	5.000	0.640	1.964	7.473
5	6	2000.	2.000	50.0	3.020	1.060	5.000	0.520	1.977	7.488

APPENDIX C1-C; Mix 21

NS	NTS	FS	CH	CS	YS	XS	YT	XT	AH	AREA
13	6	500.	0.002	0.2	1.520	12.420	2.000	11.210	1.895	7.705
15	6	500.	0.002	0.2	1.580	11.040	2.000	11.490	1.907	7.600
9	6	500.	0.020	2.0	3.310	7.620	5.000	9.910	1.927	7.564
11	6	500.	0.020	2.0	3.070	9.140	5.000	11.810	1.956	7.694
5	6	500.	0.200	10.0	8.270	3.010	10.000	1.890	1.910	7.578
7	6	500.	0.200	10.0	9.320	3.610	10.000	1.590	1.845	7.406
1	6	2000.	2.000	50.0	4.840	2.010	5.000	0.630	1.884	7.584

APPENDIX C2

Uniaxial Tension Results Taken From

Instron Chart and Records

Interpretation of Tabular Column Headings

NS . . . . . . Specimen Number

NTS . . . . . Test Set Up Number

FS . . . . . . Instron Full Scale Load Setting - Pounds

CH . . . . . . Instron Cross Head Separation Rate - in,/min.

CS . . . . . . Instron Chart Speed - in./min.

YS . . . . . . Y-Coordinate of Ultimate Load from Instron Chart - chart divisions

XS . . . . . . X-Coordinate of Ultimate Load from Instron Chart - chart divisions

YT . . . . . . Y-Coordinate of Initial Tangent from Instron Chart (selected on tangent line) - chart divisions

XT . . . . . . X-Coordinate of Initial Tangent

AH . . . . . . Average Specimen Height

AREA . . . . . Specimen Area in Shear

APPENDIX C2-A; Mix 9

NS	NTS	FS	CH	CS	YS	XS	YT	XT	AH	AREA
19	7	50.	0.002	0.2	3.800	14.800	5.000	13.000	6.025	2.266
20	3	500.	0.002	0.2	0.340	13.860	0.500	15.960	6.042	2.172
17	3	500.	0.020	2.0	0.700	13.750	1.000	15.950	6.030	2.097
18	3	500.	0.020	2.0	0.340	11.150	0.500	17.100	6.015	2.185
15	7	200.	0.200	10.0	3.150	4.850	8.000	3.850	5.932	2.128
16	7	500.	0.200	5.0	1.110	2.620	6.000	2.530	6.025	1.972
13	7	1000.	2.000	50.0	1.430	1.820	5.200	0.920	5.957	2.284
14	7	1000.	2.000	50.0	1.440	1.360	4.920	0.900	5.962	2.199

APPENDIX C2-B; Mix 10

NS	NTS	FS	CH	CS	YS	XS	YT	XT	AH	AREA
19	7	50.	0.002	0.2	4.910	13.110	5.300	9.510	5.910	2.169
20	3	500.	0.002	0.2	0.300	10.600	0.500	10.100	5.907	2.019
17	3	500.	0.020	2.0	0.500	5.400	1.000	2.200	5.905	2.093
18	7	100.	0.020	0.5	4.080	3.090	6.600	3.460	5.892	2.054
15	3	1000.	0.200	20.0	0.950	6.400	1.950	1.950	5.852	1.953
16	3	500.	0.200	20.0	2.000	6.200	2.500	1.400	5.915	2.063
13	7	1000.	2.000	50.0	2.080	1.300	4.770	0.600	5.862	2.120
14	7	1000.	2.000	50.0	2.280	0.980	4.000	0.510	5.870	2.216

Appendix C2-C; Mix 11

NS	NTS	FS	CH	CS	YS	XS	YT	XT	AH	AREA
19	7	50.	0.002	0.2	3.640	14.500	4.800	12.450	5.892	2.182
20	7	50.	0.002	0.2	3.680	14.700	5.030	13.100	5.915	2.113
17	7	100.	0.020	0.5	3.410	2.920	5.800	4.100	5.902	2.054
18	7	100.	0.020	0.5	3.680	2.870	5.390	3.260	5.905	2.128
15	7	200.	C.200	10.0	4.950	5.130	8.210	1.130	5.852	2.267
16	7	200.	0.200	10.0	5.000	4.600	8.100	1.000	5.882	2.184
13	7	1000.	2.000	50.0	3.210	1.720	7.000	0.650	5.870	2.218
14	7	1000.	2.000	50.0	2.800	1.450	7.200	0.750	5.857	2.100

APPENDIX C2-D; Mix 12

NS	NTS	FS	CH	CS	YS	XS	YT	XT	AH	AREA
19	7	50.	0.002	0.2	2.920	24.300	3.170	18.600	5.922	2.094
20	7	50.	0.002	0.2	3.120	21.590	3.240	15.390	5.945	2.020
17	7	100.	0.020	0.5	3.390	4.600	5.170	5.250	5.927	2.276
18	7	100.	0.020	0.5	2.880	4.460	4.860	5.530	5.917	2.007
16	7	200.	0.200	10.0	4.210	6.470	5.700	0.870	5.917	2.206
15	7	200.	0.200	10.0	3.990	8.260	8.000	1.370	5.975	2.349
13	7	1000.	2.000	50.0	2.520	1.750	7.080	0.800	5.992	2.323
14	7	1000.	2.000	50.0	1.960	1.880	5.000	0.560	5.990	2.123

APPENDIX C2-E; Mix 13

NS	NTS	FS	CH	CS	YS	XS	YT	XT	AH	AREA
19	7	50.	0.002	0.2	9.800	5.430	9.650	3.930	5.952	2.133
20	7	100.	0.002	0.2	4.610	5.460	7.480	4.660	5.942	1.947
17	7	100.	0.020	0.5	9.330	1.250	10.000	0.440	5.957	2.149
18	7	100.	0.020	0.5	9.130	1.140	10.000	0.440	5.952	2.101
15	7	200.	0.200	10.0	8.600	2.240	9.000	0.690	5.600	2.128
16	7	200.	0.200	10.0	8.190	2.140	9.100	0.820	5.967	1.956
13	7	1000.	2.000	50.0	3.410	0.870	4.190	0.490	5.597	2.205
14	7	1000.	2.000	50.0	3.160	0.890	4.570	0.450	5.607	2.213

APPENDIX C2-F; Mix 14

NS	NTS	FS	CH	CS	YS	XS	YT	XT	AH	AREA
19	7	100.	0.002	0.2	1.940	13.090	2.500	11.490	5.857	1.924
20	3	500.	0.002	0.2	0.400	12.000	0.300	6.000	5.840	2.034
17	7	100.	0.020	0.5	3.770	3.110	4.290	2.860	5.857	2.019
18	7	100.	0.020	0.5	4.200	2.960	6.200	3.630	5.852	2.084
15	7	200.	0.200	10.0	4.090	4.650	7.070	1.520	5.882	1.984
16	7	200.	0.200	10.0	3.990	5.020	7.190	1.820	5.830	1.991
13	7	1000.	2.000	50.0	1.420	2.500	5.240	0.900	5.870	2.052
14	7	1000.	2.000	50.0	1.530	1.560	2.830	0.360	5.902	1.904

APPENDIX C3

Uniaxial Compression Results Taken From

Instron Chart and Records

Interpretation of Tabular Column Headings

NS . . . . . Specimen Number

NTS. . . . . Test Set Up Number

FS . . . . . Instron Full Scale Load Setting - pounds

CH . . . . . Instron Cross Head Separation Rate - in./min.

CS . . . . . Instron Chart Speed - in./min.

YS . . . . . Y-Coordinate of Ultimate Load from Instron Chart - chart divisions

XS . . . . . X-Coordinate of Ultimate Load from Instron Chart - chart divisions

YT . . . . . Y-Coordinate of Ultimate Load from Instron Chart - (selected on tangent line) - chart divisions

XT . . . . . X-Coordinate of Initial Tangent

AH . . . . . Average Specimen Height

AREA . . . . Specimen Area in Shear

APPENDIX C3-A; Mix 9

NS	NTS	FS	CH	CS	YS	XS	YT	XT	AH	AREA
9	2	500.	0.002	0.2	1.620	26.350	3.000	31.850	6.020	2.185
10	2	500.	0.002	0.2	2.010	34.000	3.000	33.800	6.002	2.371
6	1	1000.	0.050	1.0	1.570	5.100	3.000	7.250	5.947	2.138
7	1	1000.	0.050	1.0	1.780	4.920	3.000	6.320	5.970	2.250
8	1	1000.	0.050	1.0	1.690	4.550	3.000	6.170	6.047	2.195
3	1	1000.	1.000	50.0	4.670	12.600	7.000	12.800	5.887	2.492
4	1	1000.	1.000	50.0	4.070	12.550	7.000	13.030	5.875	2.545
5	1	1000.	1.000	50.0	3.810	13.700	6.000	18.680	5.985	2.238
11	6	10000.	20.000	50.0	1.070	0.450	5.000	0.650	5.945	2.183
12	6	10000.	20.000	50.0	0.840	0.490	6.570	1.270	5.945	2.141

APPENDIX C3-B; Mix 10

NS	NTS	FS	CH	CS	YS	XS	YT	XT	AH	AREA
9	1	500.	0.002	0.2	2.210	24.270	3.500	27.750	5.850	2.291
10	1	500.	0.002	0.2	2.140	29.950	3.500	32.100	5.872	2.048
7	2	1000.	0.050	1.0	2.120	4.930	4.000	6.400	5.897	2.206
8	2	1000.	0.050	1.0	2.570	4.690	4.000	5.340	5.845	2.342
3	2	1000.	1.000	50.0	5.210	10.600	8.000	5.210	5.905	2.194
4	2	1000.	1.000	50.0	5.210	9.980	8.000	5.080	5.882	2.286
5	2	1000.	1.000	50.0	6.190	8.620	8.000	5.040	5.770	2.441
11	6	10000.	20.000	50.0	1.330	0.460	5.130	0.580	5.857	2.362
12	6	10000.	20.000	50.0	1.000	0.510	8.200	1.990	5.867	2.123

APPENDIX C3-C; Mix 11

NS	NTS	FS	CH	CS	YS	XS	YT	XT	AH	AREA
9	2	500.	0.002	0.2	1.870	25.940	2.500	25.000	5.900	2.227
10	1	500.	0.002	0.2	1.820	27.000	2.500	26.350	5.915	2.267
7	2	1000.	0.050	1.0	1.790	4.440	3.000	5.370	5.900	2.079
8	2	1000.	0.050	1.0	2.270	4.300	3.000	4.080	5.820	2.286
4	1	1000.	1.000	50.0	7.800	10.420	9.000	7.680	5.870	2.349
5	1	1000.	1.000	50.0	6.790	10.620	9.000	5.480	5.880	2.142
6	1	1000.	1.000	50.0	7.720	10.910	10.000	7.520	5.902	2.322
11	6	20000.	20.000	50.0	1.190	0.140	6.650	0.680	5.842	2.020
12	6	20000.	20.000	50.0	0.930	0.170	3.940	0.610	5.875	2.111

APPENDIX C3-D; Mix 12

NS	NTS	FS	CH	CS	YS	XS	YT	XT	AH	AREA
9	1	500.	0.002	0.2	1.700	32.420	2.500	32.760	5.905	2.332
10	2	500.	0.002	0.2	1.410	39.940	2.000	39.200	5.922	2.321
7	2	500.	0.050	1.0	3.240	6.720	5.000	7.020	5.992	2.091
8	2	500.	0.050	1.0	3.950	6.320	5.000	5.140	5.905	2.272
4	1	1000.	1.000	50.0	6.500	15.550	9.000	10.670	5.937	2.168
5	1	1000.	1.000	50.0	8.040	17.120	9.000	9.360	5.965	2.318
6	1	1000.	1.000	50.0	6.880	15.120	9.000	9.980	5.992	2.132
11	6	20000.	20.000	50.0	1.120	0.600	4.500	0.600	5.967	2.201
12	6	20000.	20.000	50.0	0.750	0.740	5.800	1.230	5.972	1.996

APPENDIX C3-E; Mix 13

NS	NTS	FS	CH	CS	YS	XS	YT	XT	AH	AREA
8	1	500.	0.002	0.5	5.510	28.820	7.000	27.300	5.942	2.299
9	1	500.	0.002	0.2	5.010	12.270	6.000	10.920	5.982	2.391
10	2	500.	0.002	0.2	5.630	12.300	7.000	11.010	5.980	2.410
6	2	500.	0.050	1.0	9.650	2.370	10.000	1.830	5.612	2.216
7	2	500.	0.050	1.0	8.730	2.300	10.000	1.810	5.610	2.082
3	1	1000.	1.000	20.0	9.580	2.420	10.000	1.570	5.775	2.269
4	1	1000.	1.000	20.0	9.150	2.400	10.000	1.460	5.685	2.153
11	6	20000.	20.000	50.0	1.060	0.160	6.000	0.730	5.592	2.106
12	6	10000.	20.000	50.0	1.710	0.180	5.600	0.520	5.607	2.161

APPENDIX C3-F; Mix 14

NS	NTS	FS	CH	CS	YS	XS	YT	XT	AH	AREA
9	2	500.	0.002	0.2	2.000	24.570	3.000	24.620	5.832	1.994
10	1	500.	0.002	0.2	2.030	27.310	3.000	27.210	5.852	2.179
6	1	500.	0.050	1.0	4.440	4.770	6.000	4.650	5.900	2.139
8	1	1000.	0.050	1.0	2.090	3.990	3.000	4.190	5.837	2.015
3	1	1000.	1.000	20.0	5.250	4.650	8.000	4.810	6.030	2.353
4	1	1000.	1.000	20.0	5.660	4.400	8.000	4.410	6.045	2.472
5	1	1000.	1.000	20.0	5.230	4.200	8.000	4.400	5.900	1.987
11	6	10000.	20.000	50.0	1.080	0.450	6.700	0.890	5.882	1.923
12	6	20000.	20.000	50.0	0.440	0.520	4.370	1.610	5.875	2.023

APPENDIX C4

Splitting Tension Results Taken From

Instron Chart and Records

Interpretation of Tabular Column Headings

NS . . . . . . Specimen Number

NTS. . . . . . Test Set Up Number

FS . . . . . . Instron Full Scale Load Setting - Pounds

CH . . . . . . Instron Cross Head Separation Rate - in./min.

CS . . . . . . Instron Chart Speed - in./min.

YS . . . . . . Y-Coordinate of Ultimate Load from Instron Chart - chart divisions

XS . . . . . . X-Coordinate of Ultimate Load from Instron Chart - chart divisions

YT . . . . . . Y-Coordinate of Initial Tangent from Instron Chart (selected on tangent line) - chart divisions

XT . . . . . . X-Coordinate of Initial Tangent

AH . . . . . . Average Specimen Height

AREA . . . . . Specimen Area in Shear

APPENDIX C4-A; Mix 39

NS	NTS	FS	CH	CS	YS	XS	YT	XT	AH	AREA
9	14	500.	0.020	1.0	2.700	12.450	2.600	8.250	1.945	12.560
13	14	500.	0.020	0.5	2.600	6.880	2.300	4.500	1.901	12.560
15	14	500.	0.020	0.5	2.330	8.300	2.300	6.200	1.892	12.560
5	14	1000.	0.200	10.0	3.020	12.250	2.400	7.250	1.909	12.560
6	14	500.	0.200	10.0	6.200	9.350	5.300	5.750	1.893	12.560
7	14	500.	0.200	5.0	6.000	5.540	8.300	5.750	1.913	12.560
8	14	500.	0.200	5.0	5.630	5.900	7.200	5.600	1.974	12.560
1	14	2000.	2.000	20.0	4.470	2.130	3.750	1.180	1.864	12.560
2	14	2000.	2.000	50.0	4.300	5.140	4.900	4.300	1.951	12.560
3	14	2000.	2.000	50.0	4.450	4.900	5.600	3.900	1.904	12.560
4	14	1000.	2.000	50.0	8.640	5.750	7.400	3.600	1.923	12.560
10	14	20000.	20.000	50.0	1.170	0.220	4.500	0.670	1.887	12.560
14	14	20000.	20.000	50.0	1.050	0.450	2.600	0.450	1.999	12.560
16	14	20000.	20.000	50.0	0.990	0.520	3.500	0.880	1.981	12.560

APPENDIX C4-B; Mix 43

NS	NTS	FS	CH	CS	YS	XS	YT	XT	AH	AREA
19	14	500.	0.020	1.0	8.500	4.330	7.800	2.900	1.927	12.560
24	14	500.	0.020	1.0	7.470	4.300	8.100	3.420	1.975	12.560
25	14	500.	0.020	1.0	7.620	4.570	8.300	3.780	1.972	12.560
15	14	1000.	0.200	20.0	8.600	8.810	4.000	2.760	1.946	12.560
16	14	1000.	0.200	10.0	8.970	4.670	6.900	2.720	1.925	12.560
17	14	1000.	0.200	10.0	9.000	4.620	9.000	3.200	1.880	12.560
12	14	5000.	2.000	20.0	4.500	0.830	5.400	0.700	1.984	12.560
13	14	5000.	2.000	50.0	4.270	2.290	3.400	1.230	2.023	12.560
14	14	5000.	2.000	50.0	3.780	2.350	4.800	2.150	1.899	12.560
21	14	20000.	10.000	50.0	1.530	0.380	2.800	0.500	1.993	12.560
22	14	20000.	10.000	50.0	1.540	0.390	3.500	0.590	1.994	12.560
23	14	20000.	10.000	50.0	1.550	0.360	1.800	0.280	1.904	12.560

APPENDIX C5

Hydrostatic Tension Results Taken From Instron Chart and Records

Interpretation of Tabular Column Headings

NS . . . . Specimen Number

NTS. . . . Test Set-Up Number

FS . . . . Instron Full Scale Load Setting - Pounds

CH . . . . Instron Cross Head Separation Rate - in./min.

CS . . . . Instron Chart Speed - in./min.

YS . . . . Y-Coordinate of Ultimate Load from Instron Chart - chart divisions

XS . . . . X-Coordinate of Ultimate Load from Instron Chart - chart divisions

YT . . . . Y-Coordinate of Initial Tangent from Instron Chart (selected on tangent line) - chart divisions

XT . . . . X-Coordinate of Initial Tangent

AH . . . . Average Specimen Height

AREA . . . Loaded Specimen Area

APPENDIX C5-A; Mix 16

NS	NTS	FS	CH	CS	YS	XS	YT	XT	AH	AREA
1	5	500.	0.002	0.2	8.360	1.300	9.560	1.340	0.523	12.560
2	5	500.	0.002	0.5	9.650	3.280	10.000	3.030	0.513	12.560
3	5	1000.	0.002	0.5	4.120	3.110	5.570	3.040	0.507	12.560
4	5	2000.	0.020	5.0	5.370	4.400	6.000	4.510	0.547	12.560
5	5	2000.	0.020	5.0	4.750	3.940	5.190	3.940	0.513	12.560
6	5	2000.	0.020	5.0	4.880	3.860	5.100	3.660	0.498	12.560
7	5	5000.	0.200	10.0	3.750	1.150	4.210	1.220	0.516	12.560
8	5	5000.	0.200	20.0	3.400	2.360	4.000	2.600	0.515	12.560
11	5	5000.	0.200	20.0	3.570	2.500	3.900	2.030	0.507	12.560
28	5	5000.	0.200	20.0	4.280	2.380	4.430	2.350	0.492	12.560
9	5	10000.	2.000	50.0	2.980	0.750	4.010	0.990	0.510	12.560
12	5	10000.	2.000	50.0	3.390	0.830	3.700	0.890	0.507	12.560
13	5	10000.	2.000	50.0	3.000	0.770	3.460	0.870	0.505	12.560
14	5	10000.	2.000	50.0	3.190	0.770	3.500	0.830	0.492	12.560

APPENDIX C5-B; Mix 17

NS	NTS	FS	C	CS	YS	XS	YT	XT	AH	AREA
1	5	1000.	0.002	0.5	4.440	3.190	5.210	3.250	0.594	12.560
2	5	1000.	0.002	0.5	4.650	3.250	5.750	3.550	0.579	12.560
3	5	1000.	0.002	0.5	4.390	2.850	5.340	2.980	0.599	12.560
4	5	2000.	0.020	5.0	5.880	5.250	6.740	5.490	0.588	12.560
5	5	2000.	0.020	5.0	5.890	5.070	6.460	5.170	0.568	12.560
6	5	2000.	0.020	5.0	5.570	4.960	6.420	5.160	0.626	12.560
7	5	5000.	0.200	20.0	5.400	3.100	6.430	3.500	0.595	12.560
8	5	5000.	0.200	20.0	5.300	3.260	6.250	3.680	0.609	12.560
9	5	5000.	0.200	20.0	5.340	3.160	6.100	3.490	0.585	12.560
10	5	10000.	2.000	50.0	3.760	0.890	3.150	0.970	0.624	12.560
11	5	10000.	2.000	50.0	3.410	0.870	3.880	0.980	0.623	12.560
12	5	10000.	2.000	50.0	3.620	1.010	4.550	1.240	0.617	12.560

APPENDIX C5-C; Mix 18

NS	NTS	FS	CH	CS	YS	XS	YT	XT	AH	AREA
1	5	1000.	0.002	0.5	4.570	3.510	5.410	3.570	0.595	12.560
2	5	1000.	0.002	0.5	5.470	3.710	6.400	3.810	0.582	12.560
3	5	1000.	0.002	0.5	7.460	4.050	8.450	4.150	0.590	12.560
4	5	2000.	0.020	5.0	8.240	5.910	9.110	6.110	0.583	12.560
5	5	2000.	0.020	5.0	6.770	5.510	7.320	5.510	0.584	12.560
6	5	2000.	0.020	5.0	7.970	5.150	9.150	5.570	0.593	12.560
16	5	2000.	0.020	5.0	8.730	6.440	9.610	6.640	0.585	12.560
7	5	5000.	0.200	20.0	6.020	3.330	6.220	3.390	0.615	12.560
8	5	5000.	0.200	20.0	5.260	2.950	5.540	2.980	0.591	12.560
9	5	5000.	0.200	20.0	5.750	3.090	6.060	3.190	0.596	12.560
17	5	5000.	0.200	20.0	6.170	3.500	6.510	3.660	0.590	12.560
10	5	10000.	2.000	50.0	3.570	0.830	4.020	0.930	0.603	12.560
18	5	10000.	2.000	50.0	3.400	0.870	3.950	1.000	0.585	12.560
19	5	10000.	2.000	50.0	2.800	0.750	3.200	0.850	0.573	12.560

APPENDIX C5-D; Mix 19

NS	NTS	FS	CH	CS	YS	XS	YT	XT	AH	AREA
1	5	1000.	0.002	0.5	5.030	3.620	6.390	3.720	0.581	12.560
2	5	1000.	0.002	0.5	6.030	3.920	6.910	4.000	0.583	12.560
3	5	1000.	0.002	0.5	6.470	4.120	7.820	4.370	0.581	12.560
4	5	1000.	0.002	0.5	5.480	3.870	6.660	3.970	0.577	12.560
5	5	2000.	0.020	5.0	5.190	5.130	6.140	5.330	0.621	12.560
6	5	2000.	0.020	5.0	6.070	5.010	6.650	5.010	0.581	12.560
7	5	2000.	0.020	5.0	6.300	5.250	7.020	5.350	0.580	12.560
8	5	2000.	0.020	5.0	5.670	5.220	6.590	5.460	0.599	12.560
9	5	5000.	0.200	20.0	3.780	2.800	4.240	2.800	0.586	12.560
10	5	5000.	0.200	20.0	4.590	2.800	5.170	2.880	0.590	12.560
11	5	5000.	0.200	20.0	4.640	2.890	5.210	3.020	0.584	12.560
13	5	5000.	0.200	20.0	4.420	2.780	4.950	2.880	0.578	12.560
12	5	10000.	2.000	50.0	3.390	0.860	3.680	0.920	0.584	12.560
14	5	10000.	2.000	50.0	3.720	0.930	4.050	0.970	0.582	12.560
15	5	10000.	2.000	50.0	3.960	0.960	4.400	1.030	0.581	12.560
16	5	10000.	2.000	50.0	3.530	1.000	3.860	1.020	0.581	12.560

APPENDIX C6

Bead Test Results Taken From

Instron Chart and Records

<u>Interpretation of Tabular Column Headings</u>

NS . . . . Specimen Number

NTS. . . . Test Set-Up Number

FS . . . . Instron Full Scale Load Setting - Pounds

CH . . . . Instron Cross Head Separation Rate - in./min.

CS . . . . Instron Chart Speed - in./min.

YS . . . . Y-Coordinate of Ultimate Load from Instron Chart - chart divisions

XS . . . . X-Coordinate of Ultimate Load from Instron Chart - chart divisions

YT . . . . Y-Coordinate of Initial Tangent from Instron Chart (selected on tangent line) - chart divisions

XT . . . . X-Coordinate of Initial Tangent

AH . . . . Average Specimen Height

AREA . . . Specimen Area in Shear

APPENDIX C6-A; Mix 24

NS	NTS	FS	CH	CS	YS	XS	YT	XT	AH	AREA
3	9	100.	0.020	1.0	2.400	0.490	5.400	0.700	0.620	2.904
4	9	100.	0.020	2.0	2.000	0.960	5.300	1.190	0.620	2.904
5	9	500.	0.200	20.0	3.900	1.080	6.000	1.240	0.620	2.904
6	9	500.	0.200	50.0	2.740	2.300	4.100	2.160	0.620	3.206
1	9	1000.	2.000	50.0	2.940	0.460	5.000	0.500	0.620	2.602
2	5	2000.	2.000	50.0	5.550	0.830	7.400	0.870	0.620	2.904
7	5	5000.	2.000	50.0	2.050	0.770	3.000	0.880	0.620	2.904

APPENDIX C6-B; Mix 25

NS	NTS	FS	CH	CS	YS	XS	YT	XT	AH	AREA
3	9	100.	0.020	2.0	6.770	1.090	9.200	0.960	0.346	2.880
4	9	200.	0.020	2.0	6.500	1.170	7.000	0.720	0.346	2.598
5	5	1000.	0.200	50.0	2.800	3.650	3.800	3.400	0.346	3.162
6	5	1000.	0.200	50.0	3.350	4.050	4.600	3.900	0.346	2.598
1	5	5000.	2.000	50.0	4.300	0.930	4.400	0.930	0.346	2.692
2	5	5000.	2.000	50.0	3.180	0.880	5.700	1.290	0.346	2.974

APPENDIX C6-C; Mix 26

NS	NTS	FS	CH	CS	YS	XS	YT	XT	AH	AREA
3	9	200.	0.020	5.0	8.380	2.310	9.900	2.050	0.179	2.700
4	5	500.	0.020	5.0	4.150	2.550	5.500	2.550	0.179	2.751
7	9	500.	0.020	5.0	3.530	2.200	5.500	2.300	0.179	2.474
5	5	2000.	0.200	50.0	4.050	5.600	5.100	6.100	0.179	2.373
6	5	2000.	0.200	50.0	1.120	3.620	1.500	3.320	0.179	3.128
1	5	5000.	2.000	50.0	4.250	1.000	5.200	1.130	0.179	2.499
2	5	5000.	2.000	50.0	5.380	1.020	6.200	1.100	0.179	2.726

APPENDIX D

Calibration for Machine Deformation

In this appendix, each sheet summarizes the calibration data for the "Test Set-Up Number" (NTS) indicated. The NTS used for a given test is shown on each data sheet in Appendix C. The NTS applicable for each test mode are as follows:

Test Mode	NTS
Shear	6
Uniaxial Tensile	3 and 7
Splitting Tensile	1, 2, and 6
Hydrostatic Tension	5
Bead Test	5 and 9

APPENDIX D Machine Deformation

Test Set-up Number 1 | Full Scale Load Setting: 1000 lbs | Instron Cross-Head Separation Rate: 0.005 in./min. | Instron Chart Speed: 5 in./min.

X	Y	D	F	A	B
X-Coord. from Instron Chart (Div.)	Y-Coord. from Instron Chart (Div.)	Machine Deformation (in.)	Force (lbs)	Tangent Intercept to D-F Curve (lbs)	Tangent Slope to D-F Curve (lbs/in.)
0.000	0.000	0.000E 00	0.000E 00	-0.000E 00	0.340E 05
0.500	0.170	0.500E-03	0.170E 02	-0.170E 02	0.680E 05
1.000	0.510	0.100E-02	0.510E 02	-0.230E 02	0.740E 05
1.500	0.880	0.150E-02	0.880E 02	-0.110E 02	0.660E 05
2.000	1.210	0.200E-02	0.121E 03	-0.510E 02	0.860E 05
2.500	1.640	0.250E-02	0.164E 03	-0.560E 02	0.880E 05
3.000	2.080	0.300E-02	0.208E 03	-0.800E 02	0.960E 05
3.500	2.560	0.350E-02	0.256E 03	-0.730E 02	0.940E 05
4.000	3.030	0.400E-02	0.303E 03	-0.890E 02	0.980E 05
4.500	3.520	0.450E-02	0.352E 03	-0.710E 02	0.940E 05
5.000	3.990	0.500E-02	0.399E 03	-0.121E 03	0.104E 06
5.500	4.510	0.550E-02	0.451E 03	-0.154E 03	0.110E 06
6.000	5.060	0.600E-02	0.506E 03	-0.178E 03	0.114E 06
6.500	5.630	0.650E-02	0.563E 03	-0.204E 03	0.118E 06
7.000	6.220	0.700E-02	0.622E 03	-0.190E 03	0.116E 06
8.000	7.380	0.800E-02	0.738E 03	-0.270E 03	0.126E 06
8.500	8.010	0.850E-02	0.801E 03	-0.270E 03	0.126E 06
9.000	8.640	0.900E-02	0.864E 03	-0.342E 03	0.134E 06
9.500	9.310	0.950E-02	0.931E 03	-0.380E 03	0.138E 06
10.000	10.000	0.100E-01	0.100E 04	-0.380E 03	0.138E 06

APPENDIX D Machine Deformation

Test Set-up Number 2

Full Scale Load Setting: 1000 lbs

Instron Cross-Head Separation Rate: 0.005 in./min.

Instron Chart Speed: 5 in./min.

X	Y	D	F	A	B
X-Coord. from Instron Chart (Div.)	Y-Coord. from Instron Chart (Div.)	Machine Deformation (in.)	Force (lbs)	Tangent Intercept to D-F Curve (lbs)	Tangent Slope to D-F Curve (lbs/in.)
0.000	0.000	0.000E 00	0.000E 00	-0.000E 00	0.360E 05
0.500	0.180	0.500E-03	0.180E 02	-0.150E 02	0.660E 05
1.000	0.510	0.100E-02	0.510E 02	-0.310E 02	0.820E 05
1.500	0.920	0.150E-02	0.920E 02	-0.490E 02	0.940E 05
2.000	1.390	0.200E-02	0.139E 03	-0.610E 02	0.100E 06
2.500	1.890	0.250E-02	0.189E 03	-0.960E 02	0.114E 06
3.000	2.460	0.300E-02	0.246E 03	-0.162E 03	0.136E 06
3.500	3.140	0.350E-02	0.314E 03	-0.218E 03	0.152E 06
4.000	3.900	0.400E-02	0.390E 03	-0.250E 03	0.160E 06
4.500	4.700	0.450E-02	0.470E 03	-0.295E 03	0.170E 06
5.000	5.550	0.500E-02	0.555E 03	-0.305E 03	0.172E 06
5.500	6.410	0.550E-02	0.641E 03	-0.327E 03	0.176E 06
6.000	7.290	0.600E-02	0.729E 03	-0.375E 03	0.184E 06
6.500	8.210	0.650E-02	0.821E 03	-0.427E 03	0.192E 06
7.000	9.170	0.700E-02	0.917E 03	-0.434E 03	0.193E 06
7.430	10.000	0.743E-02	0.100E 04	-0.434E 03	0.193E 06

APPENDIX D Machine Deformation

Test Set-up Number 3	Full Scale Load Setting: 500 lbs	Instron Cross-Head Separation Rate: 0.010 in./min.	Instron Chart Speed: 10 in./min.

X	Y	D	F	A	B
X-Coord. from Instron Chart (Div.)	Y-Coord. from Instron Chart (Div.)	Machine Deformation (in.)	Force (lbs)	Tangent Intercept to D-F Curve (lbs)	Tangent Slope to D-F Curve (lbs/in.)
0.000	0.000	0.000E 00	0.000E 00	-0.000E 00	0.250E 05
0.600	0.300	0.600E-03	0.150E 02	-0.600E 01	0.350E 05
1.100	0.650	0.110E-02	0.325E 02	-0.137E 02	0.420E 05
1.600	1.070	0.160E-02	0.535E 02	-0.201E 02	0.460E 05
2.100	1.530	0.210E-02	0.765E 02	-0.306E 02	0.510E 05
2.600	2.040	0.260E-02	0.102E 03	-0.436E 02	0.560E 05
3.100	2.600	0.310E-02	0.130E 03	-0.560E 02	0.600E 05
3.600	3.200	0.360E-02	0.160E 03	-0.452E 02	0.570E 05
4.100	3.770	0.410E-02	0.189E 03	-0.698E 02	0.630E 05
4.600	4.400	0.460E-02	0.220E 03	-0.102E 03	0.700E 05
5.100	5.100	0.510E-02	0.255E 03	-0.112E 03	0.720E 05
5.600	5.820	0.560E-02	0.291E 03	-0.140E 03	0.770E 05
6.100	6.590	0.610E-02	0.330E 03	-0.104E 03	0.710E 05
6.600	7.300	0.660E-02	0.365E 03	-0.163E 03	0.800E 05
7.100	8.100	0.710E-02	0.405E 03	-0.163E 03	0.800E 05
7.600	8.900	0.760E-02	0.445E 03	-0.201E 03	0.850E 05
8.100	9.750	0.810E-02	0.488E 03	-0.236E 03	0.893E 05
8.240	10.000	0.824E-02	0.500E 03	-0.236E 03	0.893E 05

APPENDIX D Machine Deformation

Test Set-up Number 5	Full Scale Load Setting: 5000 lbs	Instron Cross-Head Separation Rate: 0.010 in./min.	Instron Chart Speed: 2 in./min.

X	Y	D	F	A	B
X-Coord. from Instron Chart (Div.)	Y-Coord. from Instron Chart (Div.)	Machine Deformation (in.)	Force (lbs)	Tangent Intercept to D-F Curve (lbs)	Tangent Slope to D-F Curve (lbs/in.)
0.000	0.000	0.000E 00	0.000E 00	-0.000E 00	0.378E 05
0.450	0.170	0.225E-02	0.850E 02	-0.500E 02	0.600E 05
0.950	0.470	0.475E-02	0.235E 03	-0.135E 03	0.780E 05
1.450	0.860	0.725E-02	0.430E 03	-0.223E 03	0.900E 05
1.950	1.310	0.975E-02	0.655E 03	-0.300E 03	0.980E 05
2.450	1.800	0.122E-01	0.900E 03	-0.447E 03	0.110E 06
2.950	2.350	0.148E-01	0.118E 04	-0.477E 03	0.112E 06
3.450	2.910	0.173E-01	0.145E 04	-0.650E 03	0.122E 06
3.950	3.520	0.197E-01	0.176E 04	-0.649E 03	0.122E 06
4.450	4.130	0.223E-01	0.207E 04	-0.783E 03	0.128E 06
4.950	4.770	0.248E-01	0.239E 04	-0.783E 03	0.128E 06
5.450	5.410	0.273E-01	0.270E 04	-0.111E 04	0.140E 06
5.950	6.110	0.298E-01	0.305E 04	-0.991E 03	0.136E 06
6.450	6.790	0.322E-01	0.339E 04	-0.118E 04	0.142E 06
6.950	7.500	0.347E-01	0.375E 04	-0.125E 04	0.144E 06
7.450	8.220	0.372E-01	0.411E 04	-0.148E 04	0.150E 06
7.950	8.970	0.397E-01	0.449E 04	-0.132E 04	0.146E 06
8.450	9.700	0.422E-01	0.485E 04	-0.149E 04	0.150E 06

Test Set-up Number 6	Full Scale Load Setting: 5000 lbs	Instron Cross-Head Separation Rate: 0.010 in./min.	Instron Chart Speed: 5 in./min.

X X-Coord. from Instron Chart (Div.)	Y Y-Coord. from Instron Chart (Div.)	D Machine Deformation (in.)	F Force (lbs)	A Tangent Intercept to D-F Curve (lbs)	B Tangent Slope to D-F Curve (lbs/in.)
0.000	0.000	0.000E 00	0.000E 00	-0.000E 00	0.500E 05
0.450	0.090	0.900E-03	0.450E 02	0.458E-04	0.500E 05
0.950	0.190	0.190E-02	0.950E 02	-0.190E 02	0.600E 05
1.450	0.310	0.290E-02	0.155E 03	-0.480E 02	0.700E 05
1.950	0.450	0.390E-02	0.225E 03	-0.107E 03	0.850E 05
2.450	0.620	0.490E-02	0.310E 03	-0.204E 03	0.105E 06
2.950	0.830	0.590E-02	0.415E 03	-0.264E 03	0.115E 06
3.450	1.060	0.690E-02	0.530E 03	-0.367E 03	0.130E 06
3.950	1.320	0.790E-02	0.660E 03	-0.446E 03	0.140E 06
4.450	1.600	0.890E-02	0.800E 03	-0.668E 03	0.165E 06
4.950	1.930	0.990E-02	0.965E 03	-0.767E 03	0.175E 06
5.450	2.280	0.109E-01	0.114E 04	-0.876E 03	0.185E 06
5.950	2.650	0.119E-01	0.132E 04	-0.111E 04	0.205E 06
6.950	3.470	0.139E-01	0.174E 04	-0.122E 04	0.213E 06
7.950	4.320	0.159E-01	0.216E 04	-0.150E 04	0.230E 06
8.950	5.240	0.179E-01	0.262E 04	-0.194E 04	0.255E 06
9.950	6.260	0.199E-01	0.313E 04	-0.244E 04	0.280E 06
10.950	7.380	0.219E-01	0.369E 04	-0.299E 04	0.305E 06
11.950	8.600	0.239E-01	0.430E 04	-0.407E 04	0.350E 06
12.950	10.000	0.259E-01	0.500E 04	-0.407E 04	0.350E 06

APPENDIX D Machine Deformation

Test Set-up Number 7	Full Scale Load Set ing: 500 lbs	Instron Cross-Head Separation Rate: 0.050 in./min.	Instron Chart Speed: 20 in./min.

X	Y	D	F	A	B
X-Coord. from Instron Chart (Div.)	Y-Coord. from Instron Chart (Div.)	Machine Deformation (in.)	Force (lbs)	Tangent Intercept to D-F Curve (lbs)	Tangent Slope to D-F Curve (lbs/in.)
0.000	0.000	0.000E 00	0.000E 00	-0.000E 00	0.267E 05
0.300	0.400	0.750E-03	0.200E 02	-0.300E 01	0.307E 05
0.600	0.860	0.150E-02	0.430E 02	-0.158E 02	0.392E 05
0.850	1.350	0.212E-02	0.675E 02	-0.243E 02	0.432E 05
1.100	1.890	0.275E-02	0.945E 02	-0.287E 02	0.448E 05
1.350	2.450	0.337E-02	0.122E 03	-0.233E 02	0.432E 05
1.600	2.990	0.400E-02	0.149E 03	-0.457E 02	0.488E 05
1.850	3.600	0.462E-02	0.180E 03	-0.531E 02	0.504E 05
2.100	4.230	0.525E-02	0.211E 03	-0.699E 02	0.536E 05
2.350	4.900	0.587E-02	0.245E 03	-0.840E 02	0.560E 05
2.600	5.600	0.650E-02	0.280E 03	-0.684E 02	0.536E 05
2.850	6.270	0.712E-02	0.314E 03	-0.103E 03	0.584E 05
3.100	7.000	0.775E-02	0.350E 03	-0.115E 03	0.600E 05
3.350	7.750	0.838E-02	0.388E 03	-0.115E 03	0.600E 05
3.600	8.500	0.900E-02	0.425E 03	-0.862E 02	0.568E 05
3.850	9.210	0.962E-02	0.461E 03	-0.148E 03	0.632E 05
4.100	10.000	0.102E-01	0.500E 03	-0.148E 03	0.632E 05

APPENDIX D Machine Deformation

Test Set-up Number 9	Full Scale Load Setting: 1000 lbs	Instron Cross-Head Separation Rate: 0.010 in./min.	Instron Chart Speed: 5 in./min.

X X-Coord. from Instron Chart (Div.)	Y Y-Coord. from Instron Chart (Div.)	D Machine Deformation (in.)	F Force (lbs)	A Tangent Intercept to D-F Curve (lbs)	B Tangent Slope to D-F Curve (lbs/in.)
0.000	0.000	0.000E 00	0.000E 00	-0.000E 00	0.560E 05
0.500	0.560	0.100E-02	0.560E 02	0.200E 01	0.540E 05
1.000	1.100	0.200E-02	0.110E 03	0.600E 01	0.520E 05
1.500	1.620	0.300E-02	0.162E 03	0.600E 01	0.520E 05
2.000	2.140	0.400E-02	0.214E 03	-0.100E 02	0.560E 05
2.500	2.700	0.500E-02	0.270E 03	-0.300E 02	0.600E 05
3.000	3.300	0.600E-02	0.330E 03	-0.240E 02	0.590E 05
3.500	3.890	0.700E-02	0.389E 03	-0.380E 02	0.610E 05
4.000	4.500	0.800E-02	0.450E 03	-0.780E 02	0.660E 05
4.500	5.160	0.900E-02	0.516E 03	-0.690E 02	0.650E 05
5.000	5.810	0.100E-01	0.581E 03	-0.990E 02	0.680E 05
5.500	6.490	0.110E-01	0.649E 03	-0.132E 03	0.710E 05
6.000	7.200	0.120E-01	0.720E 03	-0.108E 03	0.690E 05
6.500	7.890	0.130E-01	0.789E 03	-0.134E 03	0.710E 05
7.000	8.600	0.140E-01	0.860E 03	-0.162E 03	0.730E 05
7.500	9.330	0.150E-01	0.933E 03	-0.236E 03	0.779E 05
7.930	10.000	0.159E-01	0.100E 04	-0.236E 03	0.779E 05

APPENDIX E1

Double Lab Shear;

Summary of Data Reduction

APPENDIX E1-A; Mix 15

NS	R	SF	TF	DMS	DIS	DMT	DIT	S	E	SEC	TAN
Sample No.	Strain Rate $\dot{\gamma}$ %/min.	Max. Force F_s (lbs)	0.5 Max. Force F_t (in.)	Machine Deform. at SF (in.)	Indicated Deform. at SF (in.)	Machine Deform. at TF (in.)	Indicated Deform. at TF (in.)	Ult. Stress τ_u (psi)	Ult. Strain γ (percent)	Sec. Mod. G_s (ksi)	Tan. Mod. G_T (ksi)
17	0.110	99.5	49.7	0.00198	0.08840	0.00100	0.03458	13.8	4.74	0.29	0.37
19	0.101	79.5	39.8	0.00159	0.08620	0.00079	0.03415	11.1	4.29	0.26	0.33
21	0.106	84.5	42.2	0.00169	0.11240	0.00084	0.05383	11.8	5.86	0.20	0.21
13	1.124	155.5	77.7	0.00291	0.07540	0.00156	0.03010	21.1	4.07	0.52	0.66
15	1.088	149.5	74.7	0.00281	0.08000	0.00150	0.02724	20.5	4.20	0.49	0.73
7	10.499	237.5	118.8	0.00373	0.06360	0.00198	0.01738	33.1	3.14	1.05	2.05
9	11.111	208.0	104.0	0.00334	0.03980	0.00173	0.01281	29.2	2.03	1.44	2.37
11	11.057	269.0	134.5	0.00410	0.04800	0.00224	0.01318	37.6	2.43	1.55	3.11
1	108.548	452.0	226.0	0.00497	0.05520	0.00266	0.01555	63.6	2.73	2.33	4.55
5	111.498	435.0	217.5	0.00539	0.04760	0.00311	0.01670	61.0	2.35	2.59	4.02

APPENDIX E1-A; Mix 15

NS Sample No.	R Strain Rate $\dot{\gamma}$ %/min.	SF Max. Force F_s (lbs)	TF 0.5 Max. Force F_t (in.)	DMS Machine Deform. at SF (in.)	DIS Indicated Deform. at SF (in.)	DMT Machine Deform. at TF (in.)	DIT Indicated Deform. at TF (in.)	S Ult. Stress τ_u (psi)	E Ult. Strain γ (percent)	SEC Sec. Mod. G_s (ksi)	TAN Tan. Mod. G_T (ksi)
17	0.110	99.5	49.7	0.00198	0.08840	0.00100	0.03458	13.8	4.74	0.29	0.37
19	0.101	79.5	39.8	0.00159	0.08620	0.00079	0.03415	11.1	4.29	0.26	0.33
21	0.106	84.5	42.2	0.00169	0.11240	0.00084	0.05383	11.8	5.86	0.20	0.21
13	1.124	155.5	77.7	0.00291	0.07540	0.00156	0.03010	21.1	4.07	0.52	0.66
15	1.088	149.5	74.7	0.00281	0.08000	0.00150	0.02724	20.5	4.20	0.49	0.73
7	10.499	237.5	118.8	0.00373	0.06360	0.00198	0.01738	33.1	3.14	1.05	2.05
9	11.111	208.0	104.0	0.00334	0.03980	0.00173	0.01281	29.2	2.03	1.44	2.37
11	11.057	269.0	134.5	0.00410	0.04800	0.00224	0.01318	37.6	2.43	1.55	3.11
1	108.548	452.0	226.0	0.00497	0.05520	0.00266	0.01555	63.6	2.73	2.33	4.55
5	111.498	435.0	217.5	0.00539	0.04760	0.00311	0.01670	61.0	2.35	2.59	4.02

APPENDIX E2

Uniaxial Tension;

Summary of Data Reduction

APPENDIX E2-A; Mix 9

NS Sample No.	R Strain Rate ε %/min.	SF Max. Force F_s (lbs)	TF 0.5 Max. Force F_t (in.)	DMS Machine Deform. at SF (in.)	DIS Indicated Deform. at SF (in.)	DMT Machine Deform. at TF (in.)	DIT Indicated Deform. at TF (in.)	S Ult. Stress σ_u (psi)	E Ult. Strain ε_u (%)	SEC Sec. Mod. E_s (ksi)	TAN Tan. Mod. E_T (ksi)
19	0.033	19.0	9.5	0.00071	0.14800	0.00036	0.04940	8.4	2.44	0.34	0.52
20	0.033	17.0	8.5	0.00066	0.13860	0.00034	0.05426	7.8	2.28	0.34	0.44
17	0.332	35.0	17.5	0.00099	0.13750	0.00050	0.05582	16.7	2.26	0.74	0.91
18	0.333	17.0	8.5	0.00066	0.11150	0.00034	0.05814	7.8	1.84	0.42	0.40
15	3.371	63.0	31.5	0.00191	0.09700	0.00103	0.01516	29.6	1.60	1.85	6.21
16	3.319	55.5	27.7	0.00172	0.10480	0.00090	0.00936	28.2	1.71	1.65	10.03
13	33.571	143.0	71.5	0.00329	0.07280	0.00166	0.00506	62.6	1.17	5.37	54.78
14	33.543	144.0	72.0	0.00331	0.05440	0.00167	0.00527	65.5	0.86	7.64	54.21

APPENDIX E2-B; Mix 10

NS	R	SF	TF	DMS	DIS	DMT	DIT	S	E	SEC	TAN
Sample No.	Strain Rate ε %/min.	Max. Force F_s (lbs)	0.5 Max. Force F_t (in.)	Machine Deform. at SF (in.)	Indicated Deform. at SF (in.)	Machine Deform. at TF (in.)	Indicated Deform. at TF (in.)	Ult. Stress σ_u (psi)	Ult. Strain ε_u (%)	Sec. Mod. E_s (ksi)	Tan. Mod. E_T (ksi)
19	0.034	24.5	12.3	0.00090	0.13110	0.00046	0.04405	11.3	2.20	0.51	0.77
20	0.034	15.0	7.5	0.00060	0.10600	0.00030	0.03030	7.4	1.78	0.42	0.73
17	0.339	25.0	12.5	0.00089	0.05400	0.00050	0.00550	11.9	0.90	1.33	7.05
18	0.339	40.8	20.4	0.00143	0.12360	0.00076	0.04278	19.9	2.07	0.96	1.39
15	3.417	95.0	47.5	0.00214	0.06400	0.00113	0.00475	48.7	1.06	4.60	39.34
16	3.381	100.0	50.0	0.00223	0.06200	0.00119	0.00560	48.5	1.01	4.80	32.52
13	34.115	208.0	104.0	0.00454	0.05200	0.00232	0.00523	98.1	0.81	12.12	98.80
14	34.072	228.0	114.0	0.00492	0.03920	0.00254	0.00581	102.9	0.58	17.62	92.38

APPENDIX E2-C; Mix 11

NS Sample No.	R Strain Rate ε %/min.	SF Max. Force F_s (lbs)	TF 0.5 Max. Force F_t (in.)	DMS Machine Deform. at SF (in.)	DIS Indicated Deform. at SF (in.)	DMT Machine Deform. at TF (in.)	DIT Indicated Deform. at TF (in.)	S Ult. Stress σ_u (psi)	E Ult. Strain ε_u (%)	SEC Sec. Mod. E_s (ksi)	TAN Tan. Mod. E_T (ksi)
19	0.034	18.2	9.1	0.00068	0.14500	0.00034	0.04721	8.3	2.45	0.34	0.52
20	0.034	18.4	9.2	0.00069	0.14700	0.00035	0.04792	8.7	2.47	0.35	0.54
17	0.339	34.1	17.0	0.00121	0.11680	0.00064	0.04821	16.6	1.96	0.85	1.03
18	0.339	36.8	18.4	0.00130	0.11480	0.00069	0.04451	17.3	1.92	0.90	1.17
15	3.417	99.0	49.5	0.00245	0.10260	0.00126	0.00681	43.7	1.71	2.55	23.02
16	3.400	100.0	50.0	0.00247	0.09200	0.00128	0.00617	45.8	1.52	3.01	27.50
13	34.072	321.0	160.5	0.00632	0.06880	0.00329	0.00596	144.7	1.06	13.60	158.94
14	34.144	280.0	140.0	0.00596	0.05800	0.00324	0.00583	133.3	0.89	15.01	150.64

APPENDIX E2-D; Mix 12

NS	R	SF	TF	DMS	DIS	DMT	DIT	S	E	SEC	TAN
Sample No.	Strain Rate ε %/min.	Max. Force F_s (lbs)	0.5 Max. Force F_t (in.)	Machine Deform. at SF (in.)	Indicated Deform. at SF (in.)	Machine Deform. at TF (in.)	Indicated Deform. at TF (in.)	Ult. Stress σ_u (psi)	Ult. Strain ε_u (%)	Sec. Mod. E_s (ksi)	Tan. Mod. E_T (ksi)
19	0.034	14.6	7.3	0.00055	0.24300	0.00027	0.08567	7.0	4.09	0.17	0.24
20	0.034	15.6	7.8	0.00059	0.21590	0.00029	0.07410	7.7	3.62	0.21	0.31
17	0.337	33.9	16.9	0.00120	0.18400	0.00064	0.06885	14.9	3.08	0.48	0.65
18	0.338	28.8	14.4	0.00104	0.17840	0.00054	0.06554	14.4	3.00	0.48	0.65
16	3.380	84.2	42.1	0.00241	0.12940	0.00137	0.00643	38.2	2.15	1.78	22.35
15	3.347	79.8	39.9	0.00231	0.16520	0.00130	0.00683	34.0	2.73	1.25	18.35
13	33.375	252.0	126.0	0.00546	0.07000	0.00292	0.00569	108.5	1.08	10.07	117.01
14	33.389	196.0	98.0	0.00430	0.07520	0.00219	0.00439	92.3	1.18	7.80	125.52

APPENDIX E2-E; Mix 13

NS Sample No.	R Strain Rate ε %/min.	SF Max. Force F_s (lbs)	TF 0.5 Max. Force F_t (in.)	DMS Machine Deform. at SF (in.)	DIS Indicated Deform. at SF (in.)	DMT Machine Deform. at TF (in.)	DIT Indicated Deform. at TF (in.)	S Ult. Stress σ_u (psi)	E Ult. Strain ε_u (%)	SEC Sec. Mod. E_s (ksi)	TAN Tan. Mod. E_T (ksi)
19	0.034	49.0	24.5	0.00156	0.05430	0.00080	0.01996	23.0	0.89	2.59	3.57
20	0.034	46.1	23.0	0.00148	0.05460	0.00075	0.01436	23.7	0.89	2.65	5.17
17	0.336	93.3	46.6	0.00232	0.05000	0.00119	0.00821	43.4	0.80	5.43	18.42
18	0.336	91.3	45.6	0.00227	0.04560	0.00116	0.00803	43.5	0.73	5.97	18.83
15	3.571	172.0	86.0	0.00390	0.04480	0.00199	0.00659	80.8	0.73	11.07	49.17
16	3.351	163.8	81.9	0.00373	0.04280	0.00190	0.00738	83.7	0.65	12.79	45.55
13	35.730	341.0	170.5	0.00666	0.03480	0.00349	0.00798	154.6	0.50	30.76	96.56
14	35.667	316.0	158.0	0.00623	0.03560	0.00324	0.00622	142.8	0.52	27.26	134.10

APPENDIX E2-F; Mix 14

NS Sample No.	R Strain Rate ε %/min.	SF Max. Force F_s (lbs)	TF 0.5 Max. Force F_t (in.)	DMS Machine Deform. at SF (in.)	DIS Indicated Deform. at SF (in.)	DMT Machine Deform. at TF (in.)	DIT Indicated Deform. at TF (in.)	S Ult. Stress σ_u (psi)	E Ult. Strain ε_u (%)	SEC Sec. Mod. E_s (ksi)	TAN Tan. Mod. E_T (ksi)
19	0.034	19.4	9.7	0.00073	0.13090	0.00036	0.04458	10.1	2.22	0.45	0.67
20	0.034	20.0	10.0	0.00074	0.12000	0.00040	0.04000	9.8	2.04	0.48	0.72
17	0.341	37.7	18.8	0.00133	0.12440	0.00071	0.05027	18.7	2.10	0.89	1.10
18	0.342	42.0	21.0	0.00137	0.11840	0.00068	0.04918	20.2	2.00	1.01	1.22
15	3.400	81.8	40.9	0.00236	0.09300	0.00133	0.00879	41.2	1.54	2.68	16.26
16	3.431	79.8	39.9	0.00231	0.10040	0.00130	0.01010	40.1	1.68	2.38	13.28
13	34.072	142.0	71.0	0.00326	0.10000	0.00164	0.00488	69.2	1.65	4.20	62.81
14	33.884	153.0	76.5	0.00351	0.06240	0.00177	0.00389	80.3	1.00	8.05	111.75

APPENDIX E3

Uniaxial Compression;

Summary of Data Reduction

APPENDIX E3-A; Mix 9

NS Sample No.	R Strain Rate $\dot{\varepsilon}$ %/min.	SF Max. Force F_s (lbs)	TF 0.5 Max. Force F_t (in.)	DMS Machine Deform. at SF (in.)	DIS Indicated Deform. at SF (in.)	DMT Machine Deform. at TF (in.)	DIT Indicated Deform. at TF (in.)	S Ult. Stress σ_u (psi)	E Ult. Strain ε_u (%)	SEC Sec. Mod. E_s (ksi)	TAN Tan. Mod. E_T (ksi)
9	0.033	81.0	40.5	0.00114	0.26350	0.00061	0.08599	37.1	4.36	0.85	1.31
10	0.033	100.5	50.3	0.00136	0.34000	0.00076	0.11323	42.4	5.64	0.75	1.13
6	0.841	157.0	78.5	0.00211	0.25500	0.00106	0.09485	73.4	4.25	1.73	2.33
7	0.838	178.0	89.0	0.00249	0.24600	0.00135	0.09375	79.1	4.08	1.94	2.56
8	0.827	169.0	84.5	0.00225	0.22750	0.00114	0.08689	77.0	3.72	2.07	2.71
3	16.985	467.0	233.5	0.00481	0.25200	0.00243	0.08539	187.4	4.20	4.46	6.65
4	17.021	407.0	203.5	0.00444	0.25100	0.00231	0.07576	159.9	4.20	3.81	6.40
5	16.708	381.0	190.5	0.00417	0.27400	0.00216	0.11862	170.2	4.51	3.78	4.37
11	336.417	1070.0	535.0	0.00768	0.18000	0.00412	0.02782	490.1	2.90	16.91	61.46
12	336.417	840.0	420.0	0.00685	0.19600	0.00365	0.03247	392.4	3.18	12.33	40.47

APPENDIX E3-B; Mix 10

NS Sample No.	R Strain Rate ε %/min.	SF Max. Force F_s (lbs)	TF 0.5 Max. Force F_t (in.)	DMS Machine Deform. at SF (in.)	DIS Indicated Deform. at SF (in.)	DMT Machine Deform. at TF (in.)	DIT Indicated Deform. at TF (in.)	S Ult. Stress σ_u (psi)	E Ult. Strain ε_u (%)	SEC Sec. Mod. E_s (ksi)	TAN Tan. Mod. E_T (ksi)
9	0.034	110.5	55.3	0.00153	0.24270	0.00075	0.08761	48.2	4.12	1.17	1.62
10	0.034	107.0	53.5	0.00148	0.29950	0.00072	0.09813	52.2	5.07	1.03	1.57
7	0.848	212.0	106.0	0.00218	0.24650	0.00113	0.08480	96.1	4.14	2.32	3.39
8	0.855	257.0	128.5	0.00256	0.23450	0.00137	0.08577	109.7	3.97	2.76	3.80
3	16.935	521.0	260.5	0.00361	0.21200	0.00192	0.03393	237.5	3.53	6.73	21.90
4	17.000	521.0	260.5	0.00361	0.19960	0.00192	0.03308	227.9	3.33	6.84	21.50
5	17.331	619.0	309.5	0.00418	0.17240	0.00228	0.03900	253.6	2.92	8.70	19.92
11	341.443	1330.0	665.0	0.00874	0.18400	0.00475	0.03007	563.0	2.99	18.82	65.11
12	340.861	1000.0	500.0	0.00781	0.20400	0.00435	0.04854	471.1	3.34	14.09	31.27

APPENDIX E3-C; Mix 11

NS	R	SF	TF	DMS	DIS	DMT	DIT	S	E	SEC	TAN
Sample No.	Strain Rate ε %/min.	Max. Force F_s (lbs)	0.5 Max. Force F_t (in.)	Machine Deform. at SF (in.)	Indicated Deform. at SF (in.)	Machine Deform. at TF (in.)	Indicated Deform. at TF (in.)	Ult. Stress σ_u (psi)	Ult. Strain ε_u (%)	Sec. Mod. E_s (ksi)	Tan. Mod. E_T (ksi)
9	0.034	93.5	46.7	0.00129	0.25940	0.00071	0.09350	42.0	4.37	0.96	1.33
10	0.034	91.0	45.5	0.00130	0.27000	0.00067	0.09591	40.1	4.54	0.88	1.25
7	0.847	179.0	89.5	0.00202	0.22200	0.00109	0.08010	86.1	3.73	2.31	3.21
8	0.859	227.0	113.5	0.00231	0.21500	0.00121	0.07718	99.3	3.65	2.72	3.80
4	17.036	780.0	390.0	0.00758	0.20840	0.00415	0.06656	332.1	3.42	9.71	15.62
5	17.007	679.0	339.5	0.00658	0.21240	0.00346	0.04134	316.9	3.50	9.05	24.60
6	16.942	772.0	386.0	0.00751	0.21820	0.00411	0.05805	332.5	3.57	9.32	18.19
11	342.319	2380.0	1190.0	0.01212	0.05600	0.00643	0.02434	1178.4	0.75	156.89	192.26
12	340.426	1860.0	930.0	0.01044	0.06800	0.00564	0.02880	881.0	0.98	89.92	111.74

APPENDIX E3-D; Mix 12

NS Sample No.	R Strain Rate ε %/min.	SF Max. Force F_s (lbs)	TF 0.5 Max. Force F_t (in.)	DMS Machine Deform. at SF (in.)	DIS Indicated Deform. at SF (in.)	DMT Machine Deform. at TF (in.)	DIT Indicated Deform. at TF (in.)	S Ult. Stress σ_u (psi)	E Ult. Strain ε_u (%)	SEC Sec. Mod. E_s (ksi)	TAN Tan. Mod. E_T (ksi)
9	0.034	85.0	42.5	0.00121	0.32420	0.00063	0.11138	36.4	5.47	0.67	0.97
10	0.034	70.5	35.2	0.00101	0.39940	0.00053	0.13818	30.4	6.73	0.45	0.65
7	0.834	162.0	81.0	0.00185	0.33600	0.00099	0.11372	77.5	5.58	1.39	2.06
8	0.847	197.5	98.7	0.00205	0.31600	0.00105	0.10151	86.9	5.32	1.63	2.55
4	16.842	650.0	325.0	0.00633	0.31100	0.00332	0.07706	299.8	5.13	5.84	12.07
5	16.764	804.0	402.0	0.00736	0.34240	0.00387	0.08362	346.9	5.62	6.18	12.97
6	16.688	688.0	344.0	0.00666	0.30240	0.00351	0.07629	322.8	4.94	6.54	13.29
11	335.149	2240.0	1120.0	0.01186	0.24000	0.00640	0.02987	1017.9	3.82	26.63	129.42
12	334.868	1500.0	750.0	0.00957	0.29600	0.00536	0.03181	751.7	4.80	15.67	84.86

APPENDIX E3-E; Mix 13

NS Sample No.	R Strain Rate ε %/min.	SF Max. Force F_s (lbs)	TF 0.5 Max. Force F_t (in.)	DMS Machine Deform. at SF (in.)	DIS Indicated Deform. at SF (in.)	DMT Machine Deform. at TF (in.)	DIT Indicated Deform. at TF (in.)	S Ult. Stress σ_u (psi)	E Ult. Strain ε_u (%)	SEC Sec. Mod. E_s (ksi)	TAN Tan. Mod. E_T (ksi)
8	0.034	275.5	137.8	0.00311	0.11528	0.00160	0.04298	119.8	1.89	6.35	8.60
9	0.033	250.5	125.3	0.00285	0.12270	0.00146	0.04559	104.8	2.00	5.23	7.10
10	0.033	281.5	140.8	0.00265	0.12300	0.00141	0.04428	116.8	2.01	5.80	8.15
6	0.891	482.5	241.2	0.00373	0.11850	0.00212	0.04415	217.7	2.04	10.65	14.53
7	0.891	436.5	218.2	0.00345	0.11500	0.00191	0.03950	209.7	1.99	10.54	15.64
3	17.316	958.0	479.0	0.00830	0.12100	0.00435	0.03760	422.3	1.95	21.64	36.67
4	17.590	915.0	457.5	0.00798	0.12000	0.00416	0.03340	424.9	1.97	21.56	41.31
11	357.622	2120.0	1060.0	0.01133	0.06400	0.00606	0.02579	1006.8	0.94	106.89	142.64
12	356.666	1710.0	855.0	0.00973	0.07200	0.00518	0.03176	791.4	1.11	71.26	83.49

APPENDIX E3-F; Mix 14

NS Sample No.	R Strain Rate $\dot{\varepsilon}$ %/min.	SF Max. Force F_s (lbs)	TF 0.5 Max. Force F_t (in.)	DMS Machine Deform. at SF (in.)	DIS Indicated Deform. at SF (in.)	DMT Machine Deform. at TF (in.)	DIT Indicated Deform. at TF (in.)	S Ult. Stress σ_u (psi)	E Ult. Strain ε_u (%)	SEC Sec. Mod. E_s (ksi)	TAN Tan. Mod. E_T (ksi)
9	0.034	100.0	50.0	0.00136	0.24570	0.00076	0.08207	50.1	4.19	1.20	1.80
10	0.034	101.5	50.7	0.00145	0.27310	0.00075	0.09206	46.6	4.64	1.00	1.49
6	0.847	222.0	111.0	0.00298	0.23850	0.00168	0.08602	103.8	3.99	2.60	3.63
8	0.857	209.0	104.5	0.00284	0.19950	0.00158	0.07298	103.7	3.37	3.08	4.24
3	16.584	525.0	262.5	0.00539	0.23250	0.00279	0.07891	223.2	3.77	5.93	8.84
4	16.543	566.0	283.0	0.00575	0.22000	0.00301	0.07800	229.0	3.54	6.46	9.23
5	16.949	523.0	261.5	0.00537	0.21000	0.00278	0.07191	263.2	3.47	7.59	11.23
11	339.991	1080.0	540.0	0.00773	0.18000	0.00415	0.02869	561.7	2.93	19.18	67.33
12	340.426	880.0	440.0	0.00709	0.20800	0.00383	0.03242	435.1	3.42	12.72	44.70

APPENDIX E4

Splitting Tension;

Summary of Data Reduction

APPENDIX E4-A; Mix 39

NS	R	SF	TF	DMS	DIS	DMT	DIT	S	E	SEC	TAN
Sample No.	Strain Rate ε %/min.	Max. Force F_s (lbs)	0.5 Max. Force F_t (in.)	Machine Deform. at SF (in.)	Indicated Deform. at SF (in.)	Machine Deform. at TF (in.)	Indicated Deform. at TF (in.)	Ult. Stress σ_u (psi)	Ult. Strain ε_u (percent)	Sec. Mod. E_s (ksi)	Tan. Mod. E_T (ksi)
9	1.028	135.0	67.5	0.00045	0.24900	0.00022	0.08567	11.1	1.67	1.46	4.08
13	1.052	130.0	65.0	0.00043	0.27520	0.00022	0.10174	10.9	1.84	1.30	3.11
15	1.057	116.5	58.2	0.00039	0.33200	0.00019	0.12562	9.8	2.22	0.97	2.53
5	10.479	302.0	151.0	0.00101	0.24500	0.00050	0.09123	25.2	1.64	3.39	7.23
6	10.563	310.0	155.0	0.00103	0.18700	0.00052	0.06726	26.1	1.25	4.60	10.95
7	10.453	300.0	150.0	0.00100	0.22160	0.00050	0.08313	25.0	1.48	3.71	13.70
8	10.133	281.5	140.8	0.00094	0.23600	0.00047	0.08758	22.7	1.58	3.17	10.93
1	107.277	894.0	447.0	0.00301	0.21300	0.00149	0.07033	76.4	1.41	11.92	30.51
2	102.512	860.0	430.0	0.00288	0.20560	0.00143	0.07547	70.2	1.36	11.35	35.42
3	105.024	890.0	445.0	0.00300	0.19600	0.00148	0.06198	74.4	1.29	12.64	50.75
4	103.986	864.0	432.0	0.00289	0.23000	0.00144	0.08406	71.5	1.52	10.33	24.31
10	1060.071	2340.0	1170.0	0.00884	0.08800	0.00459	0.03484	197.5	0.53	81.79	823.13
14	1000.667	2100.0	1050.0	0.00807	0.18000	0.00412	0.03635	167.3	1.15	31.90	421.40
16	1009.592	1980.0	990.0	0.00768	0.20800	0.00388	0.04978	159.2	1.34	26.05	401.85

APPENDIX E4-B; Mix 43

NS	R	SF	TF	DMS	DIS	DMT	DIT	S	E	SEC	TAN
Sample No.	Strain Rate $\dot{\varepsilon}$ %/min.	Max. Force F_s (lbs)	0.5 Max. Force F_t (in.)	Machine Deform. at SF (in.)	Indicated Deform. at SF (in.)	Machine Deform. at TF (in.)	Indicated Deform. at TF (in.)	Ult. Stress σ_u (psi)	Ult. Strain ε_u (percent)	Sec. Mod. E_s (ksi)	Tan. Mod. E_T (ksi)
19	1.038	425.0	212.5	0.00142	0.08660	0.00071	0.03160	35.1	0.57	13.51	34.19
24	1.012	373.5	186.8	0.00124	0.08600	0.00062	0.03154	30.1	0.57	11.65	34.62
25	1.014	381.0	190.5	0.00127	0.09140	0.00063	0.03470	30.8	0.60	11.19	32.25
15	10.276	860.0	430.0	0.00288	0.08810	0.00143	0.02967	70.4	0.57	27.06	37.99
16	10.388	897.0	448.5	0.00302	0.09340	0.00149	0.03536	74.2	0.61	26.91	55.24
17	10.636	900.0	450.0	0.00304	0.09240	0.00150	0.03200	76.2	0.60	27.96	81.92
12	100.790	2250.0	1125.0	0.00855	0.08300	0.00441	0.02917	180.6	0.50	79.50	286.92
13	98.879	2135.0	1067.5	0.00818	0.09160	0.00419	0.03089	168.1	0.56	66.05	164.27
14	105.319	1890.0	945.0	0.00739	0.09400	0.00371	0.03386	158.5	0.58	59.99	218.76
21	501.840	3060.0	1530.0	0.01117	0.07600	0.00600	0.02732	244.5	0.43	123.64	688.03
22	501.421	3080.0	1540.0	0.01123	0.07800	0.00604	0.02596	245.9	0.45	120.74	919.74
23	525.210	3100.0	1550.0	0.01129	0.07200	0.00608	0.02411	259.3	0.41	140.00	547.33

APPENDIX E5

Hydrostatic Tension;

Summary of Data Reduction

APPENDIX E5 -A; Mix 16

NS	R	SF	TF	DMS	DIS	DMT	DIT	S	E	SEC	TAN
Sample No.	Strain Rate ε %/min.	Max. Force F_s (lbs)	0.5 Max. Force F_t (in.)	Machine Deform. at SF (in.)	Indicated Deform. at SF (in.)	Machine Deform. at TF (in.)	Indicated Deform. at TF (in.)	Ult. Stress σ_u (psi)	Ult. Strain ε_u (percent)	Sec. Mod. E_s (ksi)	Tan. Mod. E_T (ksi)
1	0.382	418.0	209.0	0.00626	0.01300	0.00348	0.00586	33.3	1.29	2.59	3.67
2	0.390	482.5	241.2	0.00610	0.01312	0.00309	0.00585	38.4	1.37	2.80	3.57
3	0.395	412.0	206.0	0.00619	0.01244	0.00343	0.00450	32.8	1.23	2.66	7.81
4	3.659	1074.0	537.0	0.01136	0.01760	0.00597	0.00807	85.5	1.14	7.49	11.10
5	3.899	950.0	475.0	0.01023	0.01576	0.00528	0.00721	75.6	1.08	7.02	10.03
6	4.016	976.0	488.0	0.01047	0.01544	0.00542	0.00700	77.7	1.00	7.78	12.23
7	38.785	1875.0	937.5	0.01662	0.02300	0.00852	0.01087	149.3	1.24	12.07	16.42
8	38.810	1700.0	850.0	0.01619	0.02360	0.00867	0.01105	135.4	1.44	9.42	14.67
11	39.474	1785.0	892.5	0.01689	0.02500	0.00911	0.00929	142.1	1.60	8.88	195.66
28	40.650	2140.0	1070.0	0.01877	0.02380	0.00973	0.01135	170.4	1.02	16.66	25.80
9	392.414	2980.0	1490.0	0.02389	0.03000	0.01221	0.01471	237.3	1.20	19.79	24.17
12	394.737	3390.0	1695.0	0.02689	0.03320	0.01389	0.01631	269.9	1.25	21.67	28.31
13	395.779	3000.0	1500.0	0.02403	0.03080	0.01230	0.01509	238.9	1.34	17.84	21.62
14	406.229	3190.0	1595.0	0.02542	0.03080	0.01307	0.01513	254.0	1.09	23.24	30.41

APPENDIX E5-B; Mix 17

NS Sample No.	R Strain Rate ε %/min.	SF Max. Force F_s (lbs)	TF 0.5 Max. Force F_t (in.)	DMS Machine Deform. at SF (in.)	DIS Indicated Deform. at SF (in.)	DMT Machine Deform. at TF (in.)	DIT Indicated Deform. at TF (in.)	S Ult. Stress σ_u (psi)	E Ult. Strain ε_u (percent)	SEC Sec. Mod. E_s (ksi)	TAN Tan. Mod. E_T (ksi)
1	0.337	444.0	222.0	0.00657	0.01276	0.00370	0.00554	35.4	1.04	3.39	5.70
2	0.345	465.0	232.5	0.00681	0.01300	0.00387	0.00574	37.0	1.07	3.46	5.74
3	0.334	439.0	219.5	0.00652	0.01140	0.00366	0.00490	35.0	0.82	4.29	8.43
4	3.401	1176.0	588.0	0.01229	0.02100	0.00653	0.00958	93.6	1.48	6.32	9.04
5	3.519	1178.0	589.0	0.01230	0.02028	0.00654	0.00943	93.8	1.40	6.68	9.24
6	3.193	1114.0	557.0	0.01172	0.01984	0.00619	0.00895	88.7	1.30	6.84	10.05
7	33.613	2700.0	1350.0	0.02295	0.03100	0.01205	0.01470	215.0	1.35	15.89	24.20
8	32.823	2650.0	1325.0	0.02256	0.03260	0.01183	0.01560	211.0	1.65	12.81	17.04
9	34.188	2670.0	1335.0	0.02272	0.03160	0.01192	0.01528	212.6	1.52	14.00	18.53
10	320.342	3760.0	1880.0	0.02950	0.03560	0.01541	0.02316	299.4	0.98	30.62	12.06
11	321.027	3410.0	1705.0	0.02703	0.03480	0.01398	0.01723	271.5	1.25	21.77	26.02
12	324.324	3620.0	1810.0	0.02851	0.04040	0.01484	0.01973	288.2	1.93	14.95	18.15

APPENDIX E5-C; Mix 18

NS Sample No.	R Strain Rate ε %/min.	SF Max. Force F_s (lbs)	TF 0.5 Max. Force F_t (in.)	DMS Machine Deform. at SF (in.)	DIS Indicated Deform. at SF (in.)	DMT Machine Deform. at TF (in.)	DIT Indicated Deform. at TF (in.)	S Ult. Stress σ_u (psi)	E Ult. Strain ε_u (percent)	SEC Sec. Mod. E_s (ksi)	TAN Tan. Mod. E_T (ksi)
1	0.336	457.0	228.5	0.00672	0.01404	0.00381	0.00603	36.4	1.23	2.95	4.87
2	0.344	547.0	273.5	0.00681	0.01484	0.00351	0.00651	43.6	1.38	3.16	4.21
3	0.339	746.0	373.0	0.00894	0.01620	0.00478	0.00733	59.4	1.23	4.83	6.88
4	3.429	1648.0	824.0	0.01577	0.02364	0.00841	0.01105	131.2	1.35	9.72	14.47
5	3.427	1354.0	677.0	0.01328	0.02204	0.00691	0.01019	107.8	1.50	7.18	9.58
6	3.375	1594.0	797.0	0.01532	0.02060	0.00813	0.00970	126.9	0.89	14.25	23.94
16	3.417	1746.0	873.0	0.01657	0.02576	0.00891	0.01206	139.0	1.57	8.85	12.89
7	32.538	3010.0	1505.0	0.02410	0.03330	0.01234	0.01640	239.6	1.50	16.02	18.10
8	33.822	2630.0	1315.0	0.02241	0.02950	0.01174	0.01415	209.4	1.20	17.45	25.73
9	33.576	2875.0	1437.5	0.02421	0.03090	0.01283	0.01513	228.9	1.12	20.37	29.65
17	33.879	3085.0	1542.5	0.02465	0.03500	0.01264	0.01734	245.6	1.75	14.01	15.42
10	331.859	3570.0	1785.0	0.02816	0.03320	0.01463	0.01652	284.2	0.84	33.98	45.40
18	342.075	3400.0	1700.0	0.02696	0.03480	0.01393	0.01722	270.7	1.34	20.19	24.12
19	349.040	2800.0	1400.0	0.02367	0.03000	0.01250	0.01487	222.9	1.10	20.18	26.89

APPENDIX E5-D; Mix 19

NS	R	SF	TF	DMS	DIS	DMT	DIT	S	E	SEC	TAN
Sample No.	Strain Rate ε %/min.	Max. Force F_s (lbs)	0.5 Max. Force F_t (in.)	Machine Deform. at SF (in.)	Indicated Deform. at SF (in.)	Machine Deform. at TF (in.)	Indicated Deform. at TF (in.)	Ult. Stress σ_u (psi)	Ult. Strain ε_u (percent)	Sec. Mod. E_s (ksi)	Tan. Mod. E_T (ksi)
1	0.344	503.0	251.5	0.00632	0.01448	0.00322	0.00586	40.0	1.40	2.85	4.42
2	0.343	603.0	301.5	0.00744	0.01568	0.00387	0.00698	48.0	1.41	3.39	4.49
3	0.344	647.0	323.5	0.00792	0.01648	0.00415	0.00723	51.5	1.47	3.50	4.85
4	0.347	548.0	274.0	0.00682	0.01548	0.00351	0.00653	43.6	1.50	2.91	4.17
5	3.221	1038.0	519.0	0.01103	0.02052	0.00577	0.00901	82.6	1.53	5.41	7.91
6	3.440	1214.0	607.0	0.01263	0.02004	0.00674	0.00915	96.7	1.28	7.58	11.70
7	3.446	1260.0	630.0	0.01304	0.02100	0.00700	0.00960	100.3	1.37	7.31	11.18
8	3.339	1134.0	567.0	0.01191	0.02088	0.00630	0.00940	90.3	1.50	6.03	8.74
9	34.130	1890.0	945.0	0.01675	0.02800	0.00859	0.01248	150.5	1.92	7.84	11.33
10	33.898	2295.0	1147.5	0.01998	0.02800	0.01043	0.01278	182.7	1.36	13.44	22.91
11	34.247	2320.0	1160.0	0.02017	0.02890	0.01055	0.01345	184.7	1.49	12.36	18.58
13	34.582	2210.0	1105.0	0.01931	0.02780	0.01005	0.01286	176.0	1.47	11.99	18.09
12	342.661	3390.0	1695.0	0.02689	0.03440	0.01389	0.01695	269.9	1.29	20.97	25.77
14	343.643	3720.0	1860.0	0.02921	0.03720	0.01525	0.01782	296.2	1.37	21.59	33.49
15	344.432	3960.0	1980.0	0.03088	0.03840	0.01623	0.01854	315.3	1.29	24.36	39.62
16	344.234	3530.0	1765.0	0.02788	0.04000	0.01447	0.01866	281.1	2.09	13.47	19.49

APPENDIX E6-A; Mix 24

NS Sample No.	R Strain Rate ε %/min.	SF Max. Force F_s (lbs)	TF 0.5 Max. Force F_t (in.)	DMS Machine Deform. at SF (in.)	DIS Indicated Deform. at SF (in.)	DMT Machine Deform. at TF (in.)	DIT Indicated Deform. at TF (in.)	S Ult. Stress σ_u (psi)	E Ult. Strain ε_u (percent)	SEC Sec. Mod. E_s (ksi)	TAN Tan. Mod. E_T (ksi)
3	3.226	24.0	12.0	0.00043	0.00980	0.00021	0.00311	8.3	1.51	0.55	0.88
4	3.226	20.0	10.0	0.00036	0.00960	0.00018	0.00225	6.9	1.49	0.46	1.03
5	32.258	195.0	97.5	0.00367	0.01080	0.00181	0.00403	67.2	1.15	5.84	9.36
6	32.258	137.0	68.5	0.00256	0.00920	0.00127	0.00289	42.7	1.07	3.99	8.19
1	322.581	294.0	147.0	0.00552	0.01840	0.00283	0.00588	113.0	2.08	5.44	11.47
2	322.581	1110.0	555.0	0.01169	0.03320	0.00617	0.01305	382.2	3.47	11.02	17.22
7	322.581	1025.0	512.5	0.01091	0.03080	0.00569	0.01203	353.0	3.21	11.01	17.28

APPENDIX E6-B; Mix 25

NS	R	SF	TF	DMS	DIS	DMT	DIT	S	E	SEC	TAN
Sample No.	Strain Rate ε %/min.	Max. Force F_s (lbs)	0.5 Max. Force F_t (in.)	Machine Deform. at SF (in.)	Indicated Deform. at SF (in.)	Machine Deform. at TF (in.)	Indicated Deform. at TF (in.)	Ult. Stress σ_u (psi)	Ult. Strain ε_u (percent)	Sec. Mod. E_s (ksi)	Tan. Mod. E_T (ksi)
3	5.780	67.7	33.8	0.00122	0.01090	0.00060	0.00353	23.5	2.80	0.84	1.39
4	5.780	130.0	65.0	0.00242	0.01170	0.00120	0.00334	50.0	2.68	1.87	4.05
5	57.803	280.0	140.0	0.00449	0.01460	0.00233	0.00501	88.5	2.92	3.03	5.72
6	57.803	335.0	167.5	0.00520	0.01620	0.00279	0.00568	128.9	3.18	4.05	7.72
1	578.034	2150.0	1075.0	0.01885	0.03720	0.00977	0.01818	798.5	5.30	15.05	16.44
2	578.034	1590.0	795.0	0.01529	0.03520	0.00811	0.01439	534.6	5.75	9.29	14.72

APPENDIX E6-C; Mix 26

NS	R	SF	TF	DMS	DIS	DMT	DIT	S	E	SEC	TAN
Sample No.	Strain Rate ε %/min.	Max. Force F_s (lbs)	0.5 Max. Force F_t (in.)	Machine Deform. at SF (in.)	Indicated Deform. at SF (in.)	Machine Deform. at TF (in.)	Indicated Deform. at TF (in.)	Ult. Stress σ_u (psi)	Ult. Strain ε_u (percent)	Sec. Mod. E_s (ksi)	Tan. Mod. E_T (ksi)
3	11.173	167.6	83.8	0.00314	0.00924	0.00155	0.00347	62.1	3.41	1.82	2.90
4	11.173	207.5	103.7	0.00346	0.01020	0.00173	0.00385	75.4	3.77	2.00	3.19
7	11.173	176.5	88.2	0.00332	0.00880	0.00163	0.00295	71.3	3.06	2.33	4.84
5	111.732	810.0	405.0	0.00959	0.02240	0.00519	0.00969	341.3	7.15	4.77	6.79
6	111.732	224.0	112.0	0.00373	0.01448	0.00187	0.00496	71.6	6.00	1.19	2.07
1	1117.318	2125.0	1062.5	0.01865	0.04000	0.00966	0.01847	850.3	11.93	7.13	8.64
2	1117.318	2690.0	1345.0	0.02287	0.04080	0.01201	0.01909	987.0	10.01	9.86	12.47